Biological activity of Pyrrole-Imidazole polyamides *in vivo*.

Thesis by
Jerzy O. Szablowski

In Partial Fulfillment of the Requirements for the
degree of
Doctor of Philosophy

CALIFORNIA INSTITUTE OF TECHNOLOGY
Pasadena, California
2015
(Defended May 1st, 2015)

ACKNOWLEDGEMENTS

I would like to thank my advisor, Peter Dervan, for the enthusiasm and support of the research projects during my time in his lab. Peter challenged me to stay focused on my projects while thinking broadly about the impact of my work on science and medicine. I am also particularly grateful for his guidance in learning how to communicate ideas, present my work, and seek advice when needed. Lastly, I am very grateful for the freedom I was given to pursue research projects, which was challenging, but also essential aspect of my training that I deeply appreciate.

I would also like to thank my committee chair, Frances Arnold, for advice and support, both during my graduate studies and when I had an invaluable opportunity to work in her laboratory during my undergraduate studies. The summer of 2007 was one of the highlights of my undergraduate studies and the problem solving skills I learned are still extremely useful, many years afterwards.

I am also thankful to Rob Phillips and Steve Mayo for serving on my thesis committee and for their advice during my first year of graduate school.

I am grateful to postdocs in our lab, Jevgenij Raskatov and Nick Nichols, with whom I worked on several projects. Jevgenij has given me a brilliant advice on science, but also taught me a lot about communication with other scientists. Nick has been an invaluable help during my studies and his efficiency, focus, and critical thinking have all been very helpful in my own development as a scientist. Work in this thesis would not have been possible without their help. I would also like to thank the staff of Caltech OLAR, and in particular Karen Lencioni and Gwen Williams, for their advice and help in our *in vivo* experiments.

I have had a privilege to interact with many great students, postdocs, Dervan group alums, and collaborators. I would like to extend my gratitude for intellectually stimulating discussions and advice from Thomas Martinez, Jim Puckett, Amanda Hargrove, Alissa Hare, JenJoo Kang, Tim Welch, Fei Yang, John Phillips, Amanda Silberstein, Dave Montgomery, Ben Li, Alexis Kurmis, Jamie Wang, Sam Weisbrod, Jordan Meier, Patrick Frost, and Bogdan Olenyuk.

Many other scientists have been an inspiration before my graduate studies and I am very grateful for their help. During my high school studies in Poland, I was lucky to take part in an internship in Zylicz lab at IIMCB, with then a doctoral student Dawid Walerych, who helped me with my first foray into science. During my undergraduate studies, I have received more support from professors Alan Jasanoff and Bob Langer than I could have possibly hoped for. I am particularly grateful for working with and learning from their graduate student Mikhail Shapiro. Sharing enthusiasm for science, working long hours, and engaging in creative discussions with him were the highlights of my time at MIT. I am also grateful for work done with Ed Boyden in Synthetic Neurobiology group, which was my first attempt at performing an independent project, which was as rewarding as it was challenging. Many of my fellow students and postdocs at MIT were an inspiration, including Brian Chow, Gil Westmeyer, Saad Zaheer, and my then neighbours in my dormitory.

Lastly, I am sincerely grateful for the support of my family – my parents, siblings and my wife Ji. The journey that lead to this Ph.D. has been a long one and they have been on it with me for longer than anyone else. My parents have supported me in what must have looked impossible to any reasonable adult – attending a top research university in the US

after a Polish high school. I deeply appreciate that they allowed me to dream big despite the low odds of success. I have been lucky to meet Ji years ago. Throughout my Ph.D. studies her love and support were the reasons to come home every day, while her knowledge of medicine and advice helped me to stay focused on real-world implications of my work.

ABSTRACT

This thesis focuses on biological activity of pyrrole-imidazole polyamides *in vivo*. The work presented includes experiments underlining sequence selectivity of these compounds in living cells and potential methods to improve it. A large fraction of this thesis is devoted to activity of Py-Im in murine models of cancer. We investigated the pharmacokinetics and biodistribution of two compounds – targeted to 5'-WGGWCW-3' and 5'-WTWCGW-3' sequences – and characterized their activity by measuring their effects on tumor growth, gene expression *in vivo* and in tissue culture, and their effects on physiology of tumors. The initial theoretical studies suggested that a large fraction of genomic sites are bound by Py-Im polyamides non-specifically and experimental data shows that the programmed binding sequence is not a sole determinant of the patterns of gene regulation. Despite the likely presence of non-specific effects of Py-Im polyamides in living cells, *in vivo* administration of Py-Im polyamides resulted in tolerable host toxicity and anti-tumor activity. Py-Im polyamide targeted to Estrogen Receptor Response Element showed downregulation of ER-driven gene expression in tumor cells, while the compound targeted to hypoxia response element reduced vascularization of tumors and their growth rate, induced apoptosis of cells in hypoxic areas and reduced expression of proangiogenic and prometastatic factors. Further studies, showed that polyamides distributed to many of the tested tissues and their FITC-conjugates showed nuclear uptake. The gene expression effects were also present in murine tissues, such as liver and kidneys, indicating a potential for use for Py-Im polyamides in non-cancerous diseases.

TABLE OF CONTENTS

LIST OF ILLUSTRATIONS AND TABLES

C h a p t e r 1

INTRODUCTION

Background and significance

Biological systems are complex and difficult to understand. However, understanding and utilizing knowledge in biology can yield great benefits to mankind. Thanks to scientific development, fewer diseases threaten humanity than ever before, yet the ones that cause most harm represent some of the most complex scientific challenges known to date. To understand, and eventually treat, those diseases we will need methods to probe diseased cells in an understandable, programmable and consistent fashion. Many aspects of this problem can be understood with help of molecular recognition.

One of the most important interfaces in biology – the major and minor grooves in the DNA double helix – is essential for storing and reading biological information. However, it is also an attractive target for programmable molecules. The DNA has a predictable and repetitive structure where information is encoded in a single dimension – along its axis. No other biological interface represents a readable information in such simple format and is thus amenable for sequence-specific molecular recognition with relatively simple molecules. DNA-binding molecules have been known to biologists even prior to the discovery of the DNA structure (1); however, it was not until the 1960s when their major binding modes were recognized. Over the next decades, scientists recognized DNA intercalators (2), minor- and major-groove, and covalent binders (1).

Many of those molecules were tremendously useful in biological research and medicine, particularly in chemotherapy (3). One particular breakthrough made it possible to distinguish base-pairs in the minor groove of the DNA in a programmable and modular fashion using Pyrrole-Imidazole polyamides (Py-Im polyamides with affinities strong enough to displace transcription factors and modulate gene expression (4-10). The development of Py-Im polyamides sparked an area of research on the verge of biology and chemistry, where a structurally simple biological interface – the DNA double helix – could be affected through a

programmable (11), cell-permeable molecule (12, 13) with a well understood physical mode of action (4). An ability to probe cells with such molecules yields a great promise in deciphering complex biological systems and diseases, and potentially could result in rationally designed drugs for a large number of distinct diseases. However, before that is possible, more needs to be understood about the interaction of Py-Im polyamides and cells in living organisms.

The structure and function of Nucleic Acids

DNA is a biological polymer specialized in passing on the information in living organisms. It is composed from four building blocks, or nuclotides. These building blocks are largely similar: they all contain a sugar and a phosphate, but they also contain a nitrogen-containing base that varies between different nucleotides. The five carbon-sugar building nucleotides is a deoxyribose, covalently linked to a phosphate at 5' carbon through a phosphodiester bridge. Together, dexyribose and phosphate form a (14) bridge with 3' hydroxyl in another nucleotide, forming a polymer with chemical polarity. The nitrogen-containing bases (Adenine, Guanine, Cytosine and Thymine) are attached to nucleosides by 1' carbon and do not take part in formation of the DNA backbone. The nucleotides are typically described based on the base they contain (A – for adenine, G – for guanine, C – for cytosine, T – for thymine). Nucleotides in a DNA molecule, are often referred to as a 'strand' or a 'chain' of DNA. Two chains of DNA can interact through hydrophobic interactions and hydrogen bonding between their bases and thus form a double-stranded helix (15). The hydrogen bonding between bases is essential for the integrity of the double helix and the strength of that interaction depends greatly on the DNA sequence. Binding between some bases (A and T, or G and C) has a strong energetic advantage, which is described as pairing rules (Fig 1A). The strands in double helix are aligned in an anti-parallel configuration: one strand starts with a 3' hydroxyl and ends in 5' phosphate, whereas the other (complementary) strand runs in an opposite direction. The most commonly described DNA helix – in B-form – is a regular structure, with a pitch of approximately 34 angstroms, a width of approximately 20 angstroms, and a presence of minor and major grooves (Fig 1B). Other structures were found in experimental studies, although it is unclear if they are found in living cells (16). The presence of grooves exposes a fraction of the surface of nucleotides' bases, making them a plausible interface for molecular recognition of DNA.

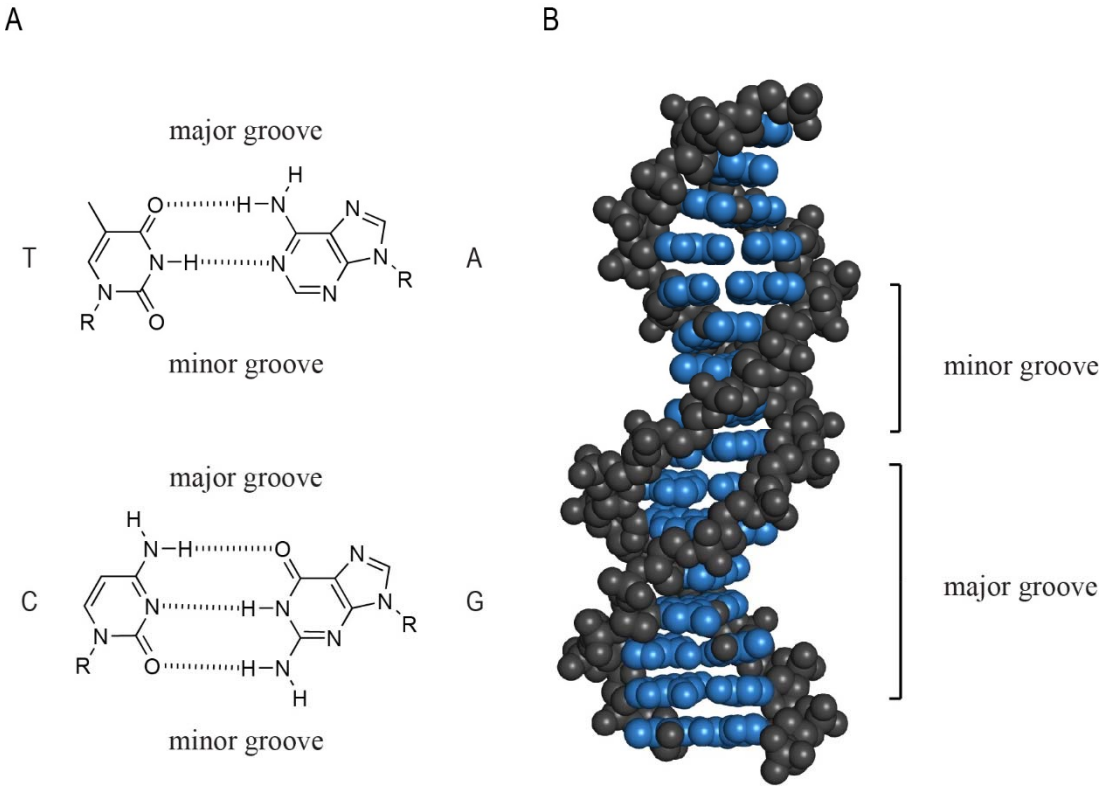

Figure 1.1 Pairing rules and the structure of DNA. A) Hydrogen bonds between bases in nucleotides gives basis to pairing rules in DNA, where Adenine (A) binds to Thymine (T), and Cytosine (C) binds to Guanine (G). B) The structure of DNA. The phosphodiester-linked sugar-phosphate backbone is colored in grey, and the Watson-Crick base pairs are depicted in blue (PDB accession code: 3BSE). Modified from Muzikar Ph.D. thesis (2011).

Molecular Recognition of DNA by minor groove binders

Properties of molecular surfaces in DNA grooves are dependent on the DNA sequence and can form a basis of sequence-specific molecular recognition. These differences are utilized by naturally occurring DNA-binding proteins, using a repertoire of interfaces (17). Most proteins bind to the major groove of DNA but minor groove binding proteins exist as well (17). Many of the DNA-binding proteins show a propensity towards binding to specific sequences – their target sites – providing control over their action throughout the genome. A particularly important class of DNA-binding proteins, transcription factors, utilize their binding sequences

to control transcription of RNA within the living cells. The presence of transcription factors allows cells to modulate production of RNA in response to external stimuli in a highly controlled manner; however, from a chemical perspective, sequence specific molecular recognition is a great challenge. Proteins utilize electrostatics, van-der Walls interactions and hydrogen bonding for sequence specific recognition. The 3-dimensional structure of the transcription factors has evolved to allow for best use of those chemical interactions, giving rise to several major classes of DNA-binding motifs (examples in Fig. 1.2) (17). Many of the transcription factors bind as monomers; however, multimeric complexes exist as well, thus allowing for binding of extended DNA sequences. Additionally, transcription factors often take part in formation of transcription complexes that include several proteins and stretch over DNA sequences longer than those that are typically bound by a single protein.

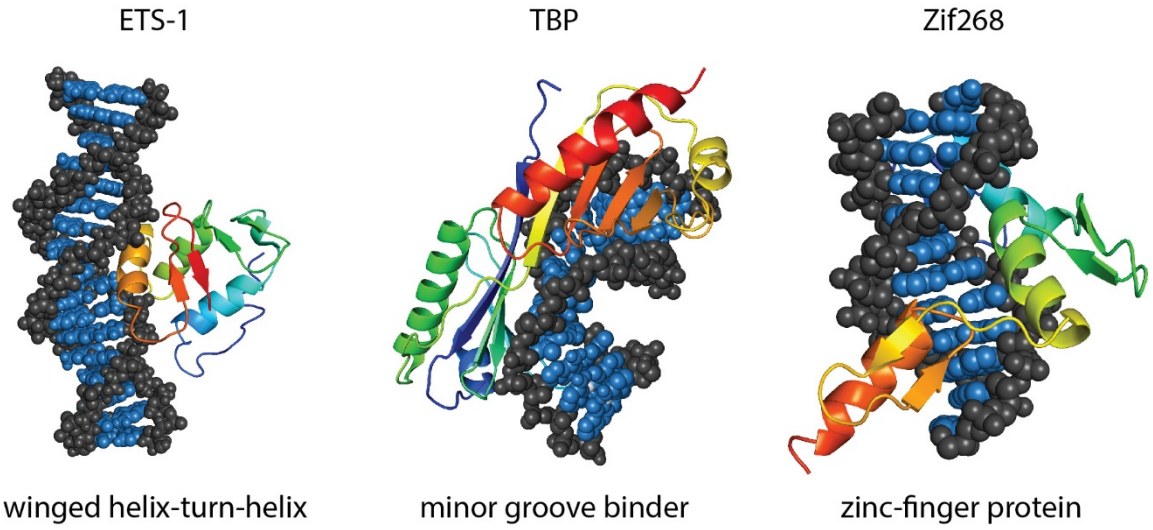

Figure 1.2 Example structure and DNA-binding motifs of three transcription factors: ETS1 (PDB: 2STW), TBP (PDB: 1TGH) and Zif268 (PDB: 1ZAA). Modified from Puckett Ph.D. thesis (2009).

In addition to DNA-binding proteins, small molecules capable of binding to DNA grooves exist as well, both in nature and chemically synthesized. The first confirmed minor groove binder was a natural product, Netropsin (18-20). Soon afterwards, a structure of Distamycin was solved (21) and a few years later a new binding mode was discovered – one where two molecules of Distamycin bind to a single minor groove (2:1 binding) (22, 23). Advances in the field of small-

molecule minor grooves inspired development of sequence-specific, heterocycles (Pyrrole-Imidazole polyamides) that were capable of binding a large repertoire of DNA sequences with affinities and specificities comparable to transcription factors (4, 24). Utilizing a structure similar to Distamycin A, oligomers containing Pyrrolle (Py) and Imidazole (Im) linked through an amide bond were developed to recognize both A:T and G:C basepairs in DNA. While a pyrrole-containing distamycin binds A:T rich sequences, the recognition of G:C was posited to be achieved using an amine in N-methylpyrrole's interacting with exoclyclic amine in guanine base (Fig. 1.3). Footprinting experiments proved that a developed Py-Im polyamide bound a predicted DNA sequence (5'-WGWCW-3'), was capable of recognizing G:C pairs, and bound in 2:1 binding mode previously seen for Distamycin A (25). Subsequent studies led to development of Py-Im polyamides of additional monomers including 3-Chlorothiophene (Ct) (26) and N-methyl-3-hydroxypyrrole (Hp) (27), both distinguishing A:T from T:A pairs. Consequently, the Py-Im polyamides became the first small molecule minor groove binder capable of distinguishing four naturally occurring Watson-Crick base pairs (27). Several methods of linking linear Py-Im polyamides were developed to increase binding affinity (28-31). The design most commonly used today is a 'hairpin' (31) polyamide where a γ-aminobutyric acid derivative ('turn' monomer) links carboxylic terminus of a Py-Im oligomer with the amino terminus of another (Fig. 1.3, bottom panel; (32)). Further improvement in binding affinity is achieved by using a chiral 2,4-diaminobutyric, or 3,4-diaminobutyric acid as a 'turn' monomer ((33, 34)). Resultant affinities for hairpin polyamides vary between low-nanomolar to sub-nanomolar (11). The GBA derivatives used confer an energetic advantage in binding to A:T, over G:C pairs (33), thus taking an activate part in DNA sequence recognition. The increased binding affinity upon inclusion of a charged amino in the 'turn' monomer is a credit to both the electrostatic interaction of the positive charge in amine and the DNA backbone and improved alignment of the Py and Im residues (31, 33-35). The alignment can be additionally improved by introduction of a structurally flexible b-alanine residue, which helps to match the curvature of Py-Im polyamide molecules with the one of DNA and targets A:T and T:A residues (36). The final structural feature of a hairpin polyamide used today is the inclusion of a 'tail' monomer on the C-terminus (typically 3,3'-diamino-N-methyl-dipropylamine) which targets T:A and A:T residues (12, 37).

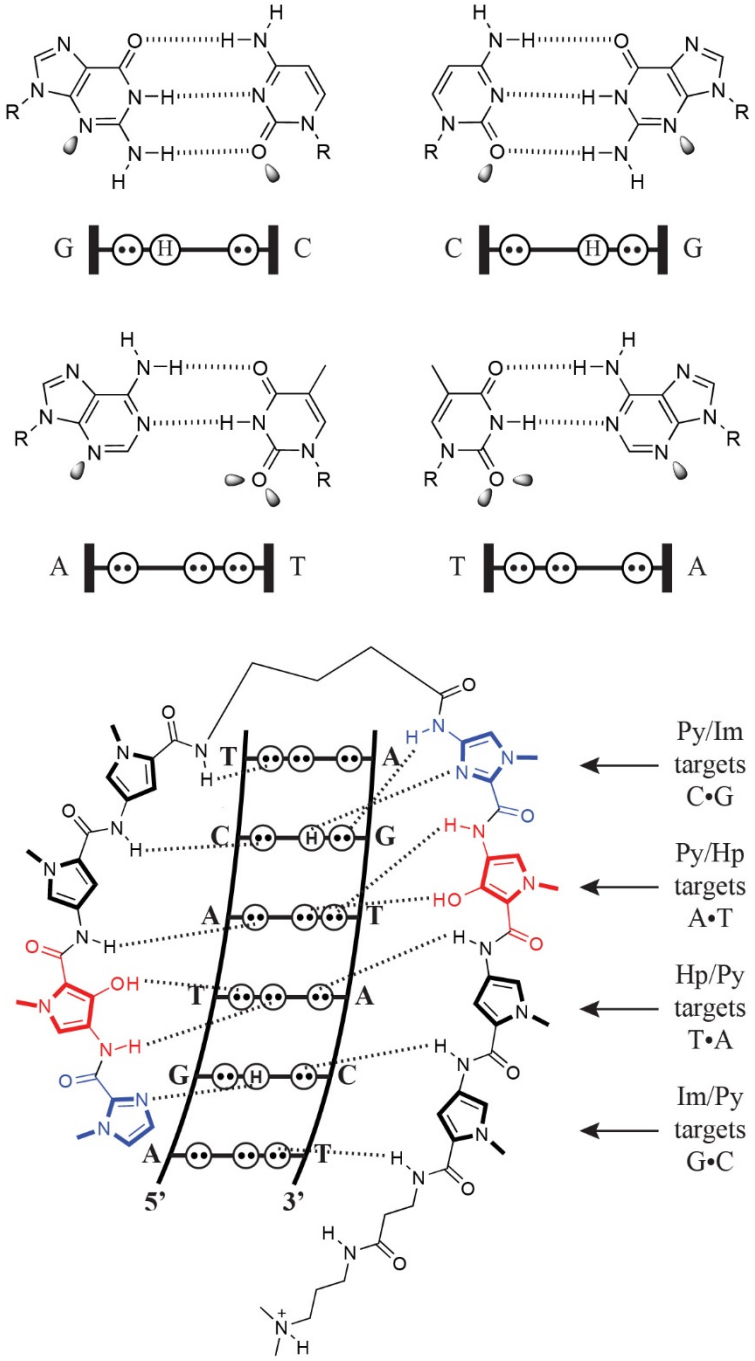

Figure 1.3 Molecular recognition of DNA minor groove by a hairpin Py-Im polyamide. (a) Hydrogen-bonding patterns in Watson-Crick base pairs with depicted lone pairs and hydrogens. Circles with dots represent electron lone pairs N(3) of purines and O(2) of pyrimidines, while H in circle represents the 2-amino group of guanine. Shaded orbitals represent lone pairs projecting into the minor groove. (b) Dashed lines represent hydrogen bonding in a complex between ImHpPyPyg-ImHpPyPy-b-Dp and a 5'-TGTACA-3' sequence(4).

Modulating gene expression with Py-Im polyamides

Hairpin Py-Im polyamides have been used to regulate gene expression in tissue culture. While the exact mechanism of gene regulation is unclear, previous *in vitro* and tissue culture experiments suggest displacement of transcription factors from DNA is one of the candidates, with possibly other effects playing a role. Hallmark experiments in our group have indicated that Py-Im polyamides are capable of displacing transcription factors in gel shift assays (9, 10, 38-42) and change their occupancy in promoters in the tissue culture setting (5, 8, 9, 39, 43). Regardless of the mechanism, Py-Im polyamides might prove useful in both research and treatment of diseases if they are capable of regulating expression of genes important for pathogenesis. The first example of gene regulation in vivo was performed in xenografts derived from A549 cells, and treated with a hairpin compound targeted to 5'-WGGWWW-3' DNA sequence (7). Soon after, Py-Im mediated gene expression modulation of Estrogen-Receptor driven reporter (6), genes related in angiogenesis and metastasis (unpublished), and tumor growth inhibition (unpublished, (43, 44)) were shown in our group. Further investigations showed possible mechanisms of polyamide-induced toxicity on cellular level (43, 45). In this work we set out to describe the anti-tumor effects of Py-Im polyamides on the organism and tissue levels.

Py-Im polyamides in treatment of disease

Transcription factors are involved in both homeostatic gene regulation and in pathogenesis of various diseases. While cancer is perhaps the most well-known example of a disease arising due to dysregulation of cellular signaling and gene expression (46), changes in activity of transcription factors is a hallmark of other diseases as well. In a research setting, Py-Im polyamides were used to inhibit function of viral proteins (41, 47), treat renal failure (48, 49), alleviate a fatty liver disease in animal models (unpublished) and notably – to inhibit growth of tumors (unpublished, (43, 44)) and reduce cancer cell invasion (50). This work focuses mainly on two of the transcription factors: Estrogen Receptor (ER), involved in progression of breast and uterine cancers, and Hypoxia-Inducible-Factor-1 (HIF-1), which plays a role in pathogenesis of diseases including many cancers, tissue fibrosis, chronic heart disease, and age-related macular degeneration (51). The first *in vivo* studies in our laboratory have shown that Py-Im polyamides can be used in living organisms with tolerable toxicity and measurable efficacy (6, 7, 44, 52, 53).

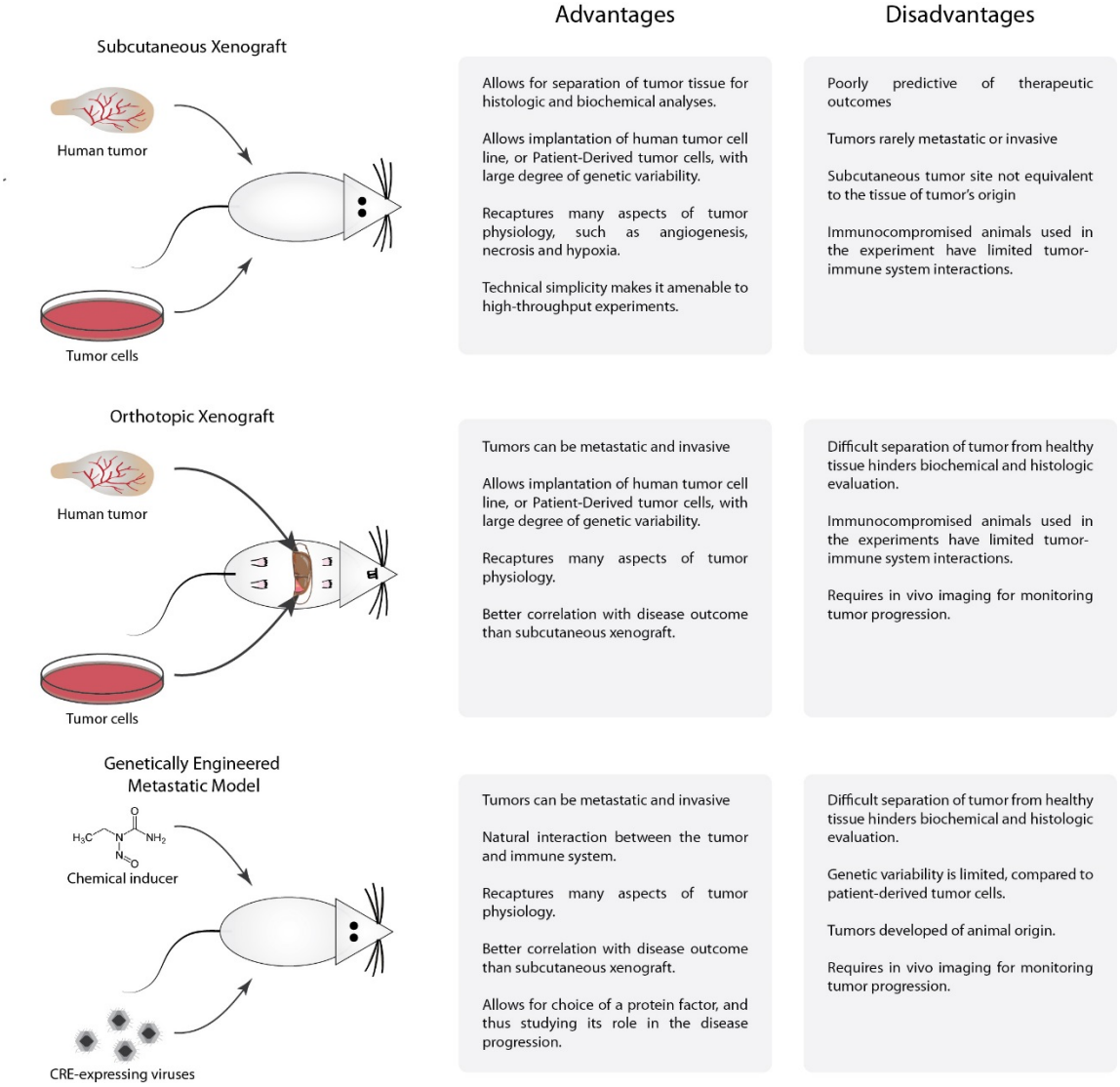

Figure 1.4. Commonly used murine cancer models: subcutaneous and orthotopic xenografts and genetically engineered models.

However, determining mechanism of action and efficacy of new compounds is a challenge. Before clinical trials, researchers typically employ use of animal models, with organisms including mice, rats, dogs, and non-human primates (54). Among them, the mice are likely the most common model organism, due to their small size and small associated research costs. There are three main classes of animal models in cancers: subcutaneous xenografts, orthotopic xenografts and genetically engineered metastatic models (GEMM) (55, 56). Each of these models has pros and cons. The subcutaneous xenograft is among the simplest of the animal models of disease.

In this model, cancer cells are implanted into a subcutaneous cavity of an immunocompromised animal using an injection of cells, with, or without an exogenous extracellular matrix (ECM), such as matrigel. This allows for a clear delineation of tumor tissue and thus a definitive histologic, biochemical, and anatomic analysis. These features make a subcutaneous xenograft a good model in understanding molecular and histologic principles behind the drug action. Another advantage of using a xenograft is an ability to implant cells derived from a human tumor along with the molecular characteristics typical of human tumors. Finally, unlike for GEMM, the results can be obtained within weeks, instead of months or even years. The disadvantages include: a relatively poor correlation in drug efficacy between a subcutaneous xenograft and human cancers, lack of metastasis in most engrafted cell lines and lack of a fully functional immune system in immunocompromised mice (54, 55). Another commonly used model of cancer – orthotopic xenograft – includes implantation of cancer cells into a mouse tissue from which the cancer cells were originally derived. This method shares many of the advantages of subcutaneous xenografts – rapid tumor growth and the ability to implant patient-derived tumor cells. Additional advantages, include a more common presence of metastasis and better correlation of drug efficacy with human disease when compared to subcutaneous xenografts (55, 57). However, the physical separation of a tumor tissue in an orthotopic xenograft is problematic, making the histologic and biochemical analyses more difficult, while tracking the disease progress requires medical imaging.

Finally, the Genetically Engineered Metastatic Models (GEMM), where an organism, typically a mouse, is genetically modified such that factors involved in cancer progression are mutated, or over- or underexpressed. These changes can be chemically induced, or can be constitutively present in mice, depending on the specific model. The genetic changes lead to increased rate of cancers that can be then studied and treated in preclinical setting. This method has many advantages: in some cases the therapeutic response in this model correlates well with responses seen in patients (58-60). It also allows for studying development of the disease with a competent immune system present and these models are, by definition, metastatic. Finally, an ability to choose a factor to be mutated allows for studying its role in tumor progression. The disadvantages are unfortunately present as well: while the mutations can be chosen to mimic human tumors, they might not fully represent the complexity and heterogeneity of the molecular

changes found in human tumors. Additionally, since the tumors obtained in GEMM are of mouse origin, and not human, and drug response might not correlate directly in a clinical setting (55).

Overall, initial studies with Py-Im polyamides are done in a subcutaneous tumor setting, due to the mechanistic nature of our investigations. However, future studies will likely focus on more advanced disease models, in order to understand the potential of Py-Im polyamides in the treatment of disease.

Scope of this work

This work aims at connecting the molecular mechanism of action of Py-Im polyamides and their action to the tissue- and organism levels. In Chapter 2 of this thesis, selectivity of polyamide in tissue culture is presented, and the limits of selectivity discussed. Chapter 3 extends the idea of Py-Im polyamide's functional selectivity and describes genomic and *in vivo* effects of a Py-Im polyamide targeted to Estrogen Receptor Elements (ERE). Chapter 4 delves into the details of polyamide biodistribution and describes the relationship between the tissue uptake of compounds and the tumor type, vasculature, and experimental methodology. Application of this knowledge is presented in Chapter 5. The text of this chapter links biological effects of Py-Im polyamide treatment to changes at molecular and tissue level. It shows that action of a polyamide targeted to Hypoxia Responsive Element (HRE) induces molecular changes in tumors that are consistent with its proposed mechanism of action: interference with hypoxic gene expression. This chapter also shows a potent anti-tumor and anti-angiogenic effects of the anti-HRE polyamide in two different cell lines. In Chapter 6, the anti-tumor effects and the inhibition of hypoxic gene expression by anti-HIF Py-Im polyamide are reinforced in another model of cancer: multiple myeloma xenografts. We explain the effects of polyamide treatment on protein expression, hypoxia-induced apoptosis and tumor growth of multiple myeloma xenografts in two different models: subcutaneous tumor and orthotopic. The final chapter links the described studies and describes possible future directions and potential utility in using polyamides for treatment in non-cancerous diseases.

References

1. Demeunynck M, Bailly C, & Wilson WD (2003) *Small molecule DNA and RNA binders : from synthesis to nucleic acid complexes* (Wiley-VCH, Weinheim).
2. Lerman LS (1961) Structural considerations in the interaction of DNA and acridines. *J Mol Biol* 3:18-30.
3. Airley R (2009) *Cancer Chemotherapy: Basic Science to the Clinic* (Wiley).
4. Dervan PB & Edelson BS (2003) Recognition of the DNA minor groove by pyrrole-imidazole polyamides. *Curr Opin Struct Biol* 13(3):284-299.
5. Nickols NG, Jacobs CS, Farkas ME, & Dervan PB (2007) Modulating hypoxia-inducible transcription by disrupting the HIF-1-DNA interface. *ACS Chem Biol* 2(8):561-571.
6. Nickols NG*, et al.* (2013) Activity of a Py-Im polyamide targeted to the estrogen response element. *Mol Cancer Ther* 12(5):675-684.
7. Raskatov JA*, et al.* (2012) Gene expression changes in a tumor xenograft by a pyrrole-imidazole polyamide. *Proc Natl Acad Sci U S A* 109(40):16041-16045.
8. Raskatov JA*, et al.* (2012) Modulation of NF-kappaB-dependent gene transcription using programmable DNA minor groove binders. *Proc Natl Acad Sci U S A* 109(4):1023-1028.
9. Nickols NG & Dervan PB (2007) Suppression of androgen receptor-mediated gene expression by a sequence-specific DNA-binding polyamide. *Proc Natl Acad Sci U S A* 104(25):10418-10423.
10. Olenyuk BZ*, et al.* (2004) Inhibition of vascular endothelial growth factor with a sequence-specific hypoxia response element antagonist. *Proc Natl Acad Sci U S A* 101(48):16768-16773.
11. Hsu CF*, et al.* (2007) Completion of a Programmable DNA-Binding Small Molecule Library. *Tetrahedron* 63(27):6146-6151.
12. Best TP, Edelson BS, Nickols NG, & Dervan PB (2003) Nuclear localization of pyrrole-imidazole polyamide-fluorescein conjugates in cell culture. *Proc Natl Acad Sci U S A* 100(21):12063-12068.
13. Nickols NG, Jacobs CS, Farkas ME, & Dervan PB (2007) Improved nuclear localization of DNA-binding polyamides. *Nucleic Acids Res* 35(2):363-370.
14. White S, Baird EE, & Dervan PB (1997) On the pairing rules for recognition in the minor groove of DNA by pyrrole-imidazole polyamides. *Chem Biol* 4(8):569-578.
15. Watson JD & Crick FH (1953) The structure of DNA. *Cold Spring Harb Symp Quant Biol* 18:123-131.
16. Brown TA (2007) *Genomes 3* (Garland Science Pub., New York) 3rd Ed pp xxii, 713 p.
17. Brändén CI & Tooze J (1999) *Introduction to Protein Structure* (Garland Pub.).
18. Kopka ML, Yoon C, Goodsell D, Pjura P, & Dickerson RE (1985) The molecular origin of DNA-drug specificity in netropsin and distamycin. *Proc Natl Acad Sci U S A* 82(5):1376-1380.
19. Kopka ML, Yoon C, Goodsell D, Pjura P, & Dickerson RE (1985) Binding of an antitumor drug to DNA, Netropsin and C-G-C-G-A-A-T-T-BrC-G-C-G. *J Mol Biol* 183(4):553-563.
20. Dickerson RE & Kopka ML (1985) Nuclear Overhauser data and stereochemical considerations suggest that netropsin binds symmetrically within the minor groove of poly(dA).poly(dT), forming hydrogen bonds with both strands of the double helix. *J Biomol Struct Dyn* 3(3):423-431.
21. Coll M, Frederick CA, Wang AH, & Rich A (1987) A bifurcated hydrogen-bonded conformation in the d(A.T) base pairs of the DNA dodecamer d(CGCAAATTTGCG) and its complex with distamycin. *Proc Natl Acad Sci U S A* 84(23):8385-8389.

22. Chen X, Ramakrishnan B, Rao ST, & Sundaralingam M (1994) Binding of two distamycin A molecules in the minor groove of an alternating B-DNA duplex. *Nat Struct Biol* 1(3):169-175.
23. Pelton JG & Wemmer DE (1989) Structural characterization of a 2:1 distamycin A.d(CGCAAATTGGC) complex by two-dimensional NMR. *Proc Natl Acad Sci U S A* 86(15):5723-5727.
24. Dervan PB (2001) Molecular recognition of DNA by small molecules. *Bioorg Med Chem* 9(9):2215-2235.
25. Mrksich M*, et al.* (1992) Antiparallel side-by-side dimeric motif for sequence-specific recognition in the minor groove of DNA by the designed peptide 1-methylimidazole-2-carboxamide netropsin. *Proc Natl Acad Sci U S A* 89(16):7586-7590.
26. Foister S, Marques MA, Doss RM, & Dervan PB (2003) Shape selective recognition of T.A base pairs by hairpin polyamides containing N-terminal 3-methoxy (and 3-chloro) thiophene residues. *Bioorg Med Chem* 11(20):4333-4340.
27. White S, Szewczyk JW, Turner JM, Baird EE, & Dervan PB (1998) Recognition of the four Watson-Crick base pairs in the DNA minor groove by synthetic ligands. *Nature* 391(6666):468-471.
28. Heckel A & Dervan PB (2003) U-pin polyamide motif for recognition of the DNA minor groove. *Chemistry-a European Journal* 9(14):3353-3366.
29. Melander C, Herman DM, & Dervan PB (2000) Discrimination of A/T sequences in the minor groove of DNA within a cyclic polyamide motif. *Chemistry-a European Journal* 6(24):4487-4497.
30. Greenberg WA, Baird EE, & Dervan PB (1998) A comparison of H-pin and hairpin polyamide motifs for the recognition of the minor groove of DNA. *Chemistry-a European Journal* 4(5):796-805.
31. Mrksich M, Parks ME, & Dervan PB (1994) Hairpin Peptide Motif. A New Class of Oligopeptides for Sequence-Specific Recognition in the Minor Groove of Double-Helical DNA. *Journal of the American Chemical Society* 116(18):7983-7988.
32. Trauger JW, Baird EE, & Dervan PB (1996) Extended hairpin polyamide motif for sequence-specific recognition in the minor groove of DNA. *Chemistry & Biology* 3(5):369-377.
33. Herman DM, Baird EE, & Dervan PB (1998) Stereochemical control of the DNA binding affinity, sequence specificity, and orientation preference of chiral hairpin polyamides in the minor groove. *Journal of the American Chemical Society* 120(7):1382-1391.
34. Dose C, Farkas ME, Chenoweth DM, & Dervan PB (2008) Next generation hairpin polyamides with (R)-3,4-diaminobutyric acid turn unit. *Journal of the American Chemical Society* 130(21):6859-6866.
35. Farkas ME, Tsai SM, & Dervan PB (2007) alpha-diaminobutyric acid-linked hairpin polyamides. *Bioorganic & Medicinal Chemistry* 15(22):6927-6936.
36. Turner JM, Swalley SE, Baird EE, & Dervan PB (1998) Aliphatic/aromatic amino acid pairings for polyamide recognition in the minor groove of DNA. *Journal of the American Chemical Society* 120(25):6219-6226.
37. Belitsky JM, Nguyen DH, Wurtz NR, & Dervan PB (2002) Solid-phase synthesis of DNA binding polyamides on oxime resin. *Bioorg Med Chem* 10(8):2767-2774.
38. Zhang Y*, et al.* (2011) Targeting a DNA binding motif of the EVI1 protein by a pyrrole-imidazole polyamide. *Biochemistry* 50(48):10431-10441.
39. Muzikar KA, Nickols NG, & Dervan PB (2009) Repression of DNA-binding dependent glucocorticoid receptor-mediated gene expression. *Proc Natl Acad Sci U S A* 106(39):16598-16603.

40. Gearhart MD*, et al.* (2005) Inhibition of DNA binding by human estrogen-related receptor 2 and estrogen receptor alpha with minor groove binding polyamides. *Biochemistry* 44(11):4196-4203.
41. Coull JJ*, et al.* (2002) Targeted derepression of the human immunodeficiency virus type 1 long terminal repeat by pyrrole-imidazole polyamides. *J Virol* 76(23):12349-12354.
42. Chiang SY*, et al.* (2000) Targeting the ets binding site of the HER2/neu promoter with pyrrole-imidazole polyamides. *J Biol Chem* 275(32):24246-24254.
43. Yang F*, et al.* (2013) Antitumor activity of a pyrrole-imidazole polyamide. *Proc Natl Acad Sci U S A* 110(5):1863-1868.
44. Yang F*, et al.* (2013) Animal toxicity of hairpin pyrrole-imidazole polyamides varies with the turn unit. *J Med Chem* 56(18):7449-7457.
45. Martinez TF*, et al.* (2014) Replication stress by Py-Im polyamides induces a non-canonical ATR-dependent checkpoint response. *Nucleic Acids Res* 42(18):11546-11559.
46. Hanahan D & Weinberg RA (2011) Hallmarks of cancer: the next generation. *Cell* 144(5):646-674.
47. Yang F, Belitsky JM, Villanueva RA, Dervan PB, & Roth MJ (2003) Inhibition of Moloney murine leukemia virus integration using polyamides targeting the long-terminal repeat sequences. *Biochemistry* 42(20):6249-6258.
48. Kajiwara M*, et al.* (2012) Development of pyrrole-imidazole polyamide targeting fc receptor common gamma chain for the treatment of immune-complex related renal disease. *Biol Pharm Bull* 35(11):2028-2035.
49. Matsuda H*, et al.* (2011) Transcriptional inhibition of progressive renal disease by gene silencing pyrrole-imidazole polyamide targeting of the transforming growth factor-beta1 promoter. *Kidney Int* 79(1):46-56.
50. Sato A*, et al.* (2013) Inhibition of MMP-9 using a pyrrole-imidazole polyamide reduces cell invasion in renal cell carcinoma. *Int J Oncol* 43(5):1441-1446.
51. Semenza GL (2014) Oxygen sensing, hypoxia-inducible factors, and disease pathophysiology. *Annu Rev Pathol* 9:47-71.
52. Synold TW*, et al.* (2012) Single-dose pharmacokinetic and toxicity analysis of pyrrole-imidazole polyamides in mice. *Cancer Chemother Pharmacol* 70(4):617-625.
53. Raskatov JA, Hargrove AE, So AY, & Dervan PB (2012) Pharmacokinetics of Py-Im polyamides depend on architecture: cyclic versus linear. *J Am Chem Soc* 134(18):7995-7999.
54. Teicher BA (2010) *Tumor Models in Cancer Research* (Humana Press).
55. Richmond A & Su Y (2008) Mouse xenograft models vs GEM models for human cancer therapeutics. *Dis Model Mech* 1(2-3):78-82.
56. de Jong M, Essers J, & van Weerden WM (2014) Imaging preclinical tumour models: improving translational power. *Nat Rev Cancer* 14(7):481-493.
57. Kerbel RS (2003) Human tumor xenografts as predictive preclinical models for anticancer drug activity in humans: better than commonly perceived-but they can be improved. *Cancer Biol Ther* 2(4 Suppl 1):S134-139.
58. Combest AJ*, et al.* (2012) Genetically Engineered Cancer Models, But Not Xenografts, Faithfully Predict Anticancer Drug Exposure in Melanoma Tumors. *Oncologist* 17(10):1303-1316.
59. Becher OJ & Holland EC (2006) Genetically engineered models have advantages over xenografts for preclinical studies. *Cancer Res* 66(7):3355-3358, discussion 3358-3359.
60. Roper J & Hung KE (2012) Priceless GEMMs: genetically engineered mouse models for colorectal cancer drug development. *Trends Pharmacol Sci* 33(8):449-455.

Chapter 2

SELECTIVITY OF PY-IM POLYAMIDES IN TISSUE CULTURE

ABSTRACT

Py-Im polyamides have excellent sequence specificity *in vitro*, yet little is known about their selectivity in the nuclei of mammalian cells. In this chapter the extent of the functional selectivity of polyamides is assessed in regulation of gene expression in Glucocorticoid signaling. First, mathematical modeling was used to find the most common GRE sequences that can be bound with 8-ring hairpin polyamides. Then a panel of 12 genes and a focused library of polyamides targeting 7 DNA different sequences was used in evaluation of polyamides as a tool for linking sequence of a response element with the gene it controls. Concurrent nuclear localization studies and in-vitro assessment of DNA binding affinity were performed on the library of polyamides to connect chemical properties of polyamides with their gene regulation patterns. Polyamides show a small degree of selectivity; however, the differences are hard to elucidate because of the low potency of some of the compounds. The potent compounds, on the other hand, show few differences in gene expression patterns. Further steps will need to be taken to increase polyamide specificity, without sacrificing potency; in particular more genes may need to tested, e.g. by using RNA-sequencing. Another possibility is using multiple compounds to target the same regulatory sequence and thus increase the specificity of Py-Im polyamides in tissue culture.

Introduction

Binding of Py-Im polyamides to DNA is sequence-specific (1, 2). While in vitro experiments have shown that a single sequence can be targeted, achieving site-specificity in a mammalian cell nucleus is a significantly more challenging task. The main problem in sequence specificity in mammalian cells is the sheer amount genetic material enclosed in the nucleus. For example, DNA in human cells contains $3x10^9$ base pairs, and a 6-base pair sequence would be expect to occur once in every 4^6 bases, assuming every base pair can be recognized. The typically used Py-Im polyamides, however, only recognize between 3 different base pairs, G, C, and W, which means an average frequency of the DNA sequence bound specifically by an 8-ring Py-Im polyamide is expected to be once in every 3^6 basepairs, an equivalent 4.1 million matched binding sites for an average Py-Im polyamide. Another factor present in mammalian cells, but not *in vitro,* is accessibility of DNA in the nucleus. Not every site in the genomic DNA is equally accessible; some of the DNA is densely packed as heterochromatin. It is currently unclear how the binding properties of polyamides change depending on the density of DNA-packing in the nuclei; however, we do know that Py-Im polyamides are capable of binding to nucleosomes (3). Finally, the time of dissociation of a commonly use hairpin polyamide and DNA match site is long ($k_{off} = 10^{-3} – 10^{-4}$ s^{-1}), half the time of dissociation which ranges from minutes to hours (4), which limits diffusion of polyamides within the nucleus. Thus, sequences most frequently bound by Py-Im polyamides might simply be those that are most accessible thanks to diffusion, or DNA packing. Recent experiments evaluated some aspects of the selectivity of Py-Im polyamides in the genome, showing that sequence-specificity might be just one factor in their genomic-DNA binding profile and the chromatin accessibility may also be important (5). In this chapter we investigated the selectivity of Py-Im polyamides in living cells, by testing the expression of a number of genes related to Glucocorticoid Receptor (GR) in the A549 cell line. We also built theoretical kinetic models of DNA-polyamide binding and calculated possible sequence specificities of Py-Im polyamides within the genome.

Background

Mammalian genes are regulated thanks to a complex network of transcription factors (6) and proteins regulating chromatin accessibility (7, 8). How transcription factors bind and control

gene expression is one of the main questions in molecular biology. Investigating the DNA sequence binding to transcription factors historically has been done through DNA-sequencing of the purified DNA bound to transcription factors (9), and subsequently by Electrophoretic Mobility Shift Assay (EMSA) (10) and DNAseI footprinting (11). These methods allowed for study of a single transcription factor binding site at a time. As a result they yielded information about binding affinity between a transcription factor and a DNA sequence, but failed to inform us about the genomic frequency and positions of these sites. It was not until the advent of high throughput genome sequencing and microarray technology that we were able to do this. Currently the most common method of determining transcription factor binding sites is Chromatin Immunoprecipitation followed by sequencing (12) (Chip-Seq), which can inform us about the position of both genes and transcription factor binding sites in the whole genome. Regrettably this method is incapable of establishing a functional link between the transcription factor sites and the genes they control. While in prokaryotes the transcription factors bind proximally to the genes, in mammalian cells this is not always the case (13, 14).

Large distance between regulatory sequences and their gene targets poses a challenging problem in identifying a functional link between them. Currently there are three Chromosome Conformation capture (3C, 4C, 5C) methods that allow one to connect the particular regulatory element with a particular gene (15-17), however the execution of these assays is often complicated (18, 19). Additionally no other method exists that could confirm the findings, and suggested problems with these methods remain untested (18). Consequently, as of now, reliably matching a transcription binding site to the gene it controls requires knocking out the regulatory sequence in cells. Unfortunately, this method requires prior knowledge of both the gene and its' regulatory sequence and many genes are controlled by multiple regulatory sequences. Because of those issues, targeted knockdown is unsuitable for genome-wide mapping. Pyrrole-Imidazole polyamides could be useful in relating regulatory DNA sequences with the gene expression patterns in a high throughput fashion.

Py-Im polyamides bind the minor groove in double-stranded DNA with affinities and specificities comparable to transcription factors. It has been achieved by combining aromatic amino acids, N-methylpyrroles (Py), N-methylimidazoles (Im), and 3-hydroxy-1-methylpyrroles

(Hp), in a short oligomer. A pair of monomers placed over each other in a minor groove can determine pairing rules between polyamides and DNA. According to those rules a Py/Im pair will recognize a C°G pair, Im/Py a G°C, wherease Py°Py pair will be capable of recognizing W°W pairs. Including a hydroxypyrrole instead of a pyrrole will bias binding of a polyamide towards T°A in the case of a Hp/Py pair and A°T in the case of a Py/Hp (1, 20) (Figs. 1.2 and 1.3). Their capability of sequence specific displacement of transcription factors from their binding sites results in an inhibition of gene expression establishing a functional link between regulatory sequences and the genes they control. However, the question that needs to be answered is whether their sequence specificity is high enough for sequence-specific gene regulation in a large mammalian genome.

Glucocorticoid receptor (GR) response pathway is a common model system for gene expression regulation in mammalian cells (7, 14). GR is a cell permeable steroid receptor binding directly (21) to a well-defined Glucocorticoid Response Element (GRE) (Fig. 2.1). There are several thousand GREs scattered across the mammalian genome implicated in gene regulation (14), each containing three highly degenerate nucleotides at positions 7,8, and 9 (Fig. 2.1B,C). These three nucleotides alone constitute 64 distinct classes of GREs that can be targeted with sequence-matched pyrrole-imidazole polyamides developed in our lab. Additionally, the other bases also show sequence variability that can be utilized for that purpose. In an observed case of one GRE driven gene (GILZ) displacement of transcription factors through polyamides results in an inhibited gene expression (22), and if that will be the case with other GRE controlled genes, we will be able to match classes of GREs to the genes they control.

Glucocorticoid receptor pathway is a useful drug target. Glucocorticoids are widely used in medicine as immunosuppresants and are some of the most potent anti-inflammatory drugs on the market (23). These effects, however, come at a price. Glucocorticoids have significant side effects, such as bone and muscle loss, psychoses, cataract and glaucoma, among many others (23). In children, prolonged use of glucocorticoids may negatively affect bone development (24). Many of those side effects, e.g. glaucoma or diabetes, are mediated through transactivation, or expression of anti-inflammatory proteins. This fact has galvanized the development of more selective glucocorticoid receptor agonists (SEGRas) which aim at decreasing transactivation

without affecting transrepression. One SEGRA (ZK 216348) has shown in animal models that the negative side effects of glucocorticoid treatment can be reduced while maintaining anti-inflammatory effects (23).

Likewise, polyamide are effective in downregulation of gene expression. While the majority of side effects of glucocorticoid treatment are due to transactivation, some of them are not. Thus targeting different sequences within GREs by polyamides administered along with standard glucocorticoids can fine-tune the effects of this anti-inflammatory treatment to minimize the side effects and maximize potency for the specific disease.

Evaluation of the genomic landscape of the GREs and polyamide binding sites

Chromatin Immunoprecipitation followed by sequencing (Chip-Seq) identified 4392 loci in the genome that are occupied by GR in human lung adenocarcinoma cells (A549) (14). The positions of these loci are, however, distant from 234 genes that are highly induced upon treatment with 100nM Dexamethasone (Dex), a synthetic agonist of GR. For genes with Dex induced expression, the median distance between the nearest GRE and a transcription start site (TSS) was 11kb, and those genes that were repressed had a median distance of 146 kb (14). The large TSS-GRE distance and its significant variability suggests that one cannot predict which genes are controlled by which GREs based solely on their relative position. The response of the genes also varies in time; particularly repressed genes are affected later in time than induced ones. This and the large distance between nearest GREs suggest that repressed genes are not controlled by promoter-proximal GR binding.

In order to further analyze the dependence of position of GREs and transcription start, I wrote a simple mathematical model assuming their random distribution. For downregulated genes, I generated random locations for both TSS and GREs and then measured their distance in the aproximately 2.1×10^9 basepairs in non-repetitive parts of the human genome (25). Even this crude estimate of the genome size and a very basic model gives a median nearest neighbour distance between TSS and GREs of 164kb, as compared to 146kb in Chip-Seq study (14). This result suggests that the position of GREs and the genes they repress are independent of each other. In this case a common assumption that the gene is controlled by its nearest neighbour is

most likely unfeasible, further suggesting that repressed genes are controlled independent of proximal GRE-promoter binding. The activated genes, on the other hand, show dependence of the position of GREs and TSSes.

I modeled their relative positions by generating set of gene positions and a random distribution of distances (GRE positions) over the mean length of a chromosome (123kb). It appears that the median distance between a TSS and the nearest neighbor (10.7 kb), assuming their random distribution, once again is very close to 11kb, as found by Chip-seq (14). The distribution of distances as modeled also matches the Chip-Seq data (Fig. 2.2). This result suggests that distance between GREs and genes they control may be distributed randomly within the chromosome. This model further supports current belief that Glucocorticoid Receptor signaling occurs through an exceptionally long range interactions (14). The code and parameters used in writing the models can be found in appendix G. Such quantitative considerations show that one cannot assume that a position of a GRE relative to TSS can predict a functional link between the two and Chromosome Conformation Capture methods maybe be necessary to establish such a link.

In order to make an informed decision on which compounds should be synthesized to exert a specific control of gene expression in A549 cells, I analyzed the GR binding sites for enrichment upon Dex induction in Chip-Seq data set from Myers lab (14). If a rare sequence is targeted with a polyamide, it is unlikely that a large number of genes will respond to it. If, on the other hand, a compound binds a wide array of sequences a larger fraction of genes in a panel is expected to be downregulated. In order to establish which sequences are most common among active GREs, I chose to computationally analyze the genome-wide occurence of sequences compatible with DNA-binding profiles of 8-ring hairpin polyamides.

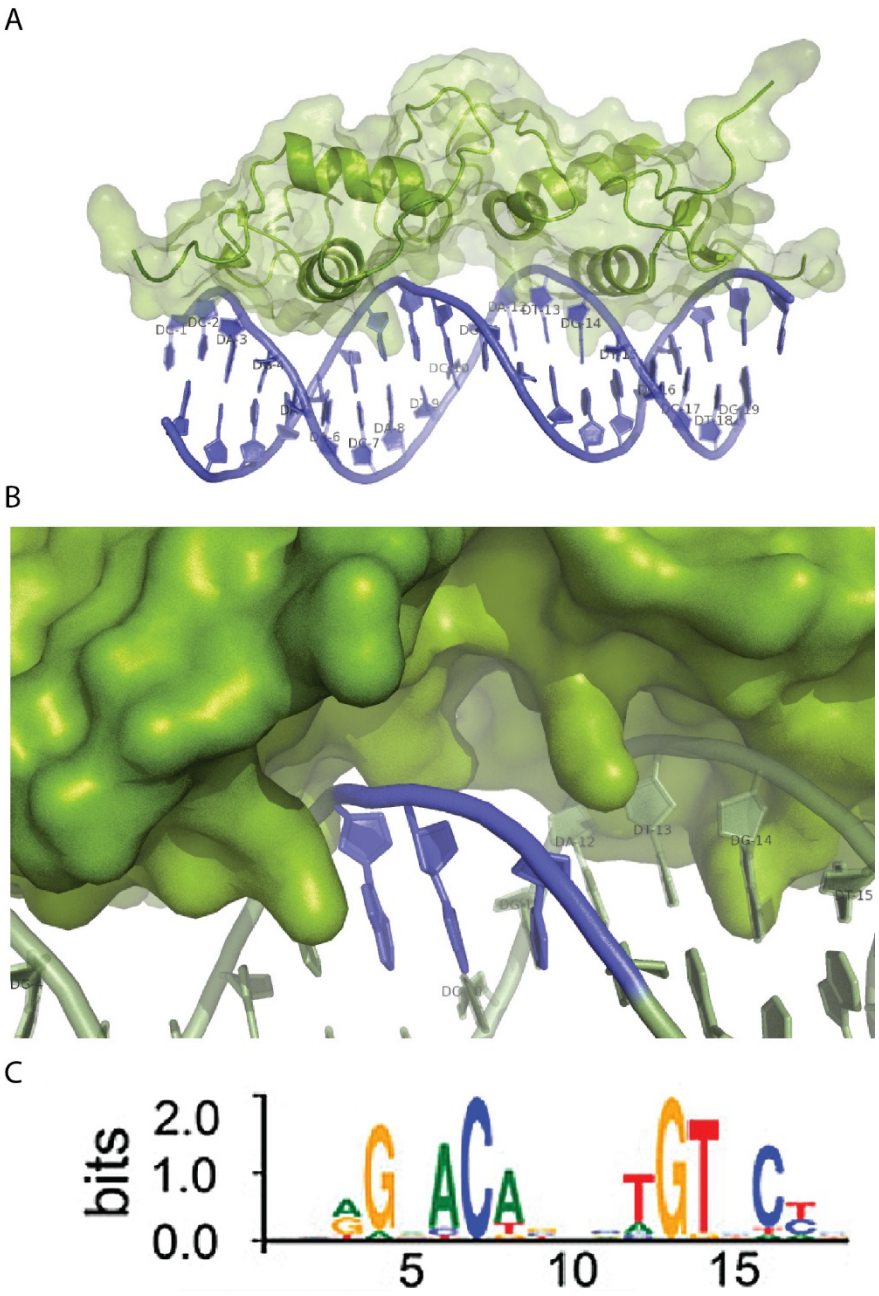

Figure 2.1 X-ray crystal structure of a Glucocorticoid Receptor (GR) bound to DNA (PDB 1R4O). (A) GR binds two DNA as a dimer. Its recognition sequences are nearly palindromic and are separated by a 3-base-pair gap, colored blue on the second inset (B). This gap corresponds to an area without physical GR-DNA interaction. (C) GRE binding motif obtained through a custom analysis of GR Chip- Seq data (14). The sequence variability of this motif allows for sequence-specific targeting of subsets of Glucocorticoid Response Elements (GREs).

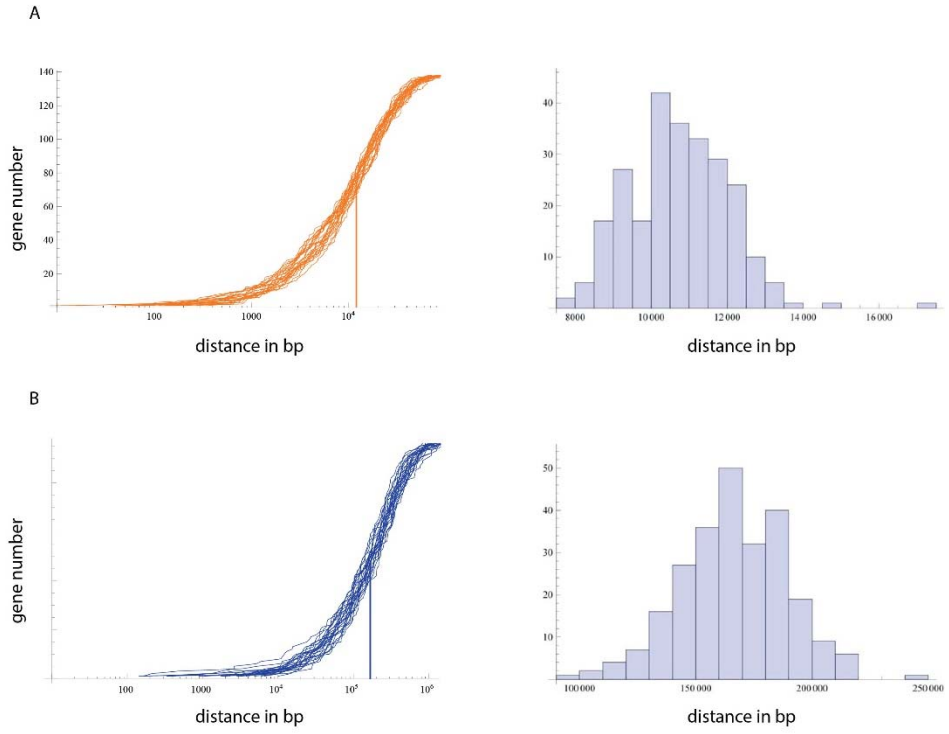

Figure 2.2 Modeling genomic distribution of GREs in relation to transcription starting sites (TSS). (A) modeling distance between GREs and Dexamethasone upregulated genes by placing GREs and TSSes at random within the average size of a human chromosome ($123kb_2$) yields comparable distribution and median distance (10.7kb, n=250) as observed by Chip-Seq (11kb). (B) Modeling distance between GREs and dexamethasone repressed genes by distributing the TSSes and GREs randomly across the whole genome yields similar distribution and median distance. (146kb for ChipSeq, versus 166.6kb for random distribution model, n=250).

The top 100 most enriched regions were scanned for a GRE consensus sequence (Fig. 2.3A), which yielded practically an identical motif as found by Chip-Seq (Fig. 2.3B) (14). I then extracted sequences with 95% homology to the GRE consensus sequence from the most enriched regions (fig 3a) and obtained 405 sequences. Using custom scripts (code in appendix D) I analyzed the frequency of motifs that can be targeted with Py-Im polyamides (Fig 2.3C). The most common sequence can be targeted by a polyamide used previously in our lab (**1**, targeted to 5'-WGWWCW-3') both *in-vitro* (26) and in gene regulation studies (22, 27). The second and third most common are targeted by the same polyamide (**2**, targeted to 5'-WGGWCW-3'), a sequence that also has gene targeted in our group previously (26). The fourth sequence (**3**, targeted to 5'-WWCWGW-3') has not been yet tested. The orthogonality of binding of polyamides **1**-**3** (Fig. 4) was determined by GRE sequence analysis, based on the previous ChIP-seq experiments (14). Comparing these three polyamides in gene regulation studies will narrow our focus to the most commonly found sequences that can be bound by 8-ring hairpin polyamides. The three

compounds can bind different sites within a GREs (Fig. 4a) and some of those sites are more conserved than others – in particular the bases 7-9, show a particularly high variability. This analysis informed the decision on which compounds should be synthesized, to exert a specific control of gene expression in A549 cells. The methods developed allow to perform this analysis for other systems, cells and polyamides.

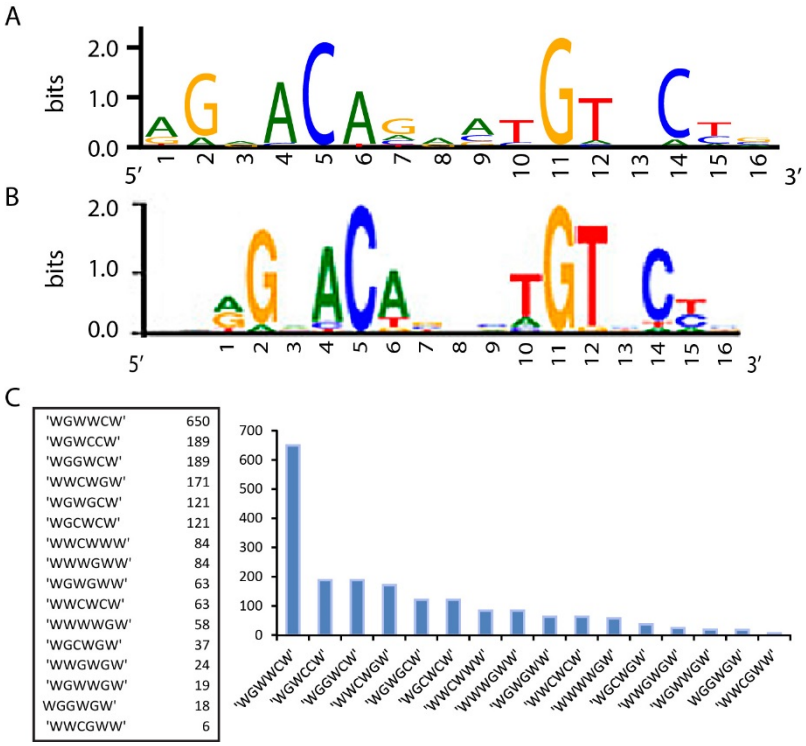

Figure 2.3 Characterizing DNA sequences binding GR. (A) Top 100 most enriched regions in Dex induced samples returned a consensus sequence that is practically identical to one obtained from uninduced cells (B). (C) The frequency of 6-basepair sequences that can be targeted by polyamides reveals WGWWCW is the most common motif among 405 GRE in a 100 regions most enriched upon Dex treatment.

Selectivity of polyamides in A549 lung adenocarcinoma cells: Gene regulation studies

The selectivity of Pyrrole-Imidazole polyamides has been tested rigorously *in vitro* (1, 28, 29); however, many questions need to be answered in the case of polyamide selectivity in cells. In order to address this issue I began gene regulation studies in A549 lung adenocarcinoma cells used previously in gene regulation studies with Py-Im polyamides (22). Since little is known

about a functional link between TSSs and GREs, I decided to investigate effects of polyamides on

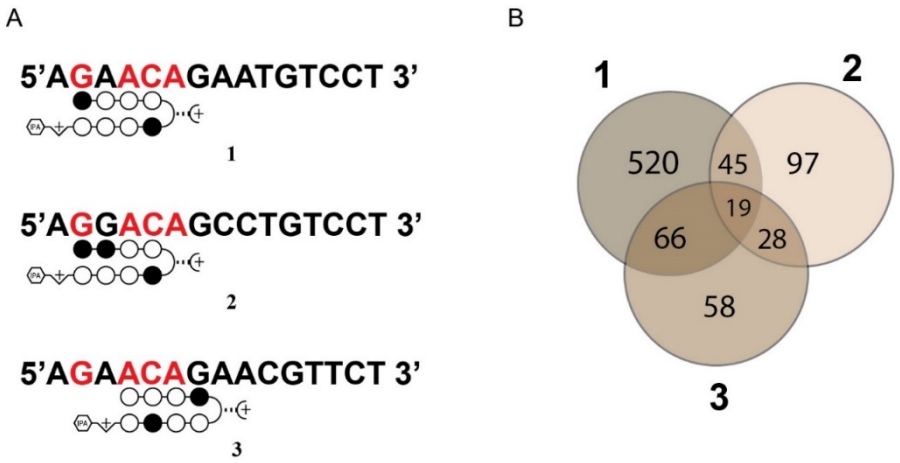

C

		1	2	3	4	5
		GWWC	GGWC	WCWG	WCWW	WCWC/GWGW
A	GWWC	650	64	85	60	44
B	GGWC	64	189	37	13	24
C	WCWG	85	37	171	43	14
D	WCWW	60	13	43	84	3
E	WCWC/GWGW	44	24	14	3	63

		GWWC	GGWC	WCWG	WCWW	WCWC/GWGW
F	GWWC	1.00	0.34	0.50	0.71	0.70
G	GGWC	0.10	1.00	0.22	0.15	0.38
H	WCWG	0.13	0.20	1.00	0.51	0.22
I	WCWW	0.09	0.07	0.25	1.00	0.05
J	WCWC/GWGW	0.07	0.13	0.08	0.04	1.00
	Promiscuity	1.39	1.73	2.05	2.42	2.35

Figure 2.4 Orthogonality and targeting sites of three polyamides recognizing the most GREs according to the data in Figure 8. (A) **1** and PA2 bind nucleotides 1-6 differ in the 3rd base of the GRE. Polyamide **3** binds a different site and shows variability in 6th and 7th bases. (B) **1** targets most sequences of the three polyamides. **3** targets mostly a subset of the sequences that are also targeted by **1**, and **2** binds mostly orthogonal sequences. (C) Polyamide specificity table shows orthogonality for other polyamides used in the study. Entries on the diagonal represent absolute number of match sequences for each polyamide. For example, entry A1 shows there are 650 WGWWCW binding sites in the tested Chip-Seq regions. The numbers of the diagonal represent a subset of GREs that can bind two different polyamides. For example, entry B2 shows there are 64 GREs that can bind both WGWWCW and WGGWCW polyamides. The bottom table (entries F1-J5) summarizes the relative promiscuity of each polyamide in the study. Each column in the top table (entries A1-E5) has been normalized to the entry on the diagonal. Promiscuity coefficients have been obtained by summing every entry in the column.

expression of a panel of genes significantly induced by GR agonist Dexamethasone (Dex), thus yielding distinguishable changes in GR-driven gene expression. According to the current models of gene expression in GR system, each of these genes should be regulated by a single or small number of GREs (14). Even though I did not know their sequences, I knew the distribution of GRE sequences genome-wide. Assuming perfect sequence specificity of polyamides, we should be able to elucidate the sequences of those GREs by observing the patterns of gene expression inhibition in a randomly selected subset of genes. I began with testing Dexamethasone induced genes identified by microarray (30) and RNA-sequencing (14). A panel of 17 genes was tested using quantitative Reverse Transcription Polymerase Chain Reaction (RT-qPCR). However, four of these genes were not upregulated significantly (Fig. 5).

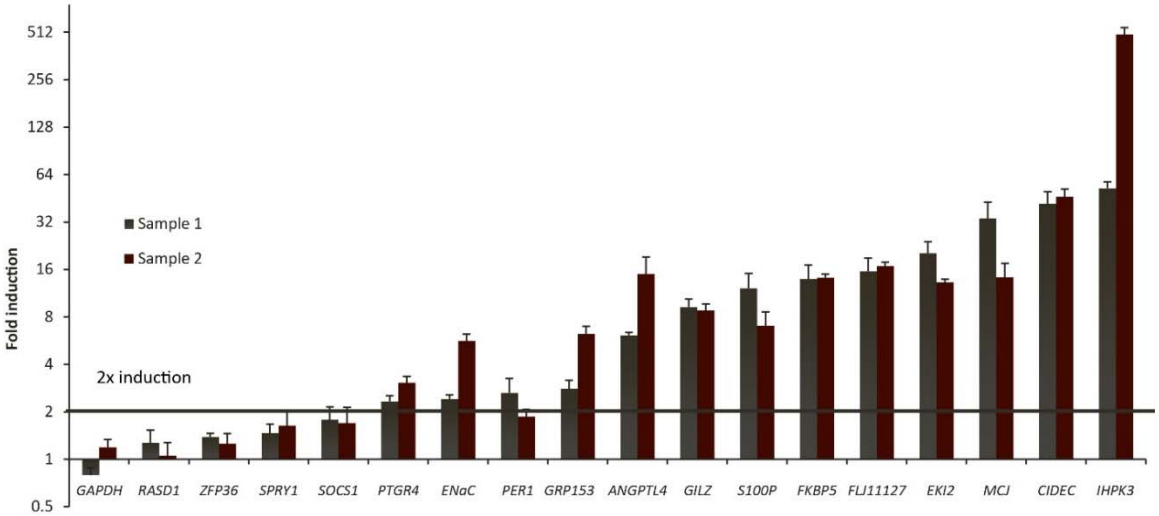

Figure 2.5 Analysis of levels of expression induced by Dexamethasone. The levels of expression were obtained by RT-qPCR. The fold induction values were obtained by dividing levels of mRNA expression obtained for Dex induced samples by uninduced ones. Genes in this panel were identified previously from microarray[7] and RNA-sequencing studies[8]. Twelve Genes that were induced at least two-fold were used for the further studies. GAPDH is a housekeeping gene and acts as a negative control. Each samples has been normalized to expression to a housekeeping gene (GUSB).

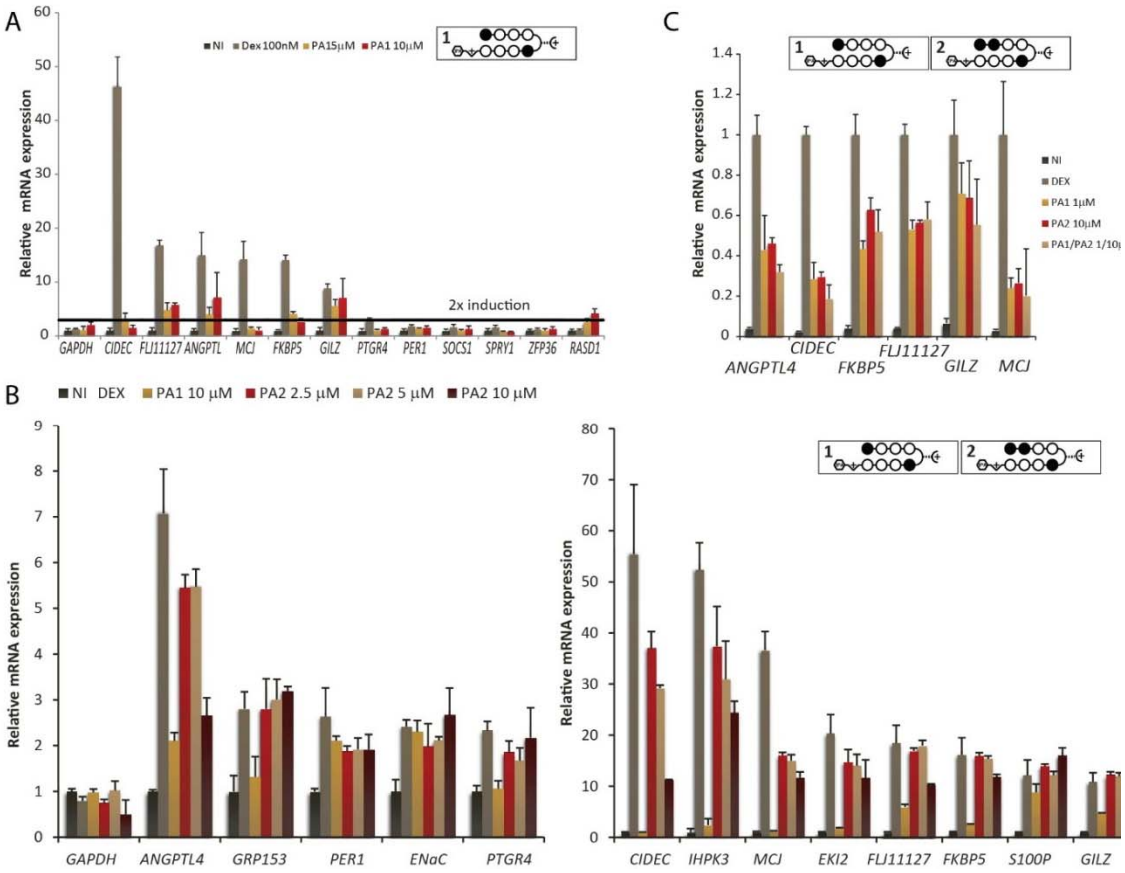

Figure 2.6 Analysis of levels of expression of genes induced by Dex and inhibited by polyamides 1 and 2. (a) Exploratory study showed that well induced genes are strongly inhibited by 1. (b) Polyamide 1 is significantly more potent than 2, but both of them downregulate the same genes. (c) Polyamide 2 is approximately 10 times less potent than 1, but the polyamides downregulated the gene expression in the same way. The correlation between the fold-induction and fold-inhibition was 0.86 for 1 and 0.74 for 2, suggesting relatively non-specific inhibition of gene expression.

I followed with the panel of 13 significantly upregulated (at least 2-fold) genes to measure the effect of polyamides on their expression. The timecourse and initial dosing was consistent with our previous studies with compound **1** in A549 cells (22). In short, the protocol included plating 12000 A549 cells/cm2 in 12 or 24 well plates for 24 hours in F12-K medium supplemented with 10% FBS, then the cells were washed twice with 1x PBS and the medium replaced with F-12K medium supplemented with 10% Charcoal Treated (CT) FBS, including the desired concentration of polyamides. After 48 hours of incubation, 100 nM dexmethasone was added directly to the medium for 6 hours, after which cells were harvested for RNA extraction. In

order to test this dosing on various genes I run a limited test on 11 genes, both upregulated and unaffected, to see if polyamides downregulated either of them (Fig. 2.6A). Confirming that all uninduced genes, with an exception of SPRY1, were unaffected by polyamide **1**, while all well induced genes were inhibited by it, I decided to compare the gene regulation capability of polyamides **1** and **2** (Fig. 2.6B).

Polyamide **1** (targeting 5' WGWWCW 3') downregulated the expression of all Dex induced genes, except two: S100P and ENaC. One of the genes, PER1, was downregulated slightly (approximately 30%) and 6 other genes, FLJ11127, FKBP5, GILZ, ANGPTL4, IHPK3, and PTGR4, were downregulated at least two-fold. Polyamide **1** at 10 μM had also completely abolished the effects of Dex in the remaining four genes, CIDEC, GRP153, MCJ and EKI2. This widespread action of polyamide 1 was not unexpected, given that the motif it targets is very common (Fig 2.3C), for the same reason one would expect polyamide **2** to target only a subset of genes, or set of genes that is different from the one downregulated by **1**. However, the dose response of polyamide **2** (Fig. 2.6B) suggests that polyamide **2** targets the same sequences, although with less potency. The same genes whose expression was most downregulated by polyamide 1, are also downregulated by polyamide **2**, albeit to a lesser extent. By running a series of exploratory experiments I was able to determine that potency of polyamide **2** is comparable to 10-fold lower concentration of polyamide **1** added to the cell media. Dosing cells with 1 μM polyamide **1** and 10 μM polyamide **2** yielded identical reponses (Fig. 2.6C), for the panel of 6 genes that were significantly downregulated in the previous experiment. It is not possible to tell whether this widespread response of both genes is due to non-specificity of polyamides in the cell nucleus, or because each of the genes inhibited happend to be regulated by several GREs containing both 5'WGWWCW3' and 5'WGGWCW3' motifs. However, when both polyamides were dosed at the same time, there was no synergistic effect (Fig. 2.6C) suggesting non-specific polyamide binding as a culprit. The extent of polyamide-mediated gene expression downregulation was correlated with the fold-induction with 100 nM dexamethasone (0.86 for **1** and 0.74 for **2**). This suggests that the most induced genes are the ones most affected by polyamides, possibly regardless of their sequence. No rigorous test exists as of now to determine the reasons for this high correlation.

Next, I tested the specificity of polyamides targeting 7th basepair in GRE motif. At first, I decided to measure the effects of polyamide **3** on the gene expression because the sequence it targets is approximately as common as for **2**. Despite following the same treatment as for compounds **1** and **2**, only two genes, ANGPTL4 and CIDEC, were affected by **3** (Fig. 2.7A) at low concentrations 2.5 μM or 5 μM. Bringing up the concentrations of these two genes showed further inhibition: ANGPTL4 was inhibited by over 50% and CIDEC by over 40%. without affecting four other highly induced genes: FKBP5, FLJ11127, GILZ, and MCJ (Fig 2.7B). Further increase in polyamide 3 concentration did not increase polyamide potency significantly, potentially because of instrument noise or polyamide solubility problems (Fig. 2.7C). Thus 10 μM concentration is either the most effective, or nearly the most effective in gene downregulation. At this concentration, the correlation between fold-induction and fold inhibition was low at 0.25, suggesting that polyamide **3** targets genes more independently of their induced activity than **1** or **2**. In an effort to improve potency of 3, I followed with its acetylation (31). Previous experience in the group suggested that this modification can improve gene downregulation (32). However, in the case of acetylated polyamide 3 (12) the gene downregulation profile was identical in both selectivity and potency.

The specificity of polyamide 3 suggested synthesis of other compounds targeting the 7th base in the GRE with N-methylpyrrole at the last position (cap). I expanded the library of compounds to target these sequences. The next sequences most commonly found in GREs can be targeted by polyamides **4** and **5** (Fig. 2.8), namely, sequences 5'WWCWW3' and 5'WWCWCW3', respectively. These compounds as well proved to be less potent than **1** or **2** but also more selective in gene downregulation. Compound **4** caused downregulation of three genes at two-fold or more: ANGPTL4, CIDEC, and MCJ (Fig. 2.9). Two of these genes, ANGPTL4 and CIDEC, were also downregulated by **3**; however, MCJ was not. Thus there is a distinguishable difference in downregulation profile between 3 and 4, even though both of them target the GRE consensus sequence. It is possible that this effect is due to DNA-binding independent events, and thus it is not yet clear if their differences in gene downregulation are due to differences in sequences of GREs influence on the gene downregulation patterns. Polyamide 6 is a potent compound with little controlling each of these three genes. It is, however, a useful feature of

these compounds and a step towards making polyamides that downregulate small subsets of genes.

Compound **5** targets a less common sequence (5'WWCWCW3') that occurs three times less commonly in the assessed region than 5'WGGWCW3' or 5'WWCWGW3' and 25% less commonly than 5'WWCWWW3'. It also happens to be even less potent than 3 and 4. Similarly to these compounds it downregulates ANGPTL4 and CIDEC, however, at 10 mM only by approximately 1.6- and 2-fold, respectively. Interestingly two other genes were downregulated slightly (albeit within the noise of the method) and showed a dose response: MCJ and FKBP5 (Fig. 2.10A). Higher concentration dosing, or additional modification to the compound 5 will be necessary to improve this potency and establish whether downregulation of these two genes is specific.

In order to distinguish whether the effects of gene expression are solely based on the sequences targeted by polyamides, or if the structural properties of the polyamide itself also matter, I decided to examine the gene regulation capabilities of polyamide **6**, which targets the same sequence as **5**, but has a different structure. It appears that the structure of the polyamide has a significant on gene expression: compound **6** affects a larger number of genes at 10 μM (Fig 2.10B), whereas polyamide **5** is more specific, but not as potent (Fig 2.10A). The former downregulated genes in a similar fashion as other N-methylimidazole capped compounds: most genes are downregulated to nearly their baseline levels, and thus compound 6, at 5 μM and 10 μM, mimicks the downregulation patterns of compound **1** (Fig. 2.10B).

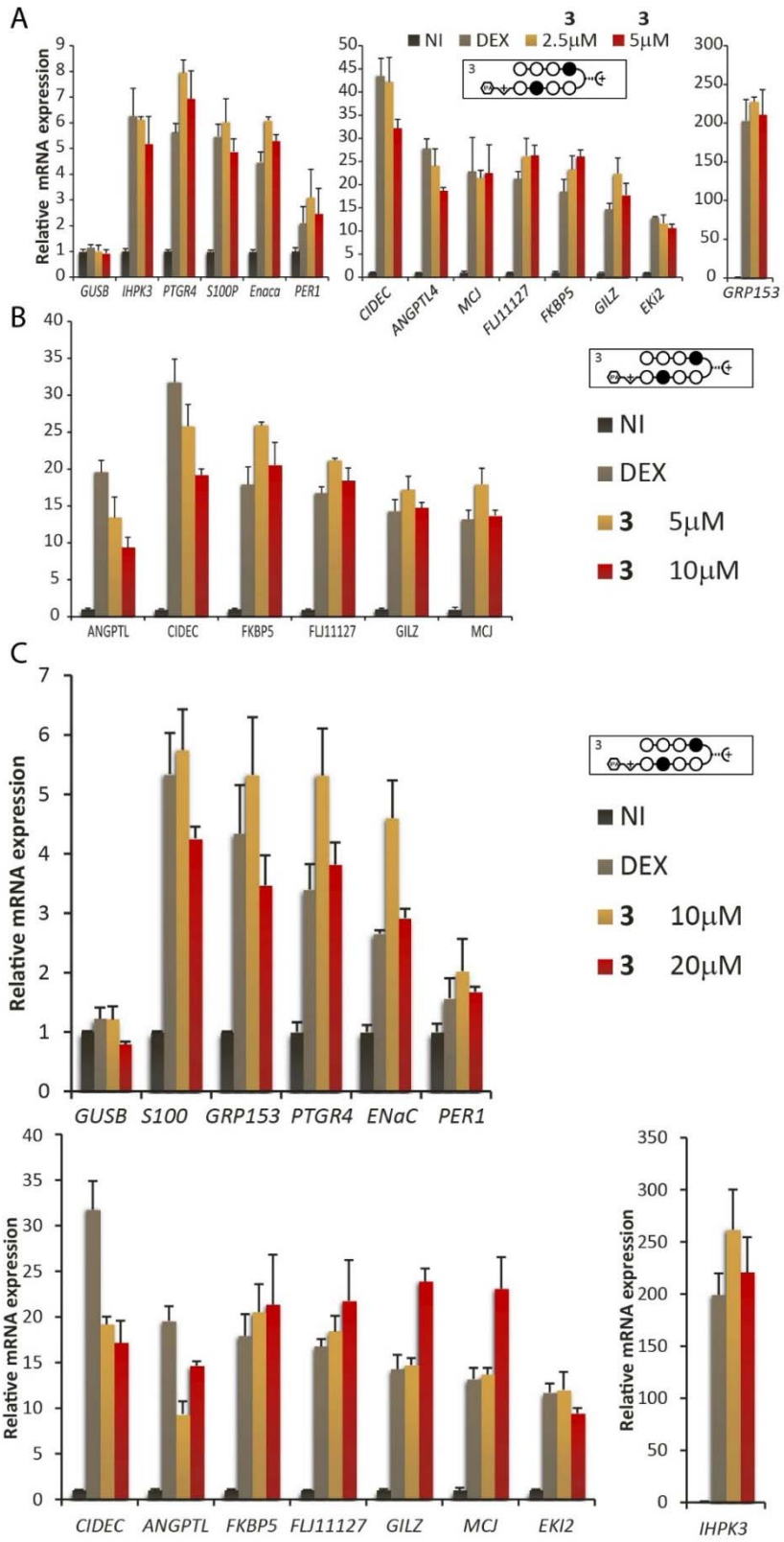

Figure 2.7 Analysis of levels of expression of genes induced by Dex and inhibited by polyamide 3. (a) At 2.5 mM and 5 mM only two genes are affected by polyamide 3. The low concentrations have been used to promote selectivity at a cost of potency. (b) Increasing the concentrations to 5 mM and 10 mM increases potency of polyamide 3 without sacrificing selectivity. Only two genes, that were affected at lower concentrations are inhibited by 3. The remaining four are negative controls and were not affected. (c) Adding even more elevated concentrations of polyamide 3 does not increase potency significantly. This could be due to a cytotoxic effect or polyamide insolubility. However, if the changes in relative mRNA expression are small, they might also not be within the instrument's sensitivity. Unlike in case of polyamides 1 and 2, the correlation between fold-induction and fold-inhibition is low at Rsq=0.25 suggesting that action of 3 is more independent on activation levels, and less on the specifics of the gene.

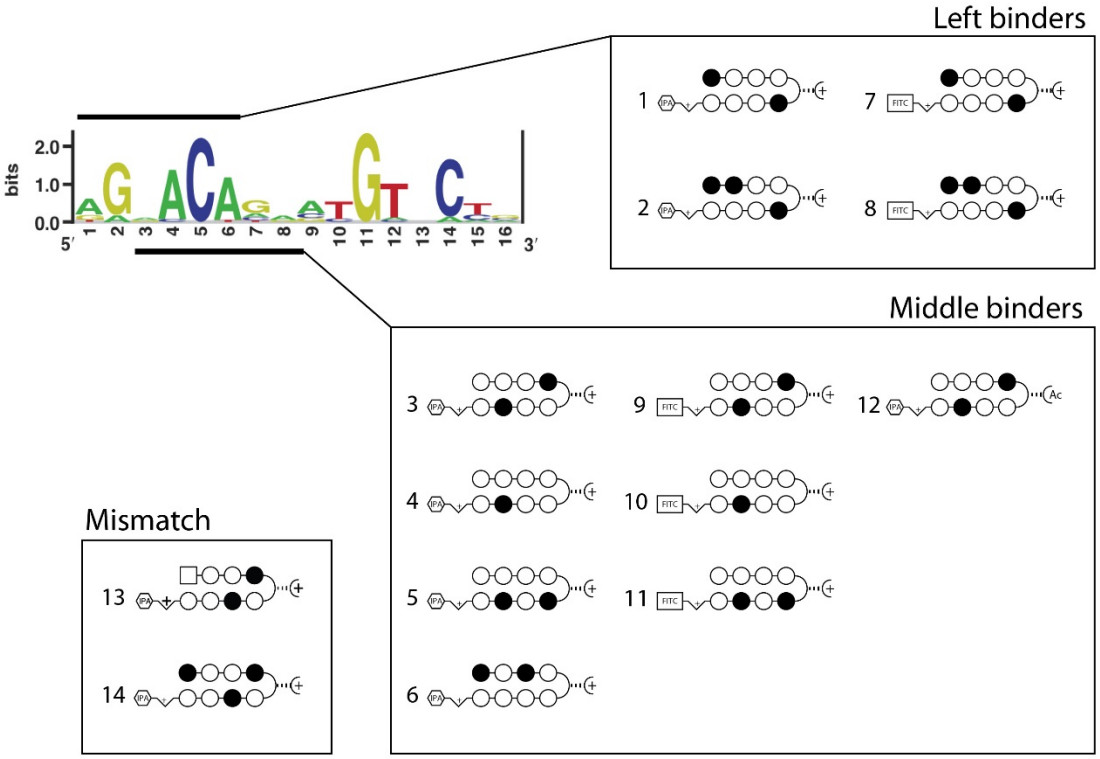

Figure 2.8 Library of synthesized polyamides. The 'left binders' include polyamides spanning bases 1 through 6 of GREs with a 3rd variable base.'Middle binders' target bases 3-8 and vary at 7th nucleotide in the GREs. Structures of polyamides drawn in Appendix A.

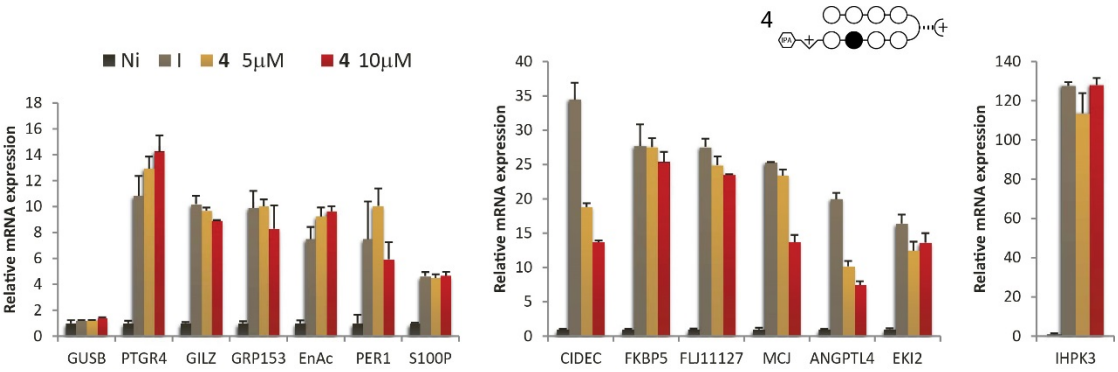

Figure 2.9 Inhibition of a panel of Dex induced genes by polyamide 4 (targeting 5'WWCWWW3' DNA sequence). The polyamide downregulated the three genes two-fold or more at 10 mM. Of those genes CIDEC and ANPGTL4 were downregulated by 3, but MCJ was not. Thus there is a difference in specificity of gene downregulation between 3 and 4.

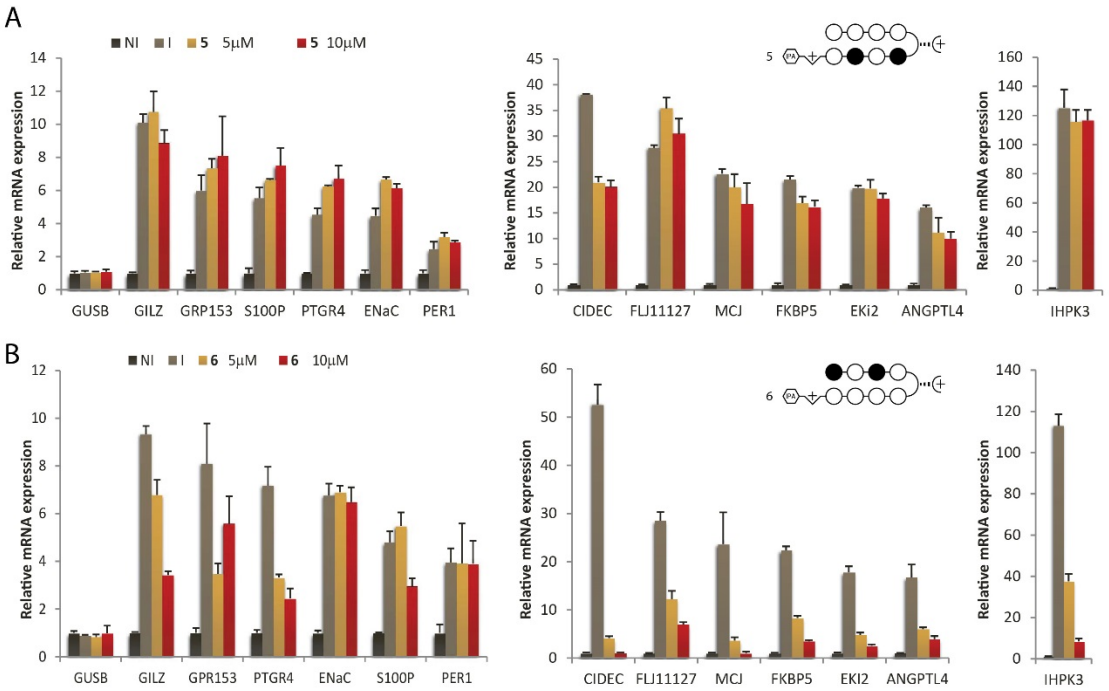

Figure 2.10 Downregulation of Dex induced genes using polyamide targeting the same sequence, but with different structures. (A) n-methylpyrrole capped polyamide, 5, downregulates the genes slightly, but selectively. (B) n-methyl-imidazole capped compound 6 downregulates the genes efficiently, but not selectively.

A negative control of sequence-specific gene regulation could be compounds targeting sequences that are not found within GREs. For example, a 5'WTWCGW3' sequence does not appear in 405 GRE motifs most responsive to Dex (Appendix E, Fig. 3C) and it can be targeted with compound **13**. In tissue culture studies **13** downregulated all genes but two whose expression was unaffected by polyamides **1** and **2** as well: S100P and ENaC. At 10 μM the most genes were downregulated to basal level. The exceptions: IHPK3, GRP153, and GILZ, were also significantly downregulated (Fig. 2.11). At 5 μM the gene downregulation effects were less prominent: most of the genes were downregulated to 4-fold the baseline expression level and two of them, IHPK3 and PTGR4, were downregulated to 10- and 2-fold the baseline. One gene, PER1, was unaffected. As a result downregulation level of most of the genes was highly correlated with the induction level: at 10 μM, the correlation coefficient between fold-induction and fold-inhibition by treatment with **4** was Rsq=0.95 at 10 μM and Rsq=0.96 at 5 μM.

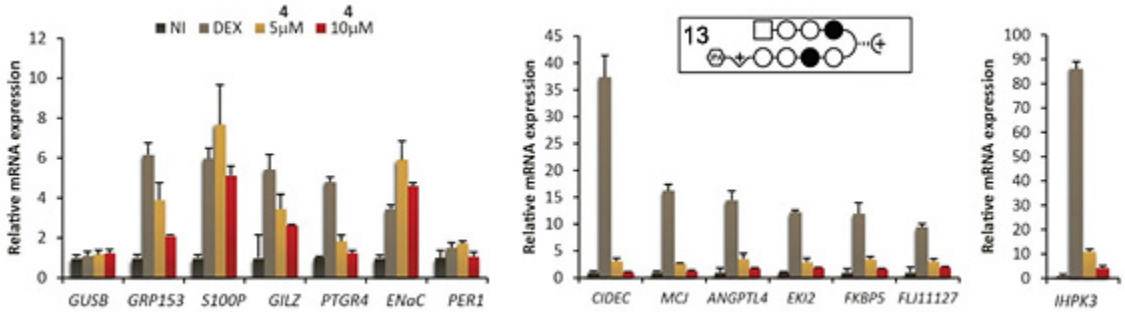

Figure 2.11 Analysis of levels of expression of genes induced by Dex and inhibited by polyamide 13. All genes, except S100P and ENaC were significantly downregulated by both 5 μM and 10 μM polyamide 13. At 10 μM most genes were downregulated to 1-2fold their baseline levels and at 5 μM - to 4-fold baseline expression. The remaining two, IHPK3 and PTGR4, were downregulated to 10-fold and 2-fold their baseline and PER1 was downregulated slightly. Overall polyamide 13 shows excellent correlation between fold-induction and fold-inhibition at both 10 μM (Rsq=0.95) and 5 μM (Rsq=0.96). This suggests that relative induction dictated polyamide inhibtioin levels, regardless of which gene was affected.

In order to compare the trends in gene downregulation studies, I pooled the RT-qPCR results into a matrix (Fig. 2.12). Three most potent polyamides (1,6 and 13, targeting 5'WGWWCW3', 5'WGWGWW3' and 5'WTWCGW3', respectively) downregulated CIDEC significantly better than ANGPTL4. However, only two of them (1,13) downregulated IHPK3 more potently than MCJ (Fig. 20a). Three less potent polyamides downregulated MCJ more potently than IHPK3 (3,4 and 5, targeting 5'WGGWCW3', 5'WWCWWW3' and 5'WWCWCW3', respectively). All but one (compound **2**) of the less potent polyamides downregulated CIDEC less potently than ANGPTL4. Polyamide **2** was overall less selective but also more potent than the other polyamides in the low-potency group (Fig. 2.6B). Only one of these compounds (**3)** downregulated ANGPTL4 and CIDEC but not MCJ.

These results show that in the GR system there is a difference between polyamides in their gene regulation patterns. These differences highlight a balance between specificity and potency. This balance could partially be due to native binding selectivity of the polyamides and partially due to potential cross talk between the genes. Interestingly, Py-Im polyamide sequence specificity alone

does not explain the patterns of gene regulation. A good example of the lack of correlation between targeted sequence and gene expression changes within the library is a mismatch compound (**13**) having a significant effect on gene expression, while a many of the 'match' polyamides such as compounds **3**, **4,** or **5** had less potent gene downregulation activity**.** Additionally, two compounds targeted to the same sequence – **5** and **6 –** show different gene regulation profiles, suggesting that Py-Im polyamide structure may play a significant role in their *in vivo* activity**.** This brought upon a question, what governs the polyamide potency and activity in tissue culture. Two possibilities include the binding affinity of Py-Im polyamides and their cellular uptake.

One explanation for potency of the synthesized compounds is their binding affinity to DNA. A compound with weaker binding could possibly have less binding energy than GR and thus could be incapable of displacing transcription factors. The binding affinity of compounds can be measured using a DNA thermal denaturation assay (32). Two sets of olignucleotids have been used for the assay: published sequences that can be compared to previous results (5' CGAnnnnnnAGC 3', where n are specific to a polyamide) and 5 oligonucleotides with sequences of GREs occuring in A549 cells. The latter have been chosen to assure that each GRE can only contain one polyamide binding site and has a match sequence of only one of the studied polyamides.

The tested polyamides included compounds **1**- **6** (Fig. 2.13). Each of the polyamides stabilized the DNA duplex in thermal denaturation thus proving its DNA-binding capability (Fig. 2.13). In order to test the specificity of polyamides in DNA thermal denaturation assay, the shorter oligonucleotides were used, to lower the melting temperatures. Both polyamides tested show a degree of sequence specificity and stabilize the match-sequence the best (Fig. 20). Importantly, however, the Py-Im polyamides with lower thermal stabilization values, and thus lower affinities ($\Delta Tm < 5.0^{o}$ C), had lower potency in gene expression inhibition. This suggests a positive correlation between Py-Im polyamide binding affinity and ability to regulate gene expression. Interestingly, however, polyamides 5 and 6 had similar effects on thermal stabilization of DNA duplexes, and thus binding affinity is not the only variable that governs potency of these compounds. Another factor that could contribute to ability of polyamides to regulate gene

expression is their cellular uptake.

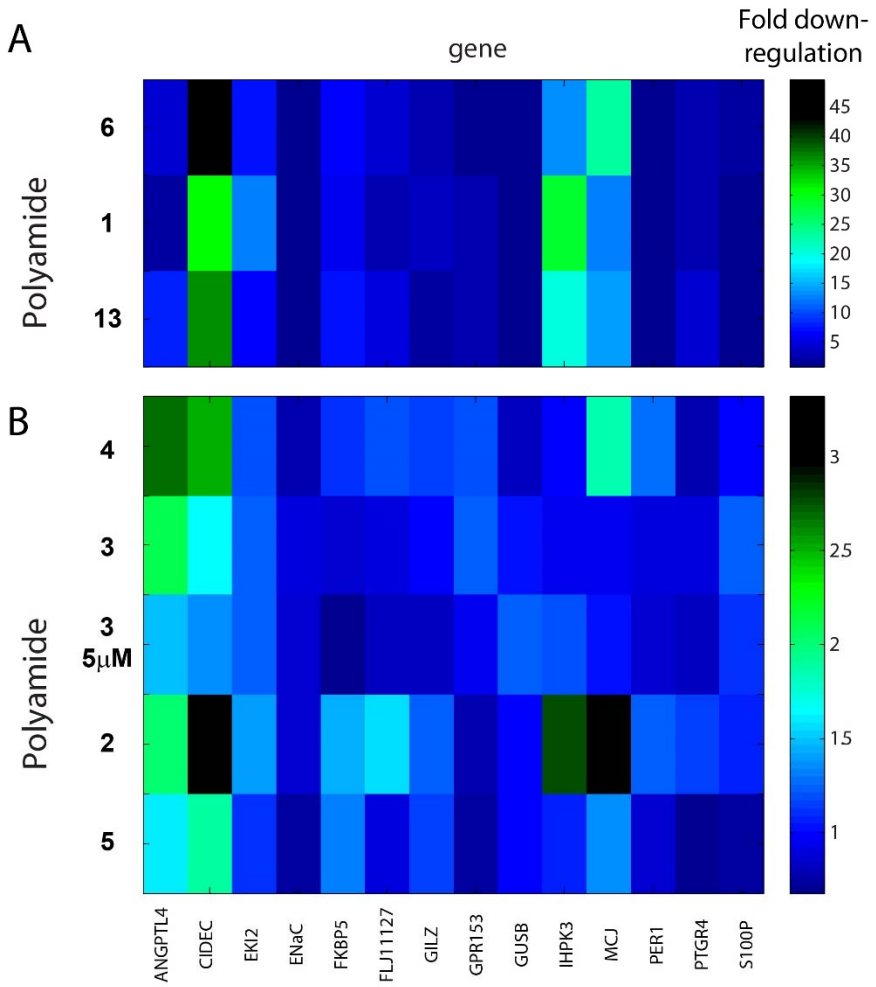

Figure 2.12 Downregulation of Dex-induced genes using Py-Im polyamides. (A) Highly potent polyamides downregulated CIDEC more efficiently than ANGPTL4. Also two out of the total number downregulated IHPK3 more potently than MCJ. (B) All but one of the less potent polyamides downregulated ANGPTL4 more potently (or comparably to) than CIDEC. Polyamide **5** downregulated MCJ as well, but 3 did not. Polyamide **2** downregulated MCJ and CIDEC more potently, but also affected several other genes. Overall, this library of GR-targeting polyamides allows for selective targeting of genes, but suffers from poor potency. Alternatively it can target a large number of genes, while suffering from poor selectivity. This issue will need to be addressed with improved dosing schemes and alternative polyamide structures.

A

	Polyamides	T_m (°C)	ΔT_m (°C)
	DNA = Respective GREs		
1		90+	?
3		80.6 (±0.3)	2.5
4		78.8 (±0.1)	4.5
5		81.9 (±0.5)	4.7
6	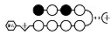	82.6 (±0.3)	5.4

B

	Polyamides	T_m (°C)	DT_m (°C)
	DNA = 5 - CGA TGTTCA AGC -3		
—		53.4 (±0.2)	—
1		72.7 (±0.4)	19.2
2		55.3 (±0.2)	1.9

C

	Polyamides	T_m (°C)	DT_m (°C)
	DNA = 5 - CGA TGGTCA AGC-3		
—		57.1 (±0.4)	—
1		69. 4 (±0.3)	16.1
2	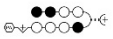	73.6 (±0.3)	20.2

Figure 2.13 Thermal denaturation assay on GREs and DNA oligos. (A) Each of the compounds synthesized stabilizes DNA duplex in thermal denaturation. Compound **3** is by far the weakest stabilizer, followed by **4** and **5** and then by **6**. Compound **1** is likely a strong stabilizer: however, it is not possible to estimate the stabilization temperature, because it's out of the range of the assay. Compound three has been tested twice to show that ΔT from polyamide binding is higher for oligos with lower melting temperarture. (B) Assay showing thermal stabilization of compound 1 and its match sequence, and compound **2** with one nucleotide mismatch. (C) Assay showing thermal stabilization of compound **2** to its match sequence, and compound **1** with one nucleotide mismatch. Compound **1** appears to be a more promiscuous binder than **2**.

Cellular uptake of polyamides

The potency of polyamides in gene regulation depend both on their DNA binding characteristics and cellular uptake. In order to decouple those two variables I performed cell-uptake studies by conjugating a Fluorescein Isothiocyanate (FITC) molecule to a polyamides' C-terminus (33). This conjugation has not affected the gene regulation potency in the past (34, 35) and is used as

a golden standard of cellular uptake in our group. We use confocal microscopy and either qualitative or software analysis of images to determine nuclear concentration of polyamides using a protocol described before (36) that has since been slightly simplified. In short, 60000 cells (A549) are plated on an optical glass in 35mm culture dishes, incubated in medium for 24 hours, and consequently dosed with Fluorescein-conjugated polyamides for 24-48 hours. Subsequently cells are washed twice with PBS and imaged on a Zeiss LSM 5 Exciter with a 63x F/1.4 objective. All tested compounds were visualized under microscope showing their nuclear uptake (Fig 2.14). The nuclear uptake of compound **7**, a FITC-conjugated version of **1**, was comparable to **9**, **10** and **11**, fluorescent counterparts of **3**,**4,** and **5**, respectively. Thus the low potency of the latter three cannot be explained by poor uptake and is more likely due to their binding properties or biological function of the sequences they bind. The poorer uptake compound **8**, on the other hand, could explain less potency in gene downregulation, as compared to **1**.

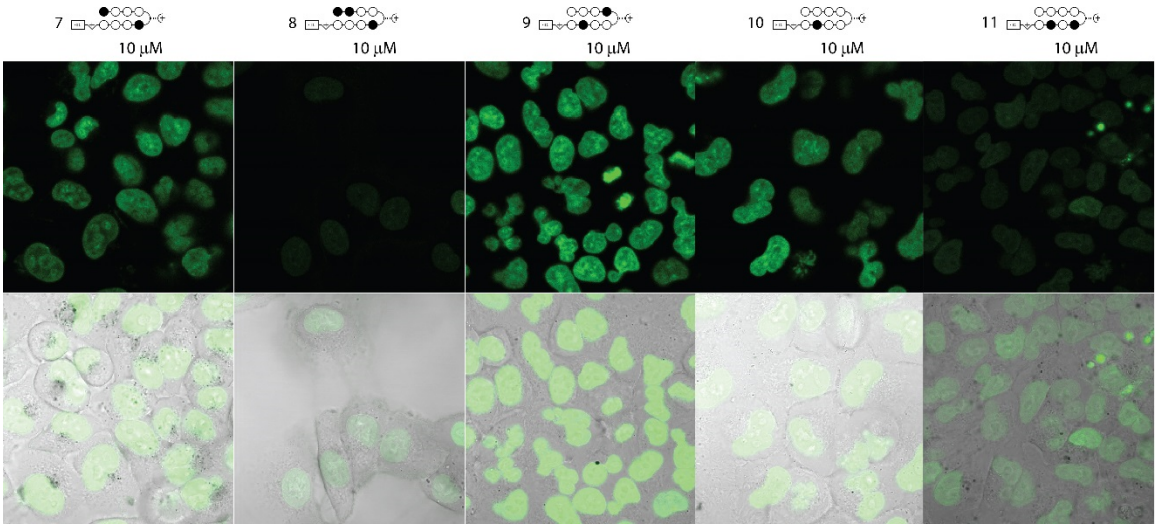

Figure 2.14 Nuclear uptake of polyamides. Compounds **7-11** were dosed at 10 μM and uptaken by A549 cells over the course of 48 hours. They were subsequently imaged on a Zeiss Exciter LSM confocal microscope. The nuclear uptake of **7** was comparable to the uptake of **9** and **10** suggesting that poor uptake cannot explain low potency of their FITC-unconjugated counterparts: **3, 4** and **5**. Poorer nuclear uptake of **8** and **11** could, however, explain low potency of **2** and **5**, respectively.

Discussion and strategies for improving polyamides specificity in-cells.

Dynamics simulations are a useful tool to understand biological processes. Polyamide binding can be modeled to give a quantitative insight into their specificity and kinetics in living cells. The developed model suggests a possible route for improvement of polyamide specificity, through elongating the targeted sequence. Currently the most attractive option is synergistic binding of multiple polyamides. In this approach no new types of molecules need to be developed: we can use molecules with well-known specificity and excellent nuclear uptake. Additionally, using several polyamides in synergy, rather than a single long polyamide, enables targeting disjoint sequences and may enable a of linear to exponential increase in selectivity with each added polyamide.

Modeling kinetics and thermodynamics of polyamide binding in-cells.

The human genome consists of approximately 3 billion bases. Most of the genome is part of intergenic sequences that are thought to have little influence on the gene expression 1 (37). A typical 8-ring hairpin polyamide can recognize 6-base pair regions that appear commonly within the genome. For example, the pattern 5'-WGWWCW-3' occurs 15 million times in the human genome, while 5'-WGGWCW-3' -- 13 million times. As a resul, targeting an expression of a small subsets of genes is difficult and requires a sufficient amount of polyamides inside the nucleus as well as proper kinetics and thermodynamics of their binding. In order to investigate the properties of polyamides that would contribute to the most selective and potent gene regulation I constructed a kinetic model of polyamide uptake and binding (Fig 2.15).

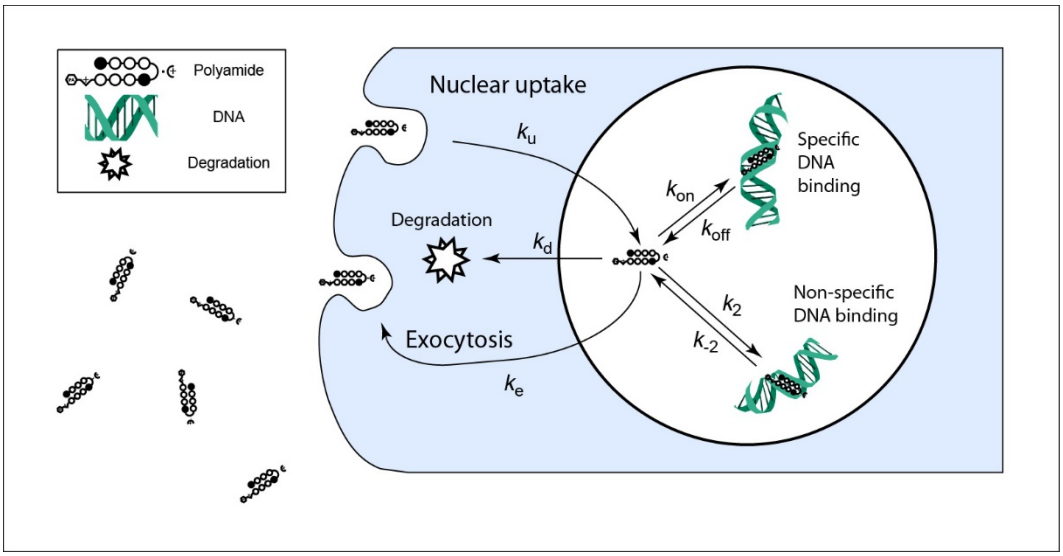

Figure 2.15 Trafficking dynamics of polyamides in living cells. Polyamides are internalized and exocytosed by cells at rates of k_u and k_e, respectively. These rates were estimated based on previous cell-uptake studies in the group. Polyamides uptaken into the nucleus can bind to either the DNA they target (rate constant of association is kon and constant of dissociation is k_{off}) or to mismatch sequences with rate of association of k_2 and rate of dissociation of k_{-2}. The rate of degradation (k_d) was added to account for thermal degradation and irreversible binding of polyamides to proteins and membranes.

Knowing the proper range of binding affinities required for selective gene regulation can guide the choice of polyamide molecules used in the study. Likewise, knowing the qualitative relation between selectivity and potency of polyamides can help in choosing the dosing scheme for a desired effect. Kinetic parameters (listed in Table 1) of several compounds have been published previously (38, 39) and I used them in simulation. In order to match cellular uptake properties I used radiography data performed in our lab in the past (Melander 2001, unpublished data). The concentrations of polyamides binding sites in A549 cell nucleus have been calculated by dividing the whole genome into 6 basepair pieces and measuring their concentration in an average volume of an A549 cell nucleus equal to 466 μm^3. This is a simple assumption that doesn't include influence of polyamides on binding in the proximity of other molecules. Even though polyamides have been shown to bind to nucleosomes (3, 40) little is known about their binding to more organized DNA structures, such as 30 nm fibers. In order to accommodate for genome accessibility, a parameter multiplying DNA concentration has been added for both mismatched and matched DNA. The lower bound of accessible genome was assumed to be the amount of

DNAse I hypersensitive DNA in A549 cells, (7) equal to 2.1% . The upper bound was the whole genome of A549 cell and midrange value chosen for representation was 10%. These three data points allow us to show trends in the effect that the amount of DNA in the nucleus has on the polyamides specificity (Fig. 16). The less DNA there is, the more likely high uptake of polyamides is going to fill up all the match-sequences. Once that happens all additional polyamide uptake decreases the specificity of binding. Depending on the amount of accessible genome, such decrease in specificity can happen at low micromolar concentrations, which is the dose we currently observe in A549 cells (41).

Table 1 Kinetic constants for polyamide binding and mismatch binding used in modeling

	K_D (M)	K_d (1/s)	K_a (1/Ms)	Specificity
15	$(5.12) \times 10^{-9}$	$(5.20) \times 10^{-4}$	$(9.76) \times 10^{4}$	149
16	$(5.57) \times 10^{-7}$	$(1.31) \times 10^{-3}$	$(2.39) \times 10^{3}$	
17	$(2.85) \times 10^{-11}$	$(2.00) \times 10^{-3}$	$(7.00) \times 10^{7}$	88
17 mismatch	$(2.52) \times 10^{-9}$	$(1.51) \times 10^{-1}$	$(6.00) \times 10^{7}$	
18	$(1.33) \times 10^{-11}$	$(2.00) \times 10^{-3}$	$(1.50) \times 10^{8}$	61
18 mismatch	$(8.10) \times 10^{-10}$	$(6.50) \times 10^{-2}$	$(8.00) \times 10^{7}$	

Abbreviations: K_A, association equilibrium constant; K_a, association rate constant; K_D, dissociation equilibrium constant; K_d, dissociation rate constant. Specificity is defined as K_A (polyamide binding)/ K_A (mismatch binding).

Table 2 Initial conditions and constants for modeling

	Value
Nuclear concentration of polyamides (M)	(0.00)
Match DNA concentration (M)	$(7.53) \times 10^{-5}$
Mismatch DNA concentration (M)	$(2.51) \times 10^{-3}$
Rate of nuclear uptake (1/s)	$(2.89) \times 10^{-6}$
Rate of nuclear exocytosis (1/s)	$(2.89) \times 10^{-4}$
Rate of degradation of free polyamide (1/s)	$(5.78) \times 10^{-6}$

Therefore once all match sites are filled, the selectivity of polyamides will get worse, but their potency will stay the same. There could thus be an upper bound at which polyamides should be dosed for maximum selectivity. Similarly, as expected, there is an upper bound to the affinity of

polyamides. Once the polyamides have very slow rate of dissociation, they take a long time to reach equilibrium and during 48 hour induction the majority of polyamides are bound in mismatch DNA regions. If their affinity is above a certain threshold, their binding could be strong enough to displace transcription factors even when bound to mismatch-sequences.

Polyamides typically show between 50-100 fold selectivity in binding different DNA sequences (39). However, given that mismatch DNA is over 30-fold more concentrated than the match sites, it is not possible to avoid nonspecific binding. Since each gene in mammalian cells can affect other ones, even few nonspecific binding events can significantly affect cellular signaling. In the case of polyamides, the extent of non-specific binding makes it very likely that polyamides change signaling in many pathways, not only the one they target. In order to alleviate this problem, we will need to drastically increase polyamide binding specificity *in vivo*.

One possibility is to increase the length of the binding site of polyamides. In the past both ours and other groups targeted DNA regions longer than 6-basepairs (7, 38, 42). However, increasing the length of sequences does not necessarily increase specificity and few studies have been done to investigate it. The polyamides recognizing 10-basepairs are shown to have very different binding affinities when binding to different sequences (38, 43). However, sequence selectivity of these molecules has not been shown.

An alternative possibility is to make use of the synergistic targeting of multiple polyamides at once. Many genes in mammalian cells are controlled by more than one transcription factor. For example, circadian gene regulatory network of tens of functionally interconnected genes (45). One of them, PER2, is controlled by GREs and other two regulatory elements: CEBP and EBOX (44). In this scenario we would use polyamides targeting 5- or 6-basepairs that show good nuclear uptake, strong potency in gene downregulation, and have known sequence specificity. Using the fact that the regulatory elements of most genes are longer than 5 -or 6-basepairs (for example GRE is 15 basepairs long) we can target each of these elements with multiple short polyamides (Fig. 2.17A). In this case the fractional occupancy at the targeted site will be significantly higher than if a single polyamide was targeted at higher concentration. Simply the fact that polyamides can bind concurrently, or one at a time, yields more possible binding

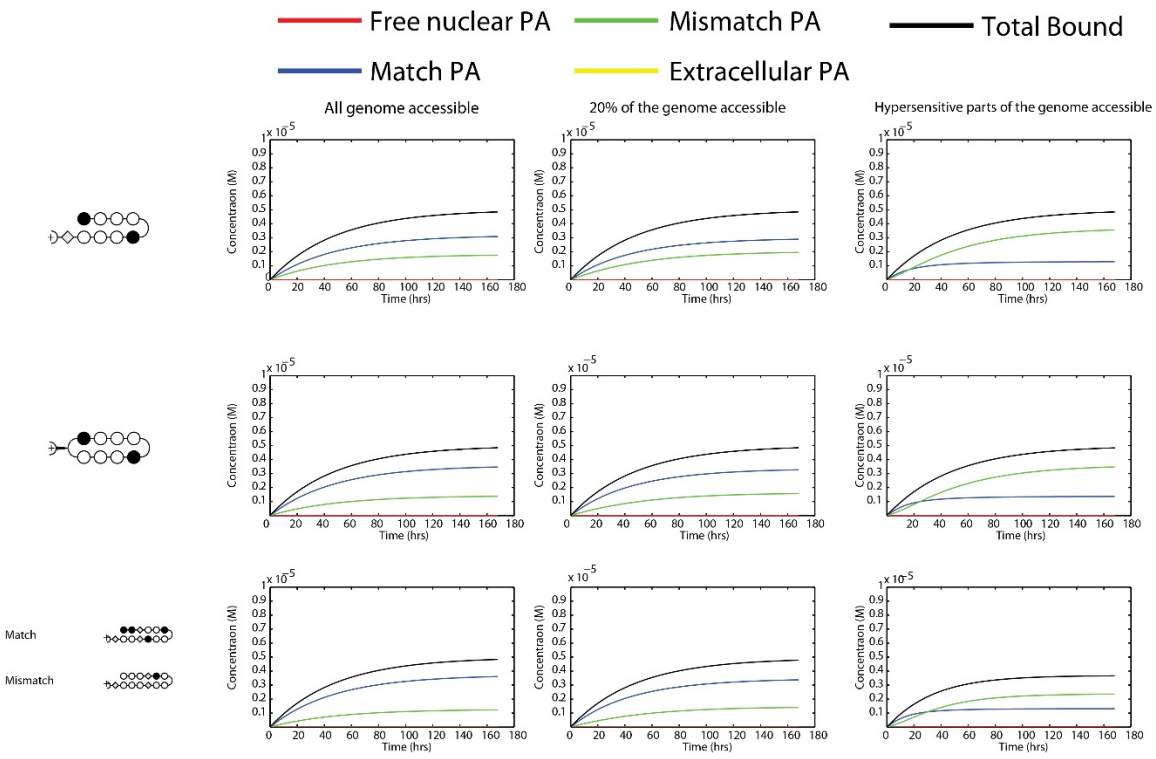

Figure 2.16 Modeling results for the three published compounds ((38, 39)) in A549 cells: a significant amount of polyamides is bound to mismatch DNA and high uptake of polyamides can lead to lower specificity. The first column shows that when all of the genome is accessible there is a constant uptake, and DNA binding, of all three polyamides. Because of the high concentration of both polyamide and nuclear DNA, a majority of polyamides are bound to DNA. This results in an initial linear accumulation of polyamides in the nucleus in time, which is consistent with the radiography data (Melander, 2001; unpublished data). All compunds reach equilibrium of binding relatively quickly and ratio of match-binding (complex Match-DNA-polyamide depicted in blue) to mismatch binding (complex of mismatch-DNA-polyamide depicted in green) is determined by the relative dissociation constants for polyamides. Even though a significant fraction of polyamides bind to (much more abundant) mismatch sites, the main species in the nucleus is DNA bound to the match polyamide. The second column represents situation when only 20% of the genome is accessible. In that case, the match sites quickly become filled with polyamide and its further uptake only increases non-specific binding. This effect is aggravated even further when only the DNAse I hypersensitive DNA is assumed to be accessible (third column). All three compounds yielded similar qualitative characteristics of nonspecific and specific binding. In conclusion, significant fraction of polyamides binds to nonspecific DNA, which will affect cellular signaling in an unpredictable fashion.

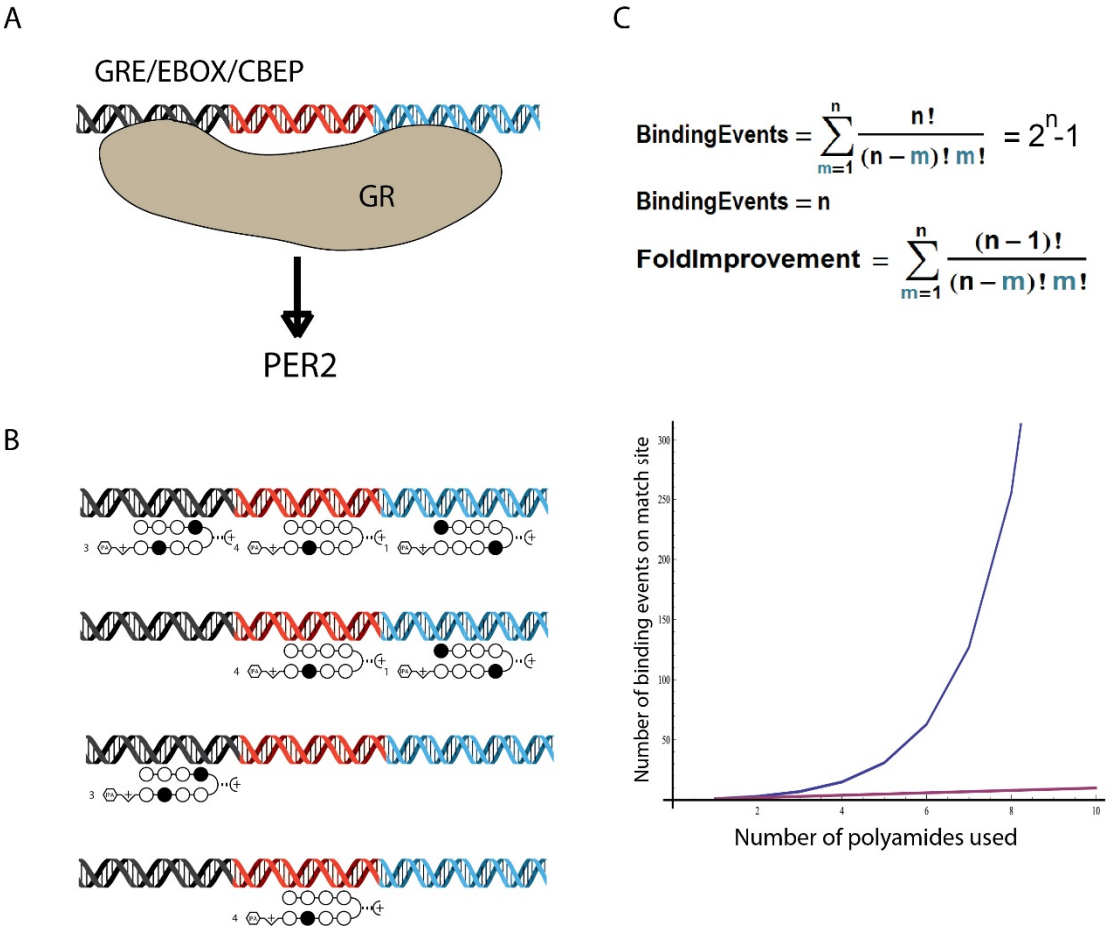

Figure 2.17 Combinatorial targeting of polyamides. (A) The circadian gene regulatory network in mouse (44) is an example of the many networks. where genes are controlled by multiple transcription factors. (B) One of the genes PER2 is controlled by GRE, EBOX and CBEP regulatory elements. (C) Each of these elements can be targeted by multiple polyamides. Since the presence of even one precludes TF binding, it is likely that more than one polyamide bound will do that as well. When multiple polyamides target long sequence, the time where at least one polyamide resides is increased exponentially for a given concentration, as opposed to linear increase in time of occupancy (D). For the same concentration of polyamides, if 10 polyamides are used instead of 1 at ten times higher concentrations, there is up to 100-fold increase in relative specificity, proviso that each polyamide is capable of regulating gene expression by itself.

Events, leading to displacement of transcription factors (Fig. 2.17B, C). In fact, for large numbers of polyamides targeted the sequence selectivity grows exponentially (with a base of 2).

This is a preferred solution because it relies on the already existing and well developed molecules. It also results in an exponential increase in specificity while allowing targeting very long sequences with 8-ring hairpin polyamides, leveraging their good cell uptake and pharmacokinetic properties.

Directions for a genome-wide evaluation of polyamide DNA-occupancy and action

The panel of 12 genes tested does not capture the complexity of the whole-genome selectivity of polaymides. Previous studies have shown that only a small number of genes are regulated differentially (22, 27, 34). The probability of finding these genes by qPCR is small, and thus we will need to use RNA-sequence to identify them. This method however is expensive, which is the reason for following with a small exploratory panel of genes at first. Since all the compounds tested have good nuclear uptake and bind DNA *in-vitro*, they are candidates for evaluation by RNA-sequencing. In order to asses the reliability of the high-throughput data, my next step will be to evaluate gene downregulation patterns of two previously published1 polyamides (targeting WGWWCW and WGWCGW). These polyamides have shown approximately forty genes that are more downregulated by the latter compound, despite its overall lower potency. In my next experiments I would like to confirm that there exist genes that are downregulated differentially. Since the second compound is overall lest potent than one targeting WGWWCW , the control we used before, showing that a mismatch polyamide (WGWCGW) does not downregulate a subset of genes is not a sufficient proof of sequence selectivity.

Appendix A: materials and methods

Synthesis of Polyamides.
All polyamides were synthesized on solid phase on Kaiser oxime resin (Nova Biochem) using protocols published previously (46, 47). The polyamides were subsequently cleaved subsequently off the resin with 3,3-diamino-N-methyldipropylamine and purified by reverse-phase HPLC. Isophtalic acid was conjugated after prior conjugation by PyBop (Nova Biochem) or PyAop (Oakwood Products, Inc) using an established protocol (34). The mass and purity of polyamides was assesed by MALDI-TOF and reverse phase HPLC.

Measurement of cellular mRNA.

A549 cells (ATCC) were plated in 12-well plates at a density at 60000 cells per well in 1ml of F12-K medium (ATCC) supplemented with 10% (vol/vol) FBS (Irvine Scientific). After 24 h, the medium was replaced with F12-K containing 10% (vol/vol) charcoal treated (CT) FBS and polyamides at desired concentrations. Cells were incubated with polyamides for 48 h and were subsequently treated with 100nM Dexamethasone (Dex). RNA was then extracted using RNEasy kit (Qiagen) and reverse-transcribed using Transcriptor first-strand kit (Roche). Quantitative real-time RT-PCR was performed with SYBR Green PCR Master Mix (Applied Biosystems) with 5 mL of 12-fold diltued RT-reaction, 1.8 μM primer and 1x master mix concentration on an ABI 7300 qPCR instrument (Applied Biosystems). The expression levels of all samples were normalised to a GUSB gene. Primer sequences were obtained from Harvard Primer bank and previously published reports (30).

DNA melting temperature assay

DNA melting assay was performed on a thermally controlled cell in a Cary 100 UV-Vis spectrophotometer in quartz cuvettes. The DNA oligonucleotides and polyamides were added to an aqueous solution of 10 mM sodium cacodylate, 10 mM KCl, 10 mM $MgCl_2$ and 5 mM $CaCl_2$ at pH 7.0, at 2 mM and 4 mM respectively. The data was recorded in a thermal cycle, where the solution was first heated to 90 C (to anneal oligonucleotides) and cooled to 25 C at 5 C/minute. Subsequently, the temperature was increased from 25C to 90C at rate of 0.5C/min and for each temperature the absorbance at 260 nm was recorded for solutions containing only oligonucleotides or both oligonucleotides and polyamides. The reported melting temperatures were defined as the maximum of the first derivative in temperature of the absorption at 260nm between 25C and 90C. The value of melting temperatures for samples with only DNA were subtracted from the samples containing both polyamides and DNA to extract the ΔT_m, or the stabilization temperature.

Confocal microscopy imaging

For nuclear uptake imaging 12000 A549 cell (ATCC) were plated on a glass optical window in 35mm dishes (MatTek product no. P35G-0-14-C). Cells were grown in 200ul of F12-K medium (ATCC) for 24 h. The cells were then washed with PBS twice and the medium was replaced with 1 ml of a fresh F12-K CT medium supplemented with FITC-labeled polyamides (at 10 mM) in DMSO (final concentration 0.1%). Subsequently the cells were incubated at 37C for 48 h washed twice with PBS and imaged in a Zeiss LSM exciter inverted confocal microscpe with a 63x/F1.4 oil immersion lens.

FITC-conjugated polyamides were imaged in multi-track mode using 488nm laser excitation with a pinhole of 375 mm and standard filter for fluorescein. All images were analyzed using Zeiss LSM software.

Appendix B: Structures of GRE targeting polyamides

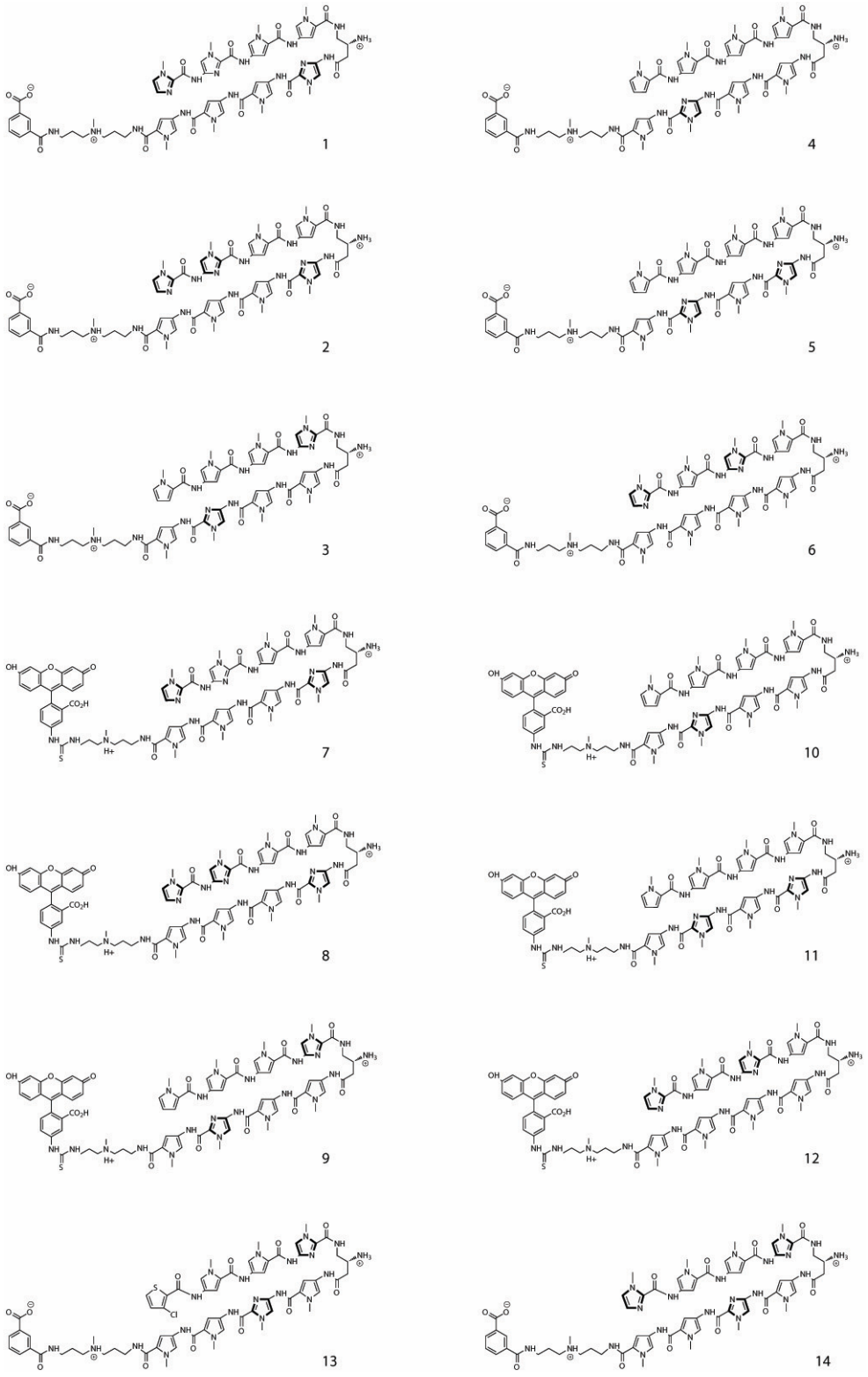

Appendix C: RT-qPCR primers used

PER1_1F CATCATGTTCTCTTGGCTGGTGG
PER1_2F GATCTTTCTTCCCCTACTCCCCG
PER1_3F GATTGGCTGGGGATCTCTTCC
PER1_1R AGGACGGCTGTCGTTTTGTTG
PER1_2R GGCGCTCAGAAAATGCTCAGTAG
PER1_3R CAGCCCTGACCTTAGTGGAGACC
ZFP36_1F CCTCTCCCTCAGTCCTTCCTGAC
ZFP36_1R GACACAGAGGAGTGGCACACAGA
PTGR4_1Fw CATCATCTGCGCCATGAGTGT
PTGR_14Re GCTTGTCCACGTAGTGGCT
PTGR4_2Fw CACTACGTGGACAAGCGATTG
PTGR4_2Re CATAGACTGCAAAGAGCGTGAG
SOCS1_Fw TTTTCGCCCTTAGCGTGAAGA
SOCS1_Re GAGGCAGTCGAAGCTCTCG
SPRY1_1Fw GCAGTGGCAGTTCGTTAGTTG
SPRY1_1Re TCTCTGACGGCTATCCAAAGAA
SPRY1_2Fw GGATAGCCGTCAGAGATTAGACT
SPRY1_2Re GCTGCCTCTTATGGCCTTGA
SPRY1_3Fw TTCGGTGGTGAAAAGACCTGC
SPRY1_3Re CCCTGGCATTACTTGGGAGT
RASD1_1Fw AGCTGAGTATCCCGGCCAA
RASD1_1Re CGAGGATGACCATGCGATAGC
RASD1_2Fw TACACGCCTACCATCGAGGA
RASD1_2Re ACACCAGGATGAAAACGTCTC
p57KIP2_FO AACGCCGAGGACCAGAA
p57KIP2_RE ACCGAGTCGCTGTCCACTT
FKBP5_FO AGGCTGCAAGACTGCAGATC
FKBP5_RE CTTGCCCATTGCTTTATTGG
ANGPTL4_FO ATTCTTTCCAGCGGCTTCTG
ANGPTL4_RE GAGGACTGGAGACGCGGAG
FLJ11127_FO GACAAGGAGCCCCACG
FLJ11127_RE GCTTGTAGCTAGCATCCAGGA
MCJ_FO AGGAGGATTTGAACAGAAAATG
MCJ_RE CTATGAGCTGTTCTAATCTTAG
Cidec1Fw TCCCTTAGCCTTCTCTACCCC
Cidec1Re AGGTACGCACTGACACATGC
Cidec2Fw TGTGTCAGTGCGTACCTCTG

Cidec2Re CCTTCCTCACGCTTCGATCC
Cidec3Fw ATTGATGTGGCCCGTGTAACG
Cidec3Re CAGCAGTGCAGATCATAGGAAA
GilzFw TGG TGG CCA TAG ACA ACA AG
GIlzRe TGC TCC TTC AGG ATC TCC AC
IHPK3_Fw TTCTCGCTGGTGGAAGACAC
IHPK3_Re CAGCAACAAGAACCGATGC
ENaC_Fw AGCACAACCGCATGAAGAC
ENaC_Re TGAGGTTGATGTTGAGGCTG
EKI2_Fw CTACTGCACCTTCCAGAATGG
EKI2_Re CCGTTGGCGTGGATAGTATG
S100P_Fw TGATGGAGAAGGAGCTACCAG
S100P_re ACTTGTGACAGGCAGACGTG
GPR153_Fw CTGGATGGTGTCCTTCATCC
GPR153_Re GATCTCAGCCACGATGAAGC

Appendix D: Code

Dynamics modeling of polyamide uptake and binding.

```
% filename: PolySim.m
%close all; % close all figures
clear; % clear variables
% Initial Conditions:
accessible=0.1;
NucPoly = 0; % Polyamide in nucleus, units M
OutPoly = 10^-5; % Polyamide in the medium, units M
DNA_match=53.8*10^-6*1.4*accessible; % Concentration of match sequences in A549, multiplied by 1.4 because cells are hypotriploid with 65ish chromosomes
DNA_mis=1.792*10^-3*1.4*accessible; % Concentration of mismatch sequences in A549, multiplied by 1.4 because cells are hypotriploid with 65ish chromosomes
selectivity=50; % Polyamide selectivity
ku=1/(96*3600); % units 1/s
ke=100*ku; % units 1/s
kd=1/(48*3600); % units 1/s
tstart = 0; % simulation start time (seconds)
tfinish_values = [3600*7*24]; % simulation end time (seconds)
options=odeset('maxstep',10); % (insures the the integration has a maximum stepsize of 1)

for i = 1:1,
```

```
% %Cycle, Baliga et al, 2001
% kon=15*10^7; % units 1/(M*s)
% koff=2*10^-3; % units 1/s
% k2=8*10^7; % units 1/(M*s)
% k_2=0.065; % units 1/s
% %2B3, Chen 2010, Molecular Therapy
% kon=9.76*10^4; % units 1/(M*s)
% koff=5.2*10^-4; % units 1/s
% k2=2.39*10^3; % units 1/(M*s)
% k_2=1.31*10^-3; % units 1/s
%
% %Hairpin, Baliga et al, 2001
% kon=7*10^7; % units 1/(M*s)
% koff=2*10^-3; % units 1/s
% k2=6*10^7; % units 1/(M*s)
% k_2=0.151; % units 1/s
%Weak binder
kon=2*10^3; % units 1/(M*s)
koff=2*10^-3; % units 1/s
k2=10^2; % units 1/(M*s)
k_2=10^-2; % units 1/s

tfinish = tfinish_values(i);
%-------------------------------------------------------------------------
% Simulate and Plot the Full ODE solution to E + S <--> ES --> E + P
initial_conditions = [ NucPoly; % initial amount of Nuclear Polyamide
OutPoly; % initial amount of E
0; % initial amount of DNAPmatch
0; % initial amount of DNAPmmismatch
DNA_match; %initial amount of DNA match
DNA_mis]'; %initial amount of DNA mismatch
tic % keep time
[t y]=ode23t('PolyFunc_nondeplet',[tstart tfinish],initial_conditions,options,ku,ke,kd,kon,koff,
k2,k_2);
t_elapse = toc; % keep time
% display the time it took to integrate full ODEs

sprintf('Time to integrate full ODEs was %3.3f seconds.',t_elapse)
```

```
Pnuc=y(:,1); % Nuclear polyamide
Pout=y(:,2); % External Polyamide
Pmatch=y(:,3); % DNA match bound polyamide
Pmis=y(:,4); % DNA mismatch bound polyamide
% plot the concentrations of S, E, ES, P as a function of time
t=t/3600;
figure(i),
plot(t,Pnuc,'-r',t,Pmatch,'-b',t,Pmis,'-g', t, Pout, '-y',t, Pmis+Pmatch,'k');
legend('Pnuc','Pmatch','Pmis','Pout','Total Bound');
xlabel('Time (hrs)');
ylabel('Concentration (M)');
titletext = ['Full ODE Solution to Polyamide binding and uptake'];
title(titletext)
hold on
figure(i+1),
plot(t, Pmis./Pmatch,'k');
legend('Pnuc','Pmatch','Pmis','Pout','Total Bound');
xlabel('Time (hrs)');
ylabel('Concentration (M)');
titletext = ['Full ODE Solution to Polyamide binding and uptake'];
title(titletext)

hold on


end
function dydt = mmfunc(t,y,flag,ku,ke,kd,kon,koff, k2,k_2)
Pinside=y(1);
Poutside=y(2);
DNAPmatch=y(3);
DNAPmis=y(4);
DNAmatch=y(5);
DNAmis=y(6);
dydt = [ku*Poutside-ke*Pinside-kon*DNAmatch*Pinside+koff*DNAPmatch-
k2*DNAmis*Pinside+k_2*DNAPmis-kd*Pinside;

0;
```

```
kon*DNAmatch*Pinside-koff*DNAPmatch;
k2*DNAmis*Pinside-k_2*DNAPmis;
-kon*DNAmatch*Pinside+koff*DNAPmatch;

-k2*DNAmis*Pinside+k_2*DNAPmis]; % d[P]/dt
```

Appendix E: Full list of sequences of top 10% most Dexamethasone-induced GREs (5'-3'):

GAGAACAGTATGTCCT	AAGGACACCGTGTGCT	CAGAACTTTCTGTACT	AGAACAACGTGTTCTG
AGAACAGTATGTCCTC	AGGACACCGTGTGCTA	CAGTACACAGTGTGCT	CGGAACACCGTGTTCT
GGGAACACTGTGTCCT	GGGACAGGATGTTCCT	AGTACACAGTGTGCTC	AAGCACATACTGTTCA
GGGAACACTATGTCCT	CAGAACATCCTGTTCT	CAGGACATTTTGTCCT	GGAACAGAATGTCCTG
AGGAACATCATGTCCT	AGAACATCCTGTTCTT	AGGACAGAATGTTCCA	AGCACATGATGTGCCC
AGGAACACTGTGTCCT	TGGAACACTCTGTCCT	GGGAACATTTTGTGCT	CAGCACAGAATGTTCT
AGGACACAGTGTTCCT	CTGGACACTCTGTCCT	TGGAACACTCTGTTCT	AGCACAGAATGTTCTG
AGGACACAGTGTTCCT	CAGGACAGCGTGTGCT	TAGGACATGGTGTTCT	AGCACACACTGTCCCA
GAGGACATACTGTTCT	AGGACAGCGTGTGCTC	AGGACATGGTGTTCTG	CAGTACACAGTGTCCT
AGGACATACTGTTCTC	AGCACAGTGTGTTCCC	AAGGACATGGTGTTCT	AGTACACAGTGTCCTC
GTGGACATGGTGTACT	AGAACAAAGTGTGCCA	AGGACATGGTGTTCTT	GAGGACACATTGTCCT
GGGACAGAATGTGCCT	TGGCACACTTTGTTCT	CTGAACAGCCTGTCCT	AGGACACATTGTCCTC
CAGAACACTATGTCCT	CTGGACATAGTGTGCT	GGGAACAGCCTGTCCT	CAGCACCTTCTGTTCT
AGAACACTATGTCCTG	AGCACAGCGTGTTCCT	AGGCACATGCTGTTCT	CAGAACATGGTGTCCT
CAGAACATTCTGTGCC	AGAACAGCATGTGCAT	TTGTACATGTTGTTCT	AGAACATGGTGTCCTG
GGTACACAATGTCCTG	CAGAACATCCTGTACC	CTGCACACTCTGTTCT	TTGAACAGGCTGTTCT
AGAACAGCCTGTACAG	CAGAACATCCTGTACC	AAGGACAGCCTGTCCT	TAGGACAATTTGTACT
AGAACAGTATGTGCAA	TGGAACATCCTGTACC	AGGACAGCCTGTCCTC	AGCACAGGGTGTTCCC
GGGTACATTCTGTCCT	CAGTACACACTGTACT	CGGTACACTGTGTCCT	GGAACAGGATGTCCTG
CAGGACACTGTGTCCT	AGTACACACTGTACTT	AAGAACAGACTGTCCT	AAGAACATGGTGTCCT
AGGACACTGTGTCCTG	GAGTACAGCTTGTCCT	AGAACAGACTGTCCTT	AGAACATGGTGTCCTG
GAGAACAGCATGTCCT	AGTACAGCTTGTCCTG	ATGTACAGCCTGTGCT	GGAACAGGATGTTCTT
AGAACAGCATGTCCTG	TGGTACACTGTGTTCT	GAGAACAAGCTGTGCT	AGCACAGACTGTTCCC
AGTACACGATGTACAA	CTGTACATACTGTGCT	AGAACAAGCTGTGCTT	AAGTACAGTATGTACT
AGAACAAGCTGTTCCT	CAGAACATCCTGTTCC	GAGGACAGTGTGTTCT	AGTACAGTATGTACTG
GGGGACATGCTGTCCT	AGGGACATTCTGTTCT	AGGACAGTGTGTTCTA	GGAACAGGATGTGCTC
CAGGACACTGTGTCCT	AGAACAGTGTGTTCAT	AGCACAGAAAGTTCTG	GGTACAGAATGTTCCA
AGGACACTGTGTCCTC	TGGGACAGCCTGTGCT	AGGGACACGCTGTTCT	AAGGACATCCTGTGCT
CAGGACACTGTGTCCT	GTGAACAGTCTGTACT	AGAACAGAGTGTTCGA	AGGACATCCTGTGCTG
AGGACACTGTGTCCTC	AGAACAGTACGTTCTG	TTGCACATGCTGTTCT	GAGAACAAGGTGTCCT
CAGGACACTGTGTCCT	AGGACAGGCTGTTCCA	GGGACAGAATGTTCAG	AGAACAAGGTGTCCTG
AGGACACTGTGTCCTC	TAGGACATGCTGTTCC	AGCACAGGACGTGCTC	AAGTACAGGGTGTTCT

CAGGACACTGTGTCCT	CAGAACACCCTGTTCT	GGAACAGAATGTTCCC	AGTACAGGGTGTTCTG
AGGACACTGTGTCCTC	AGAACACCCTGTTCTG	GAGGACATGCTGTGCT	GAGGACATACTGTACC
CAGCACAGTCTGTCCC	AAGAACATCCTGTGCC	AGGACATGCTGTGCTC	AGGACATACTGTACCT
AGCACAGTCTGTCCCC	GAGTACAACCTGTTCT	GAGGACAGAATGTTCT	GGGCACAATCTGTACT
TAGAACATTCTGTGCT	AGTACAACCTGTTCTC	AGGACAGAATGTTCTG	AGGGACATAATGTGCT
AGAACATTCTGTGCTC	GGGACACAATGTCCTC	GAGGACAGAATGTGCT	GGGACATAATGTGCTG
AGGACAGAATGTTCCA	AAGTACAATGTGTGCT	AGGACAGAATGTGCTT	CAGAACAAACTGTGCT
GGGACAGAGTGTCCTC	AGTACAATGTGTGCTA	AAGGACATTTTGTGCT	AGAACAAACTGTGCTC
TGGAACACTATGTACT	CAGAACAGCATGTACT	AAGTACATTTTGTTCT	TTGCACATGGTGTTCT
AGTACAGCCTGTTCCC	AGAACAGCATGTACTC	GGGACAGAATGTGCCT	GGGCACATGCTGTCCT
GAGAACATTGTGTTCT	AGGGACAGTTTGTTCT	GGGTACAGGCTGTACT	CTGTACACACTGTCCT
AGAACATTGTGTTCTG	AAGAACAGAATGTTCT	GAGAACAGCGTGTTCT	GAGCACATTTTGTCCT
GAGGACAGTCTGTGCT	AGAACAGAATGTTCTT	AGAACAGCGTGTTCTT	AGCACAGGATGTGCCC
AGGACAGTCTGTGCTC	CAGTACATTATGTTCC	TAGAACAGCCTGTCCT	AGTACATCATGTACAT
AAGTACAACTTGTCCT	AGTACATTATGTTCCC	AGAACAGCCTGTCCTC	GGAACAGCATGTGCTA
GAGGACACTGTGTCCT	CAGAACACTTTGTCCT	GAGTACAGAGTGTTCT	AGGACAGGATGTTCCA
AGGACACTGTGTCCTG	GAGGACAGCCTGTTCT	AGTACAGAGTGTTCTG	AGGGACACCCTGTCCT
AGAACAGTATGTTCAA	AGGACAGCCTGTTCTT	CGGAACATTTTGTCCT	CAGAACATCCTGTGCC
AGAACACACTGTACCC	AGGCACATTCTGTACT	AGGTACAGACTGTTCT	CAGAACATCCTGTGCC
TGGTACACTCTGTACT	AGGACAGAATGTTCCG	GGTACAGACTGTTCTT	CAGAACATCCTGTGCC
GAGAACACAGTGTTCT	CTGCACAATCTGTCCT	AGAACAGCATGTTCCT	CAGAACATCCTGTGCC
AGAACACAGTGTTCTA	AGGACACCATGTTCCT	CAGAACATGCTGTGCT	CAGAACATCCTGTGCC
AGCACAGAGTGTGCCA	CAGAACATCTTGTTCC	AGAACATGCTGTGCTC	CAGAACATCCTGTGCC
AGAACAGGATGTGCAT	AAGCACAGCCTGTCCT	GGAACACAATGTCCTG	CAGAACATCCTGTACC
CAGGACAGGCTGTTCT	AGCACAGCCTGTCCTT	GGGAACATCATGTTCT	CAGAACATCCTGTGCC
AGGACAGGCTGTTCTT	GAGAACAGGCTGTTCT	CAGAACAGGATGTTCT	AGCACAGGATGTCCCT
GGGACAGAATGTCCTG	AGAACAGGCTGTTCTC	AGAACAGGATGTTCTG	CAGGACATTGTGTCCA
AAGGACAGGGTGTTCT	CAGGACATCGTGTACC	AGGACAGGATGTCCCA	CAGTACATACTGTACT
AGGACAGGGTGTTCTA	CTGTACACTCTGTTCT	CAGAACACCCTGTACT	AGTACATACTGTACTG
AGGACAGTACGTTCTG	ATGAACATAATGTTCT	AGAACACCCTGTACTG	TTGAACATGTTGTACT
TGGAACACTCTGTCCT	CAGAACAGAGTGTCCT	CAGCACATTCTGTTCC	GAGCACATTTTGTTCA
CAGAACATTTTGTACC	AGAACAGAGTGTCCTG	TAGAACATTATGTTCT	TTGTACATGTTGTTCT
CAGTACAGTGTGTGCT	CAGAACAATTTGTTCT	AGAACATTATGTTCTA	AAGTACACTCTGTACT
AGTACAGTGTGTGCTT	AGAACAATTTGTTCTC	AGTACAGGGTGTCCCA	AGTACACTCTGTACTC
TTGAACATACTGTGCT	CAGAACACTGTGTACT	AGGACACCATGTCCAT	AAGAACAGAGTGTGCT
AAGTACATTTTGTCCT	AGAACACTGTGTACTC	GAGAACAGCATGTTCT	AGAACAGAGTGTGCTG
TAGGACATTTTGTTCC	GAGTACACAATGTGCT	AGAACAGCATGTTCTT	AGGACAAGTTGTACTT
GGCACAGGATGTCCTC	AGTACACAATGTGCTA	CAGCACATTCTGTCCC	GGGGACATTGTGTCCT
AGAACAGGTTGTGCCG	AGTACAAGATGTGCCC	CAGGACAGCTTGTCCT	AGGCACAGTTTGTTCT
AAGAACAGACTGTCCT	AAGAACACAATGTCCT	AGGACAGCTTGTCCTG	TGGAACATTCTGTTCC
AGAACAGACTGTCCTA	AGAACACAATGTCCTG	TAGAACATTCTGTCCC	GGAACAGAATGTACTT

AAGCACAGGATGTTCT	GGAACAGCATGTTCCA	AGGCACAGTGTGTACT	AAGAACATGATGTGCT
AGCACAGGATGTTCTT	AGGACAGGGTGTCCCG	AGGCACAGTGTGTACT	AGAACATGATGTGCTC
CAGCACAGAATGTTCT	AGCACAGTGTGTTCCA	AGGCACAGTGTGTACT	GGGGACACTCTGTTCT
AGCACAGAATGTTCTT	GGGAACAGTCTGTGCT	AGGCACAGTGTGTACT	AGCACACAATGTTCGT
AGAACAGGGTGTTCCC	GAGTACATCTTGTCCT	GGCACAAAATGTGCTT	GGGACAGCATGTTCCA
GGGACAGGATGTCCCC	CAGGACATTCTGTTCT	GGGAACAGGCTGTTCT	GGGGACATTTTGTGCT
CAGCACATTCTGTTCC	AGGACATTCTGTTCTT	AGTACACACTGTTCCT	AGAACAGAACGTTCTC
TAGGACATTCTGTTCT	GAGAACAATTTGTGCT	CAGGACATGCTGTGCT	GGAACAGGATGTTCCA
AGGACATTCTGTTCTT	AGAACAATTTGTGCTG	AGGACATGCTGTGCTG	AAGCACATCATGTCCT
GGCACAGAATGTCCCC	AGAACAGCATGTGCAG	CAGAACAGCATGTCCT	AGCACATCATGTCCTT
AAGAACAGGATGTTCT	AGCACAGGCTGTTCCT	AGAACAGCATGTCCTG	TGAACAGGATGTCCTA
AGAACAGGATGTTCTG	AGGGACAGGCTGTGCT	AGGACAGAGTGTACCG	CAGAACATGCTGTGCA
TAGGACATTCTGTGCC	AGGACAGAGTGTGCAT	GAGTACACGGTGTGCT	TGTACAGCATGTACTG
GGGGACAGCCTGTTCT	AAGTACACTCTGTCCT	AGTACACGGTGTGCTG	TTGAACATGGTGTGCT
CAGTACACTCTGTGCT	AGTACACTCTGTCCTG	GAGAACATAATGTTCT	TGGGACACACTGTCCT
AGTACACTCTGTGCTT	AGAACAAAATGTGCAT	AGAACATAATGTTCTA	TGGGACACACTGTCCT
TGGTACAGTTTGTACT	TGGAACAGTTTGTCCT	CAGGACAGGCTGTGCT	TTGTACATGGTGTTCT
TAGGACAGTGTGTGCT	GGAACAGAATGTGCTT	AGGACAGGCTGTGCTT	CAGGACAAACTGTTCT
AGGACAGTGTGTGCTC	AGCACAGGGTGTACAG	AAGTACATTCTGTTCT	AGGACAAACTGTTCTC
AGGACAGAATGTCCAC	TGGACAAAATGTACTA	AGTACATTCTGTTCTT	AGAACAGCATGTGCAA
AGTACAGCCTGTTCAG	AGGAACAGTCTGTTCT	GGGAACAGCCTGTGCT	CAGGACGTTCTGTACT
CAGGACAGACTGTGCT	CAGCACATTCTGTTCT	GAGCACATGCTGTTCA	CTGTACATGGTGTGCT
AGGACAGACTGTGCTT	AGCACATTCTGTTCTG	TGAACAGCATGTGCTC	GGAACAGAGTGTACTC
GGGCACACCCTGTGCT	GGTACAGAATGTACCC	CTGTACATTTTGTGCT	AGCACAAGATGTCCAC
TGGACAGAATGTTCTG	GGGAACATTCTGTACA	AGGACACAGTGTTCCT	TGAACAGAATGTACCG
CTGAACATTCTGTACC	CAGGACATTCTGTTCG	ATGAACATGTTGTTCT	AGGTACATACTGTCCT
AGAACAAGGTGTGCTG	AGTACAAGATGTACCT	AGGACAGGGTGTCCAT	
AGAACAGGCTGTACCC	CAGCACAGTCTGTACC	AGGGACATTCTGTGCT	
AGGACAAACTGTCCCA	AGCACAGTCTGTACCC	CAGAACAACGTGTTCT	

Appendix F: DNA oligomer sequences for thermal denaturation assay

WCWW_GRE_EMSA	GCATTGCTAGAACATTATGTTCTGCTCTCCC
WCWG_GRE_EMSA	GCATTGCAGAACAGTTTGTCCTGGCTCTCCC
WCWC_GRE_EMSA	GCATTGCAGTACACAGTGTTCTGGCTCTCCC
GWWC_Single_EMSA	GCATTGCAGTACAGGGTGTCCCAGCTCTCCC
GWWC_Double_EMSA	GCATTGCCAGAACATCCTGTTCTGCTCTCCC
WCWW_RT_GRE_EMSA	GGGAGAGCAGAACATAATGTTCTAGCAATGC
WCWG_RT_GRE_EMSA	GGGAGAGCCAGGACAAACTGTTCTGCAATGC
WCWC_RT_GRE_EMSA	GGGAGAGCCAGAACACTGTGTACTGCAATGC
GWWC_RT_Single_EMSA	GGGAGAGCTGGGACACCCTGTACTGCAATGC

GWWC_RT_Double_EMSA	GGGAGAGCAGAACAGGATGTTCTGGCAATGC
WCWC_TM_Fw	CGATACTCAAGC
WCWC_Tm_Re	GCTTGAGTATCG
WCWW_Tm_Fw	CGATACTTAAGC
WCWW_Tm_Re	GCTTAAGTATCG
WCWG_TM_Fw	CGATACTGAAGC
WCWG_Tm_Re	GCTTCAGTATCG
GWWC_TM_Fw	CGATGTTCAAGC
GWWC_TM_Re	GCTTGAACATCG
GGWC_TM_Fw	CGATGGTCAAGC
GGWC_TM_Re	GCTTGACCATCG
GCWC_TM_Fw	CGATGCTCAAGC
GCWC_TM_re	GCTTGAGCATCG
GWWC_GRE_Fw	AAGAACATCCTGTGCC
GWWC_GRE_Re	GGCACAGGATGTTCTT
GGWC_GRE_Fw	AAGGACACCGTGTGCT
GGWC_GRE_Re	AGCACACGGTGTCCTT
GW/GWC_GRE_Fw	AGGACATTCTGTTCTT
GW/GWC_GRE_Re	AAGAACAGAATGTCCT

Appendix G: Code for modeling genomic distribution of GREs and Transcription Starting Sites

(Mathematica)

```
Modeling distribution of genes and GREs in the genome
genomesizeminustelos = 0.7*3*10^9
2.1*10^9
downreg = Round[0.41*234]
96
upreg = 234 - downreg
138
plotsdistances =
Table[genes = Table[Random[], {i, 1, downreg}];
GREs = Table[Random[], {i, 1, 4392}]; genomesize = 0.7*3*10^9;
distances =
Sort[Table[
Min[Table[Min[Abs[genes[[i]] - GREs[[j]]]], {j, 1, 4392}]], {i,
1, downreg}]] ; mediandistance = 0.7*3*10^9*Median[distances];
realdistances = distances*genomesizeminustelos;
realdistancestoplot =
Table[{realdistances[[i]], i}, {i, 1, downreg}];
logtwo =
```

```
ListLogLinearPlot[{{10^3, .20*downreg}, {2*10^4, .50*
downreg}, {10^5, .85*downreg}, {2*10^6, downreg}},
AxesOrigin -> {10, 0}, PlotStyle -> Hue[0.1], Joined -> True];
logone =
ListLogLinearPlot[Reverse[realdistancestoplot],
AxesOrigin -> {10, 0}, Joined -> True]; logone, {k, 1, 25}];
mediandistancesplot =
Table[genes = Table[Random[], {i, 1, downreg}];
GREs = Table[Random[], {i, 1, 4392}]; genomesize = 3*10^9;
distances =
Sort[Table[
Min[Table[Min[Abs[genes[[i]] - GREs[[j]]]], {j, 1, 4392}]], {i,
1, downreg}]] ; notelomeres = 0.7;
mediandistance = notelomeres*genomesize*Median[distances];
mediandistance, {k, 1, 250}];
Mean[mediandistancesplot]
166589.
Print[Show[plotsdistances]]
-----------------------------------------
plotsdistances =
Table[genes = Table[Random[], {i, 1, downreg}];
GREs = Table[Random[], {i, 1, 4392}]; genomesize = 0.7*3*10^9;
distances =
Sort[Table[
Min[Table[Min[Abs[genes[[i]] - GREs[[j]]]], {j, 1, 4392}]], {i,
1, downreg}]] ; mediandistance = 0.7*3*10^9*Median[distances];
realdistances = distances*genomesizeminustelos;
realdistancestoplot =
Table[{realdistances[[i]], i}, {i, 1, downreg}];
logtwo =
ListLogLinearPlot[{{10^3, .20*downreg}, {2*10^4, .50*
downreg}, {10^5, .85*downreg}, {2*10^6, downreg}},
AxesOrigin -> {10, 0}, PlotStyle -> Hue[0.1], Joined -> True];
logone =
ListLogLinearPlot[Reverse[realdistancestoplot],
AxesOrigin -> {10, 0}, Joined -> True]; logone, {k, 1, 25}];
mediandistancesplot =
Table[genes = Table[Random[], {i, 1, downreg}];
GREs = Table[Random[], {i, 1, 4392}]; genomesize = 3*10^9;
distances =
```

```
Sort[Table[
Min[Table[Min[Abs[genes[[i]] - GREs[[j]]]], {j, 1, 4392}]], {i,
1, downreg}]] ; notelomeres = 0.7;
mediandistance = notelomeres*genomesize*Median[distances];
mediandistance, {k, 1, 250}];
Mean[mediandistancesplotup]
10732.4
Print[Show[plotsdistancesflat]]
```

References

1. White S, Szewczyk JW, Turner JM, Baird EE, & Dervan PB (1998) Recognition of the four Watson-Crick base pairs in the DNA minor groove by synthetic ligands. *Nature* 391(6666):468-471.
2. Dervan PB & Edelson BS (2003) Recognition of the DNA minor groove by pyrrole-imidazole polyamides. *Current opinion in structural biology* 13(3):284-299.
3. Gottesfeld JM*, et al.* (2001) Sequence-specific recognition of DNA in the nucleosome by pyrrole-imidazole polyamides. *J. Mol. Biol.* 309(3):615-629.
4. Meier JL, Yu AS, Korf I, Segal DJ, & Dervan PB (2012) Guiding the design of synthetic DNA-binding molecules with massively parallel sequencing. *Journal of the American Chemical Society* 134(42):17814-17822.
5. Erwin GS, Bhimsaria D, Eguchi A, & Ansari AZ (2014) Mapping polyamide-DNA interactions in human cells reveals a new design strategy for effective targeting of genomic sites. *Angew Chem Int Ed Engl* 53(38):10124-10128.
6. Bell O, Tiwari VK, Thoma NH, & Schubeler D (2011) Determinants and dynamics of genome accessibility. *Nat Rev Genet* 12(8):554-564.
7. John S*, et al.* (2011) Chromatin accessibility pre-determines glucocorticoid receptor binding patterns. *Nat. Genet.* 43(3):264-268.
8. Mitchell PJ & Tjian R (1989) Transcriptional regulation in mammalian cells by sequence-specific DNA binding proteins. *Science* 245(4916):371-378.
9. Gilbert W & Maxam A (1973) The nucleotide sequence of the lac operator. *Proc Natl Acad Sci U S A* 70(12):3581-3584.
10. Garner MM & Revzin A (1981) A gel electrophoresis method for quantifying the binding of proteins to specific DNA regions: application to components of the Escherichia coli lactose operon regulatory system. *Nucleic Acids Res* 9(13):3047-3060.
11. Galas DJ & Schmitz A (1978) DNAse footprinting: a simple method for the detection of protein-DNA binding specificity. *Nucleic Acids Res* 5(9):3157-3170.
12. Johnson DS, Mortazavi A, Myers RM, & Wold B (2007) Genome-wide mapping of in vivo protein-DNA interactions. *Science* 316(5830):1497-1502.
13. Carter D, Chakalova L, Osborne CS, Dai YF, & Fraser P (2002) Long-range chromatin regulatory interactions in vivo. *Nat Genet* 32(4):623-626.
14. Reddy TE*, et al.* (2009) Genomic determination of the glucocorticoid response reveals unexpected mechanisms of gene regulation. *Genome Res* 19(12):2163-2171.
15. Dekker J, Rippe K, Dekker M, & Kleckner N (2002) Capturing chromosome conformation. *Science* 295(5558):1306-1311.

16. Dostie J & Dekker J (2007) Mapping networks of physical interactions between genomic elements using 5C technology. *Nat Protoc* 2(4):988-1002.
17. Zhao Z*, et al.* (2006) Circular chromosome conformation capture (4C) uncovers extensive networks of epigenetically regulated intra- and interchromosomal interactions. *Nat Genet* 38(11):1341-1347.
18. Simonis M, Kooren J, & de Laat W (2007) An evaluation of 3C-based methods to capture DNA interactions. *Nat Methods* 4(11):895-901.
19. Gondor A, Rougier C, & Ohlsson R (2008) High-resolution circular chromosome conformation capture assay. *Nat Protoc* 3(2):303-313.
20. Kielkopf CL*, et al.* (1998) A structural basis for recognition of A.T and T.A base pairs in the minor groove of B-DNA. *Science* 282(5386):111-115.
21. Luisi BF*, et al.* (1991) Crystallographic analysis of the interaction of the glucocorticoid receptor with DNA. *Nature* 352(6335):497-505.
22. Muzikar KA, Nickols NG, & Dervan PB (2009) Repression of DNA-binding dependent glucocorticoid receptor-mediated gene expression. *Proc. Natl. Acad. Sci. U. S. A.* 106(39):16598-16603.
23. Buttgereit F, Burmester GR, & Lipworth BJ (2005) Optimised glucocorticoid therapy: the sharpening of an old spear. *Lancet* 365(9461):801-803.
24. Leonard MB*, et al.* (2004) Long-term, high-dose glucocorticoids and bone mineral content in childhood glucocorticoid-sensitive nephrotic syndrome. *N Engl J Med* 351(9):868-875.
25. Brown TA (2007) *Genomes 3* (Garland Science Pub., New York) 3rd Ed pp xxii, 713 p.
26. Gearhart MD*, et al.* (2005) Inhibition of DNA binding by human estrogen-related receptor 2 and estrogen receptor alpha with minor groove binding polyamides. *Biochemistry* 44(11):4196-4203.
27. Nickols NG & Dervan PB (2007) Suppression of androgen receptor-mediated gene expression by a sequence-specific DNA-binding polyamide. *Proc. Natl. Acad. Sci. U. S. A.* 104(25):10418-10423.
28. Dervan PB & Burli RW (1999) Sequence-specific DNA recognition by polyamides. *Curr Opin Chem Biol* 3(6):688-693.
29. Farkas ME, Li BC, Dose C, & Dervan PB (2009) DNA sequence selectivity of hairpin polyamide turn units. *Bioorg Med Chem Lett* 19(14):3919-3923.
30. Wang JC*, et al.* (2004) Chromatin immunoprecipitation (ChIP) scanning identifies primary glucocorticoid receptor target genes. *Proc. Natl. Acad. Sci. U. S. A.* 101(44):15603-15608.
31. Dose C, Farkas ME, Chenoweth DM, & Dervan PB (2008) Next generation hairpin polyamides with (R)-3,4-diaminobutyric acid turn unit. *J Am Chem Soc* 130(21):6859-6866.
32. Chenoweth DM, Harki DA, Phillips JW, Dose C, & Dervan PB (2009) Cyclic pyrrole-imidazole polyamides targeted to the androgen response element. *J Am Chem Soc* 131(20):7182-7188.
33. Best TP, Edelson BS, Nickols NG, & Dervan PB (2003) Nuclear localization of pyrrole-imidazole polyamide-fluorescein conjugates in cell culture. *Proc Natl Acad Sci U S A* 100(21):12063-12068.
34. Nickols NG, Jacobs CS, Farkas ME, & Dervan PB (2007) Modulating hypoxia-inducible transcription by disrupting the HIF-1-DNA interface. *ACS Chem. Biol.* 2(8):561-571.
35. Olenyuk BZ*, et al.* (2004) Inhibition of vascular endothelial growth factor with a sequence-specific hypoxia response element antagonist. *Proc. Natl. Acad. Sci. U. S. A.* 101(48):16768-16773.
36. Hsu CF & Dervan PB (2008) Quantitating the concentration of Py-Im polyamide-fluorescein conjugates in live cells. *Bioorg Med Chem Lett* 18(22):5851-5855.
37. Wiley HS, Shvartsman SY, & Lauffenburger DA (2003) Computational modeling of the EGF-receptor system: a paradigm for systems biology. *Trends Cell Biol* 13(1):43-50.

38. Chen M*, et al.* (2010) Pretranscriptional regulation of Tgf-beta1 by PI polyamide prevents scarring and accelerates wound healing of the cornea after exposure to alkali. *Mol. Ther.* 18(3):519-527.
39. Baliga R*, et al.* (2001) Kinetic consequences of covalent linkage of DNA binding polyamides. *Biochemistry* 40(1):3-8.
40. Suto RK*, et al.* (2003) Crystal structures of nucleosome core particles in complex with minor groove DNA-binding ligands. *J. Mol. Biol.* 326(2):371-380.
41. Meier JL, Montgomery DC, & Dervan PB (2012) Enhancing the cellular uptake of Py-Im polyamides through next-generation aryl turns. *Nucleic Acids Res.* 40(5):2345-2356.
42. Turner JM, Baird EE, & Dervan PB (1997) Recognition of Seven Base Pair Sequences in the Minor Groove of DNA by Ten-Ring Pyrrole−Imidazole Polyamide Hairpins. *Journal of the American Chemical Society* 119(33):7636-7644.
43. Matsuda H*, et al.* (2006) Development of gene silencing pyrrole-imidazole polyamide targeting the TGF-beta1 promoter for treatment of progressive renal diseases. *J Am Soc Nephrol* 17(2):422-432.
44. Yan J, Wang HF, Liu YT, & Shao CX (2008) Analysis of Gene Regulatory Networks in the Mammalian Circadian Rhythm. *PLoS Comput. Biol.* 4(10).
45. Yan J, Wang H, Liu Y, & Shao C (2008) Analysis of gene regulatory networks in the mammalian circadian rhythm. *PLoS Comput Biol* 4(10):e1000193.
46. Belitsky JM, Nguyen DH, Wurtz NR, & Dervan PB (2002) Solid-phase synthesis of DNA binding polyamides on oxime resin. *Bioorg. Med. Chem.* 10(8):2767-2774.
47. Puckett JW, Green JT, & Dervan PB (2012) Microwave assisted synthesis of Py-Im polyamides. *Org. Lett.* 14(11):2774-2777.

C h a p t e r 3

ACTIVITY OF A PY-IM POLYAMIDE TARGETED TO THE ESTROGEN RESPONSE ELEMENT

The text of this chapter was taken in part from a manuscript co-authored with Nicholas G. Nickols, Amanda E. Hargrove, Benjamin C. Li, Jevgenij A. Raskatov, and Peter B. Dervan.

(Nickols NG*****, **Szablowski JO***, Hargrove AE, Li BC, Raskatov JA, Dervan PB. "Activity of a Py-Im Polyamide Targeted to the Estrogen response Element," *Mol. Cancer Ther.*, **12**:675-684, (2013). *denotes equal contribution)

Abstract

Pyrrole-imidazole (Py–Im) polyamides are a class of programmable DNA minor groove binders capable of modulating the activity of DNA-binding proteins and affecting changes in gene expression. Estrogen receptor alpha (ERα) is a ligand-activated hormone receptor that binds as a homodimer to estrogen response elements (ERE) and is a driving oncogene in a majority of breast cancers. We tested a selection of structurally similar Py–Im polyamides with differing DNA sequence specificity for activity against 17β-estadiol (E2)–induced transcription and cytotoxicity in ERα positive, E2-stimulated T47DKBluc cells, which express luciferase under ERα control. The most active polyamide targeted the sequence 5′-WGGWCW-3′ (W = A or T), which is the canonical ERE half site. Whole transcriptome analysis using RNA-Seq revealed that treatment of E2-stimulated breast cancer cells with this polyamide reduced the effects of E2 on the majority of those most strongly affected by E2, but had much less effect on the majority of E2-induced transcripts. *In vivo*, this polyamide circulated at detectable levels following subcutaneous injection and reduced levels of ER-driven luciferase expression in xenografted tumors in mice after subcutaneous compound administration without significant host toxicity.

Introduction

Estrogen receptor-alpha (ERα) is a member of the nuclear hormone receptor family of transcription factors and is active in a majority of breast adenocarcinomas (1, 2). Breast tumors that express ERα and are sensitive to circulating estrogens respond to therapeutics that modulate ERα activity (3). Such therapeutics include tamoxifen, a selective ER modulator that acts as a weak agonist/antagonist by binding to the ERα ligand-binding pocket and the aromatase inhibitors that inhibit synthesis of E2 (3). A different strategy for modulation of ERα activity is inhibition of the ERα–ERE interface by a DNA-binding molecule.

Pyrrole-imidazole (Py–Im) polyamides are a class of synthetic, minor groove-binding ligands inspired by the natural product distamycin A (4, 5). Py–Im polyamides are oligomers of aromatic amino acids linked in series to fold in an antiparallel fashion when bound in the minor groove of DNA (4, 5). Sequence specificity is programmed through side-by-side pairings of the Py and Im subunits that recognize differences in the shape and hydrogen bonding pattern presented by the edges of the Watson–Crick base pairs in the floor of the minor groove (6, 7). Binding specificity has been extensively characterized by DNAse I footprinting titrations and other methods. An Im:Py pair preferentially recognizes G:C; Py:Im prefers C:G, and Py:Py is degenerate for A:T and T:A (6, 7). Py–Im polyamide binding in the minor groove also induces allosteric changes to the major groove (8, 9), and binding affinity is sufficient to modulate the binding of DNA-binding proteins (8–11).

In cell culture, selected polyamides have been used to modulate expression of genes induced by testosterone (11), TNF-α (12), hypoxia (13, 14), and dexamethasone (10). The mechanisms by which polyamides affect gene expression changes in cell culture are still

not well understood and may involve direct effects on multiple DNA-dependent processes including transcription factor occupancy, chromatin structure, RNA polymerases, and DNA replication (15). The pharmacokinetics and toxicity of a number of polyamides after intravenous and subcutaneous injection in mice and rats have been described (16–18). In mice, a selected polyamide was reported to induce changes in TGF-β expression in kidney glomeruli, and a fluorescent analog of this polyamide was observed in kidney glomeruli after tail vein injection in rats (19). Gene expression changes have also been observed in tumor xenografts in immune-compromised mice treated with a hairpin-polyamide (20).

In this study, our goal was to identify a Py–Im polyamide capable of affecting E2-stimulated gene expression in breast cancer cells and characterize its activity in cell culture and in tumor xenografts. To do this, we drew from an earlier study that reported a polyamide targeted to the estrogen response element (ERE) consensus half site 5′-WGGWCW-3′ inhibited ERα–binding to DNA in cell-free systems (21). The DNA-binding affinity and specificity of the ERE-targeted polyamide was characterized in this and other studies (21, 22). Since those publications, we have improved the nuclear uptake of polyamides via modification of the C-terminus (23). We have also shown that polyamides are bioavailable after intravenous and subcutaneous injection in mice (20, 24). We then decided to reexamine the activity of polyamides capable of disrupting ERE-driven gene expression for use *in vivo*. We have screened a focused library of polyamides for cytotoxicity and inhibition of luciferase activity using the breast cancer cell line T47D-KBluc that expresses luciferase under the control of 3 tandem, canonical EREs (25). The most active polyamide identified, which targets the consensus ERE, was further evaluated

and showed a partial suppression of E2-stimulated gene expression in cell culture. This polyamide circulated in mouse serum after subcutaneous injection and showed activity against E2-induced luciferase expression in T47D-KBluc tumor xenografts in mice with minimal host toxicity. A fluorescent analog of this polyamide distributed widely in both tumor and mouse tissue after subcutaneous injection.

Materials and Methods

Polyamide synthesis and characterization

The polyamides **1** to **5** were synthesized following previously published solid phase synthesis protocols (26). Compound purities were confirmed by analytic high-performance liquid chromatography (HPLC) and matrix-assisted laser desorption/ionization–time-of-flight (MALDI-TOF) mass spectrometry. Melting temperature analysis was conducted on a Varian Cary 100 spectrophotometer with temperature control. Oligonucleotides (IDTDNA) were dissolved in 10 mmol/L sodium cacodylate, 10 mmol/L KCl, 10 mmol/L $MgCl_2$, and 5 mmol/L $CaCl_2$ at pH 7.0 at a concentration of 2 μmol/L. Polyamides were added to oligo solution to a final concentration of 4 μmol/L in 0.1% dimethyl sulfoxide (DMSO). Oligonucleotides were annealed from 25°C to 90°C and then back to 25°C at 5°C/min. Subsequently, the temperature was elevated at a rate 0.5°C/min between 25°C and 90°C. Melting temperatures are defined as a maximum of the first derivative of absorbance at 260 nm over the range of temperatures.

Cell culture and imaging

Cell lines used were purchased directly from American Type Culture Collection (ATCC) and used within 6 months. No subsequent authentications were done by the authors. All

experiments were carried out with T47D-KBluc cells (ATCC), unless specifically mentioned otherwise. Cells were grown in RPMI-1640 and held at 37°C in 5% CO_2. Media was supplemented with 10% FBS and 1% penicillin/streptamycin. Before imaging, cells were plated in 35-mm optical dishes (MatTek) at 5×10^4 cells per dish in the presence of 10 nmol/L E2. Cells were dosed with polyamide for 24 hours. Cells were then washed twice with PBS and imaged on a confocal microscope (Exciter, Zeiss) using a ×63 oil immersion lens in a method previously described. Confocal imaging was conducted following our previously published protocols (27, 28).

Tissue processing for fluorescence imaging

The tissue sections for fluorescent imaging were obtained by fixing the tumors in 10% formaldehyde solution for 24 hours and subsequent cryoprotection in 15% sucrose (24 hours) and 30% sucrose (24 hours). The tumors were frozen in Tissue-Tek O.C.T. (Sakura Finetek) and 50 μm (for T47D-KBluc xenograft) or 10 μm (for other tissues) sections were obtained using a Leica CM 1800 cryotome. Imaging was conducted as described earlier.

Cell toxicity and luciferase assays

T47D-KBluc cells were plated at 3×10^3 cells per well in 96-well plates, incubated in standard growth media containing 10 nmol/L E2 for 48 hours, and then dosed with medium containing 10 nmol/L E2 and between 2 nmol/L and 50 μmol/L polyamides. The cells were then incubated for 96 hours and analyzed using either WST-1 assay (Roche) or luciferase assay system (Promega) according to the manufacturers' instructions.

Gene expression analysis by qRT-PCR

Cells were plated in 12 well-plates at 1.1×10^5 cells/well and incubated in the growth medium supplemented with 10 nmol/L E2 for 24 hours. Afterward, medium was exchanged with the growth medium supplemented with polyamides and 10 nmol/L E2. Quantitative real-time PCR (qRT-PCR) was conducted according to previously established protocols (3–6). Confirmation of inhibition of *TFF1* expression by polyamides 1 to 4 was carried out and qRT-PCR was conducted following the same timeline as cell toxicity and luciferase assays. Gene expression was normalized against *GUSB* as a housekeeping gene. All primers yielded single amplicons as determined by both melting denaturation analysis and agarose gel electrophoresis. The following primer pairs were used. *GUSB*: forward 5′-CTC ATT TGG AAT TTT GCC GAT T-3′; reverse 5′-CCC AGT GAA GAT CCC CTT TTT A-3′. *DOK7*: forward 5′-GAC AAG TCG GAG CGT ATC AAG-3′; reverse 5′-ATG TCC TCT AGC GTC AGG CT-3′. *WT1*: forward 5′-CAC AGC ACA GGG TAC GAG AG-3′; reverse 5′-CAA GAG TCG GGG CTA CTC CA-3. *TGFB2*: forward 5′-CAG CAC ACT CGA TAT GGA CCA-3′; reverse 5′-CCT CGG GCT CAG GAT AGT CT-3′.

Chromatin immunoprecipitation experiments

T47D-KBluc cells were plated into 500-cm^2 plates and grown in RPMI-1640 with 10% FBS until 75% confluence was reached. Plates were washed with RPMI-1640 with charcoal-treated 10% FBS, and then the media was replaced with RPMI-1640 with charcoal-treated 10% FBS with 2 μmol/L polyamide 1 and incubated for 48 hours. Plates were then treated with 10 nmol/L E2 or vehicle for 45 minutes. Cross-linked chromatin was obtained using the 2-step cross-linking methods previously described (29). Chromatin

was isolated and sheared. Antibodies to ERα (AC-066-100; Diagenode) were used to immunoprecipitate ERα–bound DNA fragments. Cross-links were reversed and PCRs using primers targeted to the regions of interest were used to assess enrichment of bound fragments as compared with negative controls. *TFF1* promoter: forward 5′-TCA GAT CCC TCA GCC AAG AT-3′; reverse 5′-TGG TCA AGC TAC ATG GAA GG-3′. Negative loci control: forward 5′-AAA GAC AAC AGT CCT GGA AAC A-3′; reverse 5′-AAA AAT TGC TCA TTG GAG ACC-3′.

Circulation and toxicity in vivo

All animal experiments were carried out according to approved Institutional Animal Care and Use Committee protocols at the California Institute of Technology (Pasadena, CA). Circulation studies were done as previously described (30). Briefly, 120 nmol of polyamide 1 was injected subcutaneously into the right flank of 4 female C57BL/6 mice in a total of 200 μL of a 20% DMSO/PBS vehicle. Blood was collected retroorbitally at serial time points. Serum was treated with methanol, analyzed via HPLC, and quantified against a standard curve of concentration versus peak area, all as previously described, to determine approximate serum concentrations (24). For toxicity studies, 5 female C57BL/6 mice were injected with 20 nmol of polyamide 1 in a total of 200 μL of a 20% DMSO/PBS vehicle on days 1, 3, 5, 8, 10, 12, and then with 30 nmol on days 15, 17, 19, 22, 24, and 26 and were weighed before each treatment day. Mice were euthanized if weight loss was more than 15% of initial body weight, if dehydration was more than 10%, or if moribund behavior was observed. None were observed in this experiment.

Engraftment of T47D-KBluc.

Experiments were carried out in appropriately shaved female NSG mice (JAX) between 8 and 12 weeks of age. Cells were injected into the left flank area of the animals as suspensions of 5.0×10^6 mL^{-1} in 50% RPMI-1640 growth medium and 50% Matrigel, 200 μL per injection. Mice also received a subcutaneous E2 pellet (0.72 mg, 60-day slow release; Innovative Research of America) implanted into the right flank on the day of engraftment.

Treatment and tumor monitoring.

Mice were treated with either 25 nmol of polyamide 1 or 50 nmol of polyamide **5**. For the short-term and fluorescent imaging studies, they were treated for 8 days after engraftment and every second day for a total of 4 injections. For long-term treatment, injections started 16 days after engraftment and were continued twice a week for the following 4 weeks. Imaging was accomplished using the IVIS Imaging System (Caliper). The animals were anesthetized with 2% to 3% isoflurane and injected intraperitoneally with 150 μL of RediJect D-luciferin (Caliper) and subsequently transferred to the imaging chamber, where isoflurane levels were reduced to 1% to 2.5%. The floor of the imager was heated to +37°C to avoid animal hypothermia. Breathing frequency was monitored and not allowed to drop below 1 per second, adjusting the isoflurane levels accordingly at all times.

Endpoint criteria and euthanasia.

Animal endpoint criteria encompassed weight loss of more than 15%, restriction of motoric function by the engrafted tumor, dehydration of more than 10%, and moribund behavior. Where appropriate, the animals were euthanized by asphyxiation in a CO_2 chamber.

Tumor tissue harvest.

Animals were resected and tumors excised using standard forceps, scissors, and surgical blades. The tumors were weighed immediately afterward. For studies with fluorescein isothiocyanate (FITC)-conjugate 5, resected tumor tissue was homogenized via blunt force and then pushed through a microfilter to achieve single cell suspensions, which were plated on glass microscopy slides for 6 hours before imaging using a Zeiss Exciter fluorescence confocal microscope.

RNA-Seq sample preparation and data processing

Cells for gene expression analysis were plated in 10-cm diameter dishes at 1.1×10^6 cells per dish and incubated in the growth medium supplemented with 10 nmol/L E2 for 24 hours. Afterward, medium was exchanged with the growth medium supplemented with polyamides and 10 nmol/L E2 and incubated for 48 hours in 5% CO_2 and 37°C. The RNA was then harvested using an RNEasy Kit (Qiagen). Subsequently, a Riboguard RNAse inhibitor was added and samples were treated with TurboDNA Free DNAse (Ambion), according to manufacturers' instructions. RNA-Seq libraries were prepared using standard Illumina reagents and protocols. Single read sequencing with the read length of 50 nucleotides were conducted on the Illumina HiSeq2000 sequencer, following manufacturers' instructions, producing 35 to 50 million reads per library. Sequencing data were mapped against the combined human (hg19) transcriptome, using the Bowtie program package 0.12.7 (31) and the refseq annotation. The open access processing package Cuffdiff was used to calculated differential gene expression. Inter-replicate statistical significance was calculated with the DEseq module (32).

Results

Design of polyamides

We synthesized 4 8-ring hairpin Py–Im polyamides to screen for activity against E2-stimulated gene expression (Fig. 3.1 and Fig. 3.2). Polyamide 1 targets 5′-WGGWCW-3′, which is the half site ERE consensus. Polyamide **2** was previously reported to inhibit a subset of dihydrotestosterone-induced gene expression in cultured prostate cancer cells (11). Polyamide 3 was recently characterized in cultured lung cancer cells and used to partially abrogate TNF-stimulated transcription (12). Polyamide 4 targets the sequence 5′ WGWCGW-3′. Polyamides 5 and 6 are FITC-conjugated analogs of polyamides 1 and 2, respectively, used to visualize cellular uptake and distribution in this study.

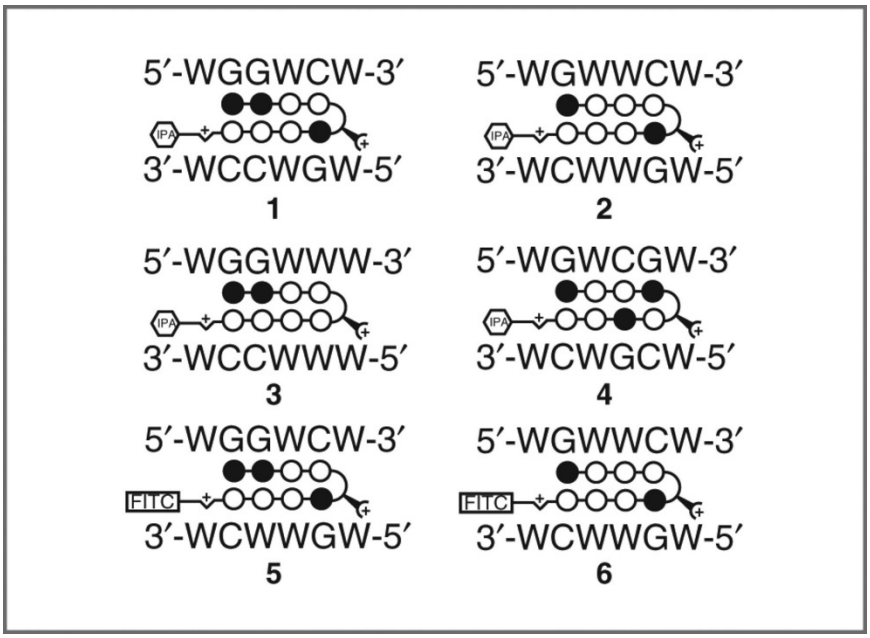

Figure 3.1 Ball-and-stick models of polyamides 1 to 6 with DNA target sequences as follows: 1, 5'-WGGWCW-3'; 2, 5'-WGWWCW-3'; 3, 5'-WGGWWW-3'; 4, 5'-WGWCGW-3'. Polyamides 5 and 6 are FITC-analogs of polyamides 1 and 2, respectively, used for fluorescence microscopy experiments. Chemical structures of polyamides 1 to 6 are in Fig. 3.2. IPA, isophthalic acid.

Evaluation of binding of polyamides to an ERE half site by DNA thermal denaturation assays

Polyamides 1 to 4 were incubated with duplex DNA 5′-CGATGGTCAAGC-3′, which contains an ERE half site consensus and melting temperatures measured (Fig. 3.3A). Duplex stabilization was greatest for polyamide 1, a polyamide that was predicted to bind this sequence based on established Py–Im polyamide pairing rules (6, 7). The other polyamides showed less stabilization of this duplex.

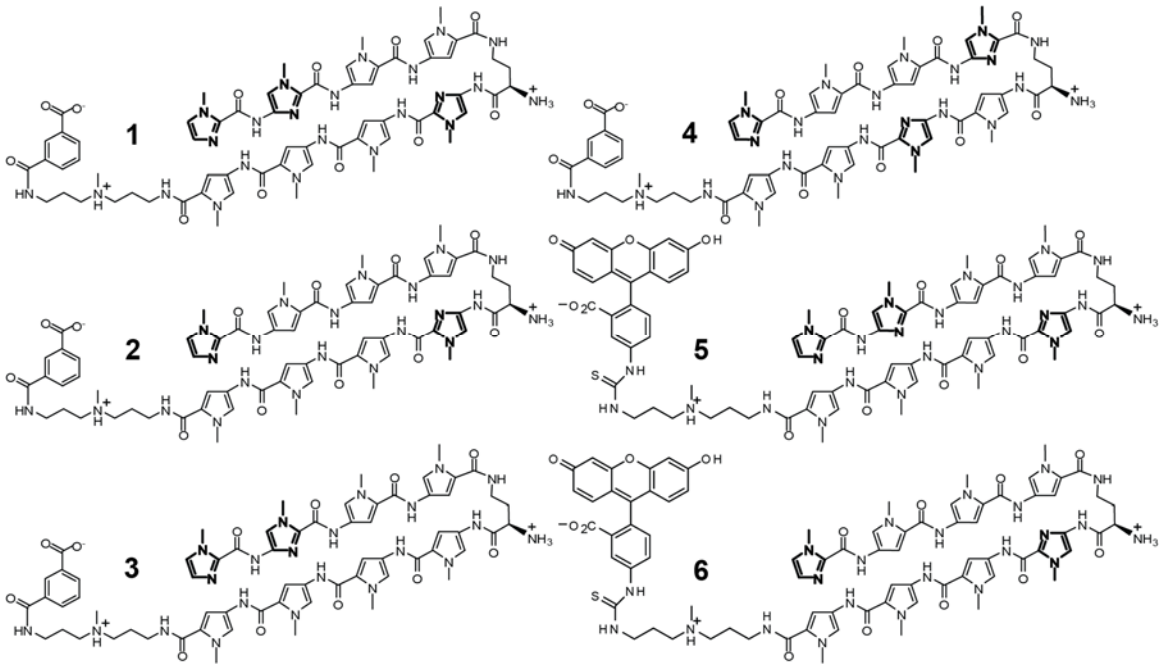

Figure 3.2 Chemical structures of compounds 1-6.

Luciferase activity and cytotoxicity in T47D-KBluc cells

The ERα–positive cell line T47D-KBluc expresses luciferase under the control of 3 tandem repeats of the sequence 5′-AGGTCACTTGACCT-3′ (25), which is the consensus sequence for the ERα–DNA homodimer (Fig. 3.3B). T47D-KBluc cells were grown in 10% FBS/RPMI-1640 media with 10 nmol/L E2 for 48 hours. Then, media was replenished with varying concentrations of polyamides 1 to 4 for 96 hours. An extended incubation time with E2 was used to approximate the *in vivo* condition of continued E2 circulation. Cell proliferation and viability was assayed using WST-1 (Roche) and luciferase output was measured (Fig. 3.3C). Both luciferase output and proliferation were affected most by treatment with polyamide 1 (IC_{50} 0.47 μmol/L for viability, 0.14 μmol/L for luciferase suppression) and least by polyamide 3 (IC_{50} > 2.5 and 1.5 μmol/L, respectively). The representative data for luciferase and WST-1 assay are shown in Fig. 3.4. We identified *TFF1* as one of the most highly induced transcripts by E2 based on published reports (33). The effects of polyamides 1 to 4 on E2-stimulated *TFF1* expression were measured to validate the luciferase screen. Polyamide 1 was again found most potent although polyamides 2 and 4 showed significant inhibition of *TFF1* as well (Fig. 3.3D). In addition, polyamide 1 shows significantly less toxicity to LNCaP, U251, and A549 cell lines (Fig. 3.5), which have low expression of ERα (34–37). Inhibition of *TFF1* mRNA by polyamide 1 is dose responsive (Fig. 3.6A) and chromatin immunoprecipitation of ERα at the *TFF1* promoter after E2 stimulation of cells pretreated with **1** showed reduced occupancy as compared with vehicle-treated cells (Fig. 3.6B, C).

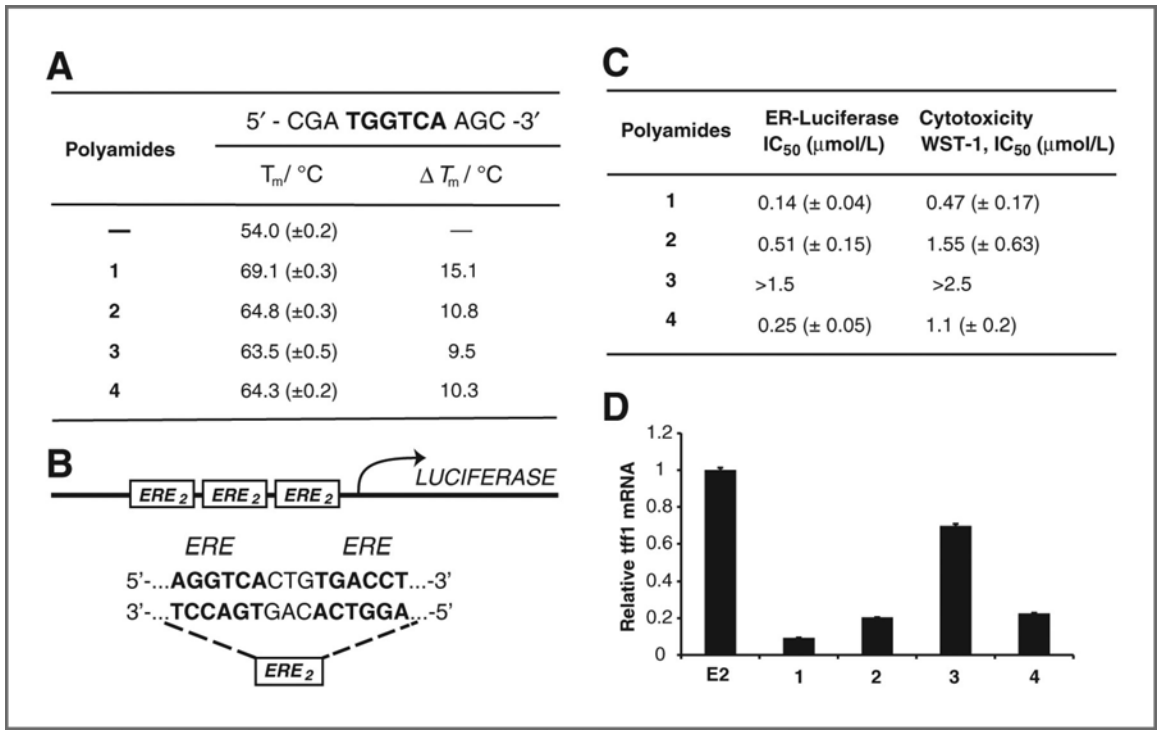

Figure 3.3 A, thermal denaturation assays of a duplex DNA oligonucleotide containing a half site ERE. Polyamide **1** shows the most stabilization. B, sequence of ERE-driven luciferase in T47D-KBLUC cells. C, polyamides **1** to **4** were screened for cytotoxicity and suppression of ER-driven luciferase. Polyamide 1 is most potent by both measures. Representative isotherms are displayed in Fig. 3.4. D, polyamides dosed at 0.3 μmol/L were screened for activity against TFF1 expression, a known ERE-driven gene. The relative activities of polyamides **1** to **4** approximately mirror what is seen in the luciferase assay at this concentration. At higher concentrations (~1 μmol/L), all four polyamides show activity.

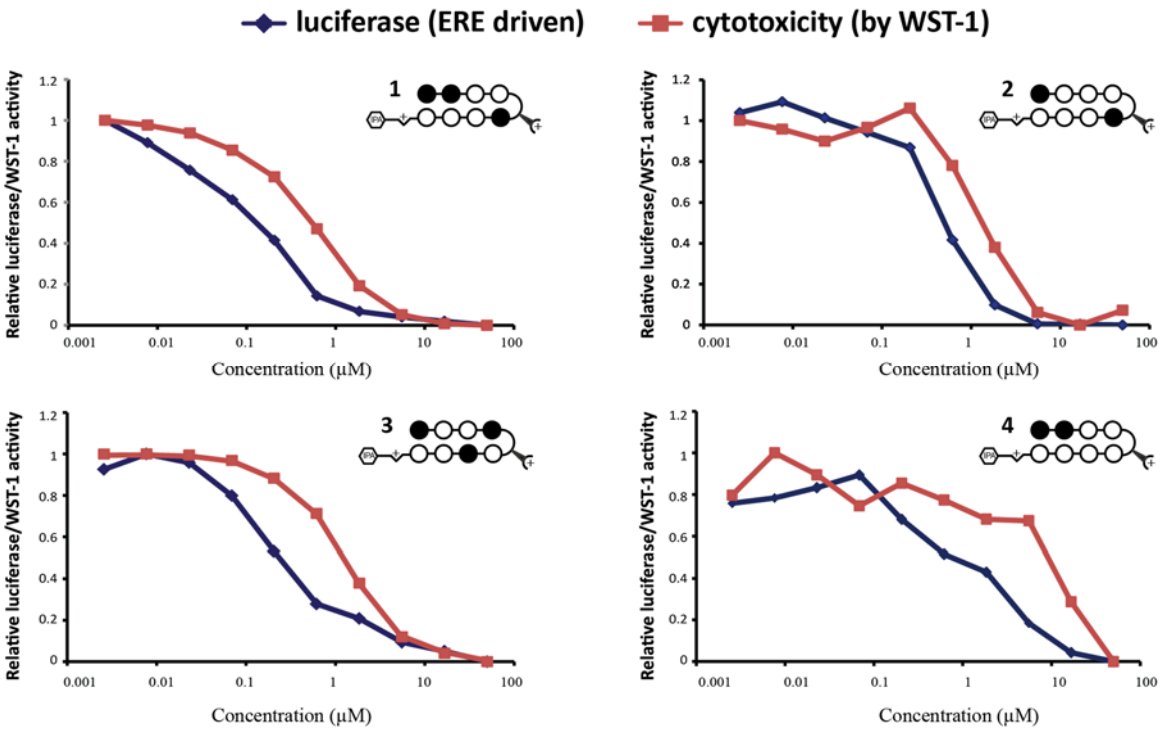

Figure 3.4. Representative data from luciferase and cytotoxicity (wst-1) assays for compounds 1-4.

Cell Line	IC50 (96h, **1**, m**M**)
T47D-KBLuc	0.47 ± 0.17
A549	8.5 ± 3.7
LNCaP	>50
U251	>50

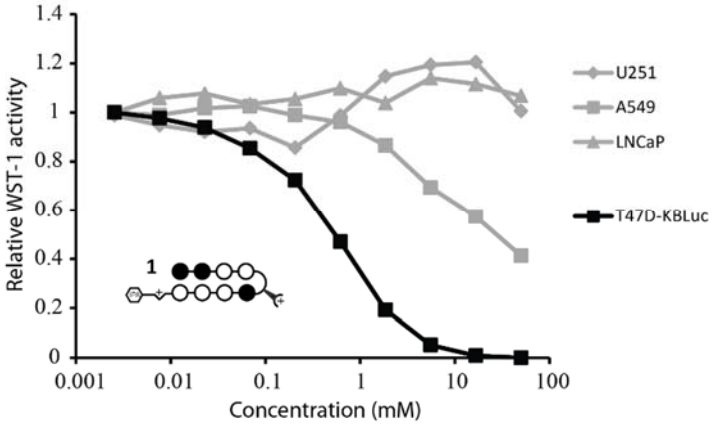

Figure 3.5 WST-1 cytotoxicity of 1 in T47D-KBLUC, LNCaP, A549, and U251 cells.

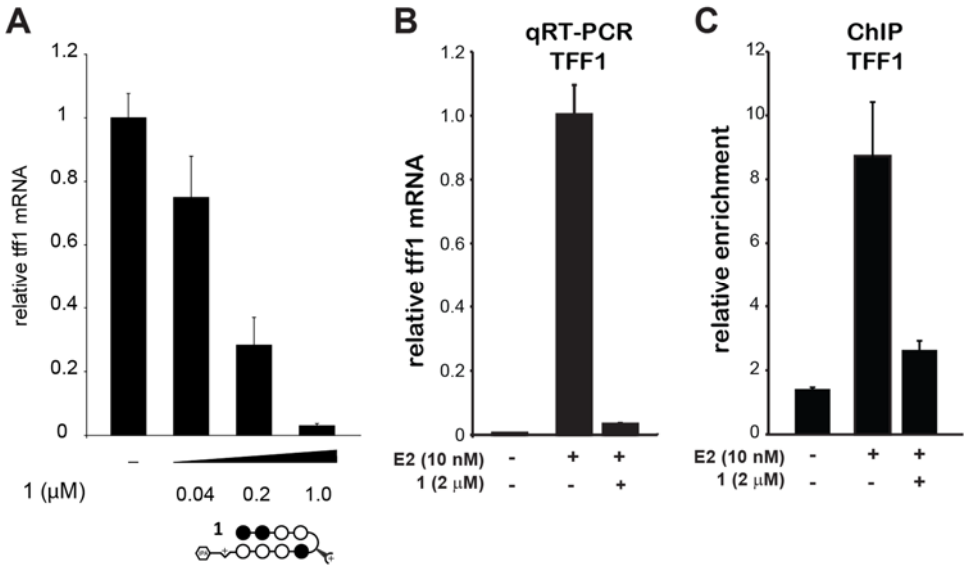

Figure 3.6 Quantitative RT-PCR analysis of Tff1 mRNA reduction after treatment with 1 for 96h is dose responsive. B, Relative mRNA of E2 induced tff1in the presence of 1 at 2 μM C, ERα occupancy at the tff1 promoter is reduced by 1. The cells were incubated with 1 for 48 hours prior to induction with E2 (10 nM) for 45 minutes. The IC50 for cytotoxicity of 1 at 48h in 10% CT-FBS/RPMI is 3.4 μM.

Genome-wide polyamide effects on E2-induced gene expression

Effects of hairpin polyamide 1 at 0.3 and 1 μmol/L on the transcriptome of E2-induced cells were measured using RNA-Seq. Reads were mapped using Hg19 reference human genome and data were analyzed using the Bowtie and CuffDiff packages (38). Only the genes with fragments per kilobase of exon per million fragments mapped (FPKM) ≥ 20 and at least 2-fold change in gene expression upon treatment with either polyamide 1 or E2 were used in the analysis (Table 3.1). Among those genes, at 1.0 μmol/L, polyamide 1 affected expression of 346 genes (0.7% of total) at least 2-fold as compared with E2-treated control. Of these genes, an equal number of genes were up- and downregulated (173 in each case). At the lower concentration of 0.3 μmol/L, expression of 127 genes (0.3% of total) was affected at least 2-fold, and a majority of these genes (77 vs. 50) were

downregulated. At the same threshold, E2 upregulated 1,003 genes (2.0%; Fig. 3.7A) and downregulated 575 genes (1.2%; Fig. 3.7B). A fraction of expression changes induced by E2 were reversed by polyamide 1 (Table 3.2), and this fraction was greater for E2-repressed genes. Among E2-upregulated genes, 43 (4.3%) were repressed by polyamide 1 at least 2-fold at 1.0 μmol/L. Among those 575 genes that were downregulated by E2, 95 (16.5%) were derepressed by **1** at 1.0 μmol/L at least 2-fold (Fig. 3.7A and B). Overall, of the 346 genes affected by polyamide 1 at 1.0 μmol/L, 138 (39.9%) represent genes whose up- or downregulation by E2 was abrogated by polyamide treatment. Genes whose expression was affected by polyamide 1 at a lower concentration (0.3 μmol/L) were largely a subset of the genes affected at 1.0 μmol/L, 103 of which (81.1%) were affected by polyamide 1 at both concentrations.

Further analysis was conducted using Euclidian distance clustering with complete linkage (Fig. 3.7C). Interestingly, while the majority of E2-affected genes are not affected by polyamide 1, out of the top 50 genes most strongly affected by E2, 28 (56%) are inhibited at least 2-fold and 38 of 50 (78%) genes are inhibited at least 1.5-fold by polyamide 1 (Fig. 3.7D). Five transcripts were selected for verification by qRT-PCR and all five showed good reproducibility of the expression changes seen by RNA-Seq (Fig. 3.8). Four were upregulated by E2 (*AREG*, *DOK7*, *TFF1*, and *WT1*) and one downregulated by E2 (*TGFB2*).

Circulation and toxicity of polyamide 1 in mice

To assess serum concentrations of **1** after subcutaneous injection, 4 female C57BL/6 mice were injected subcutaneously into the left flank with 120 nmol of polyamide 1 in a

200 µL 20% DMSO/PBS vehicle. Serial serum samples were taken via retroorbital draw and processed by methods previously described (30). Polyamide 1 was detectable in serum for up to 24 hours after injections, and reached a maximum concentration of 3 µmol/L at 6 hours after injection (Fig. 3.9A). Toxicity after repeated injections of **1** was assessed by daily weights and visual inspection of treated mice. Five female C57BL/6 mice were injected with 20 nmol of polyamide 1 subcutaneously to the left flank 3 times a week for 2 weeks without measurable weight loss. The regimen was then increased to 30 nmol for 2 weeks, again without measurable weight loss or changes in animal behavior (Fig. 3.9B).

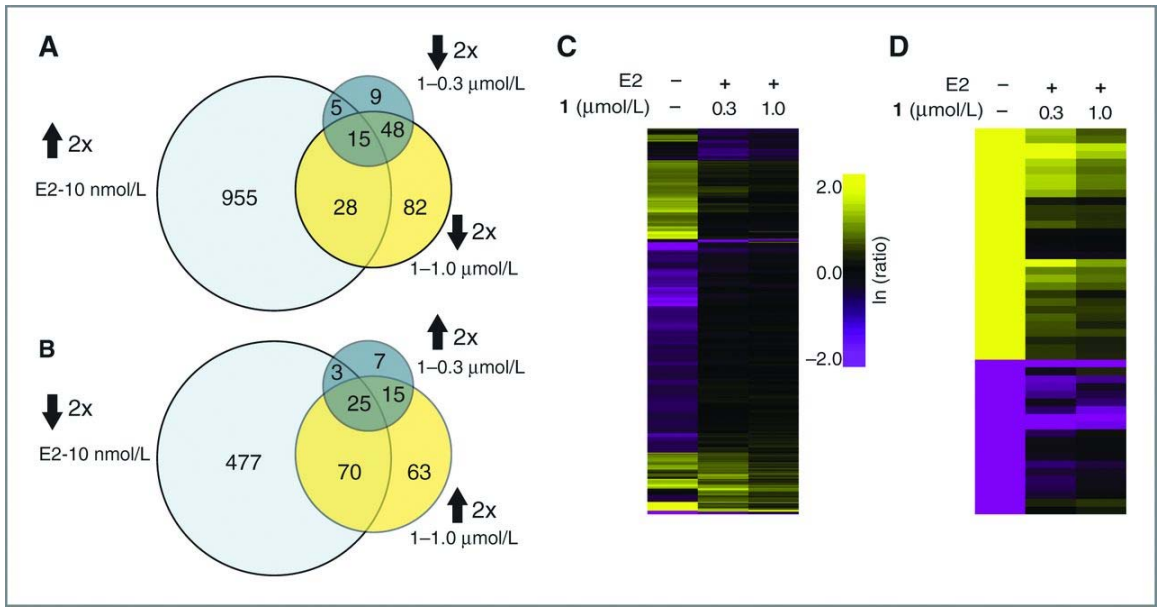

Figure 3.7 RNA-seq global transcriptome analysis. All ratios are normalized to the induced control (10 nmol/L E2). A, Venn diagrams show the overlap between genes upregulated by E2 at least 2-fold and genes downregulated by polyamide 1 at 0.3 or 1.0 µmol/L. B, Venn diagrams for the overlap of genes downregulated by E2 at least 2-fold and derepressed by polyamide 1 at 0.3 or 1.0 µmol/L. C, hierarchical clustering (Euclidian distance, complete linkage) of genes changed at least 2-fold as compared with the induced state. D, 50 genes that were most changed by E2 induction were clustered (Eucludian distance, complete linkage). Of those genes, 30 were upregulated and 20 were downregulated by E2. Fold-changes are relative to E2-induced control.

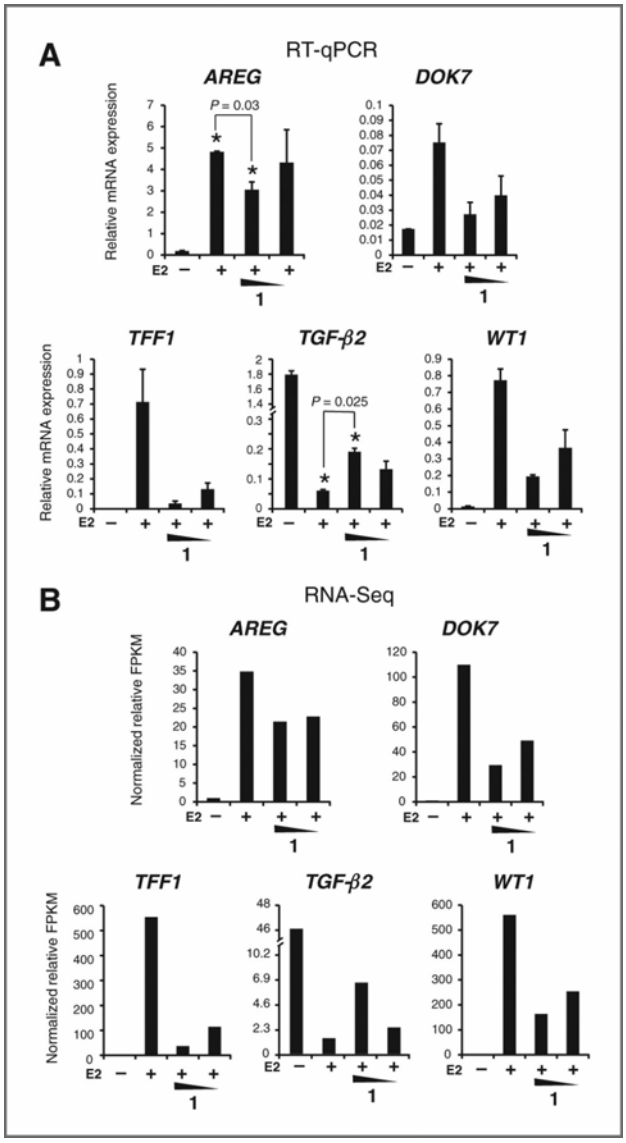

Figure 3.8 Confirmation of genome-wide polyamide effects observed by RNA-seq. Five genes (4 induced and 1 repressed by estrogen) were interrogated. A, relative mRNA levels of selected genes measured by qRT-PCR. B, relative mRNA expression values as measured by FPKM from RNA-seq. Concentrations of polyamide 1 are 1.0 and 0.3 μmol/L.

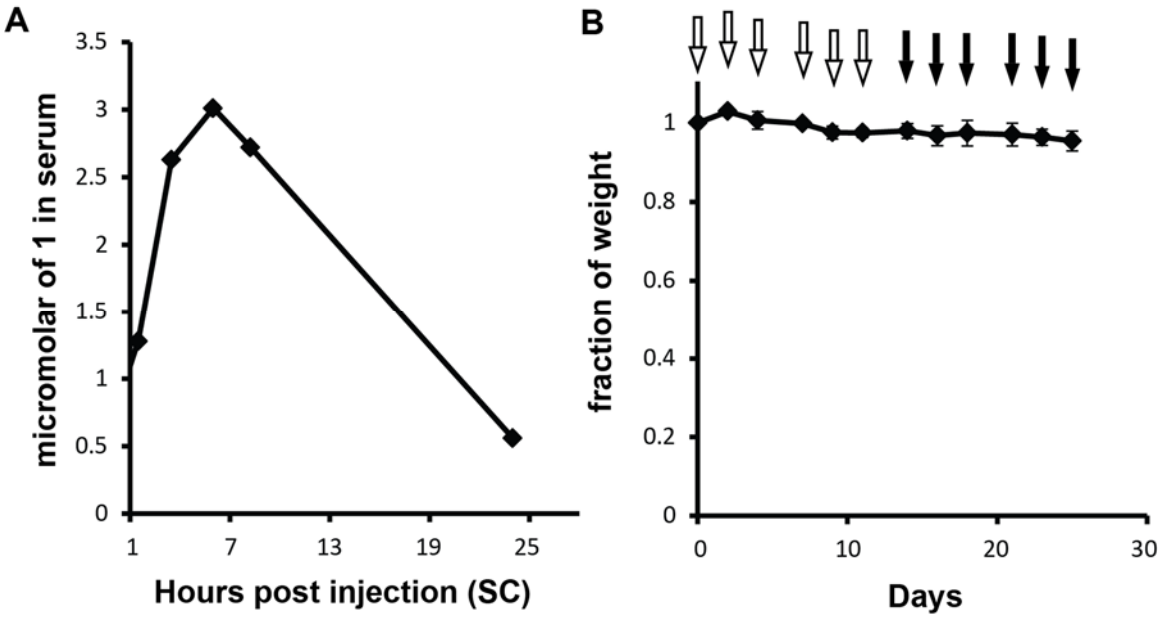

Figure 3.9 Pharmacokinetics of **1**. A, Serum concentrations of 1 after subcutaneous injection (120 nmol) into C57BL/6 mice. B, Weight curves after indicated injections of 1. Gray arrows: 20 nmol, Black arrows: 30 nmol. n = 4 mice.

Effects on ERα–mediated transcription in T47D-KBluc tumor bearing mice after short-term treatment

To measure the efficacy of polyamide 1 *in vivo* against E2-induced transcription, T47D-KBluc cells were engrafted into female nonobese diabetic/severe combined immunodeficient (NOD/SCID)-gamma (NSG) immunocompromised mice supplemented with a slow-release subcutaneous E2 pellet in the right flank to facilitate E2-induced growth. After 1 week of growth, mice were imaged using the IVIS Imaging System (Caliper) and stratified into groups of 12 mice each for vehicle and polyamide treatment. Polyamide 1 (25 nmol) in 200 μL 20% DMSO/PBS was injected subcutaneously into the left shoulder every other day for a total of 4 injections. Vehicle-treated mice received 20%

DMSO/PBS alone. After 3 injections, mice were reimaged. Luciferase output increased an average of 8-fold for the vehicle-treated mice and 3-fold for the mice treated with polyamide 1 (Fig. 3.10A). Mice were euthanized the day following the fourth injection for tumor resection. Tumors from vehicle-treated mice were 71 ± 12 mg and tumors from polyamide-treated mice 55 ± 11 mg (Fig. 3.10B), which does not explain the differences seen in luciferase expression. Representative images of mice treated with polyamide 1 or vehicle at day 6 are shown (Fig. 3.10C).

Effects on ERα–mediated transcription in T47D-KBluc tumor-bearing mice after long-term treatment

To investigate the effects of polyamide 1 in tumor-bearing mice after extended treatment, T47D-KBluc cells were again engrafted into female NSG mice supplemented with a subcutaneous E2 pellet in the right flank. Tumors were grown for 9 days before stratification of 5 mice each into polyamide 1 and vehicle treatment groups. Mice were treated with vehicle or 25 nmol of polyamide 1 in 20% DMSO/PBS, subcutaneously into the left shoulder twice a week for a course of 9 injections (25 days), beginning on day 16 after engraftment (Fig. 3.10D). Treated mice maintained their weights at more than 90% until the final days of treatment when their weights decreased to more than 85% before euthanasia. Luciferase was monitored weekly using the IVIS Imaging System. Luciferase output in the polyamide-treated mice was consistently lower than vehicle-treated mice (Fig. 3.10E). At the experimental endpoint, tumors from vehicle-treated mice were 165 ± 27 mg and tumors from polyamide-treated mice 128 ± 54 mg.

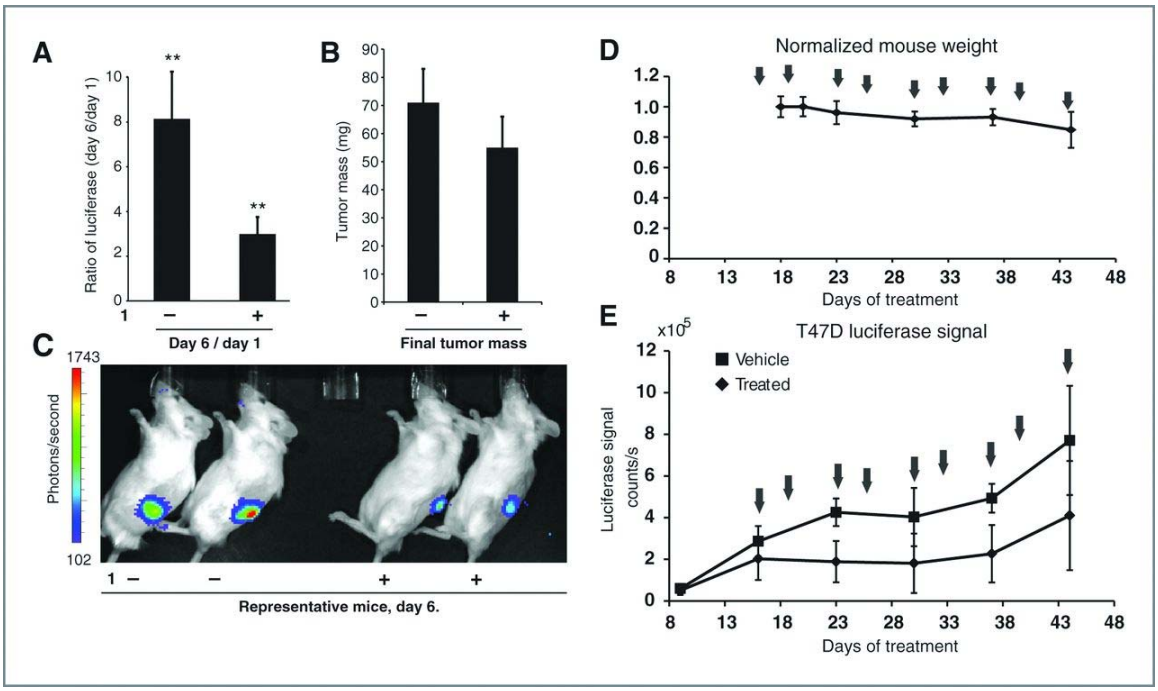

Figure 3.10 Xenograft studies. A, treatment of T47D-KBluc–bearing mice with polyamide 1 results in suppression of ER-driven luciferase. **, $P < 0.01$; $n = 12$ mice per group. Errors are 95% confidence interval (CI). B, tumor masses at experimental endpoint were vehicle: 71 ± 12 mg (95% CI); polyamide 1, 55 ± 11 mg (95% CI). C, representative luciferase output of vehicle and treated mice on day 6. D, treatment schedule for extended time-course experiments with normalized mouse weights over time. Arrows indicate treatment days. E, luciferase signal for polyamide 1 and vehicle-treated groups. Error bars are SDs. Mean tumor masses at the endpoint for animals treated with vehicle is 165 ± 27 mg (95% CI) and for animals treated with 1 is 128 ± 54 mg (95% CI).

Tissue distribution of FITC-conjugated polyamide 5 in mice bearing T47D-KBluc xenografts

Py–Im polyamide 5 is a FITC-labeled conjugate of hairpin **1** that was synthesized to evaluate tissue and subcellular localization via fluorescence microscopy. T47D-KBluc cells cultured *in vitro* and then treated with **5** showed nuclear fluorescence similar to what has been reported in other cell lines (27, 28) treated with FITC-conjugated polyamides in cell culture (Fig. 3.11). An NSG mouse engrafted with T47D-KBluc cells as described in the previous section was treated with polyamide **5** in a manner identical to that of polyamide 1, except at a dose of 50 nmol per injection. After 3 injections, the mouse was euthanized, the tumor resected, and internal organs dissected. Tissue was fixed, cryoprotected, sectioned,

and imaged immediately. Fluorescence signal was evenly distributed throughout multiple sections of the tumor xenograft. A representative section is shown (Fig. 3.12A). High magnification reveals nuclear localization in tumor tissue (Fig. 3.12B). Sections of cardiac muscle show significant cytoplasmic fluorescence in a fibrous pattern (Fig. 3.12C). Sections of kidney and liver both show nuclear fluorescence localization, with minimal cytoplasmic fluorescence (Fig. 3.12D and E). Small bowel epithelia show diffuse cellular fluorescence (Fig. 3.12F).

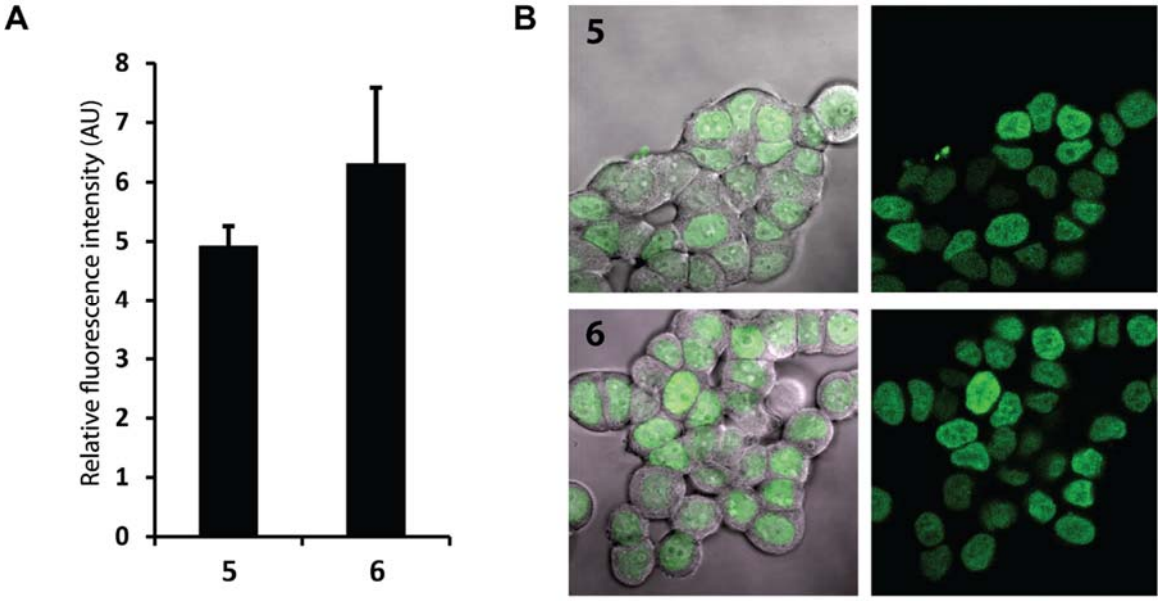

Figure 3.11. Confocal microscopy of live, cultured T47D-KBLUC cells. A, Mean intensity of fluorescence/cell averaged over three images. Errors are 95%CI. B, Representative images of polyamides 5 and 6.

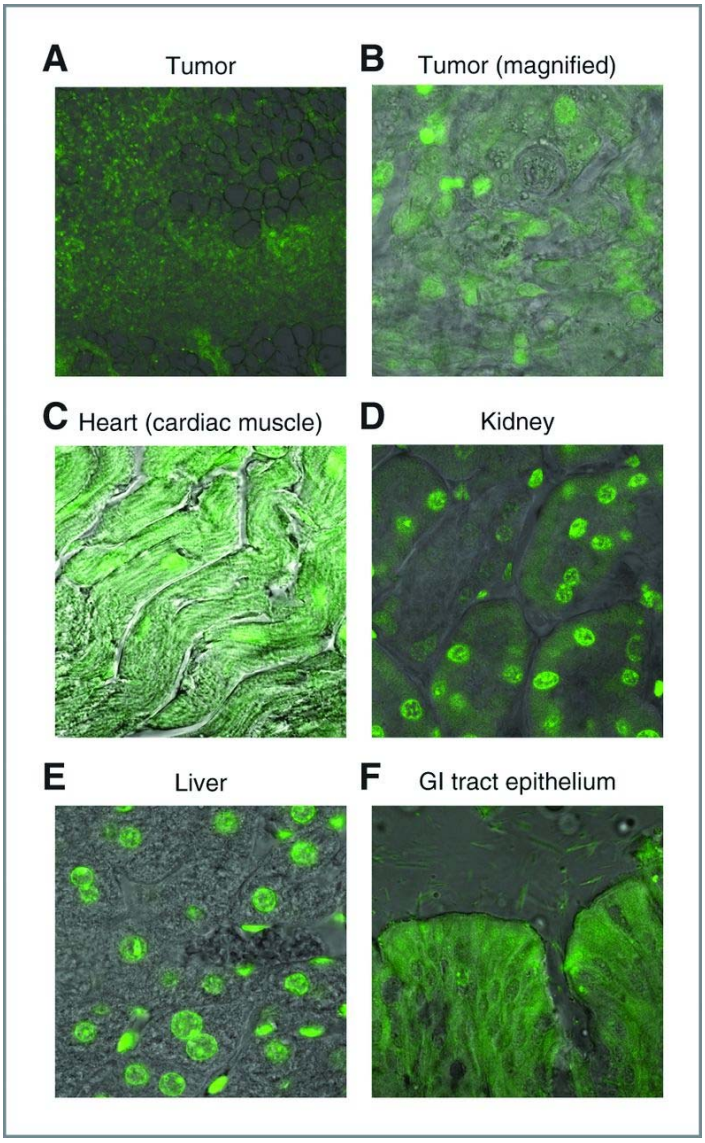

Figure 3.12 Tissue frozen sections of tissue extracted from xenograft-bearing mouse treated with polyamide 5. A, FITC-labeled Py–Im polyamide 5 distributes widely in sections of the T47D-KBluc tumor xenograft. B, high magnification shows nuclear localization of polyamide 5 in tumor cells. C, cardiac muscle sections show a fibrous pattern of fluorescence in the cytoplasm as well as nuclear staining. D, kidneys show nuclear localization of polyamide 5. E, liver sections show nuclear localization of polyamide 5. F, bowel epithelia show cytoplasmic fluorescence. GI, gastrointestinal.

To ensure that nuclear fluorescence in the xenografts was not an artifact of the fixation process, we extracted live cells from T47D-KBluc xenografted tumors from mice treated with polyamide 5 as earlier. In this experiment, cells were isolated via filtration and plated on microscope slides, and incubated for 6 hours before imaging. Cells derived from the tumor showed nuclear staining in a pattern similar to that seen in the fixed tumor sections as well as cultured cells treated with polyamide 5 *in vitro* (Fig. 3.13).

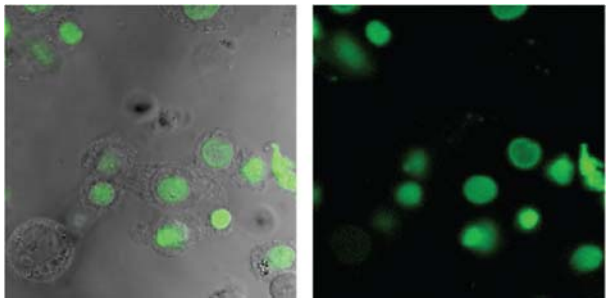

Figure 3.13 Confocal microscopy of live cells taken from T47D-KBLUC xenografts in mice treated with 5.

Discussion

In order for DNA-binding, Py–Im polyamides to be considered for therapeutic application, these molecules must possess favorable pharmacokinetic and pharmacodynamic properties and exert a desired effect in target tissues. In this study, ERα–induced transcription in xenografted breast cancer tumors was the target. A polyamide targeted to the ERE half site 5′-WGGWCW-3′ was identified from a focused screen for activity against ER-mediated transcription and cytotoxicity against ERα–positive breast cancer cells. This polyamide was further tested for its global effects on the transcriptome of E2-induced T47D-KBluc cells. Hairpin polyamide 1 showed limited toxicity and circulated at therapeutic levels in serum after subcutaneous injection. It also showed

activity against ER-driven luciferase expression in xenografted tumors in immunocompromised mice. FITC-polyamide conjugate 5 shows widespread localization in body tissues including sections through the xenografted tumor, which reveal nuclear fluorescence.

Suppression of ER-induced gene expression

We screened for both suppression of E2-induced luciferase expression and for antiproliferation by WST-1 assay using T47D-KBluc cells. Polyamide 1 was the most active by both measures, whereas polyamide 3 was inactive by either measure. These molecules differ only at a single atom, which represents the difference between a Py and Im heterocycle. Although polyamides have been shown to have differing uptake properties depending on Py–Im content and sequence (27, 28), the differences in activity in this series is likely not explained by differing uptake efficiency as confocal microscopy of FITC-polyamide conjugates 5 and 6 are similar (Fig. 3.11).

Global effects on the E2-stimulated transcriptome

E2 exerts its effects through direct DNA binding and less frequently extranuclear pathways that do not involve ERα–DNA binding (39). Our genome-wide transcriptome analysis (Fig. 4) revealed that a small fraction of gene expression changes induced by E2 treatment is suppressed by polyamide 1. From a total of 1,003 E2 upregulated genes, only 43 (0.43%) are repressed by polyamide 1 at 1.0 μmol/L, and from a total of 575 E2 downregulated genes, 95 (16.5%) were derepressed. However, among the 50 genes most strongly either induced or repressed by E2, a majority were significantly affected by polyamide 1. Among these top 50, 28 (56%) were downregulated by polyamide 1 (1.0

μmol/L) at least 2-fold. At a lower cutoff of 1.5-fold, 38 (76%) of E2-induced gene expression changes were abrogated by the action of polyamide 1 at 1.0 μmol/L. Many of these strongly E2-responsive genes play important roles in the development of tumors and are therapeutically relevant. Among them is Wilms tumor 1 (*WT1*), a gene originally identified as a tumor suppressor (40); however, more recently it has become apparent that it can also act as an oncogene (41). *WT1* expression is detectable in 90% of breast cancers (42) and high levels of *WT1* expression are correlated with poor patient survival (43). *TFF1* is a predictor for breast cancer patient survival (36). Transforming growth factor-β2 (*TGF-β2*) was observed among the most strongly E2-repressed genes and was also over 3-fold derepressed by polyamide 1 at 1.0 μmol/L. TGF-β2 is involved in cancer development that is also derepressed by traditional antiestrogens (44). We conclude that polyamide 1 acts in an antiestrogenic fashion among genes that are most potently affected by E2 but is less active for the majority of E2-responsive genes. If the mechanism by which polyamide 1 interferes with estrogen-driven gene expression is through direct interference with ER–DNA interfaces, we would not expect to affect ER-driven transcription at loci where ER signals through a tethering complex (45), such as with Ap1 and Sp1. Indirect interactions between ER and DNA through tethering with other proteins offer a partial explanation for the limited number of ER-driven transcripts affected by polyamide 1.

Most transcripts affected by polyamide 1 are not explained on the basis of E2 antagonism; 295 genes that are either up- or downregulated by polyamide 1, at least 2-fold that are not explained by effects on ER activity. Of these, 164 are upregulated and 131 downregulated by polyamide 1. To further characterize these effects, we used the DAVID functional annotation tool (46, 47). For the upregulated transcripts, enriched biologic

processes include those involved with the regulation of apoptosis and cell-death, as well as responses to endogenous and hormone stimuli, whereas downregulated genes suggested that polyamide 1 is involved in regulation of GTPase-mediated signal transduction and protein transport and biosynthesis (DAVID database, BP_FAT_GO analysis of genes changed at least 2-fold by treatment with 1 at 1 μM). The mechanisms of cell death may include the inhibition of transcription (10, 11, 13, 15), but other DNA-dependent processes may contribute and are an area of current investigation. Whether or not the effects of polyamide 1 on these biologic processes are specific to polyamide 1 or may represent a class-effect is unknown but also under study.

Polyamide treatment suppresses E2-simulated luciferase expression in vivo

T47D-KBluc cells were chosen as the cell line for our study based on previous work using T47D cells as a model for ERα–positive breast cancer. Both vehicle- and polyamide-treated groups showed an increase in total luciferase expression from the baseline measurement immediately before treatment on day 1. However, on day 6, after 3 sequential injections, this increase was significantly blunted in the polyamide-treated group as compared with vehicle (from ~8- to 3-fold), suggesting that **1** was able to reach sufficient concentrations in tumor tissue to affect luciferase expression. The approximately 2.5-fold difference in luciferase between polyamide- and vehicle-treated groups, if interpolated to the *in vitro* data, suggest an approximate concentration of 0.3 μmol/L within the xenograft tissue. Tumor masses did not differ significantly between polyamide- and vehicle-treated mice in this experiment. However, this 6-day experiment may be too brief to adequately assess effects on tumor growth.

Effects on tumor size

Although there are no published reports on the growth of T47D-KBluc xenografts in mice, data from parental T47D xenografts show a slow, linear growth pattern rather than exponential (48). To better assay for antitumor activity of polyamide 1, we conducted similar experiments over a longer period of time. T47D-KBluc xenografted tumors were grown for 2 weeks before initiating treatment, and treatment with polyamide 1 was conducted twice per week for a total of 4 weeks. We observed no significant change in tumor size at the experimental endpoint, although we found a sustained suppression of luciferase output in the polyamide-treated arm as compared with vehicle-treated, consistent with our initial observations. The IC_{50} for cytotoxicity of polyamide 1 in cell culture is 0.47 μmol/L, which we believe to be higher than the concentrations achieved within the tumor tissues in this study.

Tissue distribution of FITC-conjugate polyamide 5 in mice after repeated subcutaneous injections

Fixed, frozen sections through multiple internal organs harvested from T47D-KBluc engrafted mice treated with polyamide 5 reveal widespread organ distribution of fluorescent signal but with differing patterns of fluorescence between tissues, and with little obvious systemic toxicity. The tumor sections show nuclear fluorescence in a subcellular pattern that is similar to what is observed in cell culture (Fig. 3.12A). The liver and kidneys also show strong nuclear fluorescence (Fig. 3.12D and E), whereas sections through the intestinal epithelium and cardiac muscle show predominantly cytoplasmic and both cytoplasmic and nuclear fluorescence, respectively. A difference in the cellular uptake

of polyamide–FITC conjugates between cell types has also been observed *in vitro* (27). Recent work has shown that polyamides can form aggregates in solution (49). Whether polyamide aggregation influences distribution *in vivo* is unknown. Tissue-specific targeting of small-molecule drugs is an area of current investigation that may become relevant for this class of molecules as additional *in vivo* experiments are planned.

Conclusion

Polyamide 1 delivered by subcutaneous injection in a simple DMSO/saline vehicle distributed widely in host and tumor tissue and showed adequate bioavailability to affect luciferase expression in xenografted tumor tissue, with acceptable toxicity. Future investigations will include optimization of polyamides for lower systemic toxicity without a compromise in efficacy.

Tables

Table 3.1 Genes induced (or repressed) by either **1** (1 μM) or E2 (10 nM)

Down >2-fold 1.0 μM PA

AC034193.1	FAF1	BCKDHB	PTPRK
GMDS	FTO	SERPINA1	PEMT
TFF1	LARS2	RP13-582O9.5	ERGIC1
RALGPS1	RSRC1	TTLL5	HIBADH
TRAPPC9	TBC1D22A	AIG1	WWP2
RP11-1018J8.2	ELP4	FARP2	NIPAL2
CTD-2313N18.7	CLSTN2	GRIK3	ADK
SMYD3	FAM172A	SDCCAG8	SND1
RP11-206M11.7	KIF16B	TNIK	C9orf46
SLC39A11	JPH2	ANO10	LHPP
U6.133	SLC24A3	LARGE	C3orf21
TFF3	CUX1	RABGAP1L	FOXJ1
EXOC4	C1orf194	MSI2	TYRP1
DENND1A	THSD4	SUCLG2	IQCK
AC126407.1	PCNXL2	PAPSS2	FLT4
IMMP2L	CBARA1	HINT1	MAPK9
C11orf49	COMMD10	MGAT5	ACOT7
TIAM1	CLPB	CCDC132	COBL
PDZK1P2	CASK	TSSC1	APBB2
PDZK1P1	RSU1	AC005077.9	PET112L
PDZK1	VPS53	MAPKAP1	KIFAP3
PIP	SIPA1L2	NT5DC1	DDX10
SERPINA6	ERC1	WDR70	KREMEN1
MAD1L1	PIGU	EFCAB11	OLFM1
SPINK4	FHL2	NME7	SLC6A14
ATG7	MYO1D	ERI3	METTSD1
CCDC91	RP11-40H20.1	AC006465.3	CHST1
DOK7	PIGL	APOD	GALNT2
AE000658.30	MGP	XPR1	PLCE1
CAPSL	CWC27	UQCC	OAZ3
PCCA	TSPAN5	STAU2	MNAT1
ACOX2	CDC20B	PCCB	THADA
WT1	FN1	IQCG	SLC38A6
SUSD3	NEK11	U6.694	NCRNA00263
RP11-161E22.2	RERG	OSGIN1	PKIG
VEPH1	EXOC6	PAM	C1QTNF6
MAP2K5	ITFG1	CRADD	ETNK2
ATG10	DEPTOR	OLFML3	TBC1D5
LRBA	AC023161.1	COPG2	NSMCE2
KIAA0391	DIP2C	RGS12	MRPL48
AC010859.1	BRE	ACER3	CRAT
ADAMTS15	RBM19	STK3	EXT2
COMMD1	MYEOV	EIF2B3	SERGEF
ARL15	TAB1	DTNB	

Up> 2-fold 1.0 μM PA

GABARAPL1	ZMIZ2	AC114498.3	AC044860.2
GABBR1	PABPC1L	CD44	AC121247.1
TROVE2	SLC6A9	CD74	RP11-539L10.3
SLC25A29	AMIGO2	snoU13.267	ANKRD10
GRB7	TUFT1	J01415.22	CASP4
LZTR1	PSD4	ADM	J01415.19
VEGFA	PNRC1	PLEKHB1	RND3
TNFAIP2	MICAL1	TP53INP1	J01415.4
SIRT1	HDAC10	MEGF6	RPS26P3
GALT	C3	TSPYL2	GPX3
HIST1H3D	PDP1	DUSP1	RNASEH2B
LYPD3	RARRES3	KLHL24	HIST1H2AD
DHX58	TXNIP	TP53I11	AL593851.1
PCDH1	RPL12P4	SLC3A2	SCARNA17
PPAPDC1B	LPIN3	MUTYH	ATHL1
ENGASE	PLXNA1	ALDH2	MB
HES1	OGT	MX1	J01415.1
MDM4	PTPRU	MTUS1	AL355388.1
HIST1H2BD	RPL12P8	5S_rRNA.486	AC092143.1
RP5-857K21.14	RP3-405J24.1	RP11-466C23.3	RC3H1
NFKBIA	ABCC5	J01415.20	AQP3
C9orf3	OGFRL1	JDP2	AC136698.1
CCNG2	RP11-154D6.1	J01415.24	MTRNR2L9
IFRD1	CALD1	GPRC5A	J01415.5
AC011737.2	RP11-601I15.1	SELENBP1	J01415.8
IL1R1	AC022007.5	J01415.15	J01415.6
ZNF251	OPLAH	IFI27	snoU13.458
BAMBI	AL132821.1	RP4-697K14.7	Y_RNA.184
CC2D1B	RP11-373E16.1	hsa-mir-1977.1	TGFB2
PABPC1P10	HIST2H4B	J01415.10	TNFAIP3
ZNF302	HIST2H4A	CBS	UPK2
PARP10	RALGDS	CDC42EP3	ARRDC3
AMOTL2	MOSC1	SERTAD2	ELF3
GIGYF1	AGA	IFI6	RPL12P1
RP11-169K16.6	CLK4	RP11-383C5.4	J01415.2
OAS1	RP11-106M3.1	U6.1189	GDF15
ESPN	FAM193B	J01415.18	snoU2_19.4
BX322557.10	OSR2	ASNS	AL132988.3
RP11-434O22.1	AP005264.1	EP400NL	5_8S_rRNA.6
RP11-344H11.4	TMEM44	J01415.7	S100P
RCN1	AC064874.2	MTRNR2L2	RP5-1174J21.1
SOX4	NDRG1	RASL11B	AC005261.1
SLC7A5	AC010487.1	MGEA5	SERGEF
ISG15	CTSL1	COL6A1	

Up >4-fold 1.0 μM PA

TGFB2	ELF3	snoU2_19.4	RP5-1174J21.1
TNFAIP3	RPL12P1	AL132988.3	AC005261.1
UPK2	J01415.2	5_8S_rRNA.6	
ARRDC3	GDF15	S100P	

E2 >4-fold up

RP11-459E5.1	RP11-21L23.3	NDC80	KIF11
SPINK4	TRIP13	SPAG5	U6.694
WT1	AMZ1	HMMR	KIFC1
TFF1	RBP7	WNT10B	SLC7A1
PDZK1P2	LAT2	NBL1	C1orf97
RP11-1018J8.2	FAM65C	AC026271.3	RP11-467L20.6
DOK7	AGR3	TSKU	KIF20A
PDZK1P1	EXO1	MELK	TNFRSF10A
PDZK1	DERA	TOP2A	AZGP1
ACOX2	RP11-467L13.5	SKAP2	CCNB1
STC2	RRM2	SIPA1	CDCA2
AREGB	CCNA2	MTHFD2	TUBA1B
AREG	MND1	CDCA8	AC097711.1
OLFM1	KCTD6	DLGAP5	FAM72A
TFF3	SPC25	FAM83D	NUSAP1
AC135050.3	CDCA3	MYBL2	MCM2
SLC6A14	JPH2	HJURP	PRC1
MYEOV	DSCC1	ESPL1	TK1
PTGES	NCAPH	GINS1	TPX2
CXCL12	MKI67	U6.664	KIAA1524
TNS4	BIRC5	DTL	CCND1
SUSD3	MGP	UHRF1	HINT1
NKAIN1	CENPA	TNFRSF10C	OIP5
TP53I3	AFF3	RBM24	UBE2T
FLT4	AGR2	CDKN3	C9orf100
LY6E	THBS1	GNG11	C6orf141
PEG10	DEPDC1B	CDC20P1	FANCI
EIF4E1B	CDC6	CDC45	RP4-774G10.1
LIN28A	PLK1	ASF1B	GPSM2
PFKFB3	KIAA0101	SNCG	CCDC85B
GRIK3	CMTM7	KIF4A	RP11-379F12.3
NMU	SULF1	RP11-67L3.6	SERPINA6
RAPGEFL1	PRR11	ADCY3	PCNA
SYT12	CDCA5	LMNB1	C15orf23
NCAPG	RRM2P3	CKAP2L	PCK2
CA8	NUF2	AURKA	DEPDC1
GREB1	KIF2C	WDR76	MZT2B
FHL2	THSD4	PRIM1	AMD1
AC126407.1	UBE2C	CASC5	CRLF1
LDHB	CENPH	TACC3	OAS3
IGFBP4	TYMS	CTPS	ARHGAP11A
MYC	BUB1	AL592284.1	RP11-336N8.4
NPY1R	AC006465.4	HMGB2	RPL7AP11
AL358781.2	ABCC11	RP11-424C20.2	RP11-120E5.5
RBBP8	SLC29A1	SLC16A3	FEN1
MICB	TROAP	RP11-145M9.3	RP5-1100H13.3
PTTG1	CCNB2	CDC20	SNX24
AURKB	RERG	SH3BP1	CKS2
GALNT7	PKMYT1	BARD1	NEK2
SPC24	CEP55	NRM	RP11-417L14.1
MCM10	BUB1B	CA12	

E2 >4-fold down

CDH10	C9orf117	AP001816.1	FGFR1
AC005261.1	CDKN2B	AMT	HIST1H2AC
UPK2	CITED2	MALAT1	PYROXD2
CDHR3	MAP2	AC114498.8	ENC1
TGFB2	AC114498.3	CAPSL	J01415.12
AQP3	CCDC159	AC114498.4	FSTL1
snoU13.267	RP5-1174J21.1	PDP1	MAFK
5_8S_rRNA.6	C1orf66	NAALADL2	PLXNB1
SOD3	EPAS1	RP11-612B6.2	CALCOCO1
ZDHHC8P1	ANXA3	CD24P4	SLC25A29
AL132988.3	PNPLA7	OSR2	ID2
RP11-383C5.4	DUSP1	HIST1H2AI	AC093734.1
ARL4D	RP11-400K9.4	LCN12	SELENBP1
GPNMB	SOX2	MYO1B	TBC1D9
VTCN1	CALD1	AMIGO2	U6.133
RASL11B	CSAD	AL713999.8	HIST1H1PS1
5S_rRNA.486	HPX	KCNMA1	ERBB2
BCAS1	EPGN	LRRC46	CCDC39
CCDC154	snoU2_19.4	COL7A1	AC060834.2
NDRG1	GNMT	snoU13.458	ARRDC3
CHST1	BAMBI	ARMC3	TUFT1
CDC42EP3	TXNIP	AC064874.2	THBS3
TRIM29	HIST1H2AD	CPAMD8	HIST1H4J
hsa-mir-1977.1	J01415.11	AC136698.1	BTG1
NANOS1	IL1R1	ARHGEF37	TP53INP1
ELF3	HES1	RP4-717I23.3	GSTM2P1
HIST1H4H	J01415.9	C1orf194	MLLT4
U6.1189	ID3	MTERFD3	HIST1H3D
J01415.10	AL132988.2	RP11-539L10.3	PIK3R3
FGFR4	L1CAM	KIAA1984	FAM134B

Down >4-fold 1.0 μM PA

AC034193.1	SLC39A11	PDZK1P2
GMDS	U6.133	PDZK1P1
TFF1	TFF3	PDZK1
RALGPS1	EXOC4	PIP
TRAPPC9	DENND1A	
RP11-1018J8.2	AC126407.1	
CTD-2313N18.7	IMMP2L	
SMYD3	C11orf49	
RP11-206M11.7	TIAM1	

Table 3.2 Genes whose induction (or repression) by E2 is inhibited (or repressed by) **1 (1 μM)**

Genes upregulated by E2 >2-fold and downregulated by 1 >2-fold

SPINK4
ACOX2
OLFM1
SLC6A14
FLT4
GRIK3
FHL2
JPH2
MGP
RERG
HINT1
ACER3
AC034193.1
CLSTN2
APOD
MAPK9
OSGIN1
C9orf46
TAB1
ETNK2
AC005077.9
ACOT7
OLFML3
RP13-582O9.5
SERPINA1
VEPH1
EIF2B3
DDX10
WT1
TFF1
PDZK1P2
RP11-1018J8.2
DOK7
PDZK1P1
PDZK1
TFF3
MYEOV
SUSD3
AC126407.1
THSD4
U6.694
SERPINA6
RP11-206M11.7

Genes downregulated by E2 >2-fold and upregulated by 1 >2-fold

TGFB2
snoU13.267
5S_rRNA.486
NDRG1
hsa-mir-1977.1
J01415.10
AC114498.3
DUSP1
CALD1
BAMBI
TXNIP
IL1R1
HES1
PDP1
OSR2
AMIGO2
AC064874.2
SLC25A29
SELENBP1
TUFT1
TP53INP1
HIST1H3D
RP11-466C23.3
OPLAH
GPRC5A
MEGF6
SOX4
J01415.4
PSD4
AC022007.5
CCNG2
HIST2H4A
HIST2H4B
TMEM44
MB
ZNF251
AC010487.1
LYPD3
PNRC1
MTUS1
HIST1H2BD
LPIN3
MTRNR2L2
GABBR1
ABCC5
BX322557.10
KLHL24
CLK4
GABARAPL1
FAM193B
GRB7
RP5-857K21.14
AC044860.2
ANKRD10
C9orf3
SCARNA17
PLXNA1
JDP2
HDAC10
PABPC1L
AMOTL2
ZMIZ2
LZTR1
ESPN
RC3H1
J01415.19
TSPYL2
ENGASE
PPAPDC1B
J01415.24
AC005261.1
UPK2
AQP3
5_8S_rRNA.6
AL132988.3
RP11-383C5.4
RASL11B
CDC42EP3
ELF3
U6.1189
RP5-1174J21.1
snoU2_19.4
HIST1H2AD
snoU13.458
AC136698.1
RP11-539L10.3
ARRDC3
MTRNR2L9
J01415.1
AL593851.1
RALGDS
PTPRU
ATHL1
CC2D1B
CASP4

References

1. Kumar V, Chambon P. The estrogen receptor binds tightly to its responsive element as a ligand-induced homodimer. Cell 1988;55:145–56.

2. Manni A, Arafah B, Pearson OH. Estrogen and progesterone receptors in the prediction of response of breast-cancer to endocrine therapy. Cancer 1980;46:2838–41.

3. Burstein HJ, Prestrud AA, Seidenfeld J, Anderson H, Buchholz TA, Davidson NE, et al. American Society of Clinical Oncology clinical practice guideline: update on adjuvant endocrine therapy for women with hormone receptor-positive breast cancer. J Clin Oncol 2010;28:3784–96. Abstract/FREE Full Text

4. Dervan PB. Molecular recognition of DNA by small molecules. Biorg Med Chem 2001;9:2215–35.

5. Dervan PB, Edelson BS. Recognition of the DNA minor groove by pyrrole-imidazole polyamides. Curr Opin Struct Biol 2003;13:284–99.

6. Kielkopf CL, White S, Szewczyk JW, Turner JM, Baird EE, Dervan PB, et al. A structural basis for recognition of A•T and T•A base pairs in the minor groove of B-DNA. Science 1998;282:111–5. Abstract/FREE Full Text

7. White S, Baird EE, Dervan PB. On the pairing rules for recognition in the minor groove of DNA by pyrrole-imidazole polyamides. Chem Biol 1997;4:569–78.

8. Chenoweth DM, Dervan PB. Allosteric modulation of DNA by small molecules. Proc Natl Acad Sci U S A 2009;106:13175–9. Abstract/FREE Full Text

9. Chenoweth DM, Dervan PB. Structural basis for cyclic Py–Im polyamide allosteric inhibition of nuclear receptor binding. J Am Chem Soc 2010;132:14521–9.

10. Muzikar KA, Nickols NG, Dervan PB. Repression of DNA-binding dependent glucocorticoid receptor-mediated gene expression. Proc Natl Acad Sci U S A 2009;106:16598–603. Abstract/FREE Full Text

11. Nickols NG, Dervan PB. Suppression of androgen receptor-mediated gene expression by a sequence-specific DNA-binding polyamide. Proc Natl Acad Sci U S A 2007;104:10418–23. Abstract/FREE Full Text

12. Raskatov JA, Meier JL, Puckett JW, Yang F, Ramakrishnan P, Dervan PB. Modulation of NF-kappa B-dependent gene transcription using programmable DNA minor groove binders. Proc Natl Acad Sci U S A 2012;109:1023–8. Abstract/FREE Full Text

13. Nickols NG, Jacobs CS, Farkas ME, Dervan PB. Modulating hypoxia-inducible transcription by disrupting the HIF-1-DNA interface. ACS Chem Biol 2007;2:561–71.

14. Olenyuk BZ, Zhang GJ, Klco JM, Nickols NG, Kaelin WG, Dervan PB. Inhibition of vascular endothelial growth factor with a sequence-specific hypoxia response element antagonist. Proc Natl Acad Sci U S A 2004;101:16768–73. Abstract/FREE Full Text

15. Yang F, Nickols NG, Li BC, Marinov GK, Said JW, Dervan PB. Antitumor activity of a pyrrole-imidazole polyamide. Proc Natl Acad Sci U S A 2013;110:1863–8. Abstract/FREE Full Text

16. Fukasawa A, Aoyama T, Nagashima T, Fukuda N, Ueno T, Sugiyama H, et al. Pharmacokinetics of pyrrole-imidazole polyamides after intravenous administration in rat. Biopharm Drug Dispos 2009;30:81–9.

17. Nagashima T, Aoyama T, Fukasawa A, Watabe S, Fukuda N, Ueno T, et al. Determination of pyrrole-imidazole polyamide in rat plasma by liquid chromatography-tandem mass spectrometry. J Chromat B: Biomed Sci Appl 2009;877:1070–6. Caltech ConnectCrossRefGoogle Scholar

18. Nagashima T, Aoyama T, Yokoe T, Fukasawa A, Fukuda N, Ueno T, et al. Pharmacokinetic modeling and prediction of plasma pyrrole-imidazole polyamide concentration in rats using simultaneous urinary and biliary excretion data. Biol Pharm Bull 2009;32:921–7.

19. Matsuda H, Fukuda N, Ueno T, Katakawa M, Wang X, Watanabe T, et al. Transcriptional inhibition of progressive renal disease by gene silencing pyrrole-imidazole polyamide targeting of the transforming growth factor-beta 1 promoter. Kidney Int 2011;79:46–56.

20. Raskatov JA, Nickols NG, Hargrove AE, Marinov GK, Wold B, Dervan PB. Gene expression changes in a tumor xenograft by a pyrrole-imidazole polyamide. Proc Natl Acad Sci U S A 2012;109:16041–5. Abstract/FREE Full Text

21. Gearhart MD, Dickinson L, Ehley J, Melander C, Dervan PB, Wright PE, et al. Inhibition of DNA binding by human estrogen-related receptor 2 and estrogen receptor alpha with minor groove binding polyamides. Biochemistry 2005;44:4196–203.

22. White S, Szewczyk JW, Turner JM, Baird EE, Dervan PB. Recognition of the four Watson–Crick base pairs in the DNA minor groove by synthetic ligands. Nature 1998;391:468–71.

23. Nickols NG, Jacobs CS, Farkas ME, Dervan PB. Improved nuclear localization of DNA-binding polyamides. Nucleic Acids Res 2007;35:363–70. Abstract/FREE Full Text

24. Synold TW, Xi B, Wu J, Yen Y, Li BC, Yang F, et al. Single-dose pharmacokinetic and toxicity analysis of pyrrole-imidazole polyamides in mice. Cancer Chemother Pharmacol 2012;70:617–25.

25. Wilson VS, Bobseine K, Gray LE. Development and characterization of a cell line that stably expresses an estrogen-responsive luciferase reporter for the detection of estrogen receptor agonist and antagonists. Toxicol Sci 2004;81:69–77. Abstract/FREE Full Text

26. Puckett JW, Green JT, Dervan PB. Microwave assisted synthesis of Py–Im polyamides. Org Lett 2012;14:2774–7.

27. Best TP, Edelson BS, Nickols NG, Dervan PB. Nuclear localization of pyrrole-imidazole polyamide-fluorescein conjugates in cell culture. Proc Natl Acad Sci U S A 2003;100:12063–8. Abstract/FREE Full Text

28. Edelson BS, Best TP, Olenyuk B, Nickols NG, Doss RM, Foister S, et al. Influence of structural variation on nuclear localization of DNA-binding polyamide-fluorophore conjugates. Nucleic Acids Res 2004;32:2802–18. Abstract/FREE Full Text

29. Nowak DE, Tian B, Brasier AR. Two-step cross-linking method for identification of NF-kappa B gene network by chromatin immunoprecipitation. Biotechniques 2005;39:715–25.

30. Raskatov JA, Hargrove AE, So AY, Dervan PB. Pharmacokinetics of Py–Im polyamides depend on architecture: cyclic versus linear. J Am Chem Soc 2012;134:7995–9.

31. Langmead B, Trapnell C, Pop M, Salzberg SL. Ultrafast and memory-efficient alignment of short DNA sequences to the human genome. Genome Biol 2009;10:R25.

32. Anders S, Huber W. Differential expression analysis for sequence count data. Genome Biol 2010;11:R106.

33. Welboren WJ, van Driel MA, Janssen-Megens EM, van Heeringen SJ, Sweep FCGJ, Span PN, et al. ChIP-Seq of ER alpha and RNA polymerase II defines genes differentially responding to ligands. EMBO J 2009;28:1418–28.

34. Stabile LP, Lyker JS, Gubish CT, Zhang W, Grandis JR, Siegfried JM. Combined targeting of the estrogen receptor and the epidermal growth factor receptor in non–small cell lung cancer shows enhanced antiproliferative effects. Cancer Res 2005;65:1459–70. Abstract/FREE Full Text

35. Lau KM, LaSpina M, Long J, Ho SM. Expression of estrogen receptor (ER)-alpha and ER-beta in normal and malignant prostatic epithelial cells: regulation by methylation and involvement in growth regulation. Cancer Res 2000;60:3175–82. Abstract/FREE Full Text

36. Le Page Y, Scholze M, Kah O, Pakdel F. Assessment of xenoestrogens using three distinct estrogen receptors and the zebrafish brain aromatase gene in a highly responsive glial cell system. Environ Health Perspect 2006;114:752–8. Caltech ConnectMedlineGoogle Scholar

37. Devidze N, Fujimori K, Urade Y, Pfaff DW, Mong JA. Estradiol regulation of lipocalin-type prostaglandin D synthase promoter activity: evidence for direct and indirect mechanisms. Neurosci Lett 2010;474:17–21.

38. Trapnell C, Roberts A, Goff L, Pertea G, Kim D, Kelley DR, et al. Differential gene and transcript expression analysis of RNA-seq experiments with TopHat and Cufflinks. Nat Protoc 2012;7:562–78.

39. Madak-Erdogan Z, Kieser KJ, Kim SH, Komm B, Katzenellenbogen JA, Katzenellenbogen BS. Nuclear and extranuclear pathway inputs in the regulation of global gene expression by estrogen receptors. Mol Endocrinol 2008;22:2116–27.

40. Little M, Wells C. A clinical overview of WT1 gene mutations. Hum Mutat 1997;9:209–25.

41. Yang L, Han Y, Saurez Saiz F, Minden MD. A tumor suppressor and oncogene: the WT1 story. Leukemia 2007;21:868–76. Caltech ConnectMedlineGoogle Scholar

42. Loeb DM, Evron E, Patel CB, Sharma PM, Niranjan B, Buluwela L, et al. Wilms' tumor suppressor gene (WT1) is expressed in primary breast tumors despite tumor-specific promoter methylation. Cancer Res 2001;61:921–5. Abstract/FREE Full Text

43. Miyoshi Y, Ando A, Egawa C, Taguchi T, Tamaki Y, Tamaki H, et al. High expression of Wilms' tumor suppressor gene predicts poor prognosis in breast cancer patients. Clin Cancer Res 2002;8:1167–71. Abstract/FREE Full Text

44. Foekens JA, Rio MC, Seguin P, Vanputten WLJ, Fauque J, Nap M, et al. Prediction of relapse and survival in breast-cancer patients by PS2 protein status. Cancer Res 1990;50:3832–7. Abstract/FREE Full Text

45. Stender JD, Kim K, Charn TH, Komm B, Chang KC, Kraus WL, et al. Genome-wide analysis of estrogen receptor alpha DNA binding and tethering mechanisms identifies Runx1 as a novel tethering factor in receptor-mediated transcriptional activation. Mol Cell Biol 2010;30:3943–55. Abstract/FREE Full Text

46. Huang da W, Sherman BT, Lempicki RA. Systematic and integrative analysis of large gene lists using DAVID bioinformatics resources. Nat Protoc 2009;4:44–57.

47. Huang da W, Sherman BT, Lempicki RA. Bioinformatics enrichment tools: paths toward the comprehensive functional analysis of large gene lists. Nucleic Acids Res 2009;37:1–13. Abstract/FREE Full Text

48. Ishii Y, Waxman S, Germain D. Tamoxifen stimulates the growth of cyclin D1—overexpressing breast cancer cells by promoting the activation of signal transducer and activator of transcription 3. Cancer Res 2008;68:852–60. Abstract/FREE Full Text

49. Hargrove AE, Raskatov JA, Meier JL, Montgomery DC, Dervan PB. Characterization and solubilization of pyrrole-imidazole polyamide aggregates. J Med Chem 2012;55:5425–32.

C h a p t e r 4

TUMOR XENOGRAFT UPTAKE OF A PYRROLE–IMIDAZOLE (PY-IM) POLYAMIDE VARIES AS A FUNCTION OF CELL LINE GRAFTED

The text of this chapter was taken in part from a manuscript co-authored with Jevgenij A. Raskatov and Peter B. Dervan.

(Raskatov JA, Szablowski JO, Dervan PB, "Tumor Xenograft Uptake of a Py Im Polyamide Varies as a Function of Cell Line Grafted", J. Med Chem. 57(20):8471-6 (2013))

Abstract

Subcutaneous xenografts represent a popular approach to evaluate efficacy of prospective molecular therapeutics *in vivo*. In the present study, the C-14 labeled radioactive Py-Im polyamide 1, targeted to the 5'-WGWWCW-3' DNA sequence, was evaluated with regard to its uptake properties in subcutaneous xenografts, derived from the human tumor cell lines LNCaP (prostate), A549 (lung), and U251 (brain), respectively. Significant variation in compound tumor concentrations was seen in xenografts derived from these three cell lines. Influence of cell line grafted on systemic polyamide elimination was established. With A549, a marked variation in localization of 1 was determined between matrigel-negative and -positive xenografts. An extensive tissue distribution analysis of 1 in wild-type animals was conducted, enabling the comparison between the xenografts and the corresponding host organs of origin.

Introduction

Cancer represents a major worldwide health problem, with nearly 1.6 million new cases estimated to occur in 2014 in the US alone.[1] The past forty years of research and development of therapeutics has brought improved patients' survival[2], however, malignant neoplasias remain the second most common cause of death in the US, accounting for over 20 % of all deaths.[3] Consequentially, major efforts are being put into the development of novel therapeutic approaches.[4] Treatment strategies of various classes are currently available in the clinic. Classical approaches comprise surgery, chemotherapy, radiation therapy and immunotherapy, with the method of choice depending on tumor type and progression stage.[5] Cancer chemotherapy has recently seen important conceptual advances, such as tumor-specific tissue targeting,[6] prodrug modifications,[7] and development of small molecule inhibitors of aberrant signaling nodes in cancer.[8] A significant drawback of molecules targeted to tumor-specific features is the introduction of evolutionary pressure upon the cancer cells, which often results in the emergence of resistant clones.[9] Broadly cytotoxic chemotherapeutics (*e.g., cis*-platin or doxorubicin), on the other hand, commonly exhibit severe side-effects, such as cardio-,[10] and neurotoxicity,[11] as well as neutropenia.[12]

Py-Im polyamides are a modular class of DNA-binding small molecules, capable of binding defined sequences with affinities and specificities comparable to those of DNA-binding proteins.[13] They are cell-permeable scaffolds,[14] and have been shown to displace various transcription factors from cognate binding sites[15], leading to altered gene expression profiles. Inhibition of RNA pol II elongation was observed, accompanied by degradation of the large RNA pol II subunit and induction of the p53 stress response,

without concomitant DNA damage.[16] Most recently, our laboratory has transitioned to *in vivo* experimentation, demonstrating bioavailability,[17] and efficacy of varying Py-Im polyamides in tumor xenografts models in mouse.[16,18] Antitumor effects with limited systemic toxicity were observed with the subcutaneous LNCaP prostate cancer model.[16] Our recent C-14 based quantitation study established significant enrichment of a Py-Im polyamide in the LNCaP tumor xenograft tissue over lung and kidney.[19] The present investigation evaluates the biodistribution of the C-14 radioactively labeled Py-Im polyamide **1** (Fig. 4. 1A) in a range of tumor xenografts, addresses the influence of xenografted cell line on systemic polyamide elimination, and provides an extended biodistribution profile of the molecule.

Results

C-14 radioactively labeled Py-Im polyamide 1 exhibits differential uptake between tumor xenografts of varying cellular origin. Initial experiments compared the accumulation of compound **1** in LNCaP and A549 subcutaneous tumor xenografts (Fig. 4.1A). In order to minimize the injection-associated experimental error, both tumors were grafted on the opposing flanks of the same host animal, following the schedule displayed in Fig. 4.2. A mean compound concentration of 1.04 mg/kg (0.74 μM) was measured for the LNCaP xenograft tissue, comparable with liver-associated levels of 1.12 mg/kg (Fig. 4.1B). Strikingly, A549 tumors were found to uptake substantially lower amounts of polyamide **1** (average of 0.23 mg/kg), closely resembling the values obtained for the kidney (0.27 mg/kg), and approximately two-fold higher than lung tissue (0.15 mg/kg). Comparisons with the corresponding single-xenograft versions of the experiment were conducted for both tumor types (Fig. 4.1C). The LNCaP single tumor experiment revealed a mildly elevated concentration with respect to the double xenograft counterpart (42 %, $p < 0.05$),[19] whereas the values obtained for A549 were not distinguishable between the two experiment types. Overall, Py-Im polyamide **1** localized to LNCaP (prostate) tumors at concentrations five to seven-fold higher than those measured with A549 (lung).

To gain deeper understanding of the phenomenon, immunohistochemical analyses were conducted, assaying for tumor-associated microvessels (Figures 3 and 4). Microvessel densities were indistinguishable between the two tumor types. However, LNCaP xenografts were hemorrhagic and exhibited vascular spaces with extravasated red blood cells at the microscopic level, which were absent with A549. In order to broaden the scope

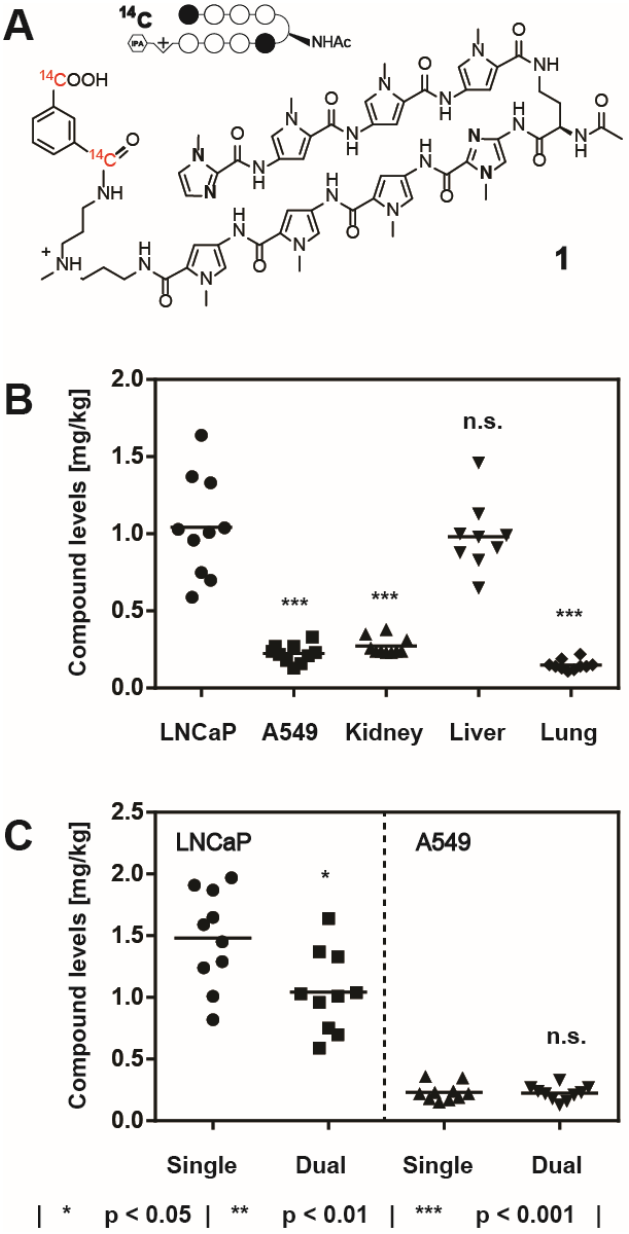

Fig. 4.1. A) The C-14 radiolabeled Py-Im polyamide **1**, targeted to the DNA sequence 5'-WGWWCW-3'. B) Compound levels of **1** in LNCaP and A549 tumor xenografts, compared against major host organs (kidney, liver, lung). Statistical comparison performed against the LNCaP tumor concentration of **1**. C) Calibration of the dual xenograft experiment against the respective single-tumor versions. All injections were performed intraperitoneally at 20 nmol per animal (NSG male mouse, N=10) and tissues harvested 24 hours following administration. Each datapoint represents an individual organ / tumor analyzed.

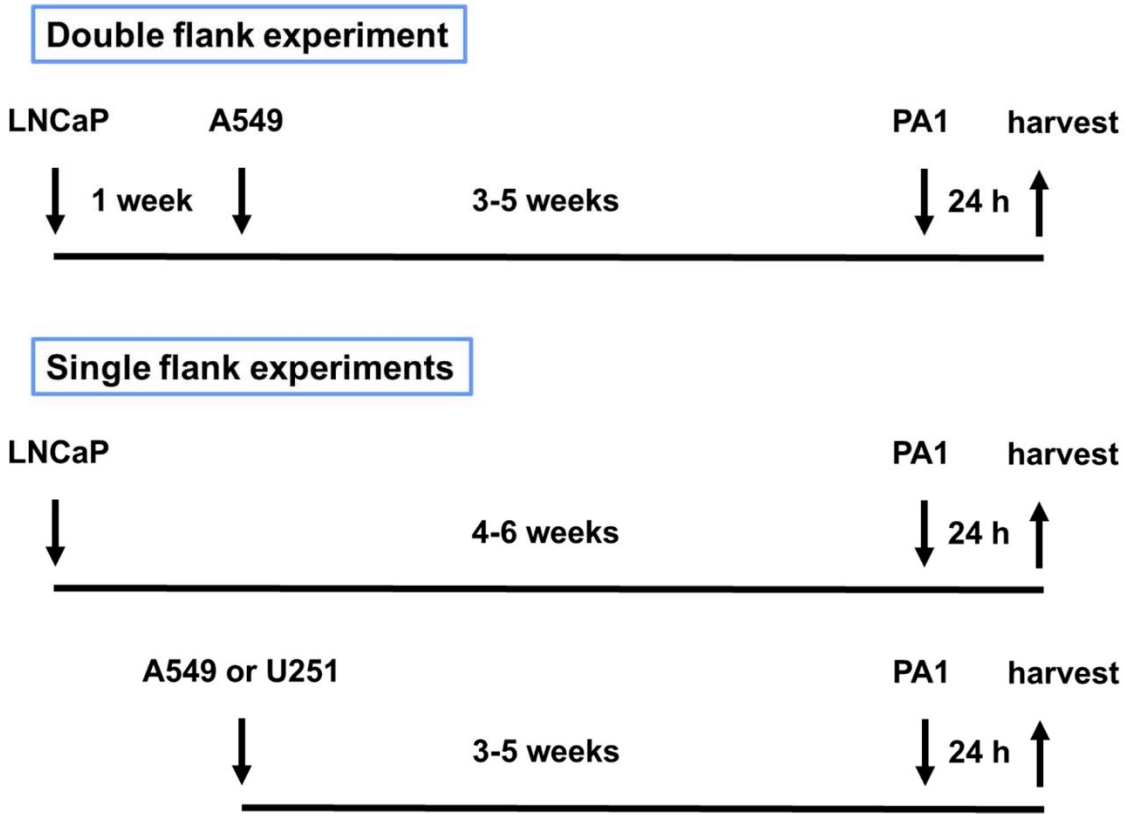

Fig. 4.2. Engraftment and polyamide administration schedules for the double flank experiment and the single flank versions.

of the investigation, the U251 (brain) cell line was additionally evaluated in the xenograft setting with regard to uptake of 1 (Fig. 4.5). A mean value of 0.65 mg/kg (0.47 μM) was measured. The U251-associated xenograft uptake profile was found to be distinct from both LNCaP and A549-derived tissues, which were 2.3-fold higher and 2.8-fold lower, respectively.

None of the tumor-associated levels of Py-Im polyamide **1**, discussed above, exhibited a correlation with tumor size over the window analyzed (Fig. 4.6A-D,F).

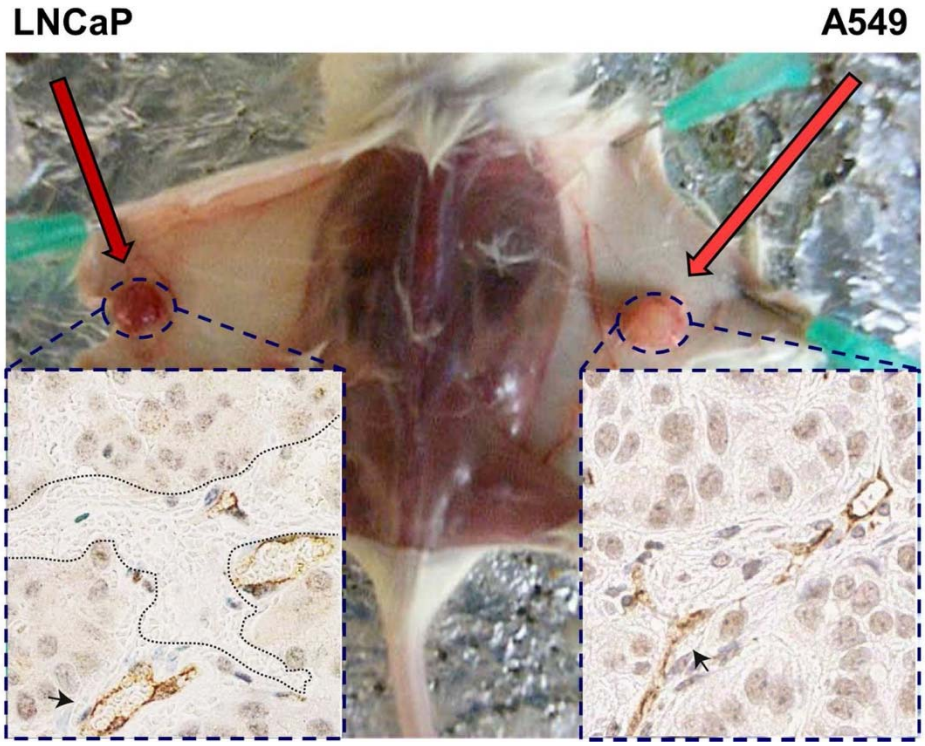

Fig. 4.3. A representative NSG male mouse that was grafted with LNCaP (2.5 x 10$_6$ in 1:1 media / matrigel) and A549 (2.5 x 10$_6$ in media), following schedule outlined in (A). Representative histological slices (CD31 stain) are displayed in the inset graphics. LNCaP tumor displays poorly defined vascular spaces with extravasated red blood cells (indicated with the dotted line), absent with A549. Arrows highlight some blood vessels.

Host organ levels of Py-Im polyamide 1 as a function of the subcutaneously grafted cell line. The major host organs kidney, liver, and lung were interrogated with regard to concentrations of **1** for all xenograft experiments, and benchmarked against the naïve background control (Fig. 4.7). Kidney concentrations spanned a range from 0.22 mg /kg (naïve control and A549 xenograft animals) to 0.27 mg/kg (double xenograft experiment).

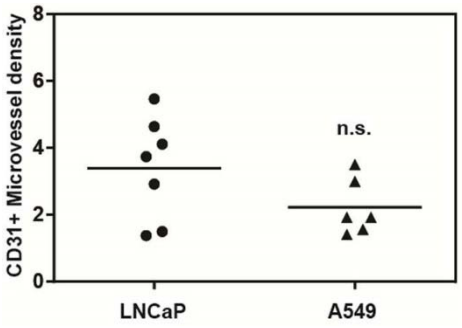

Fig. 4.4. Microvessel density quantitated for LNCaP and A549 tumor sections, respectively.

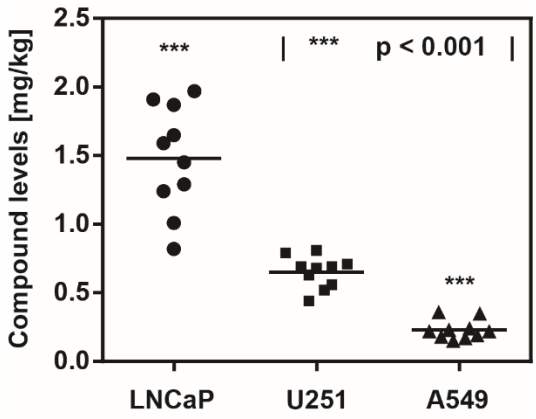

Fig. 4.5. Tumor levels of Py-Im polyamide **1** as a function of cell line engrafted. All injections were performed intraperitoneally at 20 nmol per animal (NSG male mouse, N=10) and tissues harvested 24 hours following administration. Each datapoint represents an individual tumor analyzed. Statistical comparison was performed against the U251 tumor concentration of **1**.

Lung tissue showed similar variance in concentration of **1** as a function of xenografted cell line (0.12 to 0.15 mg/kg). A more significant difference was noted for the liver-associated compound levels. Whereas naïve reference animals were indistinguishable from U251- or A549-xenograft bearers, grafting of the LNCaP cell line resulted in liver values that were about two-fold higher (1.04 mg/kg vs 0.57 mg/kg; $p < 0.001$).

Matrigel affects uptake of Py-Im polyamide 1 into A549 xenografts. We chose to evaluate the influence of matrigel on uptake of **1** for xenografts derived from the A549 cell line. Systematic analysis of tumor polyamide concentration as a function of size revealed that larger tumors accumulated substantially higher quantities of compound **1** when matrigel was employed during engraftment (Fig. 4.6F). This was in striking contrast with the observations made for the same cell line grafted without matrigel (Fig. 4.6A,C).

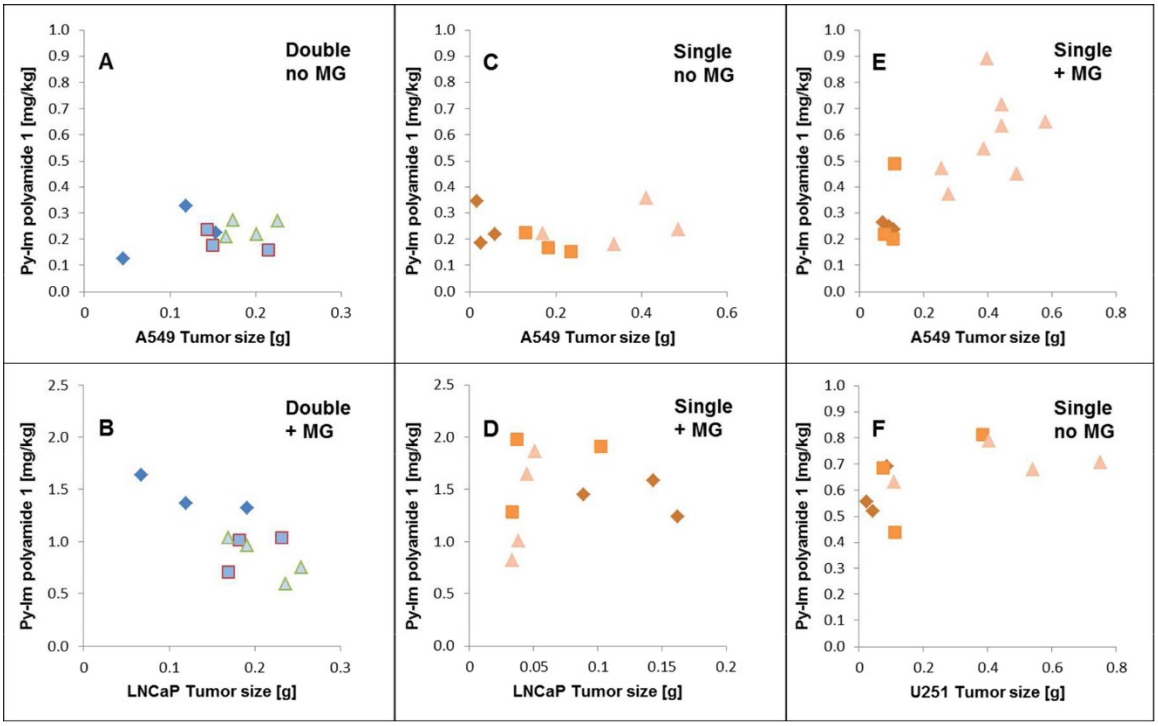

Fig. 4.6. Tumor concentration of Py-Im polyamide **1** as a function of size. MG denotes matrigel; double / single indicates whether the animals was grafted twice or once, respectively (only relevant with A549 and LNCaP). Post-engraftment time is coded by diamonds (4 weeks with LNCaP, 3 weeks with A549 or U251), squares (5 weeks with LNCaP, 4 weeks with A549 or U251), and triangles (6 weeks with LNCaP, 5 weeks with A549 or U251).

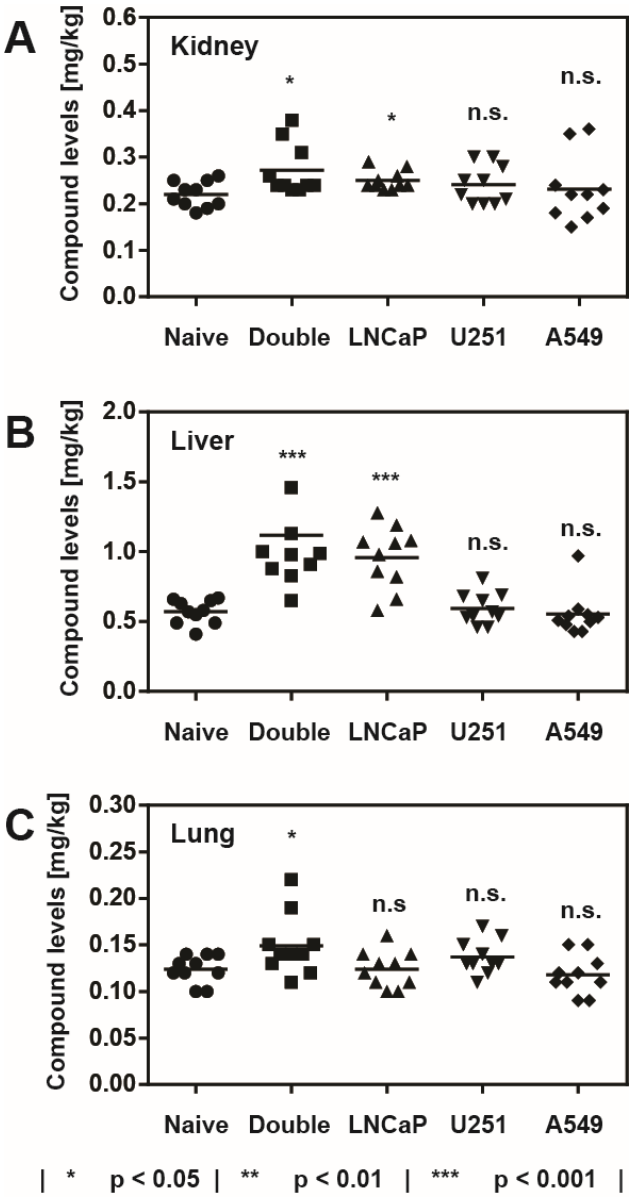

Fig. 4.7. Concentrations of polyamide **1** in the host organs kidney (A), liver (B), and lung (C) as a function of cell line engrafted. Naïve indicates reference host animals devoid of tumor graft. All injections were performed intraperitoneally at 20 nmol per animal (NSG male mouse, N=10) and tissues harvested 24 hours following administration. Each datapoint represents an individual organ analyzed.

Plotting of tumor-associated levels of **1** as a function of post-engraftment time revealed a clear trend (Fig. 4.8). Three or four weeks past engraftment, there was no statistically significant difference measurable between the A549 xenografts produced with or without matrigel, with an averaged concentration of 0.23 mg/kg (0.16 μM). Five weeks past engraftment, however, a divergence became apparent. Whereas matrigel-negative tumors showed levels of compound **1** indistinguishable from earlier timepoints (0.25mg/kg), a marked increase was noted for the matrigel-positive xenografts. A mean concentration of 0.59 mg/kg was measured ($p < 0.001$), with the highest value amounting to 0.89 mg/kg, therewith reaching values comparable to those obtained for LNCaP tumors (cf. Figures 1 and 5).

Extended tissue distribution analysis of 1 in wild-type mice. In order to obtain a more complete picture of biodistribution of Py-Im polyamide **1**, a comprehensive tissue analysis

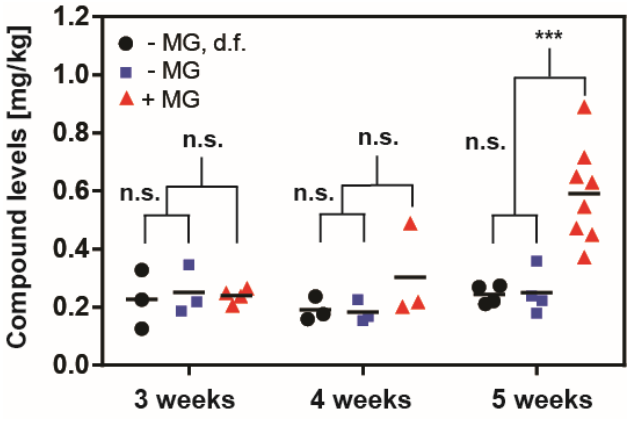

Fig. 4.8. A549 Tumor levels of Py-Im polyamide **1** as a function of time (3-5 weeks), presence of the LNCaP tumor on the opposite flank (denoted as d.f.), and matrigel used to engraft (+/- MG). All injections were performed intraperitoneally at 20 nmol per animal (NSG male mouse) and tumors harvested 24 hours following administration. Each datapoint represents an individual tumor analyzed. | *** $p < 0.001$ |

following administration of **1** was conducted in the balb/c mouse strain. Blood, bone marrow (BM), brain, fat tissue, intestinal tissue, heart, kidney, liver, lung, muscle, pancreas, prostate, and spleen were interrogated independently (Fig. 4.9). Because the balb/c male mouse of comparable age possesses a body weight that is reduced by some 25% with regard to its NSG counterpart, compound **1** was administered at 15 nmol per animal here, as opposed to 20 nmol per animal employed with NSG mice.

The majority of tissues exhibited concentrations of **1** below 0.1 mg/kg, with the brain not showing any significant evidence of polyamide uptake. Kidney and liver were found to contain comparable compound levels to those determined for the NSG strain (0.23 mg/kg vs 0.22 mg/kg and 0.57 mg/kg vs 0.49 mg/kg for kidney and liver, respectively). Interestingly, bone marrow concentration of **1** amounted to 0.24 mg/kg, therewith being over 10-fold higher than blood. The spleen exhibited a concentration of **1** of 0.32 mg/kg, whereas the pancreas contained compound **1** at 0.15 mg/kg. The majority of organs contained the Py-Im polyamide **1** at concentrations that were significantly lower than those determined for any of the tumor xenografts examined above.

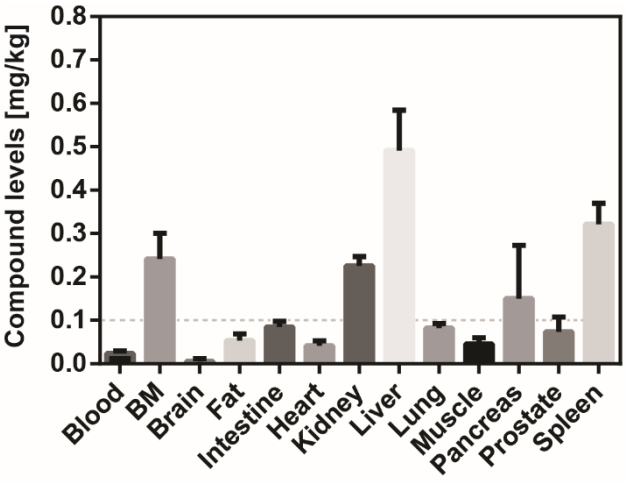

Fig. 4.9. Extended tissue distribution analysis of Py-Im polyamide **1** in wild-type mice. Injections were performed intraperitoneally at 15 nmol per animal (balb/c male mouse) and organs harvested 24 hours following administration. Error bars represent standard deviations (N = 5). BM denotes bone marrow. Dashed line indicates the 0.1 mg/kg threshold.

Discussion

The xenograft approach is a popular method to interrogate a prospective antitumor agent *in vivo*.[20] It can be subdivided into two main categories, namely subcutaneous (ectopic) and orthotopic xenografts. Orthotopic inoculation is considered to recapitulate the tumor setting more closely than the subcutaneous approach, because cancer cells are grafted into the host organ of tumor origin. With the exception of lung and blood cancer, for which orthotopic xenografts are readily achievable by tail vein injection, the approach is experimentally demanding, and requires sophisticated survival surgery. Genetically engineered animal tumor models represent an attracttive alternative to xenograft experimentation, since they tend to recapitulate certain aspects of disease progression, such as tumor vascularization, tumor-stroma interactions, and metastasis formation, more accurately.[21] They furthermore allow for conducting experiments in immunecompetent

animals. The studies are, however, elaborate to perform, requiring extended experimentation time frames and large animal group sizes. Furthermore, xenografts allow the assessment of efficacy against human cancer cell lines and primary cells, whereas genetically engineered animal models are limited to neoplasias of the species employed. Given the above, subcutaneous xenografts remain an attractive method to generate initial estimates of efficacy for molecules of interest.[22]

The present study was initiated to rationalize the apparent discrepancy between cell culture results and the corresponding xenograft experiments that we observed in preceding investigations.[16b,18a] Specifically, *in vitro* cytotoxicity evaluation for the non-radioactive analogue of **1** revealed A549 and LNCaP to possess comparable sensitivities towards polyamide treatment (IC_{50} values of 1.5 ± 0.2 μM and 2.1 ± 0.3 μM,[16b] respectively). This contrasted with the outcome of our *in vivo* investigations, with LNCaP xenografts exhibiting tumor burden reduction in response to treatment with **1** in the xenograft setting,[16b] while related studies with the A549 cell line were unsuccessful.[18a] The present investigation demonstrates this unanticipated result to be rooted, at least in part, in the pronounced difference in polyamide uptake between the two xenograft types, LNCaP tumors accumulating the compound at five- to seven-fold higher levels than their A549 counterparts (Fig. 4.1) in both the double-flank experiment and the single xenograft experiments with A549 and LNCaP.[19] Additional discrepancy may stem from the difference in the time frame employed for *in vitro* cytotoxicity measurement (3 days) and *in vivo* antitumor evaluation (at least 7 days), and the fact that the polyamide concentration is kept constant over the course of the experiment *in vitro*, but not *in vivo*.[19]

Comparison with U251 xenografts revealed an uptake profile that was distinct from both LNCaP- and A549-derived tumors (Fig. 4.2). This leads to the important realization that neither LNCaP nor A549 could be considered an outlier. Each cell line examined yielded tumors with characteristic uptake features, which, while clearly dependent on the cell line grafted, could not have been predicted from *in vitro* experiments. The U251-derived xenografts exhibited higher microvessel densities than both A549 and LNCaP tumors, without, however, possessing the vascular spaces characteristic of LNCaP.[23] This likely gave rise to distinct characteristics of U251 tumors.

It was surprising to find that liver accumulation of **1** was dependent on the cell line grafted. Whereas the grafting of A549 or U251 cells showed no influence, the presence of LNCaP-derived tumors resulted in levels that were elevated by about twofold (Fig. 4.3). This was possibly due to the increased leakiness of the tumor vasculature in LNCaP xenografts, as compared with A549 (Fig. 4.SI 2), and U251.[23] Matrigel-positive xenografts did not result in increased liver compound values as compared to their matrigel-negative counterparts (0.65 mg/kg *vs* 0.55 mg/kg, $p = 0.17$). It is possible that the leaky LNCaP tumor vasculature creates liver stress, which in turn could result in impeded clearance of Py-Im polyamide **1**. This phenomenon is likely to operate with other types of small molecule therapeutics, although the magnitude of the effect will be dependent on specifics, which could lead to alternative clearance mechanisms.

The influence of matrigel on uptake of **1** by A549 xenografts was of interest due to the common use of matrigel to facilitate engraftment of tumor cells *in vivo*.[24] An effect indeed became manifest, albeit only at the most advanced post-engraftment timepoints (Fig. 4.4 and Fig. 4.SI 4E). It appears likely that the A549 tumor architecture diverges at advanced

time points, as a function of matrigel. Supporting this, slightly higher weights were noticed in the matrigel-positive group than in the matrigel-negative control at the point of divergence (average of 409 mg *vs* 271 mg; $p < 0.05$). Influence of matrigel employment on tumor proliferation, vascularization and metastasis have been previously documented.[24] The xenograft host-tumor interface being artificial *a priori*, it is unclear, whether the matrigel-positive or -negative tumors give rise to more accurate models.

Comparisons of uptake between tumors and the corresponding healthy host tissues were of interest, in order to probe for potential enrichment in cancer lesions. The LNCaP xenografts exhibited concentrations ranging from 0.5 mg/kg to 2.0 mg/kg, thus being an order of magnitude higher than what was determined for mouse prostate, which possessed an averaged value below 0.1 mg/kg. It is therefore possible that the compound quantities measured in LNCaP subcutaneous xenografts provide optimistic estimates. However, tumor formation does perturb organ integrity, and it therefore appears likely that diseased prostate tissue should exhibit values different from the healthy organ in both the orthotopic and the genetically induced disease model setting. It should furthermore be noted that LNCaP was derived from a metastatic lymph node lesion, which, although having originated from a prostate tumor, likely possessed a distinct architecture. Tumors derived from the A549 cell line (non-small lung carcinoma) can be compared with lung tissue concentrations of **1**. With the exception of the elevated values that were determined in matrigel-positive tumors at extended time points, they averaged at approximately 0.2 mg/kg, whereas healthy lung tissue exhibited concentrations of **1** around 0.1 mg/kg. Whether this is a coincidence or indeed evidence that A549 xenografts mimic the lung tissue setting more adequately remains unclear. Lung colonization experiments may be

useful to shed further light onto this question in future studies. U251 is a glioblastoma-derived cell line, and the healthy organ of origin is the brain. The corresponding comparison between tumor and tissue of origin lacks substance, since the subcutaneous xenograft cannot be expected to recapitulate the blood brain barrier. Overall, and keeping the above-mentioned caveats in mind, tumors generally accumulated higher amounts of compound **1** than the corresponding healthy tissues of origin.

Conclusions

The present study identified a marked difference in xenograft uptake levels of Py-Im polyamide **1** in the three cell lines tested. LNCaP-derived tumors exhibited a mean concentration of the polyamide that was over fivefold higher that the corresponding A549-associated value. Compound **1** was found to localize to U251 xenografts at a concentration that was substantially lower than what was found for LNCaP, but significantly higher than A549. This demonstrates the necessity of examining uptake into tumor xenografts on a case by case basis in order to rationalize outcomes of antitumor studies and to identify viable cell lines for future xenograft experiments. Unexpectedly, elimination of **1** from the liver was impaired in LNCaP xenograft-bearing animals. Matrigel was found to influence uptake of **1**, resulting in a twofold elevation at longer post-engraftment time points with A549-derived tumors. Comparison with the corresponding healthy tissues revealed that higher concentrations of **1** were associated with xenografts, with animal prostate tissue exhibiting order of magnitude lower values than those measured with LNCaP tumors.

Experimental Section

Polyamide Synthesis and Characterization. The synthesis of polyamide **1** has been previously reported.[19] The compound was confirmed by analytical HPLC to possess a purity of >99%, and co-eluted with its non-radioactive analog. Polyamide **1** was quantitated employing liquid scintillation with the activity constants of 55 mCi/mmol, which was provided by the vendor (ARC). Quench correction was conducted against a standard curve that was reported by our laboratory in a preceding account.[19]

Cell Culture Maintenance and Xenograft Establishment. The cell lines A549, LNCaP and U251 were obtained from ATCC and cultured following provider's recommendations, and not exceeding passage number 25. Cells were only employed for xenograft experimentation where a viability of 95 % or higher was recorded (trypan blue stain). Nod-SCID-Gamma (NSG) male mice were purchased at eight weeks of age from JAX and housed in an immunocompromised facility (level A) in accordance with IACUC regulations. They were taken forward for experiments after an acclimatization period of at least three days. All engraftments were conducted subcutaneously with 2.5 M cells per inoculation in 200 μL vehicle (either media or 1:1 mixture with matrigel). Animals were monitored weekly for signs of pain and distress. Male balb/c mice were obtained from JAX and housed in a level B animal facility.

Administration of polyamide 1 and tissue harvest. Compound **1** was quantitated by liquid scintillation counting prior to injection and administered intraperitoneally at either 20 nmol (NSG) or 15 nmol (balb/c) per animal in a fume hood dedicated exclusively to C-14 *in vivo* radioexperimentation. Animals were housed in disposable cages and euthanized by CO_2 asphyxiation. Disposable cages were destroyed at the end of the experiment.

Tissues were harvested, placed into scintillation vials, and solubilized at +65 °C for at least 12 hours, employing the proprietary dissolution agent SOLVABLE (Perkin-Elmer). The resultant solutions were decolorized with 2 x 200 µL hydrogen peroxide (30 %, Sigma Aldrich) at ambient temperature for at least 2 hours, followed by heating to +65 °C for 30 min. Samples were treated with 10 mL of the scintillation cocktail HIONIC-FLUOR (Perkin-Elmer), vortexed and the amounts of C-14 quantitated by liquid scintillation counting at the Beckman Coulter LS6500 Multi-Purpose Scintillation Counter. All reported values have been quench-corrected and normalized against organ weight. Bone marrow weights were calculated as the difference between the femur and tibia bones subjected to tissue solubilization, and the insoluble residue, which was isolated subsequent to C-14 quantitation. In order to obtain dry bone residues, the scintillation fluid was decanted, the solids triturated (twice with ethanol, then three times with MeOH), and dried at +65 °C overnight.

Acknowledgements

JAR is grateful to the Alexander von Humboldt foundation for the award of a Feodor Lynen postdoctoral fellowship. We thank Bogdan Olenyuk for helpful discussions.

References

(1)Siegel, R.; Ma, J.; Zou, Z.; Jemal, A. Cancer statistics, 2014. *CA - Cancer J. Clin.* **2014**, *64*, 9-29.

(2)Ries, L. A. G. et al. SEER cancer statistics review, 1975-2005. *U.S. National Institutes of Health, National Cancer Institute,* **2008**.

(3)Hoyert, D. L.; Xu, J. Deaths: Preliminary Data for 2011. *Natl. Vital Stat. Rep.* **2012**, *61*, 1-52.

(4)Patel, J. D. et al. Clinical Cancer Advances 2013: Annual Report on Progress Against Cancer From the American Society of Clinical Oncology. *J. Clin. Oncol.* **2014**, *32*, 129-160.

(5)Huitink, J. M.; Teoh, W. H. L. Current cancer therapies – A guide for perioperative physicians. *Best Pract. Res. Cl. An.* **2013**, *27*, 481-492.

(6)Peer, D.; Karp, J. M.; Hong, S.; FaroKhzad, O. C.; Margalit, R.; Langer, R. Nanocarriers as an emerging platform for cancer therapy. *Nat. Nanotechnol.* **2007**, *2*, 751-760.

(7)Denny, W. A. Prodrug strategies in cancer therapy. *Eur. J. Med. Chem.* **2001**, *36*, 577-595.

(8)a) Druker, B. J. et al. Efficacy and safety of a specific inhibitor of the BCR-ABL tyrosine kinase in chronic myeloid leukemia. *N. Engl. J. Med.* **2001**, *344*, 1031-1037; b)

Baselga, J.; Arteaga, C. L. Critical update and emerging trends in epidermal growth factor receptor targeting in cancer. *J. Clin. Oncol.* **2005**, *23*, 2445-2459.

(9)Tsuruo, T.; Naito, M.; Tomida, A.; Fujita, N.; Mashima, T.; Sakamoto, H.; Haga, N. Molecular targeting therapy of cancer: drug resistance, apoptosis and survival signal. *Cancer Sci.* **2003**, *94*, 15-21.

(10)Pai, V. B.; Nahata, M. C. Cardiotoxicity of chemotherapeutic agents - Incidence, treatment and prevention. *Drug Saf.* **2000**, *22*, 263-302.

(11)Verstappen, C. C. P.; Heimans, J. J.; Hoekman, K.; Postma, T. J. Neurotoxic complications of chemotherapy in patients with cancer - Clinical signs and optimal management. *Drugs* **2003**, *63*, 1549-1563.

(12)Aapro, M. S. et al. EORTC guidelines for the use of granulocyte-colony stimulating factor to reduce the incidence of chemotherapy-induced febrile neutropenia in adult patients with lymphomas and solid tumours. *Eur. J. Cancer* **2006**, *42*, 2433-2453.

(13)a) Dervan, P. B.; Edelson, B. S. Recognition of the DNA minor groove by pyrrole-imidazole polyamides. *Curr. Opin. Struct. Biol.* **2003**, *13*, 284-299; b) Hsu, C. F. et al. Completion of a programmable DNA-binding small molecule library. *Tetrahedron* **2007**, *63*, 6146-6151; c) Kielkopf, C. L.; White, S.; Szewczyk, J. W.; Turner, J. M.; Baird, E. E.; Dervan, P. B.; Rees, D. C. A structural basis for recognition of A.T and T.A base pairs in the minor groove of B-DNA. *Science* **1998**, *282*, 111-115; d) White, S.; Szewczyk, J. W.; Turner, J. M.; Baird, E. E.; Dervan, P. B. Recognition of the four Watson-Crick base pairs in the DNA minor groove by synthetic ligands. *Nature* **1998**, *391*, 468-471.

(14)Edelson, B. S.; Best, T. P.; Olenyuk, B.; Nickols, N. G.; Doss, R. M.; Foister, S.; Heckel, A.; Dervan, P. B. Influence of structural variation on nuclear localization of DNA-binding polyamide-fluorophore conjugates. *Nucl. Acids Res.* **2004**, *32*, 2802-2818.

(15)a) Nickols, N. G.; Jacobs, C. S.; Farkas, M. E.; Dervan, P. B. Modulating hypoxia-inducible transcription by disrupting the HIF-1-DNA interface. *ACS Chem. Biol.* **2007**, *2*, 561-571; b) Nickols, N. G.; Dervan, P. B. Suppression of androgen receptor-mediated gene expression by a sequence-specific DNA-binding polyamide. *Proc. Natl. Acad. Sci. USA* **2007**, *104*, 10418-10423; c) Muzikar, K. A.; Nickols, N. G.; Dervan, P. B. Repression of DNA-binding dependent glucocorticoid receptor-mediated gene expression. *Proc. Natl. Acad. Sci. USA* **2009**, *106*, 16598-16603; d) Raskatov, J. A.; Meier, J. L.; Puckett, J. W.; Yang, F. T.; Ramakrishnan, P.; Dervan, P. B. Modulation of NF-κB-Dependent Gene Transcription Using Programmable DNA Minor Groove Binders. *Proc. Natl. Acad. Sci. USA* **2012**, *109*, 1023-1028.

(16)a) Yang, F.; Nickols, N. G.; Li, B. C.; Marinov, G. K.; Said, J. W.; Dervan, P. B. Antitumor activity of a pyrrole-imidazole polyamide. *Proc. Natl. Acad. Sci. U. S. A.* **2013**, *110*, 1863-1868; b) Yang, F.; Nickols, N. G.; Li, B. C.; Szablowski, J. O.; Hamilton, S. R.; Meier, J. L.; Wang, C.-M.; Dervan, P. B. Animal toxicity of hairpin pyrrole-imidazole polyamides varies with the turn unit. *J. Med. Chem.* **2013**, *56*, 7449-7457.

(17)a) Raskatov, J. A.; Hargrove, A. E.; So, A. Y.; Dervan, P. B. Pharmacokinetics of Py-Im Polyamides Depend on Architecture: Cyclic versus Linear. *J. Am. Chem. Soc.* **2012**, *134*, 7995-7999; b) Synold, T. W.; Xi, B. X.; Wu, J.; Yen, Y.; Li, B. C.; Yang, F.; Phillips,

J. W.; Nickols, N. G.; Dervan, P. B. Single-dose pharmacokinetic and toxicity analysis of pyrrole-imidazole polyamides in mice. *Cancer Chemother. Pharmacol.* **2012**, *70*, 617-625.

(18)a) Raskatov, J. A.; Nickols, N. G.; Hargrove, A. E.; Marinov, G. K.; Wold, B.; Dervan, P. B. Gene expression changes in a tumor xenograft by a pyrrole-imidazole polyamide. *Proc. Natl. Acad. Sci. U. S. A.* **2012**, *109*, 16041-16045; b) Nickols, N. G.; Szablowski, J. O.; Hargrove, A. E.; Li, B. C.; Raskatov, J. A.; Dervan, P. B. Activity of a Py-Im Polyamide Targeted to the Estrogen Response Element. *Mol. Cancer Ther.* **2013**, *12*, 675-684.

(19) Raskatov, J. A.; Puckett, J. W.; Dervan, P. B. A C-14 labeled Py–Im polyamide localizes to a subcutaneous prostate cancer tumor. *Bioorg. Med. Chem.*, http://dx.doi.org/10.1016/j.bmc.2014.1004.1010.

(20)Kerbel, R. S. Human Tumor Xenografts as Predictive Preclinical Models for Anticancer Drug Activity in Humans: Better than Commonly Perceived—But They Can Be Improved. *Cancer Biol. Ther.* **2003**, *2*, 133 - 138.

(21)a) Frese, K. K.; Tuveson, D. A. Maximizing mouse cancer models. *Nat. Rev. Cancer* **2007**, *7*, 645-658; b) Becher, O. J.; Holland, E. C. Genetically engineered models have advantages over xenografts for preclinical studies. *Cancer Res.* **2006**, *66*, 3355-3358.

(22)Sausville, E. A.; Burger, A. M. Contributions of human tumor xenografts to anticancer drug development. *Cancer Res.* **2006**, *66*, 3351-3354.

(23)Szablowski, J. O.; Raskatov, J. A.; Dervan, P. B. *Unpublished data*.

(24)a) Bao, L.; Matsumura, Y.; Baban, D.; Sun, Y.; Tarin, D. Effects of inoculation site and matrigel on growth and metastasis of human breast-cancer cells. *Br. J. Cancer* **1994**, *70*, 228-232; b) Shuhendler, A. J.; Prasad, P.; Cai, P.; Hui, K. K. W.; Henderson, J. T.; Rauth, A. M.; Wu, X. Y. Matrigel alters the pathophysiology of orthotopic human breast adenocarcinoma xenografts with implications for nanomedicine evaluation. *Nanomed.-Nanotechnol. Biol. Med.* **2013**, *9*, 795-805; c) Fridman, R.; Kibbey, M. C.; Royce, L. S.; Zain, M.; Sweeney, T. M.; Jicha, D. L.; Yannelli, J. R.; Martin, G. R.; Kleinman, H. K. Enhanced Tumor Growth of Both Primary and Established Human and Murine Tumor Cells in Athymic Mice After Coinjection With Matrigel. *J. Natl. Cancer Inst.* **1991**, *83*, 769-774.

C h a p t e r 5

AN HRE-BINDING POLYAMIDE IMPAIRS ADAPTATION OF TUMORS TO HYPOXIA

The text of this chapter was taken in part from a manuscript co-authored with Jevgenij A. Raskatov and Peter B. Dervan.

Abstract

Hypoxic gene expression contributes to the pathogenesis of many diseases, including organ fibrosis, age-related macular degeneration, and cancer. HIF-1, a transcription factor central to the hypoxic gene expression, mediates multiple processes including neovascularization, cancer metastasis, and cell survival. Py-Im polyamide 1 has been shown to inhibit HIF-1-mediated gene expression in cell culture but its activity *in vivo* was unknown. This study reports activity of polyamide 1 in subcutaneous tumors capable of mounting a hypoxic response and showing neovascularization. We show that 1 distributes into subcutaneous tumor xenografts and normal tissues, reduces the expression of several HIF-1-dependent proangiogenic and prometastatic factors, inhibits the formation of new tumor blood vessels, and suppresses tumor growth. Tumors treated with 1 show no increase in HIF-1a and have reduced ability to adapt to the hypoxic conditions, as evidenced by increased apoptosis in HIF-1a positive regions and the increased proximity of necrotic regions to vasculature. Overall, these results show that a molecule designed to block the transcriptional activity of HIF-1 has potent anti-tumor activity *in vivo*, consistent with partial inhibition of the tumor hypoxic response.

Introduction

Oxygen sensing is involved in a range of natural physiological processes such as embryonal development, wound healing, and immune response (1). However, its dysregulation can contribute to pathogenesis of multiple diseases including fibrosis, erythrocythemia, heart disease, and cancer – a group of diseases leading to nearly 600,000 deaths every year in the United States alone (2). While new cancer treatments are being developed (3, 4), many of the cancer therapies are hampered by presence of low levels of oxygen in tumors (5, 6), known as tumor hypoxia, regulated mainly by Hypoxia Inducible Factors (HIFs) (7). Among them - HIF-1 (8) – is a transcription factor that is often associated with poorer patient survival (5). HIF-1 orchestrates numerous aspects of cancer progression: tumor angiogenesis, cell survival in hypoxia, and metastasis (5, 9). Most inhibitors affect HIF-1 signaling indirectly, by targeting other proteins, including Topoisomerase I, mammalian target of rapamycin (mTOR), or microtubules (10). Established therapeutic strategies focus on modulating HIF-1 signaling by altering the HIF-1 protein levels (3, 10), its dimerization and protein interactions (11-14), or its DNA binding and transcriptional activity (15-18).

One method to inhibit transcriptional activity of HIF-1 is to displace it from its DNA-binding site, HIF-1 responsive elements (HREs), for example by echinomycin (15), or a molecule shown in this report (compound **1**. Fig. 5.1A) (16, 17). Compound **1** is a member of a class of DNA-binding small molecules, Py-Im polyamides, which can be programmed to recognize a broad repertoire of sequences with affinities and specificities comparable to those of transcription factors (19, 20). We reported that polyamides can modulate gene expression driven by many transcription factors in tissue culture (16, 17, 21-24). Our recent

mechanistic investigations expanded beyond the transcription factor:DNA interface, showing that Py-Im polyamides can induce degradation of the large subunit of RNA polymerase II, activation of the P53 stress response without concurrent DNA damage (25), and induction of DNA replication stress (26).

Experiments focused on HIF-1-DNA binding inhibition demonstrated the ability of **1** to displace the HIF-1 complex from DNA *in vitro* (16) , and by reducing HIF-1a occupancy at selected HREs in a common tissue culture model of hypoxic response - U251 cells as represented in Fig. 5.1B (17). When U251 cells were treated with Deferoxamine, a HIF-1 activator, **1** was capable of inhibiting 23% of the induced genes, establishing polyamide **1** as a partial inhibitor of HIF-1 transcriptional activity (17). The overall gene expression changes were distinct from other inhibitors, such as Echinomycin (15) or siRNA targeted to HIF-1a, but included many important proangiogenic factors, such as *VEGF*, *FLT1,* or *Endothelin-1*.

Our previous *in vivo* investigations demonstrated the bioavailability of various Py-Im polyamides upon intravenous (27), intraperitoneal, and subcutaneous administration (28). Subsequent *in vivo* xenograft studies established that polyamides could accumulate in subcutaneously grafted tumors (24, 29, 30), modulate tumor gene expression (24, 29), and inhibit growth of prostate cancer xenografts (25, 31).

We sought to evaluate the mechanism of action of **1** *in vivo* and its therapeutic potential in treatment of cancer and other HIF-1-related diseases. We hypothesized that **1** could act as a partial inhibitor of HIF-1a-driven gene expression *in vivo,* thus inhibiting tumor growth and angiogenesis. We chose a subcutaneous tumor model, due to its hypoxic nature (5) and reliability of measurements in angiogenesis, tumor growth, and gene expression. The cell

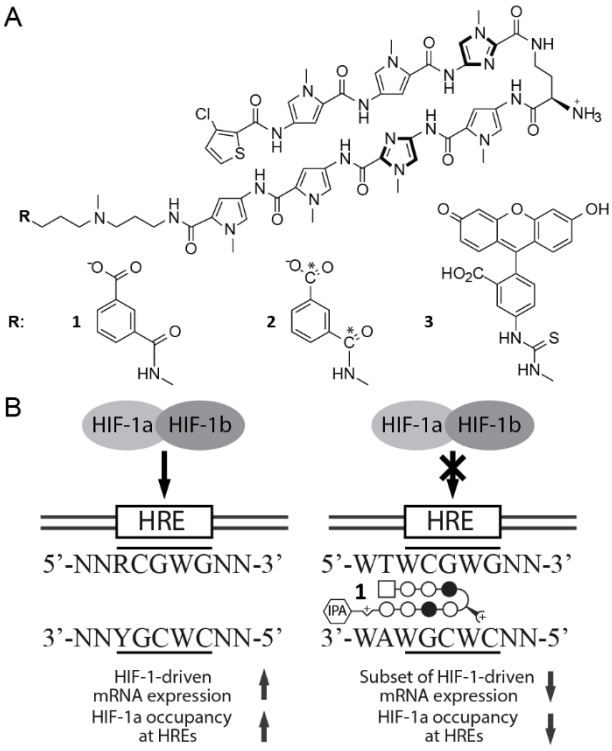

Figure 5.1 Chemical structure and biological activity of Py-Im polyamides binding HRE sequence. A) Chemical structures and ball-and-stick representation of the Py-Im polyamides **1**-**3**. N-methyl-pyrrole, N-methyl-imidazole and chlorothiophene are represented as open circles, filled circles and squares, respectively. B) Our previous studies (18) indicated that compound **1** can bind to HRE-containing sequence with nanomolar affinity and displace HIF-1 complex from in VEGF and CA9 promoters in U251 cells.

lines chosen for engraftment have been evaluated extensively in xenograft models of cancer (32-34), and hypoxic gene expression in one of them (U251) can be regulated by **1** (17) and Echinomycin (15), making it a good choice for evaluating *in vivo* mechanism of action of **1**. The second cell line, GBM39 (35), was derived from the same site as U251 cells (brain), but was maintained as subcutaneous xenografts and expanded in serum-free conditions as spheroids. The serum-free treatment maintains genetic and histologic variability of human tumors (36) and was thus our choice to ascertain the generality of the mechanism of action of polyamide **1**. The distinct profile of gene expression modulation,

favorable pharmacokinetics, and ability to modulate some aspects of hypoxic response by **1**, could establish it as an interesting candidate for treatment of HIF-1 related diseases.

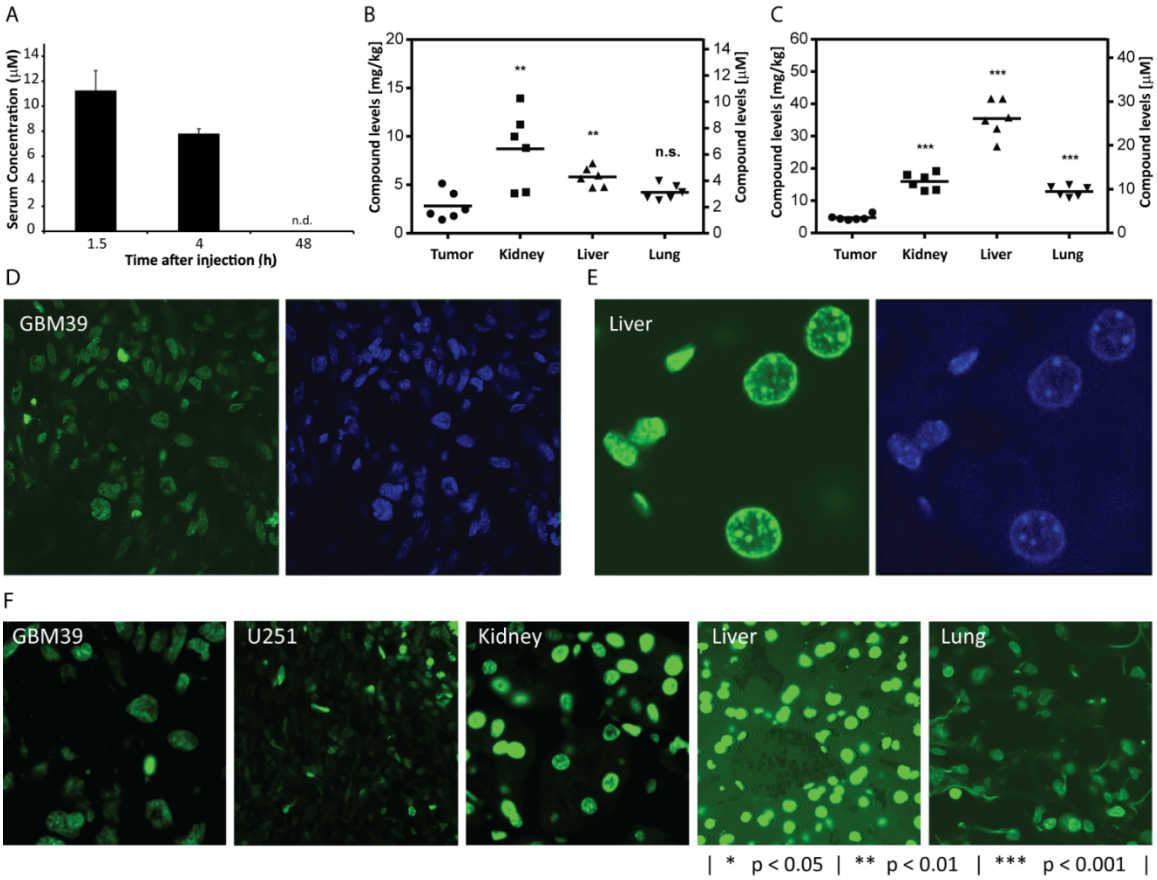

Figure 5.2. Pharmacokinetics, tissue distribution of and nuclear uptake of compounds 1-3 in-vivo. A) Serum concentration of **1** after subcutaneous injection. The C57BL6 mice were injected with **1** subcutaneously into interscapular area, after which we drew blood via retroorbital collection (n=4 per time point). B) GBM39 tumor bearing mice were injected I.P. with a 6.8mg/kg of C-14 radiolabeled polyamide **2**. The tissues were harvested 24-hours post-injection, weighed, dissolved, and quantified by scintillation. The absolute scintillation counts are normalized to organs' weight. C) GBM39 tumor bearing mice were injected I.P. with 6.8mg/kg of **2** (*Schedule A, intraperitoneal*) labeled with a radioactive C-14, harvested, and quantified 24 hours after the last injection. D) Compound **3** was injected S.C. into interscapular area at 5 μM/kg (*Schedule A*) and tissues were harvested 24 hours after the last injection. The compound **3** showed nuclear uptake in GBM39 xenograft sections. E) Compound **3** shows nuclear staining consistent with distribution of chromatin in the nucleus. F) Uptake of **3** into the tissues showing nuclear staining. The tissues were harvested 24 hours after last injection fixed with 10% NBF, co-stained with DAPI, and imaged. The left panel shows FITC channel, showing nuclear uptake of **3,** and the right panel shows a DAPI co-stain showing chromatin. Error bars denote 95% CI.

A

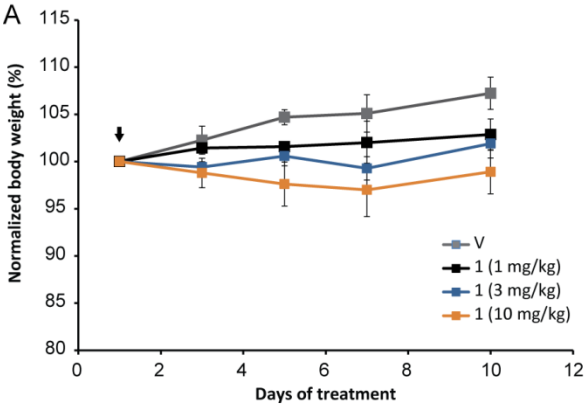

B

1 (mg/kg)	ALT (U/L)	AST (U/L)	T. Bili (mg/dL)	BUN (mg/dL)	Creat. (mg/dL)
0	100 ± 57	306 ± 286	0.13 ± 0.07	29.00 ± 1.13	0.27 ± 0.13
1	209 ± 173	303 ± 71	0.17 ± 0.07	27.33 ± 1.31	0.17 ± 0.07
3	170 ± 122	191 ± 42	0.17 ± 0.07	32.00 ± 4.53	0.20 ± 0.11
10	268 ± 308	307 ± 149	0.17 ± 0.07	29.67 ± 3.27	0.33 ± 0.13

Figure 5.3 Py-Im polyamide **1** single-dose escalation study of toxicity. A) The C57BL6 mice were injected with **1** subcutaneously and their weights were measured on days 3, 5, 7 and 10 (n=3 per condition). The maximum weight loss has been observed for **1** dosed at 10 mg/kg, reaching an average of 3% (+/- 1.4) below the original mice weight. The weight loss for the other groups was below 1% throughout the study. Arrow denotes an injection. B) A single injection of **1** was administered at doses 1-10 mg/kg in C57BL6 mice. After 10 days, blood was drown retroorbitally, serum was cleared by centrifugation and samples submitted for analysis of serum toxicity markers. No significant changes in any of the tested markers were observed after injection of **1**. Error bars and uncertainty values denote 95% CI.

Results

Py-Im polyamide 1 shows favorable preliminary pharmacokinetics and tissue distribution at tolerable doses. In order to evaluate bioavailability of **1** *in vivo*, we injected it subcutaneously (s.c.) at 6.8 mg/kg into C57BL6 mice. Compound **1** reached a serum concentration of 11.3±1.6 μM within 1.5 h and 7.8±0.4 μM at 4 h post-injection (Fig. 5.2A). A single-injection toxicity test showed that **1** did not affect animal weight, or levels of serum toxicity markers (ALT, AST, TBIL, BUN, Creat) at concentrations up to 10 mg/kg (Fig. 5.3A, B), indicating that this compound could be used *in vivo* without

significant toxicity. Taken together, these results supported evaluation of anti-tumor effects of **1** *in vivo*. The radiolabeled analogue of **1**, Py-Im polyamide **2**, was injected intraperitoneally (IP) to quantitate whole-organ compound concentrations (Fig. 5.2B, C) into immunocompromised NSG mice bearing GBM39 tumors. After 24 h, concentrations of **2** were measured in GBM39 xenografts (2.0 μM), host's kidney (6.3 μM), liver (4.2 μM) and lung (3.1 μM; Fig. 6.2B). Following 3 injections (*Schedule A,* 6.8mg/kg s.c., every other day x 3, harvest 72h post last injection), all tested tissues showed compound accumulation (Fig. 6.2C). Administration of **3** (FITC-conjugate of **1**), according to *Schedule A* in NSG mice, resulted in readily detectable nuclear staining in tumors (U251, Fig. 6.4A; GBM39, Fig. 6.2D) and tested tissues (Fig. 6.2E-F).

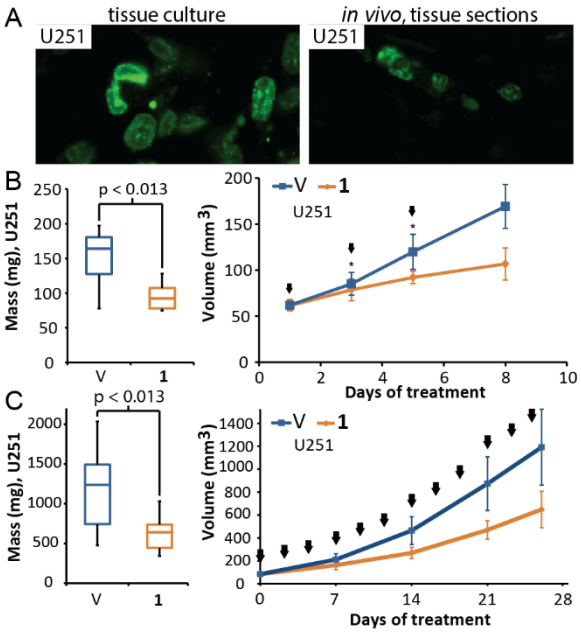

Figure 5.4 Polyamide 1 inhibits tumor growth. A) Uptake of **3** in U251 cells in tissue culture, and in s.c. xenograft sections. B) Final masses and growth curve of s.c. U251 xenografts derived from animals subjected to *Schedule A* (n=7,8, for vehicle and treated groups; for volumes, measurements at the 3rd an 5th day contain 5 data points.) C) Final masses and growth curve of U251 xenografts (*Schedule B*, n=10 per condition). Arrows denote injections. Error bars are 95% CI for growth curves and minimum-maximum values for mass graphs.

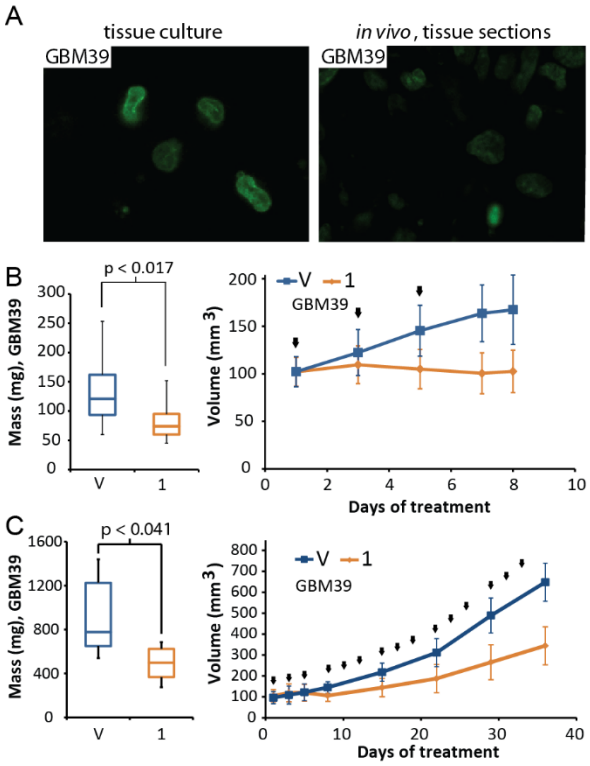

Figure 5.5 Py-Im polyamide 1 shows nuclear uptake and attenuates tumor growth in GBM39 xenografts. A) Uptake of **3** in GBM39 cells in tissue culture, and in xenograft sections. B) Final masses and growth curve of s.c. GBM39 xenografts derived from animals subjected to *Schedule A* (n=11, per condition). C) Final masses and growth curve of s.c. GBM39 xenografts (*Schedule B*, n=6 per condition). Arrows denote injections, error bars denote 95% CI for growth curves, and minimum-maximum for final mass plots.

Polyamide 1 suppresses tumor growth in subcutaneous xenografts. To test whether previously established partial inhibition of HIF-1-driven gene expression by **1** (17) would result in a decrease in tumor growth, we engrafted U251 and GBM39 cells s.c. into NOD/SCID-γ (NSG) mice. We established three dosing regiments for **1** – *Schedule A*, consisting of three s.c. injections every other day at maximum tolerated dose (6.8 mg/kg, 8 days) and *Schedules B and C*, with lower dose (4.5mg/kg, 3 inj./week) designed for prolonged treatment with low weight loss (<10%) over 4 weeks (U251 tumors) or 6 weeks (GBM39 tumors). In all cases, the tumors were harvested 72 h after last injection.

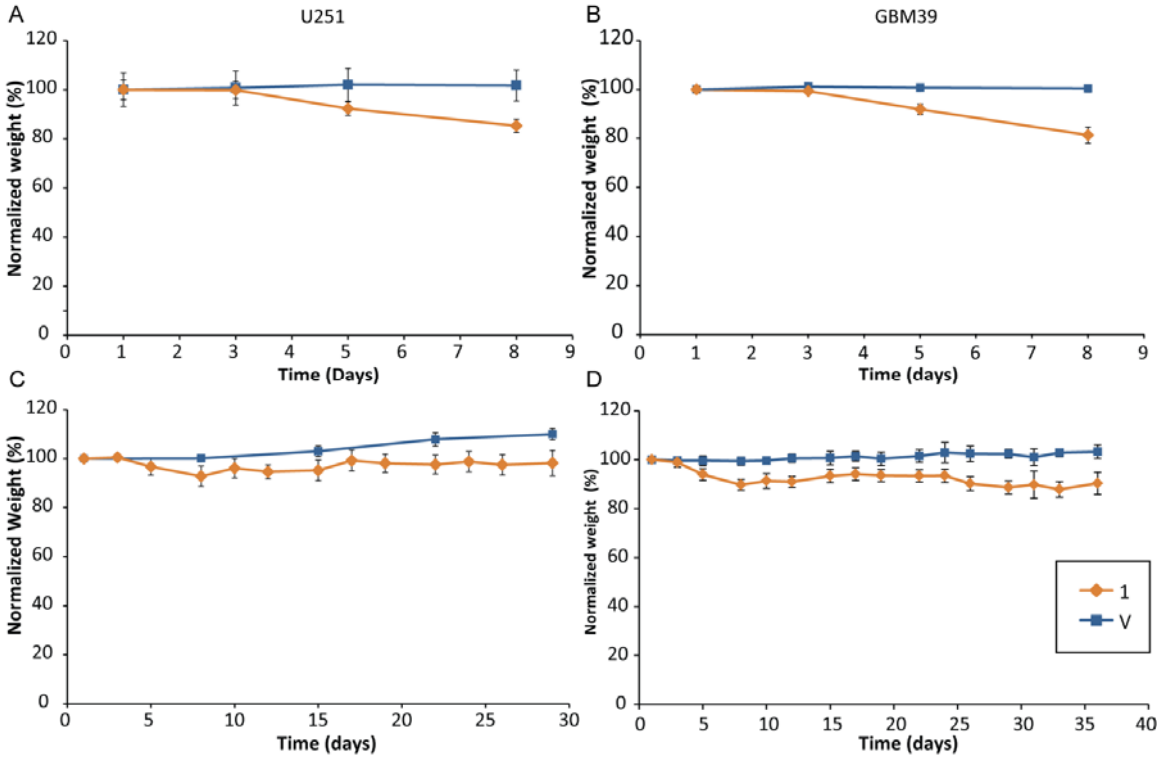

Figure 5.6. Mouse weight loss during treatment with Py-Im polyamide 1. A) Mice bearing U251 xenografts were injected with 6.8 mg/kg of **1** on the 1st, 3rd and 5th day of treatment (*Schedule A*). The weight was recorded and normalized to the initial weight for vehicle (n=7) and polyamide treated (n=8) mice. B) Analogous weight measurement or mice bearing GBM39 xenografts, treated with **1** according to schedule A (n=11, per condition). C) Weight measurements of mice with U251 tumors, treated with Py-Im polyamide **1** over 4 weeks (*Schedule B*) and of mice bearing GBM39 xenografts (D), treated with **1** according to *Schedule C*. Error bars denote 95% CI.

Mice bearing U251 tumors that were subjected to treatment with **1** (*Schedule A*) showed a median tumor burden reduction amounting to 1.8-fold ($p<0.013$; n=7, 8 for vehicle and treated groups; Fig. 6.4B;) compared to vehicle. Similarly, prolonged treatment (*Schedule B*) resulted in 1.9-fold lower median U251 tumor mass ($p<0.0125$; n=10 per condition; Fig. 6.4C). Consistent results were obtained with a primary glioma cell line (GBM39) xenograft.

Treatment according to *Schedule A* resulted in 1.8-fold lower median mass ($p<0.016$; n=11 per condition; Fig. 6.5A) and prolonged treatment (*Schedule C*) in 1.6-fold reduction ($p<0.041$; n=6 per condition; Fig. 6.5B). The treatments resulted in minor mouse weight loss; the effects were less severe (<5% average w.l. throughout the experiment) for schedules *B* and *C* (Fig. 6.6).

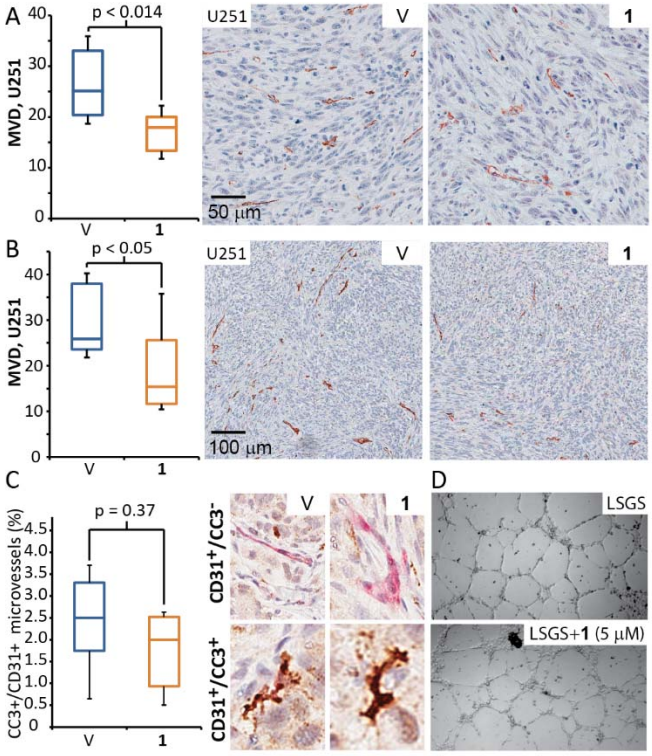

Figure 5.7 Polyamide 1 reduces microvessel density in tumors, without affecting blood vessel apoptosis or HUVEC tube formation on matrigel. A) Mice harboring xenografts were treated with 1 according to *Schedule A* and their MVD score was measured using anti-mouse CD31 immunostaining of tumor sections (For U251 n=7,8 for vehicle, and treated groups). B) Prolonged treatments, according to *Schedule B* in U251 xenografts led to comparable decrease in MVD. C) Apoptosis in blood vessels was determined by double-staining of Cleaved Caspase-3 (CC3) and mouse CD31 of GBM39 tumor sections treated according to *Schedule C*. Both vehicle and polyamide-1 treated samples exhibited low levels of blood vessel apoptosis and the differences between the groups were not significant ($p=0.37$, n=5 per condition). D) An *in vitro* angiogenesis assay - matrigel tube formation assay using HUVECs - shows treatment with 1 (5 µM) over

48h has no effect on endothelial tube formation. Error bars denote minimum and maximum.

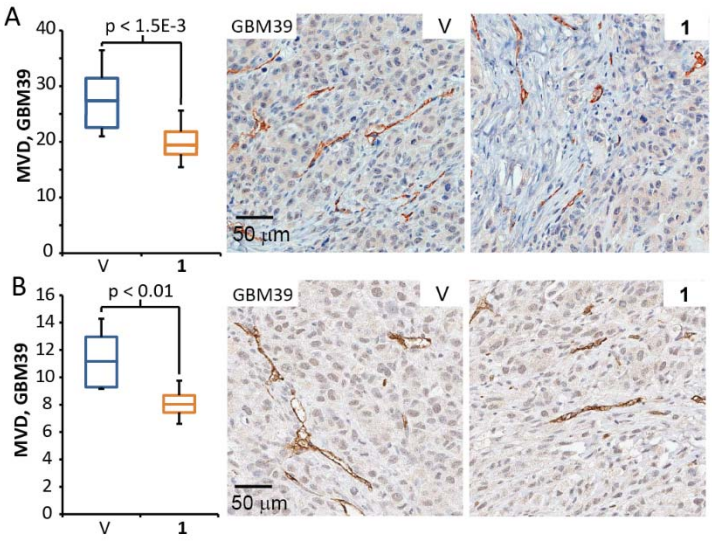

Figure 5.8 Polyamide 1 reduces microvessel density of GBM39. A) GBM39 tumors treated with **1** according to *Schedule A* show 1.4-fold reduction of MVD at the endpoint ($p<0.0015$; n=11 per condition). Similarly, when treated according to *Schedule C*, the same level of reduction was observed ($p<0.01$; n=6 per condition). Error bars denote minimum and maximum.

Polyamide 1 reduces microvessels density in xenografts, without inducing endothelial apoptosis. Hypoxic signaling is a major driver for angiogenesis and its inhibition leads to a decrease in microvessel density (MVD) (1, 10). We measured MVD using anti-mouse CD31 immunostaining of tumor sections. We observed a significant reduction of MVD in all tested scenarios. For U251 tumors, with mice subjected to *Schedule A,* we observed a 1.4-fold median reduction of MVD ($p<0.014$; n=7,8 for vehicle and treated groups; Fig. 6.7A) and a 1.7-fold median decrease for *Schedule B* ($p<0.05$, n=10 per condition*;* Fig. 6.7B). For GBM39 tumors, both treatment schedules (*A* and *C*) led to a 1.4-fold reduction in MVD ($p<0.01$; n=11 and n=6 for *Schedule A* and *C*; Fig. 6.8).

The decrease in MVD could be caused by direct effect of **1** on the endothelium, for example, rendering it either apoptotic, or unable to form blood vessels. We evaluated endothelial apoptosis by double-staining of mouse-specific CD31 and Cleaved Caspase-3 (CC3) in GBM39 tumors (Fig. 6.7C, *Schedule C*). We found no significant endothelial apoptosis in either of the treatment groups. To measure angiogenic functionality of endothelium we used *in vitro* matrigel tube formation assay with Human Umbilical Cord Endothelial Cells (HUVEC), revealing **1** (5 μM, 48 h) had no effect on tube formation (n=3, Fig. 6.7D).

Antiangiogenic effects of 1 are associated with inhibition of several aspects of hypoxic response. Decrease in MVD, without endothelial apoptosis or dysfunction, suggests **1** could interfere with the hypoxic response in tumors and possibly its primary regulator – HIF-1 (8). To further test this hypothesis we evaluated other aspects affected by hypoxic response, such as tumor cell proliferation (6), apoptosis in HIF-1 positive, perinecrotic areas (6), nuclear HIF-1a protein accumulation, and cell survival in areas distant from blood vessels (37, 38). To analyze this, we divided the tumor sections into three areas: necrotic, non-necrotic, and perinecrotic (Fig. 6.9A). The non-necrotic areas contain viable cells, while necrotic areas are decellularized. The perinecrotic area represents field of view (20x magnification) on the verge between necrosis and non-necrosis.

Antiangiogenic therapy increases hypoxia in tumors and often leads to decreased proliferation (37, 39). Upon treatment with **1** (*Schedule B*), we observed a 1.2-fold decrease ($p<0.05$; Fig. 6.9B) in proliferation marker (Ki-67) in non-necrotic areas of the U251

tumors.

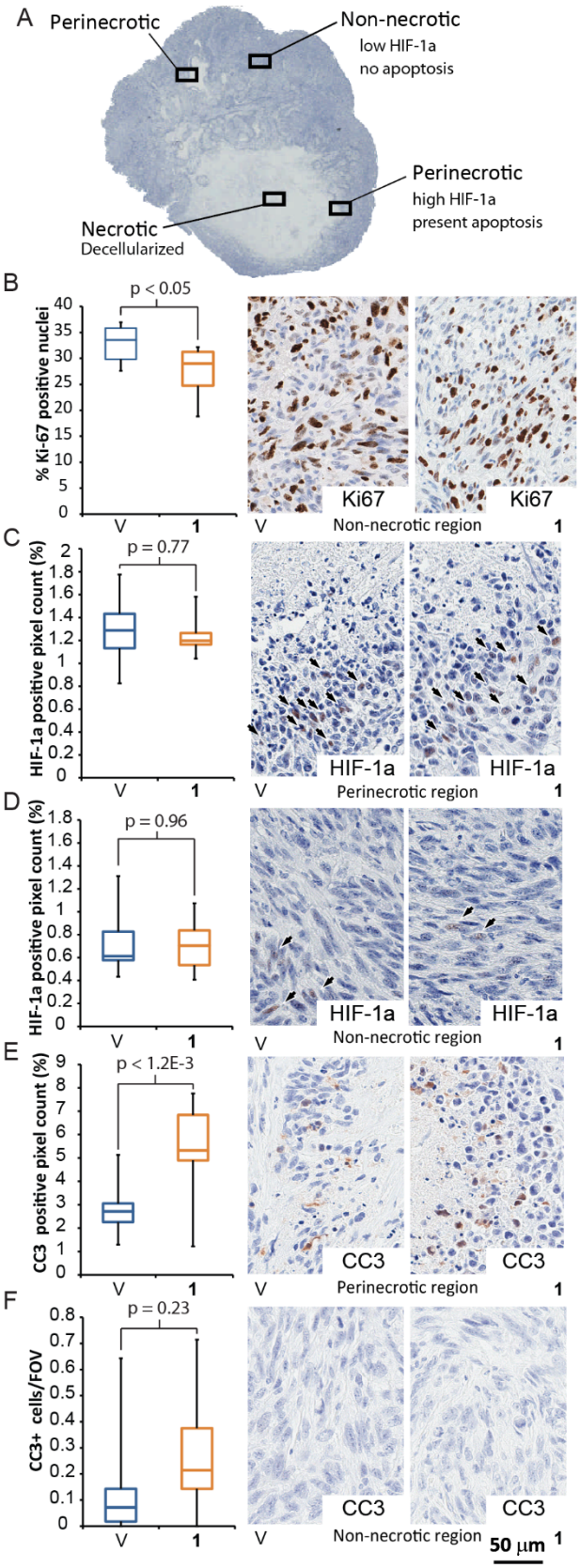

Figure 5.9 Treatment with 1 decreases tumor proliferation, induces apoptosis in HIF-1a positive areas and does not lead to HIF-1a accumulation. A) Regions used for local analysis in U251 tumors (*Schedule B* treatment). All analysis was done at 20x magnification; perinecrotic area contained 50% necrosis and 50% adjacent, non-necrotic area, as shown. B) Treatment with 1, induced a modest, but statistically significant decrease in proliferative index (Ki-67 staining). C) Non-necrotic tumor regions show no presence of apoptosis. However, cells in perinecrotic region show significant increase in CC3 staining upon treatment with 1 (D). Similarly, non-necrotic region exhibited low numbers of HIF-1a positive pixels (E) and perinecrotic area was more positive in HIF-1a (F). However, there were no differences in HIF-1a levels between the treatment groups. For each measurement n=10, per condition. Error bars denote minimum and maximum.

Another effect of induction of hypoxic response is accumulation of HIF-1a (1). However, treatment with **1** did not lead to an increase in levels of HIF-1a in either U251 (Fig. 6.9C, D) or GBM39 (Fig. 6.11A, B) tumors. Lack of HIF-1a accumulation is unlikely to be caused by its increased degradation, as **1** does not affect HIF-1a levels in tissue culture (Fig 11C). Overall, we observed a spatial distribution of HIF-1a in U251 tumor sections: perinecrotic areas showed higher HIF-1a levels compared to non-necrotic areas (1.8-fold average increase for **1**; $p<0.001$, Fig 9C, D).

Induction of hypoxic signaling can lead to apoptosis resistance in cancer cells (37). However, treatment with **1** increased apoptosis significantly in perinecrotic, HIF-1a positive, areas (1.8-fold, $p<0.0012$; Fig. 6.9E). The apoptosis was absent in non-necrotic regions of U251 tumors regardless of the treatment (Fig. 6.9F), suggesting that **1** is toxic specifically to hypoxic cells.

Hypoxic signaling mediates cell survival in areas distant from blood vessels, where oxygen pressures are the lowest. With increasing distance to blood vessels, tumor necrosis appears as a result of the death of cells with inadequate oxygen supply (1, 40). Therefore, to measure if **1** decreases ability of cells to adapt to low oxygen pressures, we measured MVD as a function of distance from the edge of necrotic areas. We found the expected lack of microvessels nearby necrotic edges. However, tumors derived from animals treated with **1** (U251, *Schedule B*) showed greater microvessel densities in areas close to the edge necrosis (3.3-fold at 150 μm and 2.3-fold for 200 μm distance, $p<0.02$ and $p<0.01$, $n=10$ per condition; Fig. 6.10A, B), suggesting that treated tumor cells could require a higher level of nutrients and oxygen for survival. Similarly, the median distances between a random

point at the edge of necrosis and the nearest blood vessels were significantly shorter in case of group treated with **1** for U251 ($p<0.001$, *Schedule B*, n=10 per condition; Fig. 6.11D) and GBM39 tumors ($p<0.01$, *Schedule C,* n=6 per condition Fig. 6.11D).

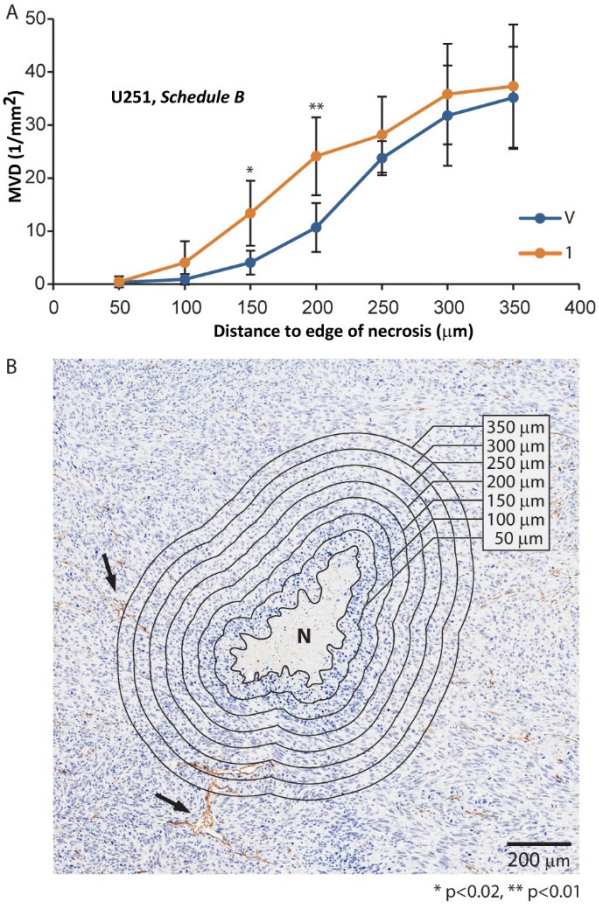

Figure 5.10. Treatment with 1 increased reliance of tumor cells on proximity to vasculature. Necrosis was delineated manually and zones were offset every 50 μm. Number of blood vessels per area was calculated for each zone and converted to MVD. A) Group treated with 1 shows higher MVD in perinecrotic areas - within 150 and 200 μm from the edge of necrosis. B) Example of necrosis along with delineation and zonal analysis of MVD. (n=10 tumor per condition, 854 total microvessels measured for a group treated with **1** and 586 for a group treated with vehicle). Arrows denote two of the large microvessels, N denotes necrosis. Error bars denote 95% CI.

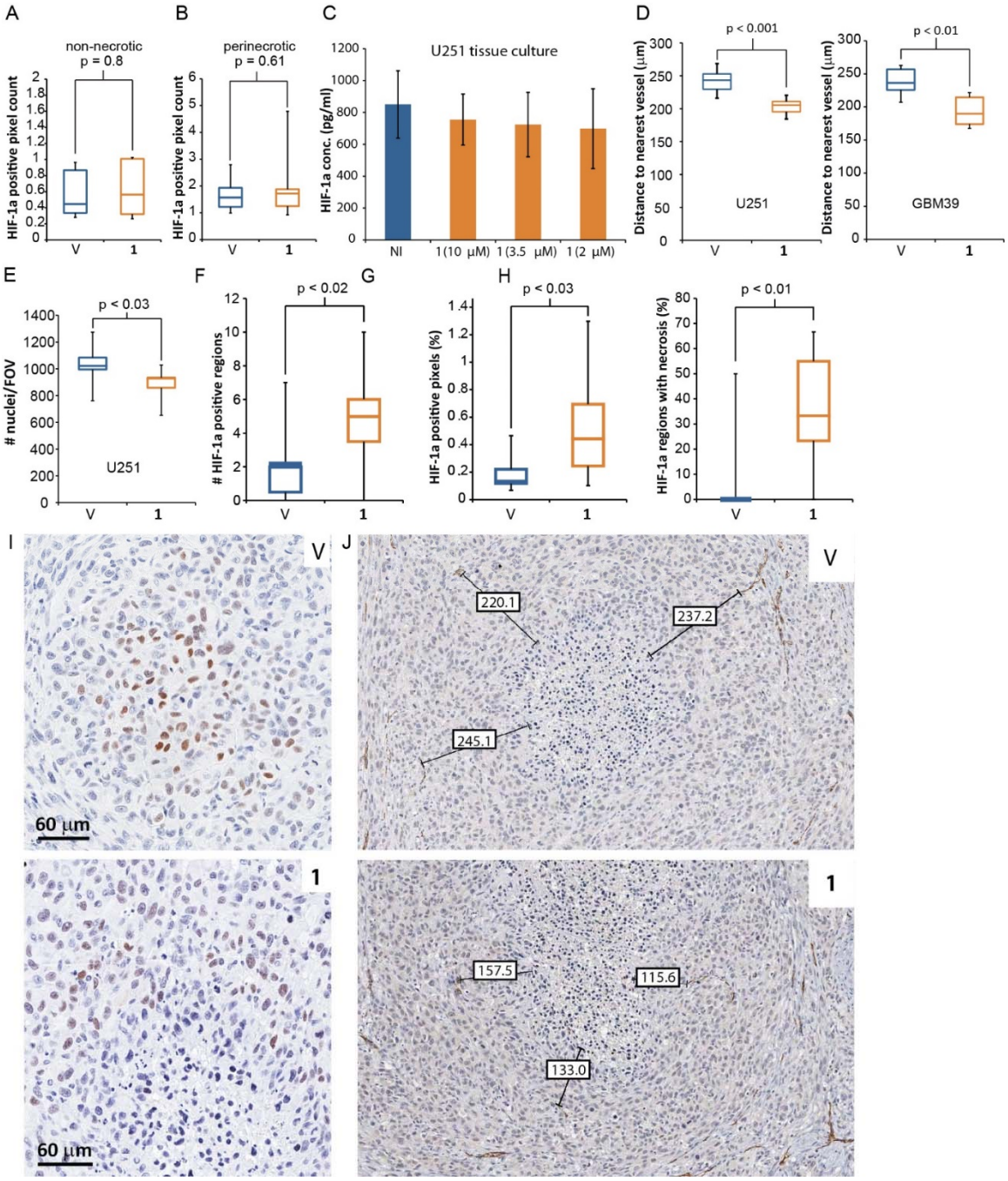

Figure 5.11 In vivo Effects of treatment with 1 are consistent between GBM39 and U251 xenografts. A) Non-necrotic region exhibited lower numbers of HIF-1a positive pixels (B) in comparison to perinecrotic region. However, we did not find increased levels of HIF-1a in treated samples, despite decreased microvessel density. C) The lack of HIF-1a induction in xenografts is unlikely to be caused by HIF-1a protein degradation as **1** did not affect HIF-1a levels in U251 cells in tissue culture. D) For both U251 and GBM39 xenografts, we found an association between presence of necrosis and distance from the nearest CD31+ microvessel closely matching distances obtained

for U251 xenografts. Interestingly, GBM39 tumors treated with **1** according to *Schedule A* showed increased presence of areas positive in HIF-1a (F-H), which often contained necrotic center (I). Further analysis shows that necrosis occurs in regions that do not contain blood vessels (J). Numbers in boxes denote distance between edge of necrotic regions and the nearest microvessel (μm). Error bars for all panels except C) denote minimum and maximum. Error bars in the panel C) denote 95% CI.

Lower MVD and lower cell survival at a distance from blood vessels should lead to an increase in necrotic area. However, the complex pattern of necrosis (micronecroses) in U251 tumors made it difficult to quantify it by a simple delineation. Instead, we decided to automatically count nuclei in the whole tumor section and found lower nuclear density in tumors treated with **1**, (10% fewer nuclei, $p<0.03$, Fig. 6.11E). Further evidence of necrosis induction by **1** was present after short-term treatment with **1** in GBM39 tumors (*Schedule A*) where transient accumulation of HIF-1a (Fig. 6.11F-H) led to presence of necrosis (Fig. 6.11I), specifically localized to HIF-1a positive areas that were distant from microvessels (Fig. 6.11I, J).

Overall, compound **1** decreases proliferation and nuclear density, selectively induces apoptosis in perinecrotic, HIF-1a positive areas, and causes necrotic areas to appear closer to vasculature, but treatment does not result in long-term HIF-1a accumulation.

Py-Im polyamide 1 reduces expression of proangiogenic and prometastatic factors in tumors. A common adverse effect of antiangiogenic treatment is upregulation of proangiogenic and prometastatic gene expression, which renders the antiangiogenic therapies less effective and is often a result of hypoxic signaling (4). We decided to test if **1** affected mRNA expression of such factors *in vivo*. NSG mice bearing U251 tumors (n=6 per condition) were treated with **1** according to *Schedule D* (6.8 mg/kg, 2 inj., on days 1

and 3; tumors harvested on day 5). Out of 10 tested proangiogenic factors, four transcripts had lower relative expression after treatment with **1** (Fig. 6.12A), and one (*VEGF*) was upregulated (1.4-fold) in both mRNA (Fig. 6.12B) and serum protein levels (Fig. 6.6C). Downregulation of mRNA expression was also apparent in the panel of prometastatic genes. Overall, 5 out of 6 tested transcripts were downregulated in the group treated with **1** (Fig. 6.12D). Results for all tested genes can be found in Table 1.

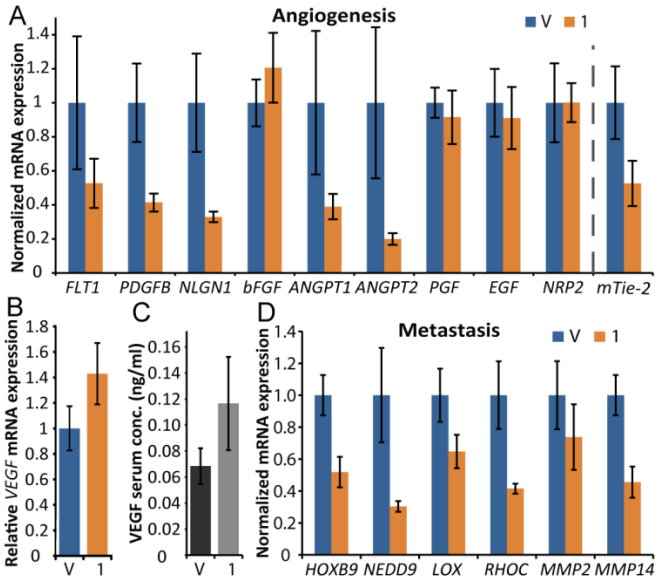

Figure 5.12. Treatment with 1 inhibits transcription of proangiogenic and prometastatic factors in tumors. Mice harboring U251 tumors were treated according to *Schedule D* to capture gene expression profile underlying the changes in tumor mass and MVD (n=8 per condition). We registered a significant downregulation of several important proangiogenic factors (A), including Angiopoietins 1 and 2 (*ANGPT1, ANGPT2*), overall tumor levels of their receptor mouse-*Tie-2* (*mTie-2*), Neuroligin 1 (*NLGN1*), as well as Plateled-Derived Growth Factor-B (*PDGFB*). Interestingly, both mRNA expression (B) and serum protein levels of a human-*VEGF* (C) were upregulated slightly in treated animals (n=8,6 for samples treated with vehicle and **1**). We selected a panel of prometastatic factors and found that **1** inhibits mRNA expression in all tested transcripts except *MMP2* (D). Error bars denote 95% CI.

Table 5.1 Percent changes in transcript expression of U251 tumors dosed with 1 according to *Schedule D* (n=8 per condition).

Gene	% change	CI95%	p-val
Significantly changed expression			
ANGPT1	-61.0	7.4	0.025
ANGPT2	-80.0	3.4	0.010
HIF1a	-33.8	15.3	0.005
HOXB9	-48.2	9.6	4.7E-05
LOX	-35.2	10.5	0.004
mTie-2	-49.4	8.4	0.003
NEDD9	-69.7	3.3	4.2E-04
NLGN1	-67.1	3.1	4.7E-04
MMP14	-54.4	9.7	0.000
PDGFB	-58.6	5.3	0.011
RHOC	-58.5	3.1	9.9E-05
VEGF	42.9	9.7	0.014
Unchanged expression			
bFGF	20.6	20.5	0.112
BNIP3	14.6	15.7	0.988
CDH1	not exp.	not exp.	n.d.
CIDEC	0.4	29.8	0.172
EGF	-8.9	18.2	0.528
FLT1	-47.3	14.5	0.053
ITGA4	-32.6	8.9	0.108
MCJ	-3.6	45.2	0.096
MMP2	-26.2	20.5	0.105
NFKB	-37.9	11.4	0.891
NRP2	0.1	11.5	0.996
PGF	-8.5	15.8	0.236

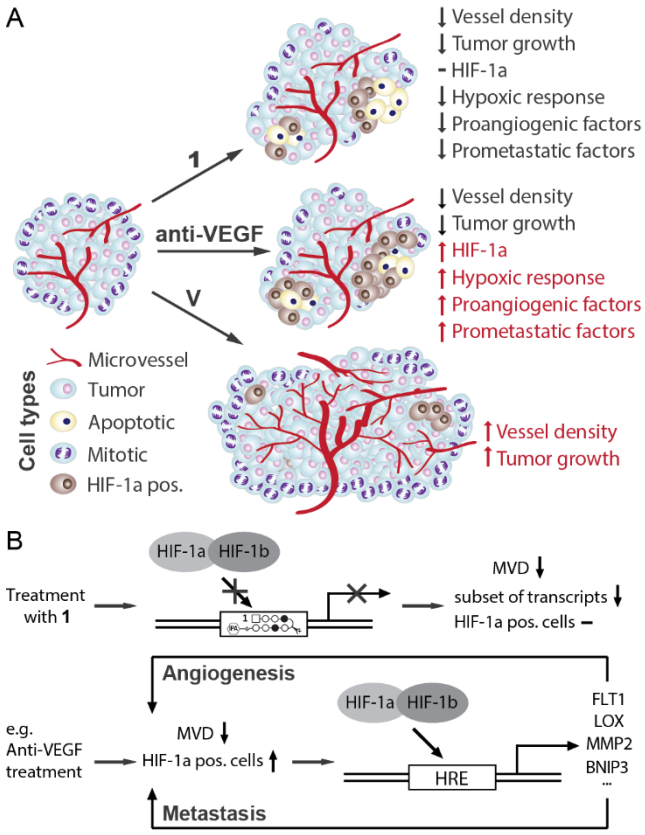

Figure 5.13. Treatment with 1 inhibits tumor growth and decreases density of vasculature in a distinct way compared to an anti-VEGF therapy. A) Compound 1 reduces microvessel density, hypoxia-related gene expression and cell proliferation, but does not increase HIF-1a levels. Presence of apoptosis in HIF-1a positive, but not HIF-1a negative, areas indicates increased sensitivity of cancer cells to hypoxia. This statement is supported by necrotic areas, being found closer to blood vessels after treatment with 1. B) Therapies targeting angiogenesis (e.g. Anti-VEGF) often lead to increased expression of prometastatic and proangiogenic factors because they do not inhibit hypoxic response. Targeting hypoxia-dependent transcription with 1 inhibits many of those factors, thus impairing adaptation of tumors to hypoxia.

Discussion

Regulation of hypoxic signaling is central to maintaining balance between health and disease. Its principal regulator, HIF-1, is essential for tumor initiation and progression, *e.g.*, vascularization, cell survival and metastasis (5, 41). Inhibition of HIF-1 activity has

suppressed tumor progression and reduced cancer resistance to available therapies (reviewed in (1, 5))**.** Our group has previously reported on the function of an HRE-binding Py-Im polyamide **1** as a partial inhibitor of HIF-1 dependent transcription in tissue culture (17). However, the *in vivo* activity and mechanism of **1** remained to be explored. We used Py-Im polyamide **1** (Fig. 6.1) to show that it inhibits tumor growth (Fig. 6.4), angiogenesis (Fig. 6.7), and several aspects of hypoxic response *in vivo* (Figs. 9 and 10). We also discovered inhibition of mRNA expression of proangiogenic and prometastatic factors that are often upregulated in hypoxic conditions (Fig. 6.12). We found that the effects of **1** are consistent with what would be expected in the case of a partial inhibition of hypoxic response (Fig. 6.13).

Polyamide tissue distribution and preliminary pharmacokinetics. Subcutaneous administration revealed that **1** distributes into serum within 1.5 h post-injection, with 31% drop in concentration 2.5 h later, indicating multi-hour long half-life. Even though **1** had favorable pharmacokinetics, its activity *in vivo* is likely dependent on the target tissue concentration. After three intraperitoneal injections (Schedule *A*), the radioactive analog **2** reached a concentration of 3.5 μM in GBM39 tumor and higher levels in other tissues. Concentrations attained for **1** in all tested tissues were thus higher than those used in our tissue culture studies (17).

Effects on tumor growth and vascularization. In the present study, inhibition of tumor growth and reduction in MVD was observed in two different cell types in response to treatment with **1**. The extent of these effects was comparable to ones exerted by Bevacizumab (42) in xenografts derived from U251 (39) and GBM39 cells (33).

Investigation of possible mechanisms of antiangiogenic action showed a lack of apoptosis in blood vessel lining, and no measurable influence on tube formation on matrigel. Lack of direct effects of **1** on endothelial cells suggests blood vessel recruitment might be impaired. One possible explanation is inhibition of expression of tumor-associated proangiogenic factors by **1**. However, systemic concentration of those proteins could also be affected.

Effects on apoptosis, proliferation and HIF-1a levels. Compound **1** induces apoptosis selectively, in HIF-1a-positive, perinecrotic areas. This suggests that **1** sensitizes cancer cells to hypoxia, which could occur by hypoxic response inhibition (5). Further support of this hypothesis is the lack of increase of HIF-1a positive cells in the tumors treated according to *Schedule B* and *C*. Since **1** did not affect HIF-1a levels in U251 cells in tissue culture, it is likely that numbers of HIF-1a positive cells were reduced as they went through apoptosis. Finally, increased reliance of cancer cells on proximity to vasculature once again suggests their hindered ability to adapt to low partial oxygen pressures, which is the main function of the hypoxic response. The transient induction of HIF-1a levels in briefly-treated GBM39 tumors could be due to two factors: concentration of **1** was insufficient to induce apoptosis of tumor cells in *Schedule A*, or overall level of hypoxia in these smaller tumors (Fig. 6.11G) was too low to induce sensitivity to **1**. The latter hypothesis is supported by comparable HIF-1a levels in non-necrotic regions of GBM39 tumors from a group treated according to *Schedule C* (Fig. 6.11A) and by tendency of smaller tumors to be less hypoxic (43). Overall, effects of **1** on apoptosis and proliferation are consistent with expected results of inhibition of hypoxic response and reduced microvessel density.

Effects on gene expression. Compound **1** reduced mRNA expression of a panel of genes involved in angiogenesis and metastasis. Many of the affected genes carry important functions in tumor adaptation to hypoxia; for example, Platelet-derived growth factor subunit B (*PDGFB*) and Angiopoietin-1 are involved in blood vessel maturation (4), whereas Lysyl Oxidase (*LOX*) or *RHOC* were involved in metastasis (44, 45). We also observed a slight elevation (1.4-fold) in both mRNA expression and serum concentration of *VEGF*, despite a visible downregulation in tissue culture (17). Reduction in microvessel density typically leads to decreased oxygen pressure and increased expression of proangiogenic factors, including *VEGF* (4, 39). However, it is not obvious whether elevation would be higher had it not been for treatment with **1**. Interestingly, elevated expression of *VEGF* did not prevent **1** from exerting antiangiogenic effect, suggesting that its mechanism of action could be *VEGF*-independent.

Conclusions

In summary, this study demonstrates that Py-Im polyamide **1** interferes with several aspects of hypoxic response *in vivo***.** Investigation of its *in vivo* mechanism of action suggests that **1** inhibits many endpoints of the hypoxic response in tumors: prometastatic and proangiogenic gene expression, tumor cell apoptosis in HIF-1a positive areas, decrease in nuclear density and proliferative index and microvessel density. This compound could potentially be useful in treatment of HIF-1 related disease as it distributes to tissues and has favorable pharmacokinetics, antitumor, and antiangiogenic activity in two different xenografts.

Pharmacokinetic and toxicity experiments. Animal experiments were carried out according to approved Institutional Animal Care and Use Committee protocols at the California Institute of Technology (Pasadena, CA). PK studies were done as previously described (28). In short, 6.8 mg/kg of **1** was administered s.c. in C57BL6 mice (CRL) and blood was collected retroorbitally (RO) at 1.5h, 4h and 48h. Serum was cleared by centrifugation (850g, 5 min), **1** extracted with 50% methanol and concentration analyzed by HPLC. Serum for analysis of toxicity markers (IDEXX) was obtained by RO collection and centrifugation (2000g, 15 min) in Serum Separator Tubes (BD Biosciences). The radioquantitation of **2** was performed as described elsewhere (46).

Table 5.2 Primers used in RT-qPCR experiments

Transcript	Forward (5'-3')	Reverse (5'-3')
ANGPT1	AGCGCCGAAGTCCAGAAAAC	TACTCTCACGACAGTTGCCAT
ANGPT2	AACTTTCGGAAGAGCATGGAC	CGAGTCATCGTATTCGAGCGG
bFGF	AGAAGAGCGACCCTCACATCA	CGGTTAGCACACACTCCTTTG
EGF	TGGATGTGCTTGATAAGCGG	ACCATGTCCTTTCCAGTGTGT
ET2	CGTCCTCATCTCATGCCCAAG	AGGCCGTAAGGAGCTGTCT
FLT1	CAGCAACATGGGAAACAGAAT	TAGAGTCAGCCACAACCAAGG
GAPDH	AGAAGGCTGGGGCTCATTTG	AGGGGCCATCCACAGTCTTC
HOXB9	CCATTTCTGGGACGCTTAGCA	TGTAAGGGTGGTAGACGGACG
LOX	AAGGTTTCTCAGCAAAGTACA	GACATCTGCCCTGTATGCTGT
MMP14	GGCTACAGCAATATGGCTACC	GATGGCCGCTGAGAGTGAC
MMP2	TACAGGATCATTGGCTACACACC	GGTCACATCGCTCCAGACT
mTie2	CAGCTTGCTCCTTTATGGAGTAG	ATCAGACACAAGAGGTAGGGAAT
NEDD9	ATGGCAAGGGCCTTATATGACA	TTCTGCTCTATGACGGTCAGG
NRLGN1	GGTGCCCCATTGACTCTCTG	GTGGGTCCACATCATCCAATTTT
NRP2	GCTGGCTATATCACCTCTCCC	TCTCGATTTCAAAGTGAGGGTTG
PDGFB	CTCGATCCGCTCCTTTGATGA	CGTTGGTGCGGTCTATGAG
PGF	GAACGGCTCGTCAGAGGTG	ACAGTGCAGATTCTCATCGCC
RHOC	GGAGGTCTACGTCCCTACTGT	CGCAGTCGATCATAGTCTTCC
VEGF	AGGGCAGAATCATCACGAAG	GGGTACTCCTGGAAGATGTCC

Quantitative Real Time-Reverse Transcription-PCR assay. Primers (Table 2) were designed using Harvard Primer bank (47). The total mRNA in tumors was extracted, analyzed and processed as in our previous studies (29).

Cell culture experiments

General Maintenance. Cell lines were characterized by StemElite ID system (Laragen). Temozolomide (TMZ) resistance of U251 cells has been assessed by Sulforhodamine B Assay (SRB) by plating 2k U251 cells per well in 96-well plates, allowing cells to attach for 24 h and then dosing TMZ up to 2 mM for 72 h. Obtained values of IC50 (sigmoidal fit) indicated TMZ resistance (IC50 = 252 ± 60 μM, 95% CI, n=6). U251 cells were maintained as adherent culture in RPMI-1640 medium (Gibco) supplemented with 10% FBS. They were sub-cultured at a ratio of 1:4-1:10 every 3 days. B) GBM39 cells were cultured as suspension culture in neurosphere growth medium, defined as F12/DMEM medium (Gibco) supplemented with b27 (diluted to 1x from a 50x solution, Gibco), EGF (20 ng/ml final, Life Technologies), bFGF (20ng/ml final, Life Technologies), heparin (50 μg/ml final, Sigma Aldrich) and Glutamax (diluted to 1x from a 100x solution, Life Technologies*)*. The EGF and bFGF growth factors were replenished every two days at concentrations listed above in presence of heparin. GBM39 cells were maintained in cell culture for up to 25 passages. After which GBM39 cell culture was re-established from a subcutaneous xenograft (~500 mm^3, male NSG, see also the xenograft methods section). The tumor was disintegrated mechanically, digested enzymatically (10% accutase in F12-K for 3 hours), and cells further disaggregated by pipetting. The cells were then cultured as described above. Human umbilical vein endothelial cells (HUVEC) were cultured in

200 PRF medium (Gibco) supplemented with Low Serum Growth Supplement (LSGS, Invitrogen). Media was exchanged every 48 h and passaged weekly. **Tube formation assay.** HUVEC cells were plated at $2x10^5$ cells per 75cm flask. After 36 hours, Py-Im polyamide **1** was added at a 5 μM final concentration, and cells incubated for 72 hours. Twelve-well plates were coated with 100 μl Geltrex (reduced growth factor basement membrane, Invitrogen) per well and allowed to solidify at 37°C for 60 min. Cells were trypsinized and taken up in 200 PRF medium at $2x10^5$ mL^{-1}, and plated in the 12-well plates at 400 μL per well. After 6-12 hours the wells were imaged on an inverted microscope by selecting 4 random fields of view.

Xenograft establishment and measurement

Male NOD-SCID-Gamma (NSG, NOD.Cg-Prkdcscid Il2rgtm1Wjl/SzJ) mice were purchased from Jackson Laboratories (JAX) and kept under defined flora pathogen-free conditions at the Association for Assessment of Laboratory Animal Care–approved Animal Facility at California Institute of Technology. U251 or GBM39 cells were implanted subcutaneously (s.c.) into left flanks of NSG mice as disaggregated cell suspensions of $2.5x10^6$ (U251) in RPMI-1640 medium or $7.5x10^5$ (GBM39) in 50% matrigel/neurosphere growth medium, using a g26 needle. Xenograft-bearing animals were treated once tumors had reached a minimum volume of 50 mm^3 as assessed by a caliper measurement (~60 mm^3 for U251 (Schedule A), and ~80mm^3 (Schedule B); ~ 100mm^3 for GBM39 xenografts). Each vehicle-treated control xenograft was paired with a xenograft of the same initial volume to be treated with **1.** Treatment was conducted by s.c. injection into the interscapular area (20% DMSO/PBS vehicle, or a stock solution of **1** at a concentration of 670 μM). Injected volumes were adjusted for animal weight, as specified *Schedule A-C*).

Animal weights were monitored at least once a week (see Supplementary Figure 1). Compound was administered s.c. interscapularly in 20% DMSO/PBS. Mice were euthanized if 15% weight loss, or more was observed.

Immunohistochemistry and histologic analysis

Immunohistochemistry and tumor sectioning was conducted at the Tissue Processing Core Laboratory (TPCL) at UCLA using protocols established at TPCL. Tumors were harvested 72 h following the last administration of **1** or vehicle, embedded in paraffin and sectioned to 5 μm thickness. Tumor microvessels were visualized using anti-mouse CD31 staining using SC-1506 antibody (SCBT) and apoptosis was assayed for using anti-human Cleaved-Caspase-3 (CC3) antibody (9664, CellSignal) and HIF-1a using CME 349 A (Biocare Medical). At least two tissue sections per slide were used for each experiment. Slides were scanned using an Aperio ScanScope AT (Aperio, Vista, CA) at a constant illumination and exposure. Images were then processed using ImageScope.

Perinecrotic area was defined as a field of view at 20x magnification that contained 50% necrosis and 50% adjacent, non-necrotic area, with edge of necrosis in the middle of the screen. Number of histologic measurements for each tissue section were chosen to limit variability of the final average value to <10%, per tumor, or until all available data in the section was counted. Measurements were averaged for each tumor, after which statistical analysis was performed for the obtained averages. All immunostaining quantifications were done at 20x magnification, unless otherwise noted.

At least 6 (CC3) or 9 (CD31) fields of view per tumor chosen randomly prior to analysis, at either 20x (CC3 staining, CD31 staining for U251, GBM39, *Schedules A* and *B*) or 40x

magnification (CD31 staining for GBM39, *Schedule C*, due to higher CD31 positive vessel counts). For analysis of frequency of apoptotic blood vessels (CC3/CD31 double staining), we counted enough high power fields (20x) containing CD31 positive vessels, to assess at least 600 microvessels per condition. Perinecrotic MVD was measured by first delineating nuclei on the edge f necrosis, and then offsetting the obtained path by an equivalent of 50 μm-350 μm, by an automatic algorithm in Adobe Illustrator CS5. The MVD was then counted manually for each 50 μm thick zone. Area of each zone was measured by an automatic integration of images and converted to mm^2, in order to obtain MVD values. At least 40 measurements per tumor were obtained, with a total of 854 measurements for a group treated with **1** and 586 for a group treated with vehicle. Measurements of the nearest blood vessel-necrosis distance were done manually using Imagescope software at 40x magnification. For GBM39 tumors, 329 measurements (n=6 per condition) were performed and 474 (n=10 per condition) measurements were done for U251 tumors. Fields of view measured per tumor sectioned varied depending on the amount of available necrotic regions with a well-defined, and thus quantifiable, border. Number of measured values per tumor section ranged between 16 and 53. Both HIF-1 and CC3 positive pixel counts were done by choosing at least 8 random fields of view at 20x magnification. Perinecrotic areas included at least n=8 measurements per tumor section and non-necrotic areas used at least n=10 per tumor section, and were higher whenever the amount of necrotic regions in the section allowed for it. Ki-67 measurements were done using Immunoratio software (48) at 20x magnification, with n=24 per tumor section. Nuclear density (and by proxy – necrosis) was assessed by automatic nuclei counting using

Image-based Tool for Counting Nuclei (ITCN), 16 fields of view were analyzed per tumor section.

Pharmacokinetics

Determination of serum concentration of **1** was performed as described previously (28). In short, **1** was injected subcutaneously into interscapular area at 6.8 mg/kg, which corresponds to 7.5 μmol/kg body weight. Blood was collected retroorbitally either at 1.5h, 4h or 48h after administration and allowed to clot for 30 minutes and centrifuged at 850 x g for 5 minutes. Serum was then mixed with two volume equivalents of methanol, vortexed and the resultant suspension centrifuged (16000 x g, 5 min). Supernatant solutions were diluted 1:1 with the HPLC loading buffer (water:acetonitrile, 80:20, acidified with 0.08 trifluoroacetic acid) and injected onto an analytical HPLC (Beckmann). Boc-Py-OMe was used as the internal standard.

Polyamide uptake and distribution *in vivo*

C-14 Radioquantitation. Quantification was performed in line with our previously reported metho. Briefly, tumor-bearing animals were injected with 6.8 mg/kg C-14 radiolabeled Py-Im polyamide **2**. After 24 hours, tissues with typical weights not exceeding 300 mg per sample were dissolved in 1 mL of the tissue solubilizing mixture SOLVABLE (Perkin-Elmer) overnight. Solutions were subsequently decolorized with 400 μl H_2O_2 (30 % w/w aqueous solution) per sample, for 1-2 hours at room temperature, then for 1 hour in 55-65 °C. HIONICFLUOR was added at 10 mL per sample and vials vortexed vigorously. Radioactivity associated with tumors, livers, kidneys and lungs was quantitated by liquid

scintillation counting on a Beckman Coulter LS6500 Multi-Purpose Scintillation Counter and quench-adjusted, as reported elsewhere (46). **Nuclear localization.** Mice were administered Py-Im polyamide **3** in three injections, every second day at 8.2 mg/kg (5 μmoles/kg). Twenty four hours post last injection tissues were harvested, fixed in formaldehyde for 24-48 hours and subsequently cryoprotected, first in 15% and then 30% aqueous sucrose (24 hours for each step). Tissue blocks were embedded in Tissue-Tek O.C.T. cryoembedding medium and sectioned at 5-10 μm of thickness. Slides were imaged on a confocal microscope capable of fluorescence detection (Zeiss LSM 510) under 63x oil immersion objective.

***In vivo* gene expression analysis, and RNA extraction**

The procedure for extraction and analysis was described elsewhere (29). In short, NSG mice bearing U251 xenografts were asphyxiated, tumors extracted and snap-frozen in LN2. They were subsequently homogenized using Tissue Tearor (BioSpec) and extracted using Trizol Plus kit, according to manufacturer's instructions. Reverse-Transcription was performed using First-Strand Transcriptor kit (Roche), using 1 μg of total RNA per reaction. RT-qPCR analysis was performed on ABI 7300 thermal cycler, using primers designed by Harvard PrimerBank and SYBR Green RT-PCR master mix (Life Technologies) and *GAPDH* as a house keeping gene as it levels were shown to be unaffected by hypoxia in U251 cells (49). For analysis of serum levels of VEGF proteins, NSG mice were dosed according to *Schedule A,* blood collected retroorbitally and serum

cleared by centrifugation (850g, 5 min). Subsequently, the VEGF protein level was measured using human-VEGF ELISA kit (R&D Biosciences).

Statistical Analysis

Each sample was analyzed using a two-tailed, student's t-test, assuming normality and unequal variance. P-value of 0.05 or less was considered statistically significant. All error bars on mean values shown are 95% confidence intervals (CI95%) and all error bars on medians, represent 25^{th}-75^{th} percentiles.

Acknowledgements

U251 cell line was a gift of Dr. Giovanni Mellilo (NCI). GBM39 cells were a gift of Dr. David Akhavan (UCLA), originally obtained from Prof. David James (UCSF). The authors thank Caltech OLAR for technical assistance with animal experiments and TPCL (UCLA) for assisting with IHC. The authors thank Drs. Nora Rozengurt and Dinesh Rao (UCLA) for helpful suggestions, discussion and preliminary pathological evaluation of tumor sections. We thank Drs. Nicholas Nickols and Bogdan Olenyuk for helpful discussions and suggestions. This work was supported by the NIH Grant GM-51747. J.O.S. was supported by NIH GM-51747. J.A.R received postdoctoral support from the Alexander von Humboldt foundation.

References

1. Semenza GL (2014) Oxygen sensing, hypoxia-inducible factors, and disease pathophysiology. Annu Rev Pathol 9:47-71.
2. Siegel R, Naishadham D, & Jemal A (2013) Cancer statistics, 2013. *CA Cancer J Clin* 63(1):11-30.
3. Xia Y, Choi HK, & Lee K (2012) Recent advances in hypoxia-inducible factor (HIF)-1 inhibitors. *Eur J Med Chem* 49:24-40.
4. Loges S, Schmidt T, & Carmeliet P (2010) Mechanisms of resistance to anti-angiogenic therapy and development of third-generation anti-angiogenic drug candidates. *Genes Cancer* 1(1):12-25.
5. Wilson WR & Hay MP (2011) Targeting hypoxia in cancer therapy. *Nat Rev Cancer* 11(6):393-410.
6. Vaupel P & Mayer A (2007) Hypoxia in cancer: significance and impact on clinical outcome. *Cancer Metastasis Rev* 26(2):225-239.
7. Semenza GL, Nejfelt MK, Chi SM, & Antonarakis SE (1991) Hypoxia-inducible nuclear factors bind to an enhancer element located 3' to the human erythropoietin gene. *Proc Natl Acad Sci U S A* 88(13):5680-5684.
8. Wang GL, Jiang BH, Rue EA, & Semenza GL (1995) Hypoxia-inducible factor 1 is a basic-helix-loop-helix-PAS heterodimer regulated by cellular O2 tension. *Proc Natl Acad Sci U S A* 92(12):5510-5514.
9. Brown JM & Wilson WR (2004) Exploiting tumour hypoxia in cancer treatment. *Nat Rev Cancer* 4(6):437-447.
10. Onnis B, Rapisarda A, & Melillo G (2009) Development of HIF-1 inhibitors for cancer therapy. *J Cell Mol Med* 13(9A):2780-2786.
11. Kung AL*, et al.* (2004) Small molecule blockade of transcriptional coactivation of the hypoxia-inducible factor pathway. *Cancer Cell* 6(1):33-43.
12. Kushal S*, et al.* (2013) Protein domain mimetics as in vivo modulators of hypoxia-inducible factor signaling. *Proc Natl Acad Sci U S A* 110(39):15602-15607.
13. Lao BB*, et al.* (2014) In vivo modulation of hypoxia-inducible signaling by topographical helix mimetics. *Proc Natl Acad Sci U S A* 111(21):7531-7536.
14. Lee K*, et al.* (2009) Acriflavine inhibits HIF-1 dimerization, tumor growth, and vascularization. *Proc Natl Acad Sci U S A* 106(42):17910-17915.
15. Kong D*, et al.* (2005) Echinomycin, a small-molecule inhibitor of hypoxia-inducible factor-1 DNA-binding activity. *Cancer Res* 65(19):9047-9055.
16. Olenyuk BZ*, et al.* (2004) Inhibition of vascular endothelial growth factor with a sequence-specific hypoxia response element antagonist. *Proc Natl Acad Sci U S A* 101(48):16768-16773.
17. Nickols NG, Jacobs CS, Farkas ME, & Dervan PB (2007) Modulating hypoxia-inducible transcription by disrupting the HIF-1-DNA interface. *ACS Chem Biol* 2(8):561-571.
18. Lee K*, et al.* (2009) Anthracycline chemotherapy inhibits HIF-1 transcriptional activity and tumor-induced mobilization of circulating angiogenic cells. *Proc Natl Acad Sci U S A* 106(7):2353-2358.
19. White S, Szewczyk JW, Turner JM, Baird EE, & Dervan PB (1998) Recognition of the four Watson-Crick base pairs in the DNA minor groove by synthetic ligands. *Nature* 391(6666):468-471.

20. Hsu CF*, et al.* (2007) Completion of a Programmable DNA-Binding Small Molecule Library. *Tetrahedron* 63(27):6146-6151.
21. Nickols NG & Dervan PB (2007) Suppression of androgen receptor-mediated gene expression by a sequence-specific DNA-binding polyamide. *Proc Natl Acad Sci U S A* 104(25):10418-10423.
22. Muzikar KA, Nickols NG, & Dervan PB (2009) Repression of DNA-binding dependent glucocorticoid receptor-mediated gene expression. *Proc Natl Acad Sci U S A* 106(39):16598-16603.
23. Raskatov JA*, et al.* (2012) Modulation of NF-kappaB-dependent gene transcription using programmable DNA minor groove binders. *Proc Natl Acad Sci U S A* 109(4):1023-1028.
24. Nickols NG*, et al.* (2013) Activity of a Py-Im polyamide targeted to the estrogen response element. *Mol Cancer Ther* 12(5):675-684.
25. Yang F*, et al.* (2013) Antitumor activity of a pyrrole-imidazole polyamide. *Proc Natl Acad Sci U S A* 110(5):1863-1868.
26. Martinez TF*, et al.* (2015) Replication stress by Py-Im polyamides induces a non-canonical ATR-dependent checkpoint response. *Nucleic Acids Res* 42(18):11546-11559.
27. Synold TW*, et al.* (2012) Single-dose pharmacokinetic and toxicity analysis of pyrrole-imidazole polyamides in mice. *Cancer Chemother Pharmacol* 70(4):617-625.
28. Raskatov JA, Hargrove AE, So AY, & Dervan PB (2012) Pharmacokinetics of Py-Im polyamides depend on architecture: cyclic versus linear. *J Am Chem Soc* 134(18):7995-7999.
29. Raskatov JA*, et al.* (2012) Gene expression changes in a tumor xenograft by a pyrrole-imidazole polyamide. *Proc Natl Acad Sci U S A* 109(40):16041-16045.
30. Raskatov JA, Szablowski JO, & Dervan PB (2014) Tumor xenograft uptake of a pyrrole-imidazole (py-im) polyamide varies as a function of cell line grafted. *J Med Chem* 57(20):8471-8476.
31. Yang F*, et al.* (2013) Animal toxicity of hairpin pyrrole-imidazole polyamides varies with the turn unit. *J Med Chem* 56(18):7449-7457.
32. Jacobs VL, Valdes PA, Hickey WF, & De Leo JA (2011) Current review of in vivo GBM rodent models: emphasis on the CNS-1 tumour model. *ASN Neuro* 3(3):e00063.
33. Hu YL*, et al.* (2012) Hypoxia-induced autophagy promotes tumor cell survival and adaptation to antiangiogenic treatment in glioblastoma. *Cancer Res* 72(7):1773-1783.
34. Akhavan D*, et al.* (2013) De-repression of PDGFRbeta transcription promotes acquired resistance to EGFR tyrosine kinase inhibitors in glioblastoma patients. *Cancer Discov* 3(5):534-547.
35. Sarkaria JN*, et al.* (2006) Use of an orthotopic xenograft model for assessing the effect of epidermal growth factor receptor amplification on glioblastoma radiation response. *Clin Cancer Res* 12(7 Pt 1):2264-2271.
36. Tentler JJ*, et al.* (2012) Patient-derived tumour xenografts as models for oncology drug development. *Nature reviews. Clin Oncol* 9(6):338-350.
37. Blagosklonny MV (2004) Antiangiogenic therapy and tumor progression. *Cancer Cell* 5(1):13-17.
38. Tang CM & Yu J (2013) Hypoxia-inducible factor-1 as a therapeutic target in cancer. *J Gastroenterol Hepatol* 28(3):401-405.
39. Rapisarda A*, et al.* (2009) Increased antitumor activity of bevacizumab in combination with hypoxia inducible factor-1 inhibition. *Mol Cancer Ther* 8(7):1867-1877.

40. Thomlinson RH & Gray LH (1955) The histological structure of some human lung cancers and the possible implications for radiotherapy. *Br J Cancer* 9(4):539-549.
41. Ryan HE, Lo J, & Johnson RS (1998) HIF-1 alpha is required for solid tumor formation and embryonic vascularization. *EMBO J* 17(11):3005-3015.
42. Presta LG*, et al.* (1997) Humanization of an anti-vascular endothelial growth factor monoclonal antibody for the therapy of solid tumors and other disorders. *Cancer Res* 57(20):4593-4599.
43. Lyng H, Skretting A, & Rofstad EK (1992) Blood flow in six human melanoma xenograft lines with different growth characteristics. *Cancer Res* 52(3):584-592.
44. Erler JT*, et al.* (2006) Lysyl oxidase is essential for hypoxia-induced metastasis. *Nature* 440(7088):1222-1226.
45. Sethi N & Kang Y (2011) Unravelling the complexity of metastasis - molecular understanding and targeted therapies. *Nat Rev Cancer* 11(10):735-748.
46. Raskatov JA, Puckett JW, & Dervan PB (2014) A C-14 labeled Py-Im polyamide localizes to a subcutaneous prostate cancer tumor. *Bioorg Med Chem* 22(16):4371– 4375
47. Spandidos A, Wang X, Wang H, & Seed B (2010) PrimerBank: a resource of human and mouse PCR primer pairs for gene expression detection and quantification. *Nucleic Acids Res* 38(Database issue):D792-799.
48. Tuominen VJ, Ruotoistenmaki S, Viitanen A, Jumppanen M, & Isola J (2010) ImmunoRatio: a publicly available web application for quantitative image analysis of estrogen receptor (ER), progesterone receptor (PR), and Ki-67. *Breast Cancer Res* 12(4):R56.
49. Said HM*, et al.* (2007) GAPDH is not regulated in human glioblastoma under hypoxic conditions. *BMC Mol Biol* 8:55.

Chapter 6

PRECLINICAL DEVELOPMENT OF PY-IM POLYAMIDES AS THERAPEUTICS FOR MULTIPLE MYELOMA

This chapter is based on a collaborative project with Patrick J. Frost (UCLA, West Los Angeles Veteran Affairs Hospital). The text of this chapter was taken in part from a MERIT grant application submitted to West Los Angeles Veteran Affairs Hospital, written by Patrick J. Frost.

Introduction

Multiple myeloma (MM) is an incurable disease of malignant plasma cells characterized by high rates of relapse, resistance to drug therapies, and, despite some recent advances in treatments, an overall median survival of just 5-6 years (1-3). It is unclear why this disease is so difficult to cure, but it has been hypothesized that physiologic characteristics of the bone marrow (BM) microenvironment confer critical growth and survival advantages that protect MM (4, 5). The BM is known to be hypoxic (pO_2 ~10-30mmHg) (6) compared to most tissues (85-150mmHg) and paradoxically, while oxygen stress can kill tumor cells (7), low pO_2 conditions also promote MM tumor progression (8), angiogenesis (9, 10), and resistance to chemotherapy (11, 12). These pro-survival effects are known to be regulated by an adaptive cellular response mediated by several oxygen-sensitive transcription factors, the most important of these being the hypoxia-inducible factors (HIFs) (for review see (13)). HIFs are composed of a constitutively expressed β-subunit (HIF1β/ARNT) and inducible α-subunits (HIF1α, 2α, and 3α) whose expression is generally dependent upon oxygen levels and is regulated by proteosome degradation (Fig. 6.1A). While the exact roles that these α-subunits play in regulating the hypoxic responses of MM in the BM microenvironment isn't well understood, recent studies do suggest that HIF1α activity supports initial survival and angiogenesis, whilst HIF2α supports subsequent MM progression and growth (3, 14). Thus, since the BM is known to have hypoxic niches that support MM growth and survival, and the adaptive cellular response to hypoxia includes

activation of HIF, we hypothesize that targeting this HIF-mediated adaptive hypoxic response will sensitize or kill MM cells engrafted within the BM microenvironment.

HIF activates about ~100-200 genes, typically in "categories" related to metabolism, angiogenesis, and apoptosis (15, 16). Because of the development of more resistant and malignant tumor phenotypes associated with hypoxia, there is increasing interest to targeting HIF-mediated gene transcription (17). Whilst targeting HIF-mediated transcription may be a promising strategy, there are numerous barriers to success. For example, many DNA targeting/binding molecules are non-specific and have significant "off target" effects against tumor and normal tissue (18). Echinomycin, a cyclic peptide in the family of quinoxaline antibiotics, can inhibit HIF/DNA binding (19), but is less sequence specific than HIF-PA (20). Programmable HIF inhibitors, such as siRNA or zinc-finger peptides, are sequence specific but suffer from poor bioavailability and the need for specific targeting strategies (21). Hairpin polyamides have an advantage for targeting gene transcription; they are small synthetic molecules, are cell permeable, localize to the nuclei, and can recognize and bind specific regions of the minor groove of double helical DNA with high affinity (22). The sequence specificity is conferred by the pattern of side-by-side pairs of Py and Im residues: Im-Py targets a G-C base pair, Py-Im targets a C-G base pair, and Py-Py targets T-A or A-T base pair (Fig. 6.1B) (23). Polyamide binding results in allosteric changes to the DNA helix that interferes with DNA-protein interactions and modifies endogenous gene expression (22). Specific PA compounds have been developed to recognize and target the promoter regions of enhancer and transcription factor binding elements, including androgen receptor (AR) (24), glucocorticoid receptor (GR) (25), NF-

κB (26), and the TGF-β1 promoter region (27). In xenograft studies, polyamides emonstrated anti-tumor efficacy related to their ability to inhibit specific gene expression, thereby providing a strong justification for further pre-clinical studies (28-32). Olenyuk et al (33) developed a PA that targets the 5'-WTWCGW-3' (W= A or T) sequence that modulates a subset of hypoxia-induced genes and confirmed that HIF/DNA targeting PA could be specific inhibitors of HIF activity (20).

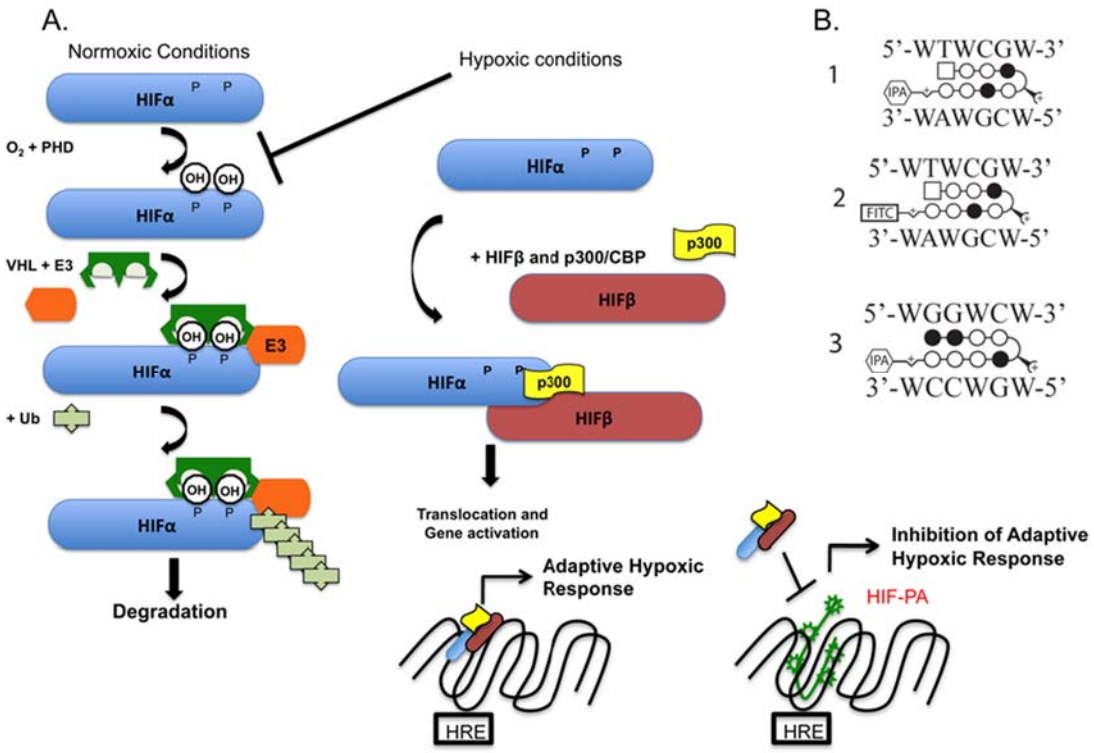

Fig 1: (A) Cartoon of HIF regulation showing O2-dependent stabilization of HIFα and dimerization with HIFβ. (B) Cartoon of PA used in this study (I) HIF-PA, (2) FITC-HIF-PA, (3) CO-PA.

This hypothesis was tested using a class of synthetically derived, sequence-specific DNA-binding pyrrole-imidazole (Py-Im) polyamide (PA) molecules that are composed of the aromatic rings of N-methylpyrrole and N-methylimidazole amino acids that recognize

the promoter regions of enhancer and transcription factor binding elements within DNA sequences (Fig. 6.1B) (33). The binding of Py-Im PA compounds results in allosteric changes to the DNA helix that interferes with DNA-protein interactions and modifies gene expression (22). These compounds have multiple advantages for targeting gene transcription: they are cell permeable, localize to the nuclei, and recognize and bind to specific regions of the minor groove of double helical DNA with affinity similar to transcriptional factors, such as HIF (22). Previous studies show antitumor effects of Py-Im polyamides in xenografts (20, 26, 28, 30); however, the effects of Py-Im polyamide treatment on Multiple Myeloma models have not been examined. Herein we evaluate those effects using a Py-Im polyamide (HIF-PA) that is capable of displacing heterodimer from binding to its cognate DNA sequences and inhibiting hypoxia-mediated gene transcription including pro-angiogenic factors (33). The choice of compound is dictated by observed heightened expression of angiogenic factors, such as VEGF, increased angiogenesis within MM tumors, and a strong correlation of these characteristics with disease development and progression in the BM and poor patient prognosis (34-37). Currently used VEGF-targeting drugs, such as bevacizumab (Avastin) inhibit angiogenesis in MM tumors; however, only modest and transient anti-tumor effects were observed (38), calling into question the overall clinical effectiveness of using a mono-therapeutic strategy targeting angiogenesis to treat myeloma. One explanation for the underwhelming effects of bevacizumab could be explained by a concomitant increase of hypoxia resulting from the inhibition of angiogenesis (39). In this scenario, low pO_2 (a natural component of the BM niche) may actually support MM progression and facilitate the adaptive hypoxic response via

activation HIF signaling and transcription of survival factors. In fact, a growing body of evidence supports the idea that HIF activity confers resistance to hypoxia-mediated apoptosis in solid tumors (40) and chemotherapy-mediated apoptosis in MM (12, 41). Thus, anti-angiogenesis strategies that don't address the HIF-mediated adaptive response to hypoxia may potentiate MM survival. Here, we present preliminary data demonstrating that synthetically derived PA compounds specifically inhibit the HIF-mediated adaptive hypoxic response in MM cells and overcome their resistance to hypoxia-mediated apoptosis. We investigated hypoxic signaling and HIF-PA response in a panel of MM cell lines (U266, H929, OPM-2, MM1.S, 8226) and the IL-6 dependent ANBL-6 isogenic MM cell line that has been transfected with mutated *N-RAS* or *K-RAS* (42). ANBL-6 is an interesting model because oncogenic mutations of *RAS* occur in 30-40% of MM patients and are associated with progressive disease, resistance to therapy, poor survival, and induction of HIF1α (43, 44), which makes them a good candidate for targeting HIF activity. Another cell model used are isogenic U266 cells transfected with a constitutively activated AKT allele (45). The 8226 cells were used to establish subcutaneous and orthotopic (bone marrow) xenografts and showed potential anti-tumor effects of HIF-PA-mediated. Finally, our preliminary experiments silencing HIF1α expression mirror our results of targeting HIF activity with polyamides, thereby validating our overall strategy. Our results showing differential expression and regulation of HIFα-subunits to low pO_2 highlights the importance of understanding the role that these transcriptional factors play in mediating the hypoxic response of MM engrafted in the BM.

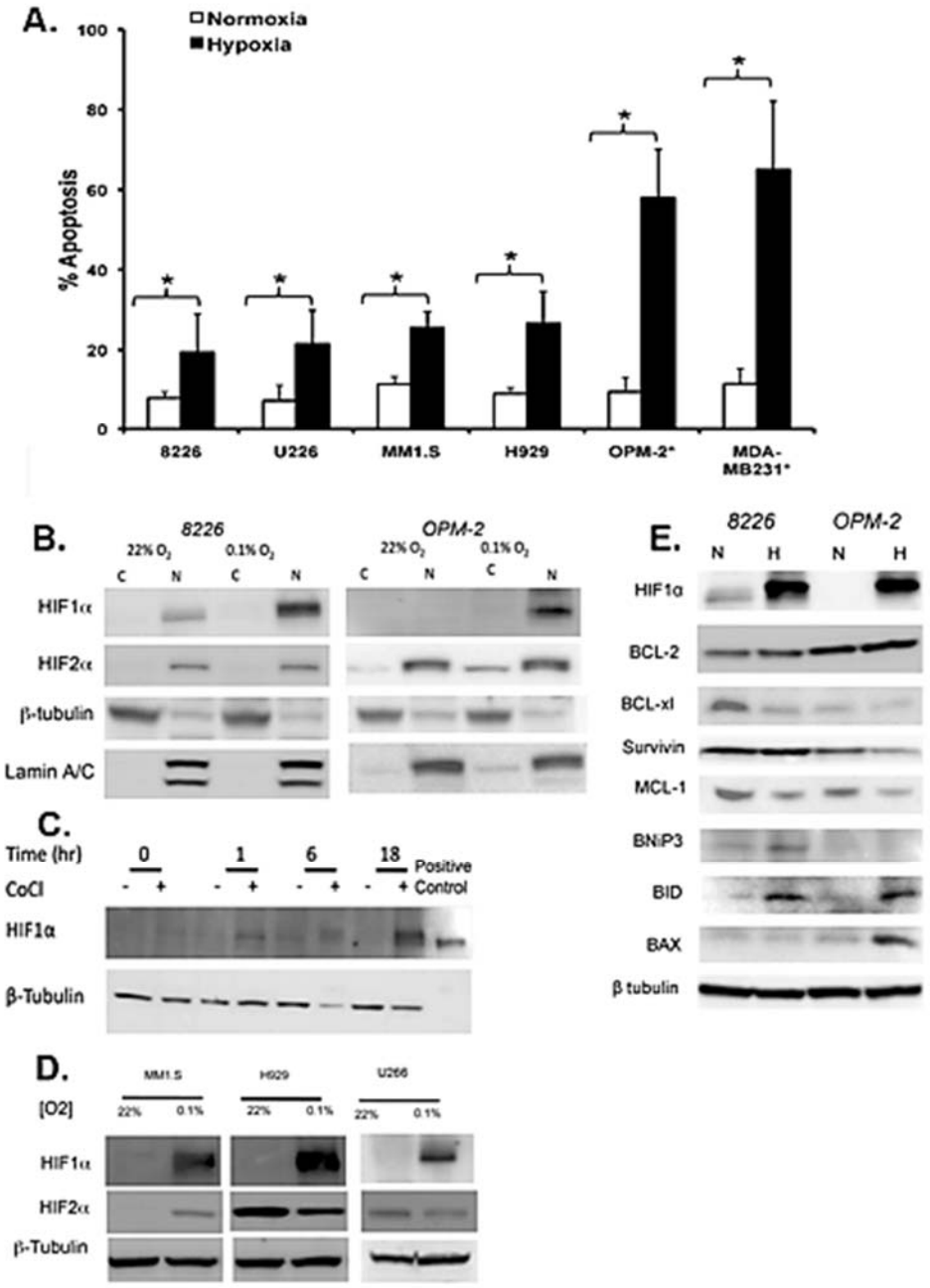

Fig 2. (A) Hypoxia-mediated apoptosis in MM cells cultured under normoxia (22%) or hypoxia (0.1%) for 72hr. Brackets indicate significance ($p<0.05$). OPM2 and MDA-MB-231 cells were cultured at 0.1% O_2 for 48hr. Mean ± Std dev of 4 independent experiments. (B) Immunoblots of HIF1α and 2α expression and translocation under normoxia or hypoxia for 24 hrs. C=cytoplasm fraction, N=nuclear fraction. (C) $CoCl_2$ induction of HIF1α in OPM2. Lysates were collected at indicated times. (D) Immunoblots of hypoxia-mediated induction of HIF1α and 2α in MM cells. (E) Immunoblots showing effect of 24 hr hypoxia on anti- and pro-apoptotic factors in 8226 and OPM2 cells. N=normoxia (22%), H=hypoxia (0.1%).

Results

Regulation of hypoxic gene expression in polyamides

MM cell lines have been reported to be resistant to hypoxia (3), but variations in the pO_2 levels studied, use of hypoxia mimicking agents (i.e., $CoCl_2$) and variation in cell lines has introduced discrepancies between studies. To establish our own baseline model, we used a hypoxia chamber to test the sensitivity of MM cell lines cultured under standard "normoxic" conditions (i.e., ~22% O_2, 5% CO_2) or "hypoxic" conditions (from 2% down to 0.1% O_2). The O_2 levels (2-0.1%) we report here are similar to the actual pO_2 levels observed in mouse BM; Spencer et al (6) measured pO_2 in mouse bone marrow to be <32 mmHg, but in some BM niches it could be as low as 9.9 mmHg, or about 1% O_2 (range of 2-0.6%) in the extravascular spaces. We found that pO_2 levels >1% were only modestly cytotoxic to MM cells, even when cultured up to 72 hrs (data not shown). At low oxygen conditions (e.g., 0.5-0.1% O_2), we observed a statistically significant (T-test, $p<0.05$) increase in hypoxia-mediated apoptosis (Fig. 6.2A) with 8226 and U266 cells being the most resistant (an increase of ~15-20% apoptosis), whilst H929 and MM1.S were intermediately sensitive (~25% apoptosis). In contrast, OPM2 was the most sensitive (>50% apoptosis compared) and this affect occurred by 48 hr. As a positive control for hypoxia-mediated apoptosis, we used the breast cancer cell line, MDA-MB-231, which is known to be sensitive to low pO_2 (46). The hypoxia-resistant 8226 cells constitutively expressed HIF1α, but this was strongly upregulated by hypoxia (0.1%, 24 hrs) (Fig. 6.2B left panel). HIF1α was not observed in the hypoxia-sensitive OPM2 under normoxic

baseline conditions, but was induced by low pO_2 (Fig. 6.2B, right panel). Interestingly, HIF2α expression was independent of O_2 levels in both cell lines. This is interesting because both

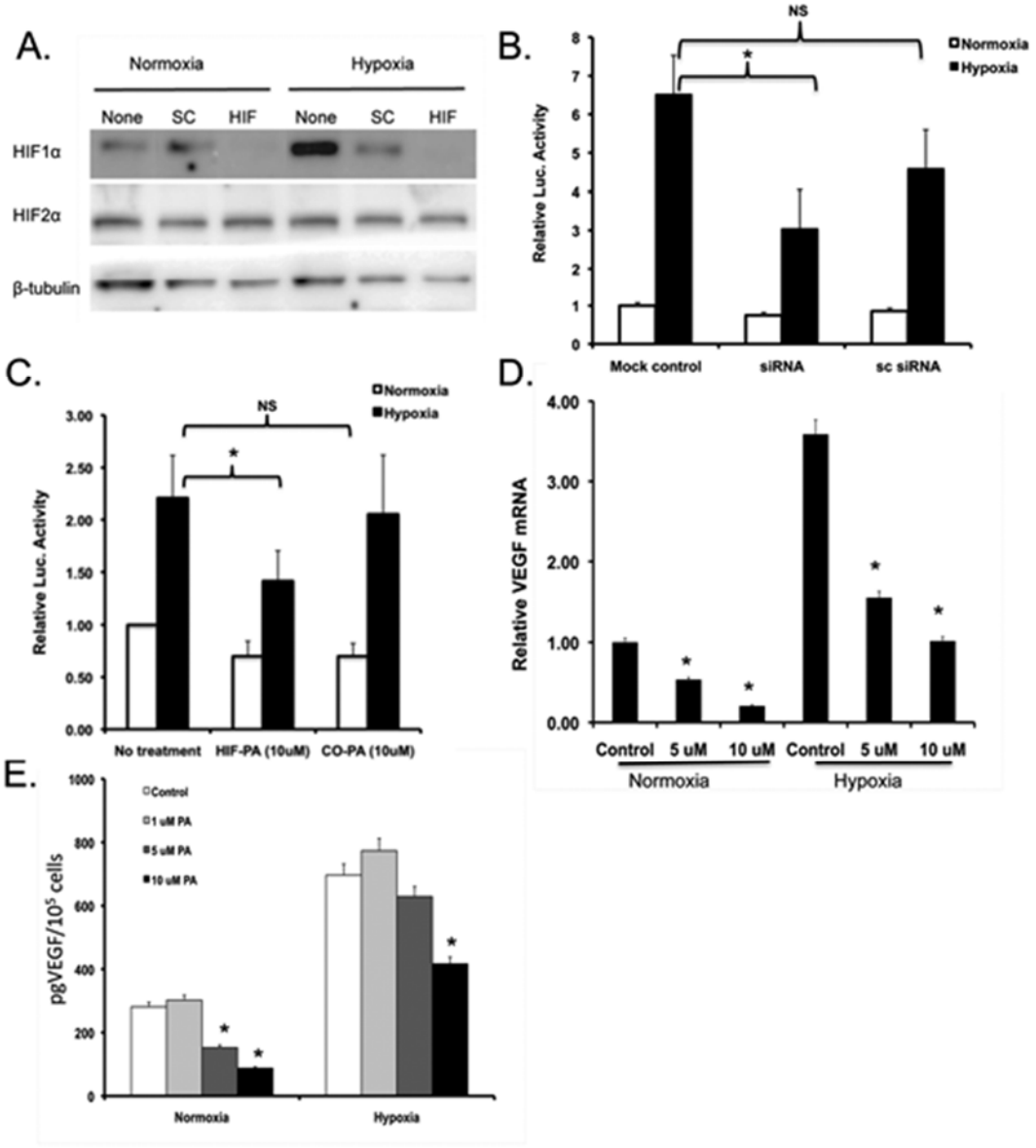

Fig. 6.3. (A) 8226 cells transfected with mock (None), HIF1α siRNA (HIF) or scrambled siRNA (SC) and HIF1α and HIF2α measured by WB. (B). HRE-LUC reporter activity in 8226 cells transfected with HIF siRNA or SC siRNA as described above. Values are means ±std of 3 independent experiments. NS=non significant ($p>0.05$), *=$p<0.05$. Hypoxic conditions were set at 0.1% for 24hrs. (C) HRE-LUC activity in 8226 cells under normoxic or hypoxic conditions and

treated with PA as indicated above. (D) HIF-PA-mediated inhibition of VEGF mRNA by RT-PCR (*=$p<0.05$). (E) HIF-PA-mediated inhibition of VEGF in supernatants by ELISA (*=$p<0.05$).

α-subunits are controlled via the PHD/VHL ubiquination pathway, yet it isn't clear why HIF2α, but not HIF1α, is constitutively expressed in these cells, and may lend credence to our hypothesis that the α-subunits have differential roles in MM. The rapid upregulation of HIF1α in OPM2 was confirmed using the hypoxia mimic, $CoCl_2$, which induced HIF1α by 1hr and reached a maximum by 18hrs (Fig. 6.2C). HIF1α expression was also induced by low pO_2 in MM1S, H929, Mosby, and U266 cell lines (Fig. 6.2D). In contrast, MM1.S was the only cell line tested in which HIF2α expression was O_2-dependent. These findings are generally similar to other reports describing HIF1α expression in MM cells (3, 10, 14). Culturing 8226 and OPM2 with low oxygen (0.1% 24hrs) didn't affect the expression of the pro-survival factor Bcl-2, but did inhibit Bcl-xl and MCL-1 in OPM2 and 8226, whilst survivin was only downregulated in OPM2 cells (Fig. 6.2E). Survivin has previously been reported to play a role in HIF-regulated survival of myeloma cells and thus may be an important target for future studies (12). Low pO_2 also upregulated the pro-apoptotic factors, BNiP3 (a known HIF target), BID, and BAX. We wish to point out that it isn't clear if the changes described above are specifically due to HIF activation (and as such could be a target for HIF-PA) or represent general physiological stresses in cell caused by low pO_2.

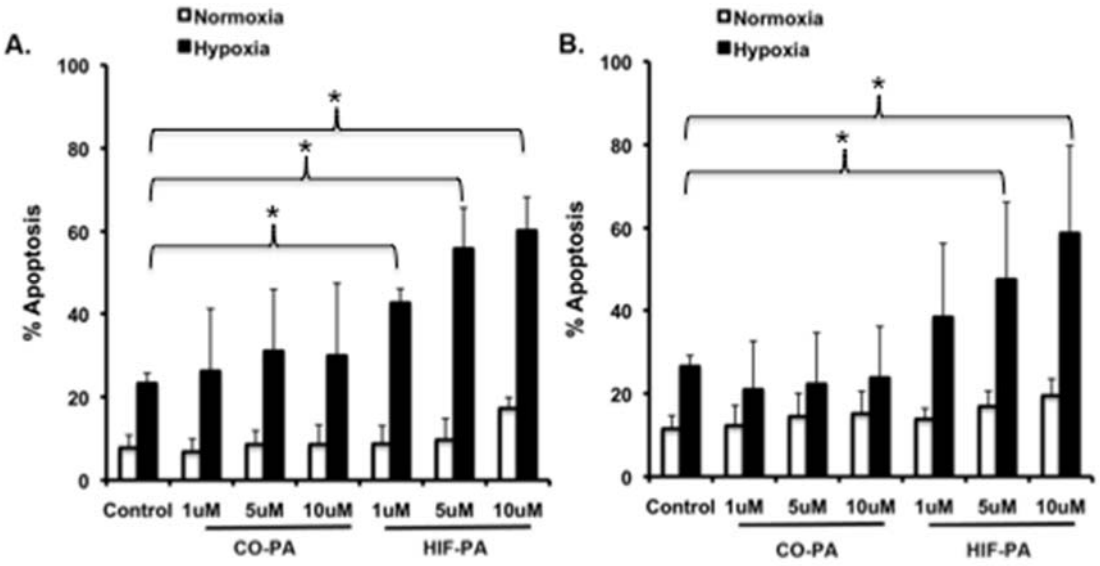

Fig. 6.4. HIP-PA sensitizes MM cells to hypoxia. (A) 8226 treated for 72 hr. (B) OPM2 treated for 24 hours. Apoptosis was measured by cleaved caspse 3. Cells were cultured under normoxic (22%O_2) or hypoxic conditions (0.1% O_2) with indicated concentration of HIF-PA or control PA. Data are means ± SEM of 3 independent experiments. Brackets comparing control with treatment *=$p<0.05$.

HIF-PA inhibits the hypoxic response in MM cells

HIF1α siRNA was used to knockdown the baseline HIF1α expression in 8226 cells (Fig. 6.3A), and importantly, this also inhibited the hypoxia-mediated upregulation of HIF1α (Fig. 6.3A compare lanes 1 and 3 and 4 and 6) but not the expression of HIF2α protein. Silencing HIF1α with siRNA significantly inhibits HRE-LUC reporter activity in 8226 HRE-luciferase (HRE-LUC) transfected reporter cells (Fig. 6.3B). It should be noted that in these experiments, HIF1α siRNA only inhibited about 50% of the HRE-LUC activity, which we believe is due to HIF2α-mediated LUC activity, thus explaining the partial response we see. We also found that HIF-PA could inhibit the hypoxic response in 8226 reporter cells. As shown in Fig. 6.3C, hypoxic conditions (0.1% O_2, 24hr) induced (by ~2-3 fold) LUC activity compared to baseline and HIF-PA inhibited about 40-50% (4

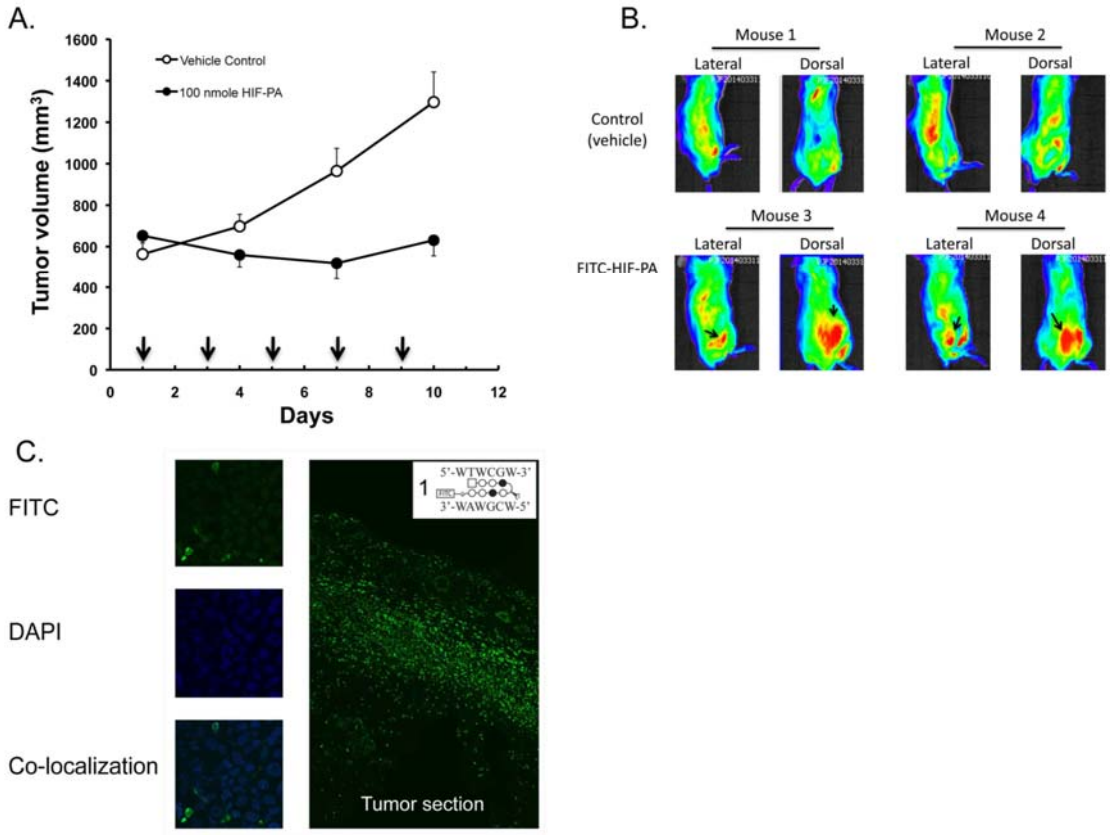

Fig 6.5. HIF-PA inhibits 8226 tumor growth in SQ xenograft model. (A) Change in 8226 tumor volume in HIF-PA treated NOD/SCID mice. Arrows indicate days of injection. * $p<0.05$ (B) Uptake of FITC-labeled HIF-PA (3 injections, every other day) assayed using fluorescent imaging of live animals. Arrows indicate location of SQ 8226 tumors. (C) Confocal fluorescent microscopy of excised tumors, demonstrating nuclear uptake of HIF-PA.

independent experiments, $p<0.05$) of this hypoxia-induced effect. As a negative control, non-HRE-sequence targeting CO-PA recognizing the unrelated sequence, 5'-WGGWCW-3', didn't significantly inhibit LUC activity. Similar results were seen in HRE-LUC expressing U266 and OPM2 cell lines (data not shown). In a previous study, it was shown that treatment with HIF-PA affected expression of a subset of hypoxia-induced genes containing HREs of the sequence 5′-(T/A)ACGTG-3′ that was similar to the level of inhibition observed when HIF was silenced by siRNA and by the DNA binding drug,

Echinomycin (20). However, in this study, the effect of HIF-PA-mediated inhibition of gene expression was not studied for cells cultured under hypoxic conditions. To address this, we tested if VEGF gene transcription (a known target of HIF) was inhibited by HIF-PA in MM cells. As shown in Fig. 6.3D, culturing 8226 cells under hypoxic conditions (0.1% O_2, 24hrs) induced VEGF mRNA (by ~3-4 folds) and HIF-PA significantly (3 independent experiments $p<0.05$) inhibited this effect. Additionally, VEGF protein (measured by ELISA) in the supernatant of cells cultured in low pO_2 was also significantly downregulated ($p<0.05$)(Fig. 6.3E). Altogether, these data support the hypothesis that HIF-PA can inhibit the HIF-mediated adaptive hypoxic response in MM.

HIF-PA sensitizes MM to hypoxia

We expect that inhibiting the adaptive hypoxic response will sensitize MM cells to hypoxia-mediated apoptosis based on our preliminary data. To test this, we cultured MM cells under normoxic or hypoxic conditions (0.1% O_2, 72 hours) in the presence of HIF-PA or control. As shown in Fig. 6.4, HIF-PA had little effect on normoxic 8226 cells (Fig. 6.4 white bars), but HIF-PA treatment of hypoxic 8226 cells induced a significant and dose-dependent hypoxia-mediated killing (an increase in ~20% to ~60%)(ANOVA, $P<0.05$) (Fig. 6.4A left panel). OPM2 cell lines were even more sensitive to hypoxia and HIF-PA, (ANOVA, $P<0.05$) with similar increases in apoptosis being observed by only 24 hrs (Fig. 6.4B right panel). The control, CO-PA, had no effect on hypoxia-mediated apoptosis in either cell line. Similar results on hypoxia-mediated sensitization were seen with MM1S and U266 cells (data not shown). These data represent the results of 3 independent

experiments and support our hypothesis that inhibiting the adaptive hypoxic response with HIF-PA can overcome MM resistance to hypoxia-mediated apoptosis.

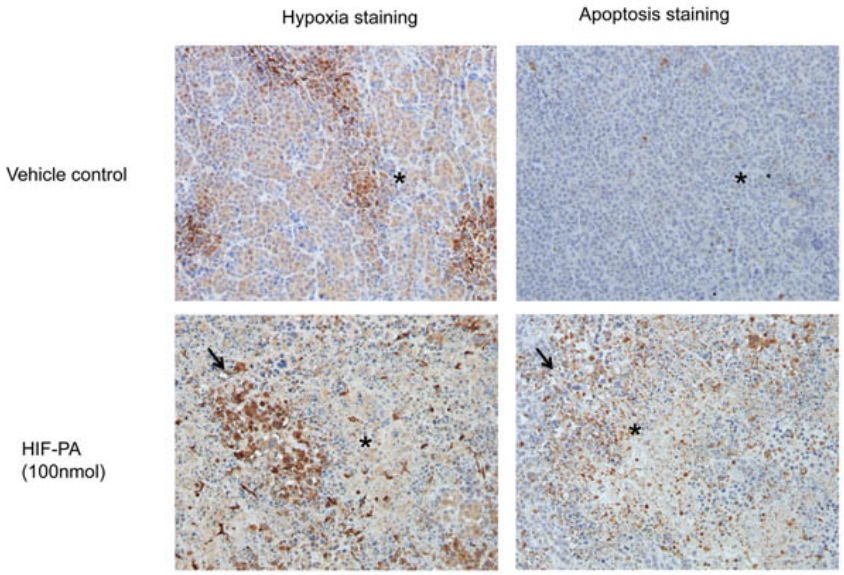

Fig. 6.6. Photomicrographs of serial tumor sections from control or HIF-PA treated mice stained for hypoxia (brown stain) and apoptosis (cleaved caspase 3). *=corresponding geographic regions. Arrow=areas of hypoxia and associated apoptosis.

As an *in vivo* correlate of the above data, the anti-MM effects of HIF-PA were also tested in a NOD/SCID xenograft model of subcutaneous (SQ) 8226 tumors (47-49). The mice were treated with 5 IP injections of HIF-PA (100nmol) or vehicle control every other day and the change in tumor volume was measured with calipers. HIF-PA treatment was well tolerated by the mice, with only a small transient decrease in weight. HIF-PA induced a significant inhibition of tumor growth in treated mice compared to control mice ($p<0.05$) (Fig. 6.5A). In order to confirm uptake of HIF-PA, an additional group of mice (N=2 mice/group) were given FITC-conjugated HIF-PA to measure compound uptake by fluorescent imaging (Fig. 6.5B). There was some auto-fluorescence signal in the bladder

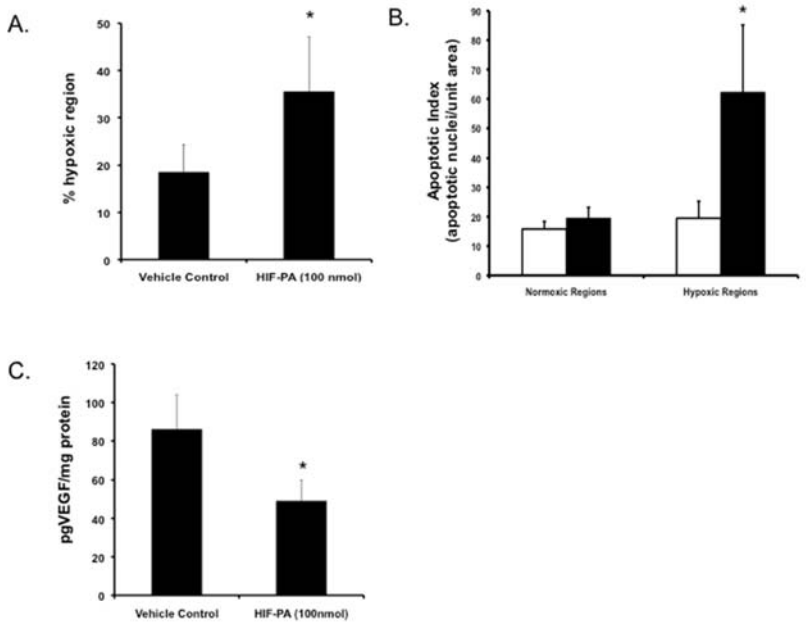

Fig 6.7. (A) Area of hypoxic regions in tissue sections stained for pimonidazole. (B). Apoptotic index, a measure of #apoptotic nuclei/unit area with regions of hypoxia or "normoxia". (C) ELISA analysis of VEGF concentration in tumor lysate. *=P<0.05. Values are means +/- 95% CI.

and gut (Fig. 6.5B, mice #1 and #2) of control mice. However, in FITC-HIF-PA treated mice, a positive signal in the tumor nodules was noted (Fig. 6.5B see arrow in mouse #3 and #4) and was confirmed by fluorescent confocal microscopy of excised tumors (Fig. 6.5C). IHC for hypoxia and apoptosis of serial tumor sections is shown in Fig. 6.6 as described previously (49). Both control (top left panel) and HIF-PA (bottom left panel) treated tumors had regions of hypoxia (the brown stained areas), but the extent of hypoxia (as well as areas of necrosis) was greater in the HIF-PA treated tumors. Quantification of hypoxic regions (determined by area of positive staining) (10 tumors/group, 10 fields/tumor) was ~35% in nodules harvested from the HIF-PA treated mice, compared to about 18% in the tumors from mice treated with vehicle control ($p<0.05$) (Fig. 6.7A). Necrotic regions within the HIF-PA treated tumors were greater than in control tumors,

and there was a strong physical correlation between areas of hypoxia and apoptosis (Fig. 6.6, bottom right panel), whilst apoptotic cells were evenly distributed in the control tumors (Fig. 6.6, top right panel). The apoptotic index (number of apoptotic cells/unit area) was used to quantify cell death by examining serial sections for hypoxic (determined by brown staining), and "normoxic" (determined by a lack of staining) regions and counting the number of apoptotic cells in the corresponding areas (10 tumors/group, 10 fields/region). As shown in Fig. 6.7B, there was an approximate 3-4 fold increase in apoptotic cells in the hypoxic regions of tumors from the HIF-PA treated mice compared to hypoxic regions of the control tumors ($p<0.05$). HIF-PA also significantly inhibited VEGF expression in tumor lysate by ~50% when compared to control tumors (Fig. 6.7C). Our data supports the hypothesis that HIF-PA can target VEGF and angiogenesis *in vivo* but we don't think that inhibition of VEGF-mediated inhibition of angiogenesis is the only explanation for these results. For example, HIF-PA sensitized MM cells to hypoxia-mediated apoptosis *in vitro*, a situation in which VEGF and angiogenesis is likely not important to MM survival.

Anti-tumor effects of HIF-PA against MM engrafted in the BM.

We've developed an orthotopic, "disseminated" BM-engrafted model (based on that of Miyakawa (50, 51)) using LUC2-transfected 8226 cells that will allow us to study MM engrafted in the BM. As shown in Fig. 6.8A, NOG mice challenged with 8226LUC cells developed engrafted tumors determined by using bioluminescence and X-ray analysis (Fig. 6.8A). In these mice, 20-50% of the bone marrow cells from inoculated mice were positive for human CD45 as confirmed by flow cytometry using FITC-conjugated anti-huCD45

antibody (Fig. 6.8B) and by IHC of *in situ* CD45+ 8226 cells in the mouse femurs. Gross histological analysis of the mice didn't show tumor formation in other tissues (i.e., liver, lung, spleen, or kidney). Other MM cell lines (e.g., OPM2, U266, and H929) are currently being developed and tested using this model.

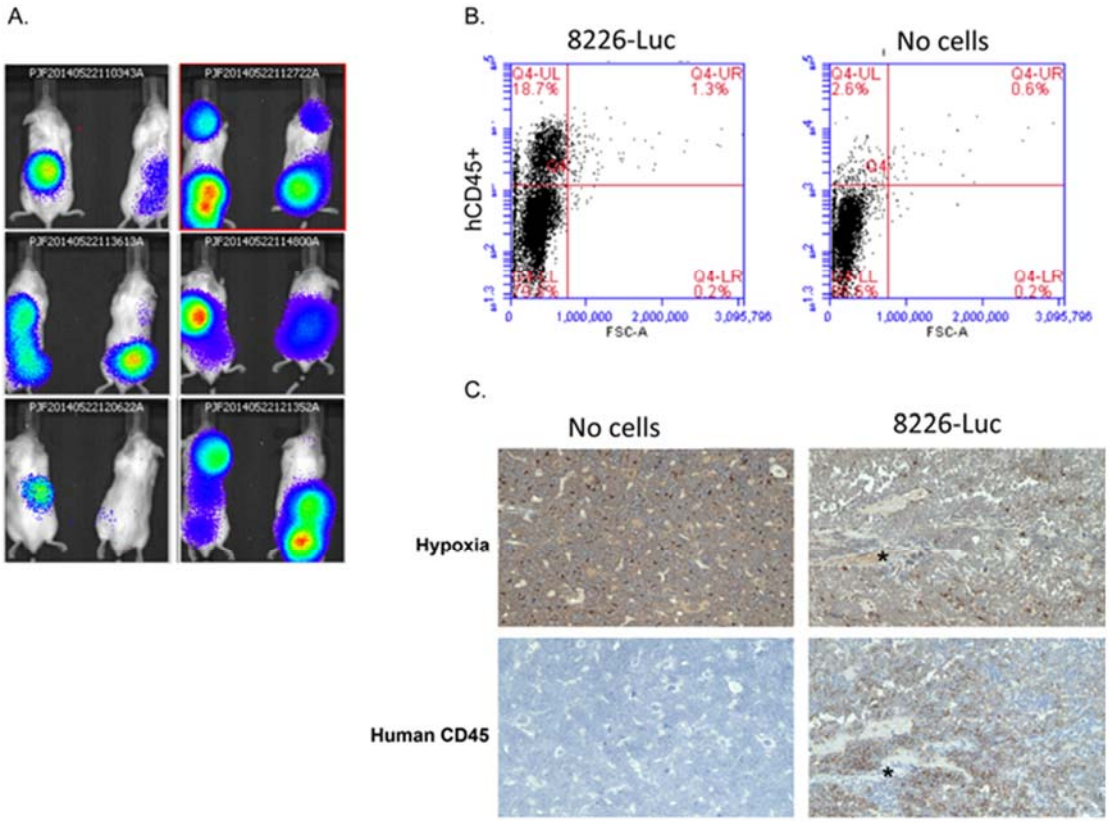

Fig 6.8. NOG mice challenged IV with 8226-LUC expressing cells. (A) Imaging of 12 mice on day +20 post-challenge with 8226LUC showing positive signal associated with long bones, skull, and spine. (B) BM harvested from mice challenged with 8226LUC or PBS and stained for huCD45 antibody (C). IHC of femurs of mice challenged with 8226LUC or PBS. Serial sections were stained with pimonidazole or huCD45.

Next, we performed a pilot experiment in which NOG mice (N=8 mice/group) with BM engrafted 8226LUC cells were given HIF-PA or vehicle control as described above for our SQ model. Fig. 6.9A shows that there was no significant (ANOVA, $p<0.10$) inhibition of

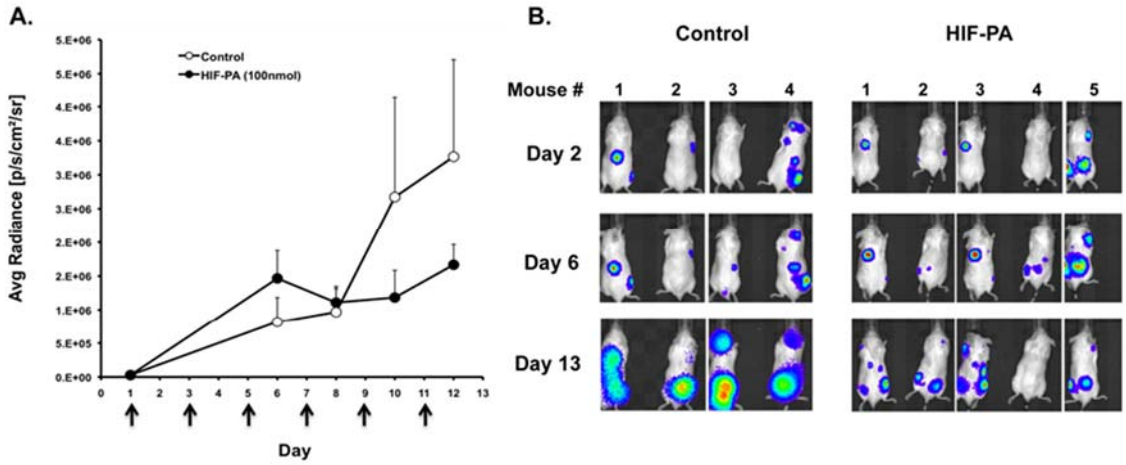

Fig 6.9. HIF-PA inhibits 8226 tumor growth in BM. (A). NOG (8/group) were challenged IV with 8226-LUC cells. Animals were given 5 IP injections of HIFA (100nmol) or vehicle control (arrows indicate days of injection). Luciferin bioluminescence was measured and data is presented as average radiance ± 95% CI. *p<0.10. (B) Representative pictures of mice imaged on day 2, day 6, and day 13 in control and HIF-PA treated mice showing change in Luciferin activity.

tumor growth in the BM and that increasing samples size will be required. Lack of significance was probably due to the small N and large variations in bioluminescence signal in the control mice. Representative images taken on day +2, +6 and +13 show both a decrease in LUC activity as well as a general shrinkage of individual tumor foci in the HIF-PA treated mice (Fig. 6.9B). In fact, we noted that in control mice, the tumor foci tended to grow and merge during the course of the experiment, in contrast to HIF-PA treated mice, in which the foci remain relatively small and isolated. This suggests to us that HIF-PA may inhibit both tumor growth and migration within the skeleton, suggesting further experiments to test this hypothesis.

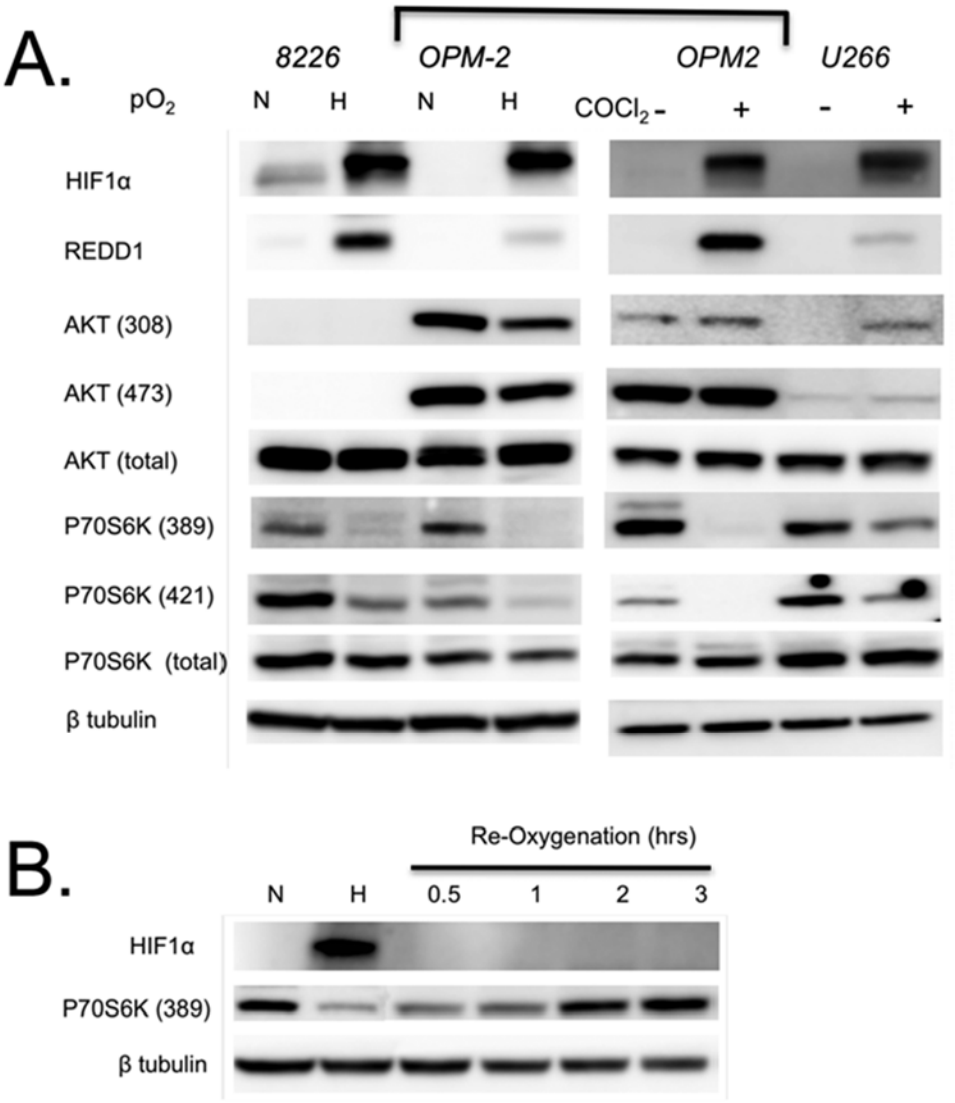

Fig 6.10. (A) Differential sensitivity of AKT/mTOR pathway in MM cells to 24hr hypoxia (0.1%) or $CoCl_2$ (100μM) treatment. Bracket indicates OPM2 treated with either hypoxia or $CoCl_2$. (B) OPM2 cells were cultured under normoxic or hypoxic (0.1%) conditions for 24 hrs and then allowed to re-oxygenate under normoxic culturing conditions for indicated time periods.

Effects of AKT/mTOR pathway activation on regulation of HIF-PA sensitivity: We have previously demonstrated that sensitivity of MM cells to mTOR inhibitors was correlated to heightened AKT activity *in vivo* and this was correlated with the inhibition of VEGF and angiogenesis (45, 47-49). Based on that we initially hypothesized that simply the induction of hypoxic stress could kill MM cells. However, as shown in Fig. 6.2, oxygen stress alone doesn't explain our *in vivo* observations, as MM tend to be resistant to low pO_2. In fact, MM cells that are most resistant to mTOR inhibition (and are characterized by quiescent AKT) also tend to be the most resistant to hypoxia (ie., 8226 and U266), whilst cells with hyperactive AKT tended to be the most sensitive (i.e.,OPM2) (52).

One potential mechanism is that hypoxia induces REDD1 expression, a hypoxia-sensitive inhibitor of mTOR (53). Therefore, we asked what were the effects of hypoxia on the mTOR pathway in our model. As shown in Fig. 6.10, hypoxia (or treatment with the hypoxia mimic CoCl2) induces REDD1 expression and inhibits the phosphorylation of p70S6 kinase, a downstream target of mTOR (54) (Fig. 6.10A). Hypoxia mediated inhibition of p70 was transient, returning to normal within 2 hr following reoxygenation of the cells (Fig. 6.10B). On the other hand, hypoxia has only slight effects on AKT phophorylation in 8226 and OPM2 cells and actually increases AKT phosphorylation at T308 in U266 cells. There is also evidence that IGF-1 and IL-6-mediated signaling via AKT induces HIF activity and potentiates survival in MM cells (12). Finally, mutions in PTEN (tumor supresson gene that regulates AKT) leads to increase HIF activity (55). Therefore, based on this and our previous work, we will test if sensitivity to HIF-PA is regulated by the activation of AKT/mTOR pathway in MM cells. To achieve this, we'll

use isogenic U266 cells that express a constitutively active AKT allele (45) as well as in ANBL-6 cells. The effects of HIF will be validated using our knockdown cells as described above. Specifically, we'll test if sensitivity to HIF-PA is correlated to AKT/mTOR activity.

In recent studies, it was shown that the hypoxia confers resistance to melphalan- or bortezomib-mediated apoptosis in MM cells, and silencing HIF1α expression restored sensitivity (12, 41). However, targeting HIF using siRNA may not be clinically feasible approach, and may be limited due to its failure to target HIF2α. Therefore, we would argue that abrogating HIF's ability to bind to the HRE using HIF-PA is a more effective way to overcome chemoresistance in MM. To test this hypothesis, MM cell lines and patient samples will be cultured *in vitro* under normoxic or hypoxic conditions and treated with HIF-PA in combination with bortezomib, melphalan, or mTOR inhibitors. These drugs were selected because they are either currently utilized anti-MM therapies (bortezomib and melphalan) or have been implicated in hypoxia-mediated apoptosis (mTOR inhibitors) in MM. In initial experiments, we'll measure the viability (by MTT assay), cell cycle transit (by hypotonic PI), and induction of apoptosis (using a cleaved caspase-3 assay kit) at various time points. We'll also collect RNA and protein to study the effects combination therapy on gene expression. The evaluation of drug-drug and drug-hypoxia interactions will be determined by isobologram and combination index (CI) analysis as previously described in our recently published study (56).

Our past studies have established that 8226 cells are resistant to mTOR inhibitors due, at least in part, to AKT dependent regulation of the internal ribosome entry site (IRES)-

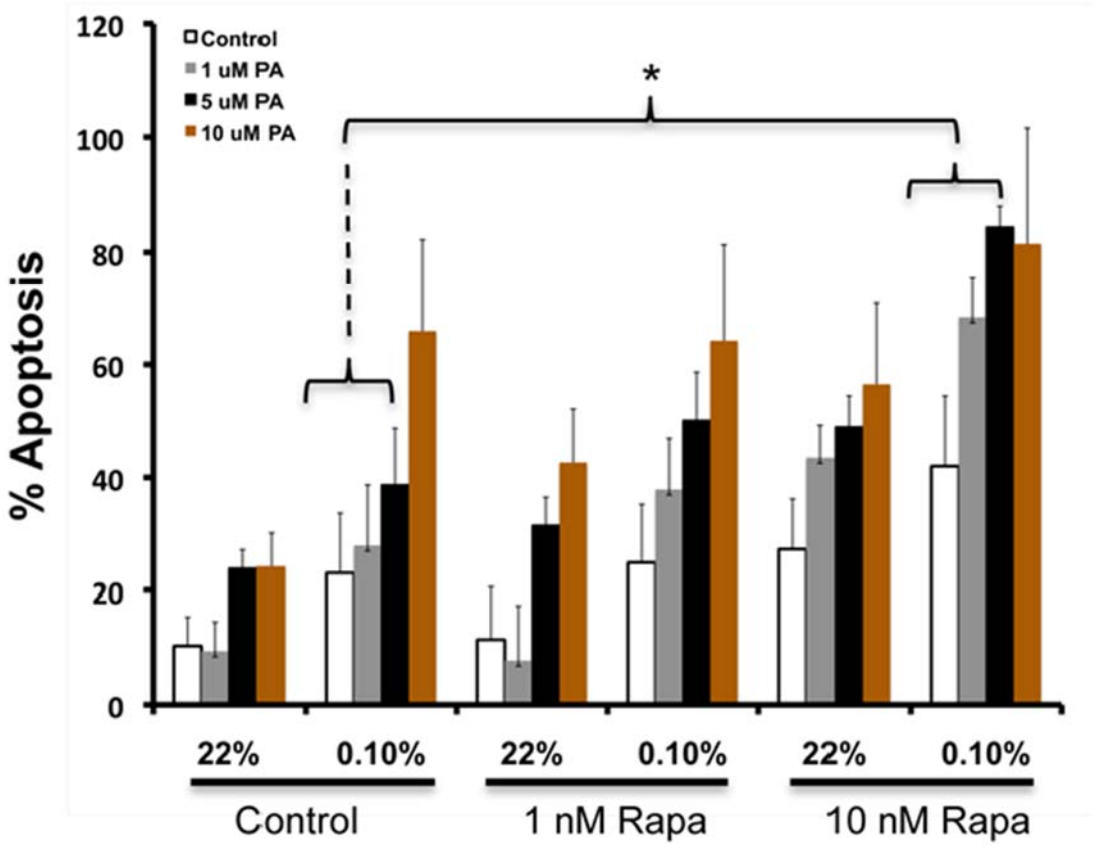

Fig 6.11. Combination of HIF-PA and Rapa treatment overcome resistance to hypoxia-mediated apoptosis. Cells were cultured under normoxic or hypoxic (0.1%) conditions with indicated drugs for 72hr. Values are mean ± SEM of 3 independent experiments. Brackets and * indicates * $p<0.05$).

mediated cap-independent salvage pathway that allows for translation of critical RNA species in the face of mTOR inhibition by rapalogs (i.e., rapamycin (RAPA) and temsirolimus) (45, 48, 49, 57, 58). We also demonstrated a correlation between RAPA-mediated inhibition of VEGF expression and angiogenesis with the induction of apoptosis in MM tumors *in vivo* (47, 48). Since hypoxia inhibits the mTOR pathway (53, 59, 60)

and cap-dependent translation (61), this suggests a role of IRES activity in regulating MM sensitivity to hypoxia (62). However, as shown in Fig. 6.2A, hypoxia alone isn't sufficient to kill 8226 MM cells. Therefore, we tested whether or not inhibiting mTOR-mediated translation could overcome resistance to hypoxia, the rationale being that inhibition of protein translation induced by the hypoxic response could sensitize the cells to apoptosis. Surprisingly, we found that mTOR inhibition had only a modest effect on apoptosis in MM cells cultured under hypoxic (0.1% O_2) conditions (Fig. 6.11, see white bars). However, the RAPA-resistant cell line, 8226, demonstrated a significant and synergistic HIF-PA-mediated sensitization to apoptosis in combination with RAPA, suggesting that targeting both the transcription and translation of hypoxia-induced genes would be an effective anti-MM strategy (Fig. 6.11, see grey and black bars and bracketed area). To expand on these findings, we'll study combination treatment of HIF-PA and mTOR inhibitors, including members of the rapalog family (e.g. rapamcyin, temsirolimus) that inhibit the mTOR complex 1 (mTORC1) and the new family of mTOR complex 1 and complex 2 (mTORC1/2) inhibitors (e.g., PP242) (63). Finally, we'll also study combination therapy of HIF-PA with bortezomib (a proteosome inhibitor) and melphalan (a nitrogen mustard alkylating agent) that were selected because they represent standard therapies for MM. As stated above, very interesting data has been presented indicating that hypoxia can confer resistance to these drugs in MM. Since these therapeutics are standard for treating MM, we believe that determining if HIF-PA can overcoming MM resistance is clinically relevant and will be a major goal of this AIM.

Data and Statistical Analysis: All data collected will be compiled and maintained using the computer program Excel. Initial data exploration and analysis of all variables will be performed using summary tables (mean, standard deviation, and ranges) box plots, and line graphs. The null hypothesis (that there is no difference from the control) will be tested using one-way analysis of variance (ANOVA), Student *t*-tests, multiple linear regression models, and *post hoc* Tukey-Kramer pair-wise comparisons. A P-value < 0.05 will be considered statistically significant for rejecting the null hypothesis. The PI has access the UCLA Semel Institute Statistics Core that will provide expert guidance and consultation in the design and analysis of experiments with the appropriate level of statistical power.

Power analysis for mouse studies: A power analysis predicts 95% power to detect differences of 30% or greater in changes in our primary variable (tumor volume) using a sample size of 8 mice/group. The effect size for changes in tumor volume in drug-treated mice compared to controls was estimated from our preliminary data and previous studies to be between 30-50%. However, only approximately 75-100% of mice challenged with tumor cells (depending upon cell line) develop a SQ or BM engrafted tumors. Thus, to ensure 8 mice/group, a total of 10-16 mice will be injected with tumor cells per experiment. Overall, we expect to utilize about 200 mice/year.

Power analysis for patient samples: We assumed that the ED50 for HIF-PA-mediated cytotoxicity will be a continual variable under hypoxic conditions and dichotomized samples into high (i.e. constitutive expression) or low (no expression) for HIF1α protein

examples. We also assumed that 33% of patient samples express "high" HIF1α based on previous literature (9). Thus, we estimate we'll need 25 patients to have 80% power and detect at least a 2x fold difference in the ED50 at a significance level of α=0.05 (calculated by a 2 sided *t*-test). In consultation with Dr. Lichtenstein, we anticipate recruiting ~7-10 patient samples/year, which should allow us to complete these studies in the time frame of this MERIT. We are cognizant of the fact that patient history (such as newly diagnosed versus relapsed disease) will contribute to the variability of our model, but would argue that addressing these variables are outside the initial scope of this application. However, if our pre-clinical results are promising, we will expand our experimental design to incorporate these additional factors.

References

1. Kumar SK*, et al.* (2008) Improved survival in multiple myeloma and the impact of novel therapies. *Blood* 111(5):2516-2520.
2. Lonial S, Mitsiades CS, & Richardson PG (2011) Treatment options for relapsed and refractory multiple myeloma. *Clin Cancer Res* 17(6):1264-1277.
3. Martin SK, Diamond P, Gronthos S, Peet DJ, & Zannettino AC (2011) The emerging role of hypoxia, HIF-1 and HIF-2 in multiple myeloma. *Leukemia* 25(10):1533-1542.
4. Hideshima T*, et al.* (2001) Novel therapies targeting the myeloma cell and its bone marrow microenvironment. *Semin Oncol* 28(6):607-612.
5. Podar K, Chauhan D, & Anderson KC (2009) Bone marrow microenvironment and the identification of new targets for myeloma therapy. *Leukemia* 23(1):10-24.
6. Spencer JA*, et al.* (2014) Direct measurement of local oxygen concentration in the bone marrow of live animals. *Nature* 508(7495):269-273.
7. Hockel M & Vaupel P (2001) Biological consequences of tumor hypoxia. *Semin Oncol* 28(2 Suppl 8):36-41.
8. Asosingh K*, et al.* (2005) Role of the hypoxic bone marrow microenvironment in 5T2MM murine myeloma tumor progression. *Haematologica* 90(6):810-817.
9. Giatromanolaki A*, et al.* (2010) Hypoxia and activated VEGF/receptor pathway in multiple myeloma. *Anticancer Res* 30(7):2831-2836.
10. Storti P*, et al.* (2013) Hypoxia-inducible factor (HIF)-1alpha suppression in myeloma cells blocks tumoral growth in vivo inhibiting angiogenesis and bone destruction. *Leukemia* 27(8):1697-1706.
11. Hu J*, et al.* (2010) Targeting the multiple myeloma hypoxic niche with TH-302, a hypoxia-activated prodrug. *Blood* 116(9):1524-1527.
12. Hu Y*, et al.* (2009) Inhibition of hypoxia-inducible factor-1 function enhances the sensitivity of multiple myeloma cells to melphalan. *Mol Cancer Ther* 8(8):2329-2338.
13. Greer SN, Metcalf JL, Wang Y, & Ohh M (2012) The updated biology of hypoxia-inducible factor. *Embo J* 31(11):2448-2460.
14. Martin SK*, et al.* (2010) Hypoxia-inducible factor-2 is a novel regulator of aberrant CXCL12 expression in multiple myeloma plasma cells. *Haematologica* 95(5):776-784.
15. Pouyssegur J, Dayan F, & Mazure NM (2006) Hypoxia signalling in cancer and approaches to enforce tumour regression. *Nature* 441(7092):437-443.
16. Semenza GL (2011) Oxygen sensing, homeostasis, and disease. *N Engl J Med* 365(6):537-547.
17. Podar K & Anderson KC (2010) A therapeutic role for targeting c-Myc/Hif-1-dependent signaling pathways. *Cell Cycle* 9(9):1722-1728.
18. Gilmore IR, Fox SP, Hollins AJ, Sohail M, & Akhtar S (2004) The design and exogenous delivery of siRNA for post-transcriptional gene silencing. *J Drug Target* 12(6):315-340.
19. Kong D*, et al.* (2005) Echinomycin, a small-molecule inhibitor of hypoxia-inducible factor-1 DNA-binding activity. *Cancer Res.* 65(19):9047-9055.
20. Nickols NG, Jacobs CS, Farkas ME, & Dervan PB (2007) Modulating hypoxia-inducible transcription by disrupting the HIF-1-DNA interface. *Acs Chemical Biology* 2(8):561-571.

21. Cheng JC, Moore TB, & Sakamoto KM (2003) RNA interference and human disease. *Mol Genet Metab* 80(1-2):121-128.
22. Edelson BS*, et al.* (2004) Influence of structural variation on nuclear localization of DNA-binding polyamide-fluorophore conjugates. *Nucleic Acids Res* 32(9):2802-2818.
23. Dervan PB & Edelson BS (2003) Recognition of the DNA minor groove by pyrrole-imidazole polyamides. *Curr Opin Struct Biol* 13(3):284-299.
24. Nickols NG & Dervan PB (2007) Suppression of androgen receptor-mediated gene expression by a sequence-specific DNA-binding polyamide. *Proc. Natl. Acad. Sci. U. S. A.* 104(25):10418-10423.
25. Muzikar KA, Nickols NG, & Dervan PB (2009) Repression of DNA-binding dependent glucocorticoid receptor-mediated gene expression. *Proc. Natl. Acad. Sci. U. S. A.* 106(39):16598-16603.
26. Raskatov JA*, et al.* (2012) Modulation of NF-kappaB-dependent gene transcription using programmable DNA minor groove binders. *Proc. Natl. Acad. Sci. U. S. A.* 109(4):1023-1028.
27. Matsuda H*, et al.* (2006) Development of gene silencing pyrrole-imidazole polyamide targeting the TGF-beta1 promoter for treatment of progressive renal diseases. *J Am Soc Nephrol* 17(2):422-432.
28. Yang F*, et al.* (2013) Antitumor activity of a pyrrole-imidazole polyamide. *Proc. Natl. Acad. Sci. U. S. A.* 110(5):1863-1868.
29. Synold TW*, et al.* (2012) Single-dose pharmacokinetic and toxicity analysis of pyrrole-imidazole polyamides in mice. *Cancer Chemother. Pharmacol.* 70(4):617-625.
30. Raskatov JA*, et al.* (2012) Gene expression changes in a tumor xenograft by a pyrrole-imidazole polyamide. *Proc. Natl. Acad. Sci. U. S. A.* 109(40):16041-16045.
31. Kashiwazaki G*, et al.* (2012) Synthesis and biological properties of highly sequence-specific-alkylating N-methylpyrrole-N-methylimidazole polyamide conjugates. *J Med Chem* 55(5):2057-2066.
32. Wang X*, et al.* (2010) Inhibition of MMP-9 transcription and suppression of tumor metastasis by pyrrole-imidazole polyamide. *Cancer Sci* 101(3):759-766.
33. Olenyuk BZ*, et al.* (2004) Inhibition of vascular endothelial growth factor with a sequence-specific hypoxia response element antagonist. *Proc. Natl. Acad. Sci. U. S. A.* 101(48):16768-16773.
34. Vacca A*, et al.* (1994) Bone marrow angiogenesis and progression in multiple myeloma. *Br J Haematol* 87(3):503-508.
35. Vacca A*, et al.* (1995) Bone marrow of patients with active multiple myeloma: angiogenesis and plasma cell adhesion molecules LFA-1, VLA-4, LAM-1, and CD44. *Am J Hematol* 50(1):9-14.
36. Rajkumar SV*, et al.* (2000) Prognostic value of bone marrow angiogenesis in multiple myeloma. *Clin Cancer Res* 6(8):3111-3116.
37. Kumar S*, et al.* (2004) Effect of thalidomide therapy on bone marrow angiogenesis in multiple myeloma. *Leukemia* 18(3):624-627.
38. White D*, et al.* (2013) Results from AMBER, a randomized phase 2 study of bevacizumab and bortezomib versus bortezomib in relapsed or refractory multiple myeloma. *Cancer* 119(2):339-347.
39. Blagosklonny MV (2004) Antiangiogenic therapy and tumor progression. *Cancer Cell* 5(1):13-17.

40. Warfel NA & El-Deiry WS (2014) HIF-1 signaling in drug resistance to chemotherapy. *Curr Med Chem* 21(26):3021-3028.
41. Hu J*, et al.* (2013) Synergistic induction of apoptosis in multiple myeloma cells by bortezomib and hypoxia-activated prodrug TH-302, in vivo and in vitro. *Mol Cancer Ther* 12(9):1763-1773.
42. Billadeau D*, et al.* (1997) Activating mutations in the N- and K-ras oncogenes differentially affect the growth properties of the IL-6-dependent myeloma cell line ANBL6. *Cancer Res* 57(11):2268-2275.
43. Chun SY*, et al.* (2010) Oncogenic KRAS modulates mitochondrial metabolism in human colon cancer cells by inducing HIF-1alpha and HIF-2alpha target genes. *Mol Cancer* 9:293.
44. Hoang B*, et al.* (2006) Oncogenic RAS mutations in myeloma cells selectively induce cox-2 expression, which participates in enhanced adhesion to fibronectin and chemoresistance. *Blood* 107(11):4484-4490.
45. Frost P, Shi Y, Hoang B, Gera J, & Lichtenstein A (2009) Regulation of D-cyclin translation inhibition in myeloma cells treated with mammalian target of rapamycin inhibitors: rationale for combined treatment with extracellular signal-regulated kinase inhibitors and rapamycin. *Mol Cancer Ther* 8(1):83-93.
46. Ahmadi M*, et al.* (2014) Hypoxia modulates the activity of a series of clinically approved tyrosine kinase inhibitors. *British journal of pharmacology* 171(1):224-236.
47. Frost P*, et al.* (2004) In vivo antitumor effects of the mTOR inhibitor CCI-779 against human multiple myeloma cells in a xenograft model. *Blood* 104(13):4181-4187.
48. Frost P, Shi Y, Hoang B, & Lichtenstein A (2007) AKT activity regulates the ability of mTOR inhibitors to prevent angiogenesis and VEGF expression in multiple myeloma cells. *Oncogene* 26:2255-2262.
49. Frost P*, et al.* (2013) Mammalian target of rapamycin inhibitors induce tumor cell apoptosis in vivo primarily by inhibiting VEGF expression and angiogenesis. *J Oncol* 2013:897025.
50. Miyakawa Y*, et al.* (2004) Establishment of a new model of human multiple myeloma using NOD/SCID/gammac(null) (NOG) mice. *Biochem Biophys Res Commun* 313(2):258-262.
51. Dewan MZ*, et al.* (2004) Prompt tumor formation and maintenance of constitutive NF-kappaB activity of multiple myeloma cells in NOD/SCID/gammacnull mice. *Cancer Sci* 95(7):564-568.
52. Shi Y*, et al.* (2002) Enhanced sensitivity of multiple myeloma cells containing PTEN mutations to CCI-779. *Cancer Res* 62(17):5027-5034.
53. Brugarolas J*, et al.* (2004) Regulation of mTOR function in response to hypoxia by REDD1 and the TSC1/TSC2 tumor suppressor complex. *Genes Dev.* 18(23):2893-2904.
54. Vadysirisack DD & Ellisen LW (2012) mTOR activity under hypoxia. *Methods Mol. Biol.* 821:45-58.
55. Semenza GL (2013) HIF-1 mediates metabolic responses to intratumoral hypoxia and oncogenic mutations. *J. Clin. Invest.* 123(9):3664-3671.
56. Hoang B, Benavides A, Shi Y, Frost P, & Lichtenstein A (2009) Effect of autophagy on multiple myeloma cell viability. *Mol Cancer Ther* 8(7):1974-1984.
57. Shi Y*, et al.* (2011) IL-6-induced enhancement of c-myc translation in multiple myeloma cells: critical role of cytoplasmic localization of the RNA-binding protein hnRNP A1. *J Biol Chem* 286(1):67-78.

58. Shi Y*, et al.* (2013) MNK kinases facilitate c-myc IRES activity in rapamycin-treated multiple myeloma cells. *Oncogene* 32(2):190-197.
59. Arsham AM, Howell JJ, & Simon MC (2003) A novel hypoxia-inducible factor-independent hypoxic response regulating mammalian target of rapamycin and its targets. *J Biol Chem* 278(32):29655-29660.
60. Sofer A, Lei K, Johannessen CM, & Ellisen LW (2005) Regulation of mTOR and cell growth in response to energy stress by REDD1. *Mol Cell Biol* 25(14):5834-5845.
61. Braunstein S*, et al.* (2007) A hypoxia-controlled cap-dependent to cap-independent translation switch in breast cancer. *Mol Cell* 28(3):501-512.
62. Stein I*, et al.* (1998) Translation of vascular endothelial growth factor mRNA by internal ribosome entry: implications for translation under hypoxia. *Mol Cell Biol* 18(6):3112-3119.
63. Hoang B*, et al.* (2012) The PP242 mammalian target of rapamycin (mTOR) inhibitor activates extracellular signal-regulated kinase (ERK) in multiple myeloma cells via a target of rapamycin complex 1 (TORC1)/eukaryotic translation initiation factor 4E (eIF-4E)/RAF pathway and activation is a mechanism of resistance. *J Biol Chem* 287(26):21796-21805.

Chapter 7

A BRIEF STUDY OF SYSTEMIC EFFECTS OF PY-IM POLYAMIDE TARGETED TO HYPOXIA-RESPONSE ELEMENT

Introduction

Oxygen regulation is essential for maintaining homeostasis in mammals. As a result, many human diseases are affected by hypoxic gene expression and in some cases these diseases can be alleviated, or prevented, by inhibiting the response to hypoxia. In particular, inhibition of hypoxic signaling could be useful in treatment of cancers, age-related macular degeneration, liver and kidney fibroses, systemic hypertension associated with apnea, and some aspects of a chronic heart disease (1, 2). In our *in vivo* studies Py-Im polyamides were administered systemically and were found in many organs at micromolar levels, often higher than those found in tumors (see chapter 5, (3, 4)). Additionally, we found that the FITC-conjugates of Py-Im polyamides were present in the nuclei of tested organs, such as livers, kidneys, or lungs (see chapter 5, (5, 6)). This raised a question if that gene expression in the tested organs can be regulated by Py-Im polyamides, and if the disease of those organs could potentially be alleviated with use of Py-Im polyamides.

Results and discussion

Py-Im polyamide 1 uptake in mouse tissues. The compound 1 (Fig 7.1A) was injected into balb/c mice intraperitoneally at 15 nmoles per mouse and the tissues were harvested after 24 hours. They were subsequently dissolved in Solvable reagent and analyzed for concentration as previously reported (7). The concentrations of 1 were analyzed for 14 organs and tissues and were the highest for liver, spleen, lungs, and kidneys (Fig 7.1B). We found comparatively low amounts of 1 in blood, brain, and both cardia and skeletal muscles (Fig. 7.1B).

These results suggested, that upon systemic administration of 1 we should expect more pronounced changes in gene expression in tissues such as liver, kidney, spleen, or lungs.

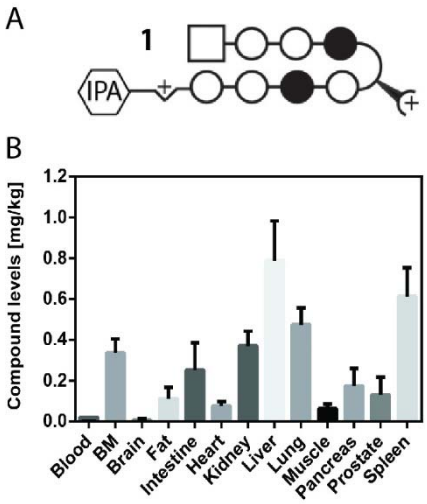

Figure 7.1 Uptake of 1 in tissues of Balb/C mice.A) Compound **1** used in the study in ball and stick notation – open circles represent N-methyl-Pyrroles, filled circles N-methyl-Imidazoles and open square 3-Chlorothiophene, as described in the Chapter 1. B) Levels of a C-14 labeled polyamide **1** in tested tissues of Balb/C mice (n=5). (Raskatov JA, 2014, unpublished data)

Gene expression changes in mouse tissues. We decided to analyze gene expression in three of the tested tissues: liver and kidneys that showed good uptake of **1,** and muscles, that showed significantly lower amounts of **1**. A panel of genes was used to determine gene expression changes in the tissues upon treatment of C57BL6 mice (NSG mice in case of muscles) with **1** (2 x s.c. inj., on day 1 and 3 at 6.8 mg/kg, tissues harvested on day 5). The organs were frozen immediately upon harvesting and RNA extracted using Trizol as described previously (see Chapter 4, Materials and Methods). RNA was then reverse-transcribed to cDNA and its levels quantified by RT-qPCR. The two tissues that have shown compound uptake levels above 0.2 mg/kg showed significant changes in gene

expression levels, while muscle, with lower uptake levels, showed no significant gene expression changes.

The presence of gene expression changes that correlated with uptake of compound 1 into the tissues suggested that action of 1 *in vivo* could be tissue specific, likely due to differences in tissue distribution. Significant uptake into livers, kidneys, or spleens suggests a possibility of regulating gene expression in those organs at lower levels than used in our previous xenograft studies. Thus studies with orthotopic xenografts or animal models of disease could show better therapeutic index of **1** than would be expected for subcutaneous xenografts used in our previous study (see Chapter 5).

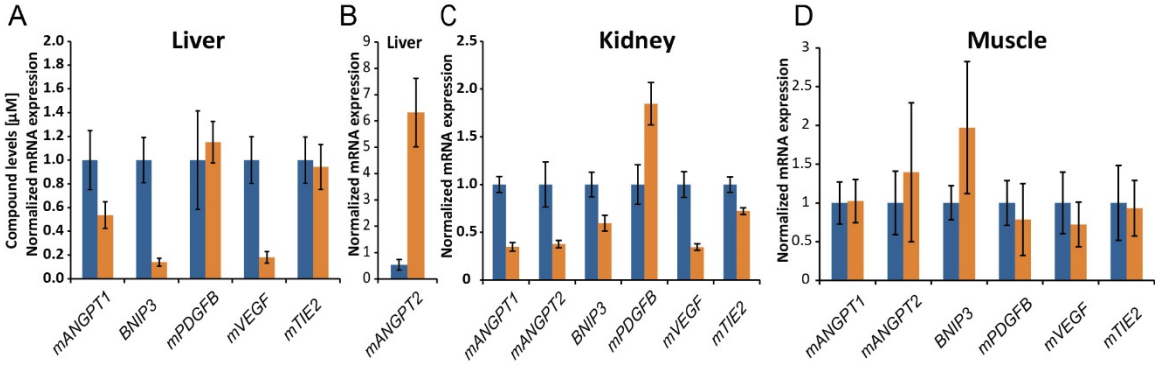

Figure 7.2 Gene expression changes in select organs. A) Proangiogenic gene were regulated by **1** in livers. Three of the tested genes, BNIP3, ANGPT1, and VEGF were downregulated, while ANGPT2 (B) was upregulated, possible due to liver toxicity (8). C) Similarly, in kidneys all genes were downregulated by **1** with the exception of PDGFB. D) In muscles, we observed no significant changes in gene expression, which could be explained by low amounts of compound **1** found after IP injection (Fig 7.1B)

References

1. Semenza GL (2014) Oxygen sensing, hypoxia-inducible factors, and disease pathophysiology. *Annu. Rev. Pathol.* 9:47-71.
2. Semenza GL (2014) Hypoxia-inducible factor 1 and cardiovascular disease. *Annu. Rev. Physiol.* 76:39-56.
3. Raskatov JA, Puckett JW, & Dervan PB (2014) A C-14 labeled Py-Im polyamide localizes to a subcutaneous prostate cancer tumor. *Bioorg. Med. Chem.*
4. Raskatov JA, Szablowski JO, & Dervan PB (2014) Tumor xenograft uptake of a pyrrole-imidazole (Py-Im) polyamide varies as a function of cell line grafted. *J. Med. Chem.* 57(20):8471-8476.
5. Nickols NG*, et al.* (2013) Activity of a Py-Im polyamide targeted to the estrogen response element. *Mol. Cancer Ther.* 12(5):675-684.
6. Yang F*, et al.* (2013) Animal toxicity of hairpin pyrrole-imidazole polyamides varies with the turn unit. *J. Med. Chem.* 56(18):7449-7457.
7. Raskatov JA, Puckett JW, & Dervan PB (2014) A C-14 labeled Py-Im polyamide localizes to a subcutaneous prostate cancer tumor. *Bioorg. Med. Chem.* 22(16):4371-4375.
8. Hadem J*, et al.* (2012) Angiopoietin-2 in acute liver failure. *Crit. Care Med.* 40(5):1499-1505.

INDEX